UNIVERSAL
LIBRARY
OU_162915
UNIVERSAL
LIBRARY

OSMANIA UNIVERSITY LIBRARY

Call No. 539.7/Vai/Pro Accession No. 3412

Author Vaidya, P. N.

Title Progress in nuclear physics

This book should be returned on or before the date last marked below.

PROGRESS SERIES

NUCLEAR PHYSICS

PROGRESS IN NUCLEAR PHYSICS

1

Editor

O. R. FRISCH, O.B.E., F.R.S.

LONDON

BUTTERWORTH-SPRINGER LTD

1950

BUTTERWORTH-SPRINGER LTD
BELL YARD · TEMPLE BAR · LONDON, W.C.2

BUTTERWORTH & CO (AFRICA) LTD · DURBAN

BUTTERWORTH & CO (AUSTRALIA) LTD · SYDNEY
MELBOURNE · BRISBANE · WELLINGTON · AUCKLAND

BUTTERWORTH & CO (CANADA) LTD · TORONTO

U.S.A. edition published by

ACADEMIC PRESS INC., PUBLISHERS
125 EAST 23RD STREET,
NEW YORK 10, NEW YORK

September 1950

Set in Monotype Times New Roman Type
Printed in Great Britain by The Eastern Press, Ltd., London and Reading.

CONTENTS

		PAGE
FOREWORD		*vii*
ACKNOWLEDGEMENTS		*viii*
1 CYCLOTRONS	*T. G. Pickavance*	1
2 HIGH VOLTAGE DIRECT CURRENT GENERATORS	*R. L. Fortescue*	21
3 PHOTOGRAPHIC EMULSION TECHNIQUE	*J. Rotblat*	37
4 ELECTRONIC CIRCUITS FOR NUCLEAR DETECTORS	*G. G. Scarrott*	73
5 THEORY OF BETA-DECAY	*T. Skyrme*	115
6 SPECTROSCOPY OF BETA- AND GAMMA-RAYS	*P. E. Cavanagh*	140
7 THE SZILARD-CHALMERS PROCESS	*H. A. C. McKay*	168
8 THE SCATTERING OF NEUTRONS BY CRYSTALS	*J. M. Cassels*	185
NAME INDEX		217
SUBJECT INDEX		223

FOREWORD

NUCLEAR PHYSICS has firmly established itself as a separate branch of physical science, and indeed within its field segregation is taking place: some researchers specialize in the construction of accelerating machines, some in the design of detecting equipment, others in the mathematical interpretation of results. This specialization we may regret, but we cannot prevent it. The best we can do is to minimize its ill effects by making it easier for the physicist to obtain information outside his special field.

This volume is intended to help both the nuclear physicist in finding information in fields adjacent to his own, and the other scientist in getting an introduction to some technique in nuclear physics which he may wish to use for his own purpose. It is planned that a similar volume will appear every year.

The choice of topics has been somewhat arbitrary. Some important topics were not included, for a variety of reasons. For instance, nuclear forces have been very recently reviewed in Rosenfeld's admirable work, and the subject is furthermore in turbulent development just now. Other topics, for instance, the reactions between light nuclei, were shelved for the opposite reason: that no very exciting developments have taken place during the last year or two. Next year's volume should fill some of those gaps. The publication of this volume has suffered some unexpected delays, but efforts have been made to add later information wherever possible. We hope that next year the gap between writing and publication will be substantially shorter.

O. R. FRISCH

ACKNOWLEDGEMENTS

The editor and publishers wish to thank the following authorities, and the authors concerned, for permission to reproduce the following illustrations :

American Institute of Physics: *Figures 8*, p 32; *2*, p 147
Arkiv för Matematik, Astronomi och Fysik : Figure 3, p 150
Institution of Electrical Engineers: *Figure 3*, p 25
Journal of Physical and Colloid Chemistry : Figures 1, p 181; *2*, p 182
Journal of Scientific Instruments : Figure 43, p 100
Nature, London : Figure 9, p 58
Physical Review : Figures 4, p 153; *2*, p 209; *3* and *4*, p 210
The Physical Society, London: *Figure 9*, p 33
Radiation Laboratory, University of California: *Figures 5*, p 12; *8*, p 19

1

CYCLOTRONS

T. G. Pickavance

WITHIN the last three years important developments in the design of cyclotrons have greatly extended their usefulness in nuclear research. As a result there are now cyclotrons of two distinct types. The conventional type has been developed steadily from the original apparatus built by LAWRENCE and LIVINGSTON[1], and many examples are in use in the United States and in Europe. The newer type, the frequency modulated cyclotron or synchrocyclotron, referred to here as the FM cyclotron, was first developed by Lawrence's team in Berkeley, California, and has opened a new field of research since it can provide beams of ions with energies in the region of hundreds of Mev. It is the principal subject of this article, but some discussion of the conventional cyclotron is necessary as an introduction. Gaussian units (electrical quantities in e.s.u, magnetic quantities in e.m.u) are used throughout except where otherwise stated.

THE CONVENTIONAL CYCLOTRON

The technique of the conventional cyclotron is well covered by the literature [2-8] and a brief survey will be sufficient here.

Principle of operation—The operation of the conventional cyclotron depends upon the fact that, for non-relativistic velocities, the time of flight of a particle around an orbit in a uniform magnetic field is independent of the velocity of the particle. It is given by

$$t=2\pi Mc/eH \qquad \ldots . (1)$$

where M = the mass of the particle (gram)
e = the charge on the particle (e.s.u)
H = the magnetic field intensity (oersted)
c = velocity of light (cm/sec)

Figure 1 shows diagrammatically the plan view of a cyclotron. Two hollow semicircular electrodes, the dees, are fixed in a vacuum chamber between the poles of a magnet, and carry an alternating potential difference. The particles to be accelerated, which are usually protons, deuterons or helium

nuclei, are emitted from an ion source in the centre of the system. Those particles which are affected by the electric field between the dees are accelerated and travel in paths determined by the magnetic and electric fields until, after they have travelled through 180° of arc, they reach the accelerating gap once more. The frequency of the alternating dee potential is adjusted to correspond to the angular velocity of the particles in their orbits, so that the particles are accelerated at each traversal of the dee gap. After many circuits they reach the edge of the system and may be extracted by means of a static deflecting field and allowed to strike an external target. High energy particles are thus produced by the successive application of relatively small potentials. The method is not suitable for electrons, since the relativity effect causes appreciable deviation from the rest value of the mass at quite low energies.

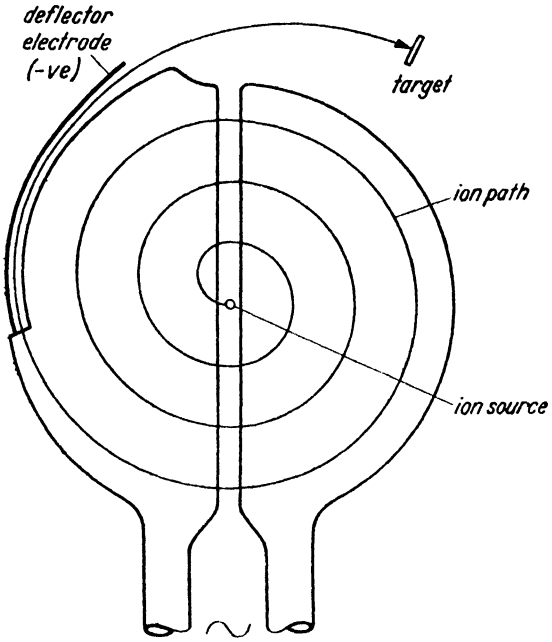


Figure 1. Schematic plan of a cyclotron

Putting into equation 1 the values of magnetic field economically obtainable (15,000 to 20,000 oersted), and the values of M/e for the particles, we get frequencies of oscillation for the dee potential about 20—30 megacycle per second for protons and 10—15 megacycle per second for deuterons or helium nuclei. The dee voltage generator is, therefore, a short-wave radio oscillator.

Some cyclotron formulae

$$H = 2\pi(Mc/e)f \quad \ldots . (2)$$

$$W = 2\pi^2 Mf^2r^2 \quad \ldots . (3)$$

$$r_N = 2(NVMc^2/eH^2)^{\frac{1}{2}} \quad \ldots . (4)$$

$$W_{max} = 4{\cdot}87\times 10^4(2V_0AZ\sin\theta_0)^{\frac{1}{2}} \quad \ldots . (5)$$

where H = magnetic field (oersted)
f = frequency of dee voltage (cycles/second)
W = kinetic energy of particle
r = radius of ion orbit (cm)
r_N = radius of ion orbit after N accelerations
$2V$ = acceleration potential per traversal of dee gap

W_{max} = maximum energy obtainable from a cyclotron (electron volts)
$2V_0$ = peak voltage between the dees
θ_0 = phase angle with respect to dee voltage in first ion orbit.

Values derived from equations 2—5 for protons, deuterons and helium nuclei are given in *Table I*, where W is in electron volts.

Table I. Field and Energy Data for Particles in Cyclotron

	Protons	*Deuterons*	*Helium nuclei*
H	$6{\cdot}52\times10^{-4}f$	$1{\cdot}304\times10^{-3}f$	$1{\cdot}304\times10^{-3}f$
W	$2{\cdot}05\times10^{-11}f^2r^2$	$4{\cdot}10\times10^{-11}f^2r^2$	$8{\cdot}20\times10^{-11}f^2r^2$
W_{max}	$4{\cdot}87\times10^4\,(2V_0\sin\theta_0)^{\frac{1}{2}}$	$6{\cdot}89\times10^4\,(2V_0\sin\theta_0)^{\frac{1}{2}}$	$1{\cdot}38\times10^5\,(2V_0\sin\theta_0)^{\frac{1}{2}}$

Equation 5 was originally given by ROSE[6]. It is derived for a magnetic field distribution which just gives adequate focusing.

Relativistic limitation of energy—The value of M in equation 1 is assumed constant in the conventional cyclotron, but the relativistic mass $M=M_0\,(1-\beta^2)^{-\frac{1}{2}}$, should be used. Thus the time of flight in an orbit increases with the energy, and the particles will gradually lag in phase with respect to the oscillations of the dee voltage if the magnetic field is uniform. Moreover, scattering of the particles by residual gas in the vacuum chamber and deviations from their paths caused by magnetic field in homogeneities will cause the beam to be lost unless some focusing influence exists. Near the centre, where the energy is low, the ions are focused by the electric field between the dees[6, 7], but this is ineffective at higher energies. The only method of focusing which has proved practicable is provided by suitably 'shaping' the magnetic field to apply a restoring force to ions off the median plane of the magnet. This requires the field to diminish as the radius increases, whereas correct synchronism of the orbits in the relativistic case demands a magnetic field increasing with radius. Thus the phase lag is increased, and a practical limit of energy obtainable with a conventional cyclotron is imposed. The difficulty can be offset by increasing the dee voltage and so reducing the number of turns and the total phase lag, but as has been shown by WILSON[7] and others, the radiofrequency power requirements rise very rapidly with the particle energy, about as W^4, and would probably become economically impracticable for energies much above 15 Mev and 30 Mev for protons and deuterons respectively.

Practical features—After continuous development in various laboratories for some years, conventional cyclotrons have become reliable sources of intense beams of ions. The largest, at Berkeley, California, and at Birmingham,

have magnets with pole-face diameters 60 inch (152 cm) and 61·5 inch (156 cm) respectively, weighing about 200 ton (203 tonne). About 100 kilowatt of radiofrequency power are required for machines of this size, with dee potentials of about 200 kilovolt. The Berkeley machine can produce a deflected beam of several microamperes of about 45 Mev helium nuclei or much greater currents of about 25 Mev deuterons. Where target materials can be used on a probe between the dees *e.g.* for the production of neutrons by deuteron bombardment of beryllium or for the production of certain tracer elements, beam currents of about 1 milliampere have been regularly obtained in several laboratories; external deflected beams, led into a separate target chamber provided with an air-lock, so that targets may be changed without disturbing the vacuum in the main chamber, vary from about 10 to 300 microamperes or more. With an energy of 12 to 20 Mev these intensities raise serious problems of heat dissipation in the targets, and oscillating or rotating water-cooled targets[5] have been used extensively. Further problems are erosion of the dees, particularly near the centre, under intense ion bombardment, and in the large machines the growth of long-period radioactivity in the dees from the reaction Cu^{65} (d, 2n) Zn^{65} (250 days). Comprehensive reviews of conventional cyclotron practice, which include many references, are given in an article by LIVINGSTON[5], and a book, *Le Cyclotron*, by NAHMIAS[8].

THE FREQUENCY-MODULATED CYCLOTRON

Phase stability—In 1945 it was shown independently by VEKSLER[9] and MCMILLAN[10] that charged particle orbits in magnetic and alternating electric fields, as in a cyclotron, can possess the property of phase stability. Suppose that a particle is circulating in a cyclotron with a frequency equal to the frequency of the dee potential, and with a phase such that it crosses the gap between the dees when the dee potential is zero, and about to become positive (decelerating). If now, for some reason, the ion velocity increases, then its time of flight back to the dee gap will increase on account of the relativistic increase of mass. The dee voltage will therefore have passed through zero on the next arrival at the dee gap and the ion will be slowed down. Similarly, a spurious effect resulting in reduced velocity will eventually be offset by an acceleration on the next passage across the dee gap. Neglecting effects such as scattering of the particle by gas in the acceleration chamber, the ion will circulate indefinitely in its orbit, executing stable oscillations of phase and energy about the equilibrium values. Veksler and McMillan pointed out that, by increasing the magnetic field or reducing the frequency of the dee voltage, or both, the particle orbits could be made to expand and the energy to increase. In 1943 Oliphant proposed an accelerator based on this principle. If such a variation is made sufficiently slowly the phase

stability is preserved during acceleration. In the synchrotron, for electrons, the frequency is fixed and the magnetic field is increased during acceleration; in the proton synchrotron the field and the frequency are both varied. In both these accelerators the orbit radius remains practically constant. Variation of the frequency during acceleration, keeping the magnetic field constant, is the principle of operation of the FM cyclotron.

Practical consequences of phase stability—The practical limit on the particle energy obtainable in a cyclotron, imposed by the relativistic increase of mass, is removed by the attainment of phase stability, and it is no longer necessary to find a compromise between adequate magnetic focusing and the conflicting requirement of synchronism. In an FM cyclotron adequate magnetic focusing can be provided, the frequency variation being made sufficiently great to allow for the combined effect on the time of flight of the increase of mass and the reduction of magnetic field at large radii.

The mean free paths of protons, deuterons or helium nuclei, in gases at pressures readily obtainable with conventional vacuum practice (about 10^{-5} mm Hg), are such that many thousands of circulations may be made during acceleration with small loss of particles from the beam, given a practicable amount of magnetic focusing. There is a well known process in which a fast ion encounters a slow neutral atom and captures an electron in flight, giving rise to a fast neutral atom and a slow ion; this process has been observed in the large Berkeley FM cyclotron (private communication) but appears to cause negligible loss of ions from the beam. The results of the theory of phase stability worked out by BOHM and FOLDY[11, 12] show that the ions can make many circulations once they have been captured in the phase stable orbits. Thus no obstacles to the acceleration of ions to high energies are inherent in the method, and an energy gain of a few kilovolt per turn is quite practicable. To test the validity of this theory the 37 inch (94 cm) Berkeley cyclotron was converted to operate as an FM machine and successfully operated[13] under conditions simulating acceleration of deuterons to 200 Mev, and later the 184 inch (467 cm) FM cyclotron was successfully operated[14] at this energy.

Formulae for the FM cyclotron—The notation is that of the papers of BOHM and FOLDY[11,12].

The equilibrium orbit is that in which a particle rotates at a frequency equal to the frequency of the dee voltage.

The total (rest and kinetic) energy E_s of a particle in the equilibrium orbit is

$$E_s = ecH/\omega_s \text{ ergs} = \frac{9\times10^{12}H}{2\pi f} \text{ electron volt (protons, deuterons)}$$

$$= \frac{1{\cdot}8\times10^{13}H}{2\pi f} \text{ (helium nuclei)} \qquad \ldots\ (6)$$

The phase angle ϕ_s of a particle in the equilibrium orbit with respect to the dee potential is given by

$$\frac{eV\sin\phi_s}{E_s} = -\left(\frac{2\pi}{k\omega_s^2}\right)\frac{d\omega_s}{dt} \qquad \ldots.(7)$$

where $k = 1 + \frac{n}{1-n}\frac{c^2}{v^2}$, $\qquad n = -\frac{r}{H}\frac{\partial H}{\partial r} = -\frac{\partial \log H}{\partial \log r}$

eV = the maximum possible energy gain per turn

$eV\sin\phi_s$ = the average energy gain per turn in a phase stable orbit,

and ρ is defined by: $\rho = eV\sin\phi_s/eV = \sin\phi_s$ $\qquad \ldots.(8)$

The equation of motion of the phase ϕ of any particle in the FM cyclotron

is $$\frac{d}{dt}\left(\frac{E_s}{\omega_s^2 k}\frac{d\phi}{dt}\right) + \frac{eV}{2\pi}\sin\phi = \frac{eV}{2\pi}\sin\phi_s \qquad \ldots.(9)$$

and $$\frac{d\phi}{dt} = \omega - \omega_s$$

The frequency $\omega_p/2\pi$ of the phase oscillations which occur about the value ϕ_s is approximately given by

$$\omega_p = (eVk\cos\phi_s/2\pi E_s)^{\frac{1}{2}} \qquad \ldots.(10)$$

The particles also execute free vertical and radial oscillations, with frequencies $\omega_v/2\pi$, $\omega_r/2\pi$ given by

$$\omega_r = (1-n)^{\frac{1}{2}}\omega \qquad \ldots.(11)$$

$$\omega_v = n^{\frac{1}{2}}\omega \qquad \ldots.(12)$$

The radius r of the orbit of a particle is

$$r = (E^2 - E_0^2)^{\frac{1}{2}}/300H = (2E_0W + W^2)^{\frac{1}{2}}/300H \qquad \ldots.(13)$$

if E, E_0, W are in electron volts

Definitions of symbols

H = vertical component of magnetic field at radius r cm (oersted)
e = charge on the particle (e.s.u.)
c = velocity of light
ω_s = angular frequency of dee potential (radians/second)
ω = angular velocity of the particle (radians/second)
E = total energy of the particle in an orbit of radius r cm
E_0 = rest energy of the particle (= 938 Mev for protons)
W = kinetic energy of the particle
f = frequency of dee potential (cycles/second)
v = velocity of the particle

Size versus energy—The factors which determine in practice the energy obtainable in an FM cyclotron are the diameter of the magnet poles and the flux density obtainable in the pole gap. The flux density is fixed, usually in

the range 15,000 to 20,000 oersted, by economic considerations, and for a given value of the flux density the particle energy increases a little less rapidly than the square of the pole diameter (equation 13). For magnets of similar geometrical shape the weight varies as the cube of the diameter and so the particle energy will vary roughly as (magnet weight)$^{\frac{2}{3}}$. It is often found possible to make the pole gap relatively smaller in larger cyclotrons; thus the weight may increase rather less rapidly than the cube of the diameter. *Table II* shows some representative figures, corresponding to cyclotrons at present under construction.

Table II. Cyclotron Characteristics

Location	*Magnet pole diameter*	*Centre field (oersted)*	*Weight of magnet steel*	*Energy expected (protons)*
Harwell	110 *inch* (280 *cm*)	17,000	670 *ton* (680 *tonne*)	180 *Mev*
Liverpool	156 *inch* (396 *cm*)	18,800	1,640 *ton* (1,660 *tonne*)	400 *Mev*
Chicago	170 *inch* (431 *cm*)	18,600	2,070 *ton* (2,100 *tonne*)	450 *Mev*

In a large cyclotron the magnet is the most costly item of equipment; it will often be more expensive than the buildings and laboratory rooms, including the elaborate shielding arrangements. This factor, rather than technical limitations, seems likely to determine the upper limit of energy which will be obtained with FM cyclotrons, and for energies beyond about 10^9 ev the economic gain from using a type of machine in which the orbit radius remains roughly constant during acceleration (thus requiring a magnetic field over a much smaller volume for a given orbit radius) would be considerable. Such machines are under construction[15,16], but none has yet operated at high energy and discussion of them is therefore inappropriate here.

The magnet—For the reasons indicated above the economical design of magnets for FM cyclotrons has received considerable attention. Low carbon steel, usually about 0·1 per cent carbon, is used for the yoke. This has been in general practice for conventional cyclotrons also, although some have used more expensive special magnet steels. The yoke is built from rectangular rolled steel plates varying in thickness from about 3 to about 12 inch (7.5 to 30 cm) in various designs, or from large forgings or castings weighing 60 tons (61 tonnes) or more. The thicker plates, and especially the forgings, have the advantage of reducing the area of steel surface to be machined and of simplifying the problem of maintaining close dimensional tolerances for the finished magnet. The choice of yoke plates, conductor material and of a method of cooling the windings is strongly affected by local considerations of machining capacity, transport facilities, costs of conductor material in various sections, steel costs, and similar factors. The optimum ratio of steel weight to conductor weight is affected by a balance of

capital costs against the cost of electrical power, further complicated by uncertainty as to the probable useful life of the machine. Since the useful life will in general be short compared with that of ordinary equipment such as electrical generating plant, the scrap value of the materials used may be a fairly important factor. In addition, a balance must be sought between the maximum particle energy for given expense and the provision of adequate working space for the vital parts of the cyclotron and for experimental work. The power consumption of existing or contemplated large magnets varies from 200 to 1,000 kw.

Three main types of winding are generally used: ' pancake ' windings of paper insulated strips, separated by water-cooled pads: similar pancake windings immersed in transformer oil, cooled by an external heat exchanger, and a hollow conductor cooled by high pressure water circulation.

The last usually gives the most efficient cooling but is often expensive to construct. In some places the cost of the hollow conductor material seems to be very high compared with that of the strip used in the more normal windings, and sometimes it is available only in short lengths so that numerous joints are required. For magnets of identical design, the current density in the windings varies inversely with the linear dimensions for a given magnetic flux density, so that the windings can be made relatively smaller in larger magnets without incurring excessive power consumption. For this reason several large magnets have aluminium conductors, where local supply conditions and costs make aluminium a more suitable material than copper, despite its greater electrical resistance, and consequently the greater bulk required for equivalent power consumption.

A departure from the standard practice is being adopted at the Carnegie Institute of Technology, Pittsburgh, United States (private communication), where the windings are to be made of copper sheet fabricated to form a helix, so that one turn extends continuously from the pole periphery to the outer diameter of the coil and each pancake is effectively a single annulus of copper. A much greater ratio of conductor volume to insulation volume is achieved than with conventional designs, with very effective cooling, and consequently a gain in particle energy for a given weight of steel and copper is achieved. A special ' homopolar ' generator is being developed to produce the high current at low voltage required by the windings, which have a much smaller number of turns and much lower resistance than conventional windings of the same volume.

Magnetic pole design—Once the yoke and winding designs and power input have been decided, the remaining problem is to determine the pole shape which will give the highest particle energy *i.e.* the maximum value of the product Hr, where r is the radius of the last stable orbit and H the vertical component of the magnetic field at that radius. Ideally, the last stable orbit corresponds to $n=1$, where $n=(-r/H)\partial H/\partial r$ (the factor defined in equation

7). In this region the magnetic field is diminishing rapidly with increasing radius on account of 'fringing', and further acceleration would cause the particles to fly off at a tangent. It has been found experimentally that on this criterion a slight gain in energy is usually obtained by using straight sided poles in place of the tapered ones[5] adopted in conventional cyclotrons, and straight sided poles are being used on almost all the FM cyclotrons under construction, following the practice on the Berkeley 184 inch machine. The contours of the pole faces are shaped to produce the desired radial field distribution, with azimuthal symmetry and symmetry about the geometric median plane. From the theory of BOHM and FOLDY[12] the distribution should be approximately parabolic for optimum phase stability conditions, and the field should therefore decrease slowly at small radii and more rapidly at larger radii, but other factors influence the problem, including the necessity for adequate magnetic focusing and the necessity to maintain the highest possible field in the $n=1$ region near the edge of the poles to avoid a reduction of the particle energy. Accordingly, a linear reduction of field with increasing radius was used in the Berkeley 184 inch cyclotron[12] and this practice has been followed elsewhere, except for the original FM operation of the Berkeley 37 inch cyclotron[13]. This is achieved by the use of fixed shims on the pole faces, giving an increasing gap with increasing radius until, near the edge, the gap is reduced progressively to compensate for the effects of leakage to as great a radius as is feasible, in the manner originally suggested by ROSE[17] (*Figure 2.*) The use of a fixed shim, designed from an experimental field survey, is in contrast with the trial and error shimming process which is often laborious with conventional cyclotrons[5]; it is possible because an FM cyclotron needs much less critical shimming.

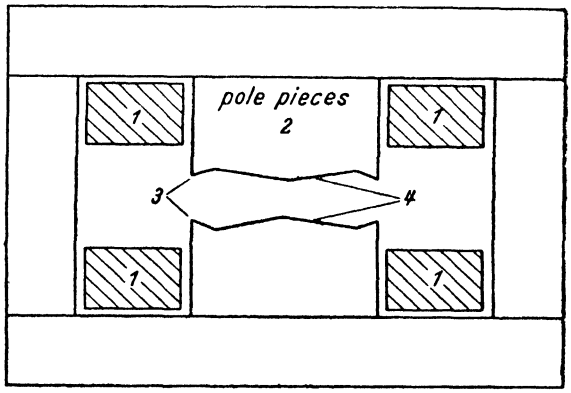


Figure 2. Schematic section of FM cyclotron magnet. Pole gap ~ 0·1 × pole diameter; radius of last ion orbit ~ 0·9 × pole radius. The focusing shim gives $\delta H/\delta r$ ~ − 0·02 per cent cm^{-1}

The ideal of acceleration to a radius near that where $n=1$ seems unlikely to be achieved in large FM cyclotrons, since it has been found impossible to accelerate ions in the Berkeley 184 inch cyclotron[18] beyond an n value of 0·2. This effect, which is discussed in some detail below, does not affect the above argument except to make it desirable to cause the field to diminish as rapidly as possible beyond the position where $n=0{\cdot}2$, to aid beam extraction.

The use of straight sided poles with shims of this kind makes it impossible to vary the final particle energy by varying the magnetic field and the starting

frequency of the dee voltage, as is frequently done with conventional cyclotrons. The reason for this is that the flux density in the Rose shim and the edges of the pole tips is much higher than elsewhere in the magnet, and thus the effect of the steel in this region is very sensitive to the value of the centre field. The FM cyclotron designed on the criterion of maximum energy for a given magnet size is thus a fixed energy machine; the provision of readily variable shims would be very difficult and would probably necessitate a reduction of the maximum energy obtainable. If an external beam of variable energy were required it could, of course, be obtained by the use of absorbers in the path of the beam at full energy, followed by magnetic analysis of the particles to eliminate the effect of straggling; this would cause a reduction of beam intensity. Operation at a fixed value of the final particle energy is not a serious disadvantage at present, since many experiments can be performed at variable energy with an internal beam, using an adjustable probe target.

The radiofrequency system—The frequency of rotation of an ion in a cyclotron orbit in a magnetic field H is given by $f=f_0H/(1+W/E_0)H_0$ where f_0 is the frequency for very small kinetic energy, and equals $eH_0/2\pi Mc$ (equation 1), H_0 is the magnetic field at the centre, W is the kinetic energy of the particle, and E_0 is the rest energy of the particle.

This relation enables the required frequency range to be calculated. The ideal frequency-time variation would be a linear reduction of frequency during acceleration, and then a rapid rise to the value f_0 for a repetition of the process. This ' saw-tooth ' variation cannot be obtained in practice, and some margin of frequency variation must be provided at each extremity of the curve. It has been shown experimentally[19] that considerable departure from linearity of the frequency-time curve causes little loss of ions. For proton acceleration, in the cyclotrons at present being built, the starting frequency f_0 is about 25 to 30 Mc/sec depending on the value of H_0 chosen, and the final frequency about 15 to 20 Mc/sec depending on the value of H and upon the particle energy. For deuterons or helium nuclei, f_0 has half the proton value and the percentage depth of modulation is smaller than that for protons, in the same cyclotron.

At frequencies of this order, the conventional two dee system with radiofrequency current fed into the diametral edges as in *Figure 1* would have appreciable potential variations along the dees in a large cyclotron, where the dee diameter is an appreciable fraction of a wavelength. Accordingly a single dee is used, with a grounded sheath to concentrate the accelerating field and with the radiofrequency current flowing at right angles to the diametral edge (*Figure 3*).

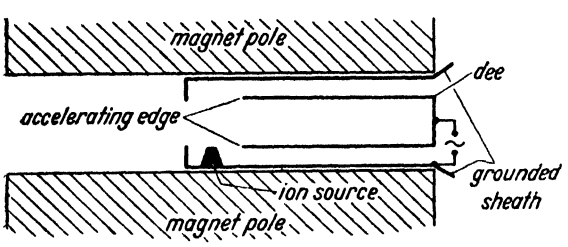


Figure 3. Schematic section of single dee cyclotron

Although, as can easily be shown, the use of a single dee causes a reduction of peak potential for a given power input, this is of small consequence since the accelerating potentials required are much smaller than those commonly used in conventional cyclotrons; moreover, considerable mechanical advantages are obtained with a single dee system.

Electronic means of frequency modulation were originally considered but were thought to be less practical than mechanical methods, using a rotating condenser with a resonant line system and a grounded grid oscillator[20]. The lines and condenser can be arranged in various ways, some of which have been discussed by SCHMIDT[21]. Some methods are illustrated in *Figure 4*. A choice of method will be influenced by the frequency range required and by engineering problems. For example, with the system shown in *Figure 4*a, where the back of the dee is grounded and the condenser is connected to the

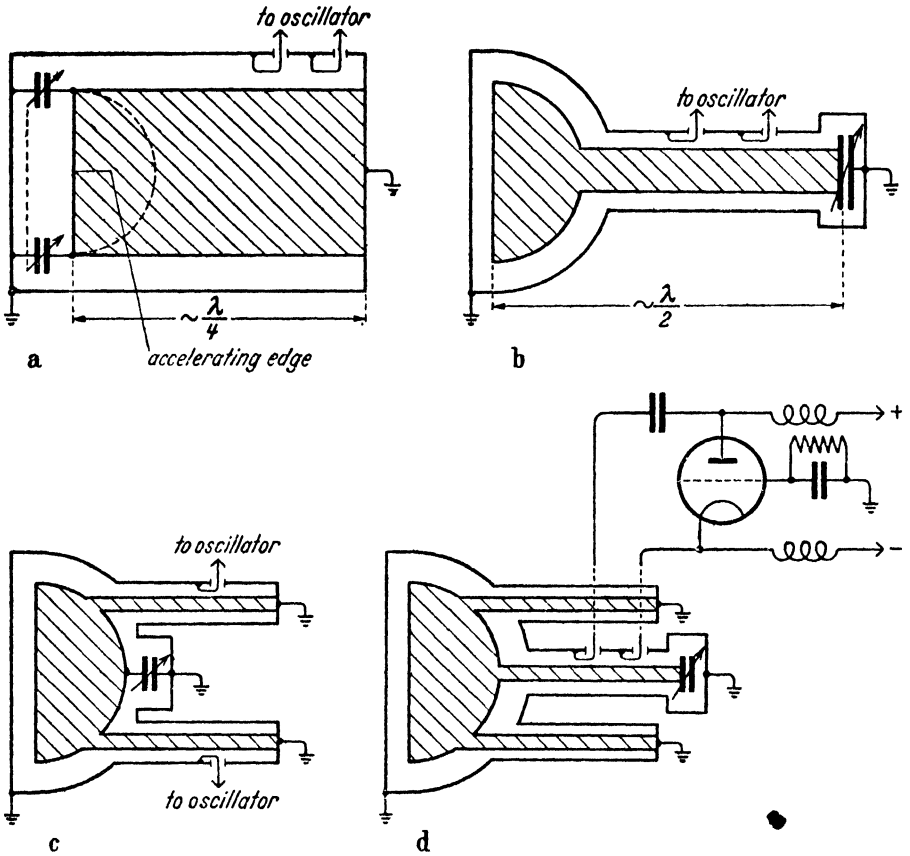


Figure 4. Some FM radiofrequency systems (schematic)

accelerating edges, the depth of modulation is determined only by the obtainable ratio of maximum to minimum capacity, whereas the half-wave system of *Figure 4*b can only produce a frequency variation of 2:1 even in the ideal case where the capacity varies from zero to infinity. On the other hand the system of *Figure 4*a requires a condenser in the magnet gap where there is little space, and where the strong magnetic field will lead to eddy current heating in

rotating metal parts; these troubles are absent in the system of *Figure 4*b. It is known that cyclotrons are under construction using the systems of *Figure 4*a, c and d, and the Berkeley 37 inch and 184 inch FM cyclotrons used the *Figure 4*b system for the acceleration of deuterons[20, 30].

All the systems embody one or more short wave transmitting valves coupled to the dee lines to form a grounded grid oscillator. The coupling system often involves transmission lines of appreciable electrical length, which must be made as insensitive to frequency as possible. Most of the design of the radiofrequency system can be done by experiments with scale models at frequencies inversely proportional to the linear scaling factor.

A new three-quarter wave system has been devised by MacKenzie[22] for the conversion of the Berkeley 184 inch cyclotron to proton acceleration. This system, illustrated diagrammatically in *Figure 5*, was found in model tests to produce a frequency variation of 2·4:1 which makes it suitable for proton energies of 500 Mev or more. With such a wide frequency band the system can be made to accelerate protons or deuterons with little modification, and problems of eddy-current losses, layout and length of coupling lines are readily solved by its use. It is being adopted for other large cyclotrons.

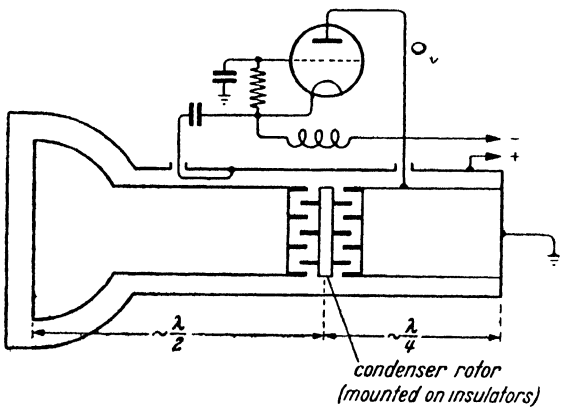


Figure 5. Three-quarter wave radiofrequency system for FM cyclotron (schematic)

The radiofrequency power required will depend upon the size of the cyclotron, the particular system used *i.e.* the Q value achieved for the resonant circuit, and upon the repetition rate of the FM cycle. It is not likely to be less than about 20 kw in a large cyclotron and therefore the system has to be cooled. The condenser shaft and vanes are usually water cooled, and it is customary to blow air over the insulators which have to be used in the condenser and, very often, at points of support for the dee and lines. Experience at Berkeley[20] shows that insulators made of zircon porcelain are more reliable in operation that those of ordinary electrical porcelains. Zircon porcelains combine low radiofrequency losses with high resistance to thermal shock, such as would be caused by local ion or electron bombardment, high mechanical strength and high thermal conductivity.

A further technical problem is the occurrence of discharges at low voltages, due to the oscillation and multiplication by collision of electrons in the radiofrequency field[20, 30]. These discharges load the oscillator, which

obtains its excitation from the dee system, and prevent the setting up of a sufficiently high dee voltage. The effect was overcome at Berkeley by the application of a D.C. sweeping potential to the dee line and condenser stator[20,30].

Dee potentials normally used or at present contemplated are about 10 to 30 kilovolt, and FM repetition frequencies about 50 to 500 cycles per second. It is possible to pulse the oscillator so that it functions only on the correct halves of the FM cycles[22] *i.e.* when the frequency is decreasing. This leads to a saving of about half the mean power consumption of the oscillator.

ACCESSORIES

The vacuum system—It is necessary to maintain a pressure of about 10^{-5} mm Hg or less in the acceleration chamber and rotary condenser. Such pressures have been obtained in continuously evacuated, demountable apparatus for many years by means of oil diffusion pumps backed by mechanical pumps, and no new techniques are required for large cyclotrons. The only new features, as compared with conventional cyclotrons, are concerned with the volume to be evacuated and consequently the size of the pumps. A general description of cyclotron vacuum practice has been given by LIVINGSTON[5]. He states as a rule of thumb that the pumping speed, in the useful operating region of the diffusion pumps, should be 1 litre per second for each litre of volume to be evacuated. This rule can still be applied. If anything, it errs on the side of generosity for large cyclotrons. Multi-stage oil diffusion pumps of 20 to 32 inch (50 to 80 cm) diameter are being used, often with refrigerated oil baffles, with re-distilled mineral oils such as *Lytton* and *Apiezon.*

Vacuum seals using double rubber gaskets separated by pumpout spaces are frequently used, and where rotary or sliding motion is required Wilson seals[23] or commercially made shaft oil seals are used. Since there is no need for adjustable magnetic shimming in FM cyclotrons, the shimming air gap has been dispensed with and the magnet pole tips are made to form the lid and base of the vacuum chamber, and are bolted through the poles and yoke to provide support against atmospheric pressure. Rubber rings are used to seal the vacuum chamber to the sides of the pole tips.

Welded mild steel and, near the magnet poles, non-magnetic steels are used for vacuum vessels; normal arc welding technique is satisfactory. Large castings are generally avoided since they are frequently porous, and component parts are commonly fabricated by hard-soldering worked brass or copper.

The ion source—RICHARDSON[19] showed that no special technique was required in order to inject ions into the phase stable orbits, and that a few per cent of the ions produced in the conventional way at the centre of the cyclotron could be accelerated in an FM cyclotron. The ion sources known to

be in use or under construction are of the well known[24] low voltage arc type, in which a discharge is maintained by electrons from a hot tungsten filament in a chamber containing the gas to be ionized (hydrogen, deuterium or helium) at a pressure of about 10 micron. The electron beam and a stream of gas, and some positive ions, emerge from an orifice in the top of the source. The material now favoured for the top is graphite[19], which resists sputtering and can be run at high temperatures. Direct current heating[19] is used for the filament in place of the radiofrequency heating which was once popular in conventional cyclotrons. Since the FM cyclotron beam reaches the target in pulses there is no need to operate the ion source continuously, and pulsed operation is therefore used. The pulses are triggered at a suitable point on the frequency time curve. This lengthens the life of the filament and improves the operation of the cyclotron by reducing the number of unwanted ions. *Figure 6* is a sectional view of a cyclotron ion source.

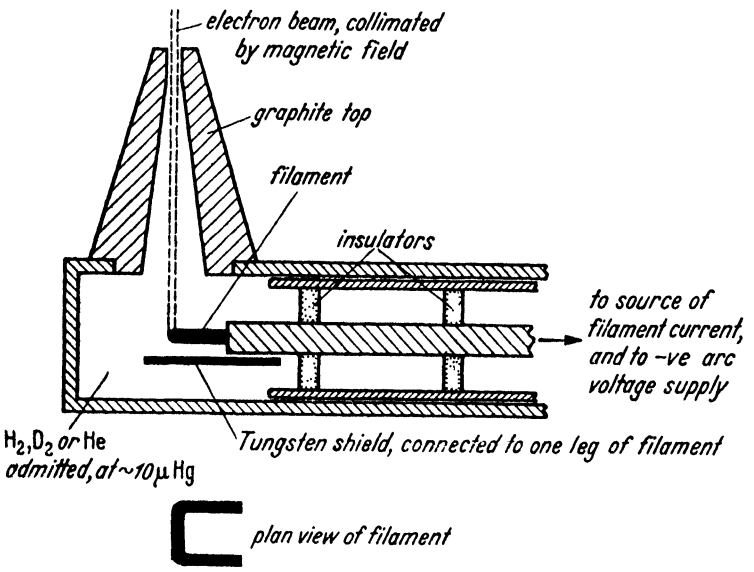


Figure 6. Section of cyclotron ion source

The targets—Since a single dee is used there is adequate space for internal targets, with little difficulty from pickup of radiofrequency currents. A movable probe enables particles of any desired energy up to the maximum to be intercepted on an internal target. With present techniques the mean ion currents are much smaller than those produced by conventional cyclotrons, since ions can only be accepted into the phase stable orbits for a small proportion of the time; the current is about 1 microampere[12], and at 400 Mev this represents 400 watt dissipated in stopping all the particles. The range of the particles is very great, and the heat dissipated per unit volume is much smaller than in conventional cyclotrons.

Extraction of the beam—The problem of beam extraction in a large FM cyclotron is complicated by the following factors:

1 The separation of consecutive orbits at large radii is very small (~ 0·1 mm) on account of the small fractional energy pickup per turn; in a conventional cyclotron the spacing is much greater (~ 5mm).

2 From the behaviour of the Berkeley 184 inch cyclotron it is probable that beam extraction will have to start at a radius where the factor n is just less than 0·2, and consequently the deflecting force must be applied over a proportionately greater distance than in a conventional cyclotron, where the value $n=1$ can be approached.

3 Radial oscillations of the ions have quite large amplitudes ($\sim$ 5 cm) at large radii.

For these reasons it seems unlikely that the conventional deflection technique[6], using a transverse electrostatic field applied between an insulated electrode and a thin septum fixed to the dee (or grounded), will be used successfully in large cyclotrons. It has, however, been used in the FM conversion of the Berkeley 37 inch cyclotron[19]. The method used in the Berkeley 184 inch cyclotron is shown in *Figure 7*. It employs a pulsed electric field between four copper bars covering 120° of arc, deflecting the ion inwards towards the centre. On leaving the deflector the ions travel outwards until their distance from the centre reaches a maximum value approximately 240° of arc beyond the end of the deflector. They are then about 3 inch farther from the centre than they were before deflection. In achieving this displacement account has to be taken of the radial oscillations. The electric field is applied at a time when most of the ions are beginning to move inwards in the radial oscillation cycle, and the deflector bars are so shaped as to allow for this. The pulse amplitude is about 200 kv and its duration a few tenths of a microsecond. The deflection produced is insufficient to extract the beam from the cyclotron magnet, and at the point of maximum displacement the ions enter a region where the magnetic field has been substantially reduced by a magnetic shield, and pass out of the machine. There is, of course, considerable loss of ions in the process of deflection. This deflector system has been discussed in detail by POWELL *et al*[26], and the pulse modulator by FARLY *et al*[27].

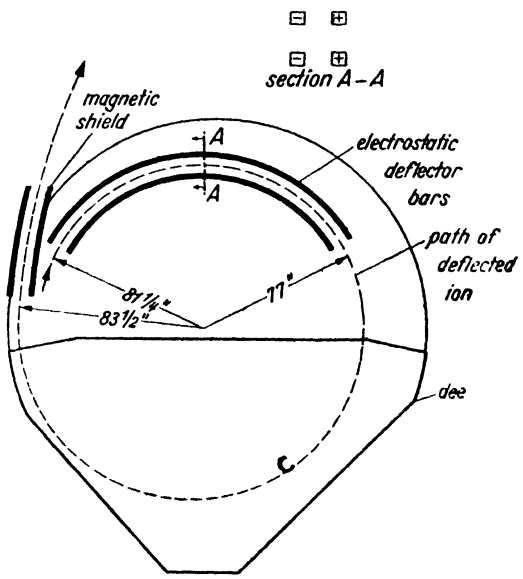


Figure 7. Diagrammatic plan of pulsed deflector for FM cyclotron (Berkeley 184 inch)

The shielding problem—Large numbers of high energy neutrons are ejected when the beam of ions strikes a target. The ions, in the energy region of hundreds of Mev, have low ionization loss and have sufficient kinetic energy to cause many nuclear disintegrations. Moreover, the neutrons are more

penetrating than those released by conventional cyclotrons. HILDEBRAND and MOYER[28] have shown that neutrons produced by 200 Mev deutrons have a half-value distance of about 9 inch (23 cm) in ordinary concrete, under conditions of measurement relevant to the determination of shielding efficiency. Despite the relatively small beam currents so far obtained, thick shielding walls are required, and the machine must be remotely controlled as are ordinary cyclotrons[6]. Light hydrogenous substances are found less effective than heavier materials for stopping high energy neutrons; ordinary structural concrete or earth is satisfactory.

The shielding methods employed are of three main types:

1 the installation is above ground and surrounded by blocks of concrete, staggered to avoid straight cracks and 10 feet (3 metres) or more in thickness, with rather less concrete overhead;

2 the laboratory is built by digging into the side of a hill to provide shielding on three sides, and the excavated earth is banked against retaining walls to shield the remainder;

3 the cyclotron is installed underground with several feet of concrete overhead.

Local conditions of terrain, building costs and density of population are factors influencing a choice of layout. Method *2* seems to offer the best compromise between accessibility and adequate shielding at reasonable cost, where suitable sites can be found.

OUTPUT

Pulsed character of the beam—The ion current is pulsed at a repetition rate equal to the rate of frequency modulation, and with a pulse duration determined by a number of factors including the dee voltage, repetition rate and orbit radius. Typical values are 50 microseconds repeated at 100 c/s, and the mean circulating current is likely to be about 1 microampere. Unless extraction methods can be greatly improved, the mean deflected beam current is unlikely to be much greater than 1 per cent of the circulating beam. Moreover the pulse deflection method causes a bunching of the ions since ions in numerous orbits are ejected simultaneously. The duration of the pulse of ions leaving the deflector is about 1 microsecond ; this is a serious disadvantage in experiments using counters, with present counting techniques.

The pulses in the circulating beam are each made of shorter pulses with varying amplitude. This has been demonstrated experimentally at Berkeley, where photographs of pulses displayed on a triggered cathode ray oscilloscope have been published by SEWELL *et al*[25]. The frequency and number of these shorter pulses and the total pulse duration are found to depend on the radius at which the probe target is placed. This fine structure of the beam pulses is attributed to a combination of two types of oscillations which are

performed by the ions in an FM cyclotron. Free radial oscillations of the ions have an angular frequency given by $\omega_r = (1-n)^{\frac{1}{2}}\omega$ where $n = (-r/H)(\partial H/\partial r)$, and ω=angular frequency of rotation.

The combination of these radial oscillations and the rotation of an ion in its orbit produces a precession of the centre of rotation, the frequency of which is $\omega_{prec} = \{1 - (1-n)^{\frac{1}{2}}\}\omega$

This is the frequency of oscillation of the ions in the beam pulse with respect to the probe target. The experimental values of the time intervals between the short pulses agree well with this expression[25]. The phenomenon of precession has been discussed by RICHARDSON *et al* in an account of the FM operation of the 37 inch Berkeley cyclotron[19]. The precession enabled a conventional D.C. deflector to be used in this case, by increasing the effective orbit separation.

In addition to the radial oscillations, the ions execute oscillations of phase and energy about equilibrium values. Since a change of the energy of an ion will cause its radius of curvature to change, there will be oscillations of radius super-imposed upon those mentioned above. The phase oscillations are much slower than the free radial oscillations, and have a frequency which agrees well[29] with that of the amplitude modulation of the short pulses.

There is also a hyperfine structure of the beam pulses corresponding to the radiofrequency oscillations of the dee potential ($\sim 2\times 10^7$ cycles/sec).

Instability at n=0·2—It has already been stated that acceleration of particles beyond a radius corresponding to n=0·2 could not be achieved in the Berkeley 184 inch cyclotron. This has been shown experimentally[18, 25] to be due to a vertical divergence of the beam at this radius, and this has been attributed[25] to a coupling between the free radial oscillations and the vertical oscillations of the ions. The vertical oscillations have a frequency given by

$$\omega_v = n^{\frac{1}{2}}\omega$$

and when n=0·2, $\omega_r/\omega_v = 2$

Thus if any coupling exists between the two forms of oscillations, energy will be fed into the vertical oscillations by the radial oscillations at a radius corresponding to this value of n. Integral values of the ratio will also occur at n=0·1 and at smaller values, but here the ratio is so high that the coupling would have to be much stronger for the effect to be observed, and it has evidently not occurred at Berkeley. At n=0·5, however, the radial and vertical frequencies are equal and so if the problem of acceleration past the n=0·2 region can be solved, it will appear again at a larger radius. The energy gain achieved by acceleration to n=0·5 would be very small, but the problem of extraction of the beam would be substantially simplified. This phenomenon

has caused the shimming of a cyclotron magnet to be aimed at the maintenance of a value of n much less than 0·2 to as great a radius as possible, followed by a rapid increase of n with increasing radius.

The effect will presumably occur with any accelerator in which particles travel long distances in a region where $n=0{\cdot}2$. These conditions exist in a very large FM cyclotron, where the rate of change of orbit radius near the edge is very small and consequently the particles make numerous circulations in the resonant region. The coupling between the radial and vertical oscillations contains a term proportional to $\delta^2 H/\delta r^2$, in addition to higher order terms, so that in principle the effect might be overcome by shimming the magnet in such a way as to make $\delta^2 H/\delta r^2$ very small at $n=0{\cdot}2$. It seems, however, that the practical difficulties involved would be too great for this to be feasible.

Modulation frequency—The beam is not particularly sensitive to the modulation frequency. The theoretical graph of beam current against modulation frequency[12] with constant dee voltage shows a broad maximum at a frequency corresponding to $\rho=0{\cdot}5$, where ρ=energy gain per acceleration/peak dee potential=$\sin\phi_s$. An experimental curve (RICHARDSON[19] *et al*) follows this fairly closely, but with a slightly broader maximum and showing evidence that ions can be accelerated over several FM cycles. For a constant value of ρ the beam current increases rapidly with the dee voltage for various reasons. For example the efficiency of collection of ions into the phase stable orbits and the number of ions extracted from the ion source both increase with the dee voltage, and the loss of ions by the capture of electrons in flight and by scattering will be reduced when the path length is reduced by raising the dee voltage and the modulation frequency[19].

Relative merits—Nuclear experiments with the FM cyclotron have to be performed in a considerable background of fast neutrons and recoil protons from materials in the neighbourhood. The beam current is difficult to measure with reasonable accuracy on account of the great range of the particles, and secondary effects. On the credit side, however, the use of a single dee and the large volume of the magnet gap enable experimental arrangements to be set up inside the main vacuum chamber so that many experiments can be performed with an internal beam. The absence of ion erosion and of limiting heat dissipation problems makes the FM cyclotron very reliable in operation. The well collimated neutron beam of fairly well defined energy[29] produced by high energy deuterons provides a very useful experimental tool. Although the beam current is small with present technique the yield in terms of nuclear events is ample with the important exception (at the time of writing) of the yield of mesons which, however, should be very much larger when protons of 400 Mev or so are available.

The rate of energy loss by ionization is small for protons of hundreds of Mev. *Figure 8* is an approximate range-energy curve. It should be pointed

out that a large proportion of the protons will be stopped, or converted into neutrons in an exchange process, in nuclear collisions, before reaching the end of their range. Development of frequency modulation has extended the life of the cyclotron in the role of the most valuable source of particles in nuclear physics. Many FM cyclotrons are being built, and several are believed to be planned for eventual conversion from large conventional machines. In addition the FM conversion of small machines such as the Berkeley 37 inch produces protons of 12 to 20 Mev, a region in which little work has been done. The large FM cyclotrons in existence or being built are listed in *Table III.*

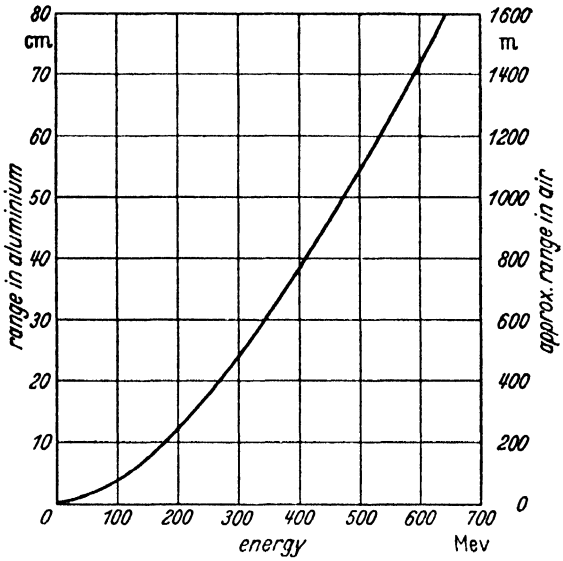


Figure 8. Range-energy curve for fast protons

Table III. Large FM Cyclotrons

Laboratory	*Pole face diameter (approximately) inches*	*Particle energy (approximately)*
Berkeley, California	184	350 *Mev protons* 190 *Mev deuterons*
University of Chicago	170	450 *Mev protons*
Columbia University, New York	170	450 *Mev protons*
Carnegie Institute of Technology, Pittsburgh	142	440 *Mev protons*
University of Rochester	130	250 *Mev protons*
Harvard University	95 (*tapered pole, root diameter* 112)	170 *Mev protons*
McGill University, Montreal	82	100 *Mev protons*
A.E.R.E. Harwell	110	180 *Mev protons*
University of Liverpool	156	400 *Mev protons*
University of Uppsala	110 *pole, root diameter*	180 *Mev protons*
University of Amsterdam	60 (*tapered pole*)	35 *Mev deuterons*

Of these, the Berkeley 184 inch machine has operated with deuterons and helium nuclei since early 1947, and is now producing 340 Mev protons. Several cyclotrons have come into operation since this article was written. They are those at Rochester[31], McGill[32], Harwell[33], Harvard (140 Mev), Amsterdam and Columbia (385 Mev). Some performance figures of the 110 in cyclotron at Harwell are as overleaf.

Pole gap—12 in (30 cm) nominal; Particle energy—180 Mev protons at 50 in (127 cm) radius; Frequency range—26.9–20.4 Mc/s (useful range 25.8–20.5 Mc/s); Beam current—1.5–2 μa mean; Pulse duration—500 μsec for full energy; Repetition rate—100 c/s; Distance travelled during acceleration—about 300 miles (480 km); D.C. power input to oscillator—25 kw mean; Peak dee voltage—10 kv mean, variation over frequency band about 2 : 1 ; Ion source operation—D.C. or pulsed arc, with no appreciable difference in filament life or beam current.

These values are fairly representative of FM cyclotrons, with the exception of the beam pulse duration which is longer than usual. The long pulse is explained partly by the value of ρ used, and partly by the shape of the frequency modulation function of the oscillator at the low frequency end.

A more complete report of the operating characteristics of the Berkeley 184 in machine has been published by HENRICH *et al*[34]. An alternative method of beam extraction, whereby small angle scattering in a heavy foil (uranium or thorium) is followed by extraction through a magnetic shield, has been adopted independently at Berkeley[35] and at Harwell. This method has the advantages of simplicity and of preserving the long beam pulse, and the disadvantage that the intensity is only a few per cent of that produced by the pulse method; its particular value is in counting experiments.

REFERENCES

1 LAWRENCE, E. O. and LIVINGSTON, M. S. *Phys. Rev.* 38 (1931) 834
2 — and EDELFSEN, N. E. *Science* 72 (1930) 376
3 — and LIVINGSTON, M. S. *Phys. Rev.* 40 (1932) 19
4 — *et al* *ibid* 56 (1939) 124
5 LIVINGSTON, M. S. *J. applied Phys.* 15 (1944) 2; 15 (1944) 128
6 ROSE, M. E. *Phys. Rev.* 53 (1938) 392
7 WILSON, R. R. *ibid* 53 (1938) 408
8 NAHMIAS, M. E. *Le Cyclotron* Paris, 1945
9 VEKSLER, V. *J. Phys. U.S.S.R.* 9 (1945) 153
10 MCMILLAN, E. M. *Phys. Rev.* 68 (1945) 143
11 BOHM, D. and FOLDY, L. L. *ibid* 70 (1946) 249
12 — — *ibid* 72 (1947) 649
13 RICHARDSON, J. R. *et al* *ibid* 69 (1946) 669
14 BROBECK, W. M. *et al* *ibid* 71 (1947) 449
15 OLIPHANT, M. L. *et al* *Proc. phys. Soc.* 59 (1947) 666
16 BROBECK, W. M. *Rev. sci. Instrum.* 19 (1948) 545
17 ROSE, M. E. *Phys. Rev.* 53 (1938) 545
18 VALE, J. *American Declassified Report MDDC* 984 (1947)
19 RICHARDSON, J. R. *et al* *Phys. Rev.* 73 (1948) 424
20 MACKENZIE, K. R. and WAITHMAN, V. B. *Rev. sci. Instrum.* 18 (1947) 900
21 SCHMIDT, F. H. *ibid* 17 (1946) 301
22 MACKENZIE, K. R. *Phys. Rev.* 74 (1948) 104
23 WILSON, R. R. *Rev. sci. Instrum.* 12 (1941) 91
24 LIVINGSTON, M. S. *Rev. mod. Phys.* 18 (1946) 293
25 SEWELL, D. C. *et al* *American Declassified Report MDDC* 1092 (1947)
26 POWELL, W. M. *et al* *Rev. sci. Instrum.* 19 (1948) 506
27 FARLY, G. M. *et al* *ibid* 19 (1948) 899
28 HILDEBRAND, R. and MOYER, B. J. *Phys. Rev.* 72 (1947) 1258
29 HELMHOLZ, A. C. *et al* *ibid* 72 (1947) 1003
30 MACKENZIE, K. R. *et al* *Rev. sci. Instrum.* 20 (1949) 126
31 BARNES, S. W. *et al* *Phys. Rev.* 75 (1949) 983
32 FOSTER, J. S. Presidential Address *Trans. roy. Soc. Canada* 1949
33 PICKAVANCE, T. G. *et al* *Nature, Lond.* 165 (1950) 90
34 HENRICH, L. R. *et al* *Rev. sci. Instrum.* 20 (1949) 887
35 LEITH, C. E. *Bull. Amer. phys. Soc.* 24 (1949) 13

2

HIGH VOLTAGE DIRECT CURRENT GENERATORS FOR NUCLEAR RESEARCH

R. L. Fortescue

HIGH VOLTAGE direct current generators provided the first sources of artificially accelerated particles used in nuclear physics. Where acceleration to the highest possible energy is required, they have now been superseded by machines using time-varying fields and circular accelerating paths, which enable repeated impulses to be given to the particles. When precise control of particle energy is needed, however, the direct current generator is still the most satisfactory accelerator. There is therefore a considerable inducement to designers to develop generators of this type with improved performance, and in particular to design machines of increased voltage for more exact examination of the higher energy regions so far accessible only to the other types of generator.

Direct current generators of the rectifier type, which were the first to be used for nuclear physics, are at present in use for voltages below a maximum of 2 Mv. New developments may extend this to 3—5 Mv, but no such generator has yet been constructed. Relatively high beam intensities are used, currents up to 5—10 ma being available, of which up to 30 per cent may be useful protons or deuterons under favourable circumstances, while 50—90 per cent may be obtained as electrons. Energy definition is limited mainly by ripple remaining on the rectified A.C. voltage. This has been as much as 5 per cent of the output voltage on heavy loads in some existing equipments, but it can certainly be kept down to the order of 1 per cent by modern design methods, and for smaller outputs 0·1 per cent should be possible.

Electrostatic generators have been used up to about 4 Mv, and, in the United States, construction has been started on machines designed to give voltages around 15 Mv. At voltages below about 0·5 Mv the electrostatic machine is likely to be more complicated and to give less output than a rectifier set. The region of overlap between the two types is thus around 0·5—1·5 Mv. The energy definition available from electrostatic generators has been as good as 1 in 10^4. 1 in 10^3 is fairly easily obtained, while 1 in 10^5 may be possible with some development of existing techniques. On the other hand, the current output is usually less than can be obtained from rectifiers. Though 1—2 ma has been obtained, 200—500 μa is a more usual upper limit. Of this, only 0·1—20μa may be available as proton beam, but again almost the full output can be obtained as electrons.

It will be convenient here to treat the two types of D.C. generator separately, in respect of their main design features as sources of high D.C. voltage. These sections are then followed by others dealing with the accelerating tubes, ion sources, and methods of stabilization, which are in principle suitable for use with either type of generator, though in practice most of the more recent developments in these fields have been applied to electrostatic machines.

HIGH VOLTAGE RECTIFIER EQUIPMENT

The possibility of obtaining D.C. at high voltage from a number of rectifiers, each of only moderate voltage, in series, has been the subject of much study since x-rays became important medically, and the nomenclature of circuit arrangements has grown up primarily in connection with this application. The basic principle of most of the various systems used, however, is the same. The individual rectifier circuits are connected so that their D.C. outputs are in series, while the A.C. inputs are fed in parallel through condensers which isolate this parallel connection from the D.C. output. Some of these isolating condensers are normally used, in addition, to provide the smoothing required on the D.C. output. For very high voltages it is almost the invariable practice to feed A.C. to each rectifier circuit by cascade connection in parallel with the previous stage, so that no condenser need be rated at more than the single stage voltage. The circuit arrived at is then as shown in *Figure 1*. Each stage is rated identically in respect of voltage, except for voltage drops due to load and other currents.

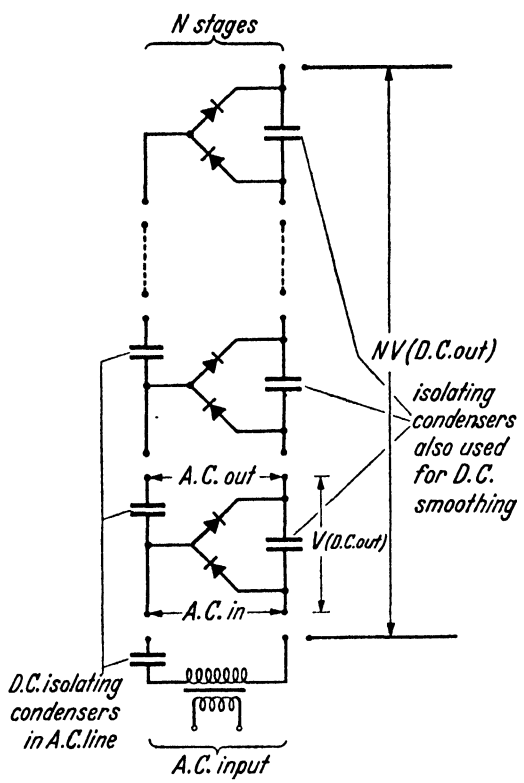


Figure 1. High voltage rectifier circuit arrangement

Detailed analysis of the operation of multiplier circuits of this kind can be made [1,2]. In general this is not necessary. The important quantities for preliminary design are derived from the stage voltage V and mean output current I as: condenser D.C. working voltage $= V$, rectifier peak inverse working voltage $= V$, amplitude of sinusoidal A.C. input voltage $= V/2$, D.C. working voltage for condenser in series with input

transformer $= V/2$, R.M.S. current rating for transformer secondary where N is the number of stages $=$ (5 to 10) $\times NI$

The capacity of condenser required is determined, as usual, by the frequency of the supply and by the ripple and voltage drop on load requirements of the D.C. output. This sets a lower limit to the capacity. An upper limit, set by allowed peak/mean or R.M.S/mean current ratio for the rectifier used, may also have to be considered. The condenser capacity influences the operation by virtue of the A.C. voltage drop it produces as well as by the drop in D.C. voltage between charging periods, and stages farthest from the transformer give the lowest output when current is taken. A limit to the number of stages that can usefully be connected in series is set by this effect, depending upon condenser size, supply frequency, and load current. Even on open circuit, leakage resistances and stray capacity and inductance will produce deviations from calculated voltages in circuits using many stages. If more than three stages are to be used in series, therefore, it is advisable to set up a scale model at low voltage (radio type rectifiers can conveniently be used) in order to decide on the size of condenser. This also enables one to determine the optimum distribution of the capacity which can be larger in the stages near the transformer, which have to pass large A.C. currents on to subsequent stages, than in the later stages. Small series inductances may also be used to reduce A.C. voltage drop. If the current scale is not changed in the model, the scale for impedance is, of course, the reciprocal of the voltage scale.

Originally these rectifier sets were intended to give the highest possible D.C. output voltage, but now they are used more as a convenient source of fairly high D.C. voltage which can be made up from relatively simple components. Such components may frequently have been developed for other applications, and in general, transformers, condensers, and rectifiers will be designed and supplied by specialist firms. Rectifiers may, however, be of various types. The most convenient is probably the barrier-layer dry rectifier made up from treated copper or selenium units[3,4]. These will only handle low voltages (about 10 v per barrier layer) but the elements are cheap and simple and can be connected in series in great numbers to give high voltage units. Thermionic rectifiers can be made to withstand voltages up to about 200 kv in single units, but such units need very careful design and a further complication is involved in providing isolated filament heating generators driven through insulating belts or rods. Radiofrequency heating[2,5] has been tried as an alternative for this purpose. Interest has been revived recently in rotating gap and needle gap rectifiers[6, 7], but they do not seem to have been applied in sets intended for nuclear physics use. The use of 2,000 c.p.s alternators in aircraft has now provided a source of standard high frequency generators, which are very suitable for use in small units where reduction of condenser size is a considerable advantage.

The general layout of the high voltage set is invariably based on vertical construction. Resin bound laminated insulators are frequently used to provide supporting frameworks, and large radius of curvature conductors, generally in the form of spun aluminium balls and cylinders, serve to terminate the main field. Screens of insulating material have been used between the high voltage electrodes and the earthed objects and room walls surrounding them, to reduce corona[8]. For compact operation components have been enclosed in oil-filled vessels and a rectifier set entirely enclosed in compressed gas insulation is at present being developed.

A description of the 1 Mv rectifier set used for nuclear physics at the Cavendish Laboratory, Cambridge, has been given by BURCHAM[9]. A very simple unit used for neutron production with incident beams of 300—400 kv is described by GRAY *et al*[10]. Details of a dry rectifier unit for 10 ma at 500 kv used for x-ray production in France have been given by REYVAL[11].

ELECTROSTATIC GENERATORS

Electrostatic generators differ in principle from rectifier sets, for energy is supplied by conversion from mechanical work instead of retaining electrical form throughout. The output voltage is maintained by transfer of charge, attached to a moving insulating medium, against the electrostatic field. Electrical machines using glass or ebonite disks for this purpose have been used in laboratories for over 100 years. The fundamental difference between this system and that of the electromagnetic generator is, however, not clearly set out in the literature. In both the charge transfer against the field gives rise to mechanical forces proportional to the rate of transfer, but the electromagnetic generator uses a conducting medium for this transfer, the electrostatic force then being overcome by an electromagnetic force on the charge, arising from its transverse motion in the magnetic field. The electrostatic system is thus unable to utilize the large currents that can be obtained by drift of charge inside a conductor; on the other hand it can produce this motion of charge against far greater electric fields than electromagnetic forces can resist in practice.

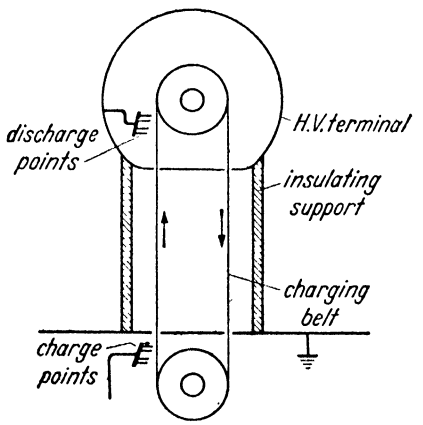


Figure 2. Van de Graaff generator (schematic)

The current output of electrostatic generators is thus a fundamental design factor. In modern machines a belt running round pulleys acts as the moving insulator (*Figure 2*). This system was introduced by VAN DE GRAAFF in a generator, the design of which was outlined[12] in 1931. To enable the

insulating surface to be charged and discharged, a local breakdown of insulation is obtained from an excitation voltage of 10—100 kv, applied between a number of sharp points near the belt and a conductor, usually the belt pulley, situated behind its surface. This first machine of Van de Graaff's introduced another feature common to all modern generators in locating the belt discharge system inside a rounded hollow conductor which formed the high voltage electrode. This gives almost complete electrostatic screening of the discharge points and the breakdown voltage at these points is then independent of the voltage between electrode and ground. More important still, the local insulation breakdown required for discharging does not tend to spread into a breakdown between high voltage electrode and ground. These general principles were incorporated in a generator used for nuclear physics by TUVE[13] in 1933-35.

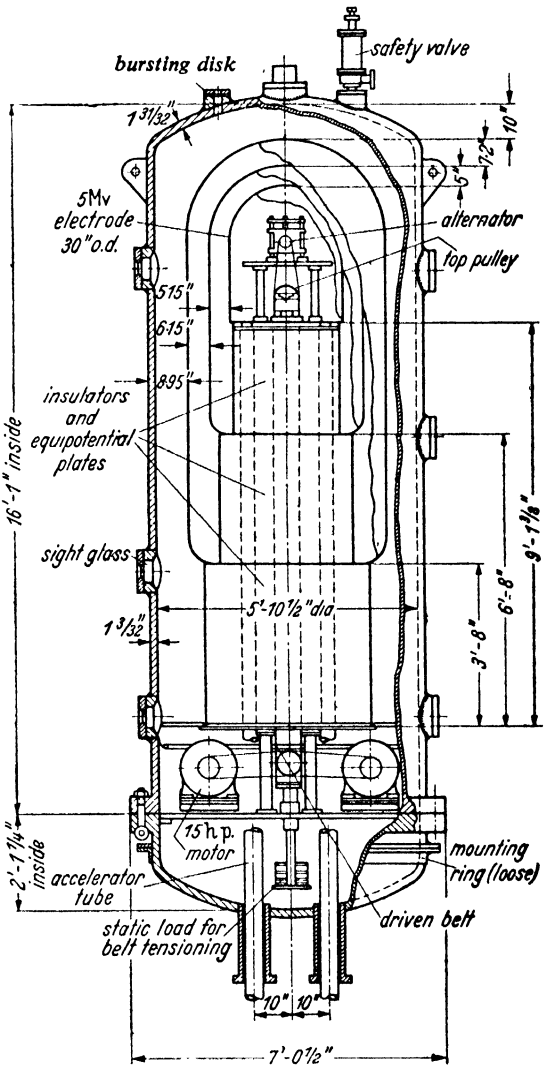


Figure 3. Arrangement of modern 5 Mv electrostatic generator

Experimental work has been carried out on non-belt generators in which the moving insulator may take the form of disks[14] or streams of gas, dust, vapour, or liquid[15–17]. Conducting plates or particles on or in the insulator have also been tried. In general, such methods have not yet been developed to a state where their practical value to nuclear physics is comparable to that of the belt generator.

The current conveyed by a moving belt is limited by *i* the maximum charge density that can be built up before the field strength it produces causes insulation breakdown, *ii* the width of the belt and *iii* its speed. *iii* has usually been restricted to about 5,000 ft/min by the desire to conform to normal engineering practice. Wide and multiple belts have been employed to increase factor *ii*. Factor *i* has been increased by the introduction of compressed air insulation, which was used by BARTON[18] in 1932, primarily

to improve voltage performance. Enclosure of the generator in a vessel containing high pressure air or gas is now invariably the practice where high currents or voltages are required (*Figure 3*).

Other factors contributing to maximum charge density on the belt, and therefore to current output, are the choice of suitable belt material and the reduction of electric field concentration near the surface. Woven cotton or rubberized canvas are preferred at present for belt materials. Metal rods placed near the belt surface have been used to minimize potential gradients in the plane of the belt and to provide surfaces of reasonably large curvature on which the lines of force from the belt can end[19]. Reduction of current capacity may arise from the elimination of any excitation voltage at the discharge points inside the high voltage electrode, the belt charge density being allowed to increase sufficiently to produce corona breakdown in virtue of its own field as it passes these points. This system, while simple, results in the belt running at a higher mean charge density than is necessary. By the use of discharge excitation[20] ideally the mean density may be reduced to zero, although in fact there is charge of one sign on one run of the belt and equal charge of the opposite sign on the run moving in the opposite direction. Such discharge excitation may be provided by the generator output itself[20] but there are then difficulties in obtaining simple control of excitation voltage. It is for this reason that self-excitation has not been used for charging the belt at the grounded end of the system.

Non-uniformity of belt charge density, and consequent reduction of current output, also arises from the finite belt width, from belt leakage conductivity, and from the behaviour of the charging and discharging points which, particularly in high pressure air or gas, may tend to spark rather than give a uniform corona on to the belt. As a result of these factors it is found that the maximum output current is less, by a factor of 2 or more, than that which can be simply calculated from belt width, speed, and flash-over charge density.

The voltage produced by an electrostatic generator is decided by the current which it is adjusted to give and the load connected to it, through which this current is passed. This is an impedance-inversion of the behaviour of electromagnetic generators, which have set voltages and give currents decided by their loading. Thus the maximum voltage which can be obtained from the electrostatic machine is limited by breakdown of its insulation, including that of its accelerating tube (load). The early generators of VAN DE GRAAFF and TUVE followed accepted principles of high voltage engineering in using the largest possible dimensions and avoiding shapes of high curvature which would give rise to field concentrations. HERB's machines[21], described in 1935 and 1937, followed the principle introduced by BARTON[18] and secured a great advantage in reduced dimensions and increased voltage limit, by the use of compressed air insulation. This principle has been followed in almost

all modern generators, although vertical insulating columns have often replaced Herb's horizontal cantilever support for the electrode, and nitrogen has been used instead of air in some cases to reduce fire risks. The increase in output voltage from pressurizing may amount to a factor of 7—10, for though the strength of gas insulation increases with pressure, with uniform fields, according to a nearly linear relation, this rise does not continue linearly to the voltages of interest in present designs. As with increased dimensions, the advantage obtained from increase of pressure seems to be much reduced after voltages of about 2 Mv have been obtained. This effect is even more pronounced in the failure of solid insulation in relation to length of path. It can be minimized by sub-dividing the insulator by conductors held at graded potentials. A generator described by HERB[22] in 1940 also incorporated this potential grading of gas and solid insulation. It is now general practice in the design of electrostatic machines. Metal corona hoops or plates with rounded edges are used to divide the solid insulation, their potentials being set by resistance or corona point potential dividers. Dome-shaped metal electrodes are fitted concentric with the high voltage electrode to provide similar gradient equalization in the gas gap when connected to appropriate points on the same potential dividing system (*Figure 3*). In this way the strength of gas insulation may be increased by up to 50 per cent.

The compressed air insulation can be improved further by the addition of certain special gases. An increase in voltage by 15 per cent was reported by HERB[23] in 1938 on using CCl_2F_2 (*Freon*, a commercial refrigerant). It is now often used in mixtures of up to 10 per cent partial pressure and may improve voltage performance by up to 30 per cent. The gas SF_6 has been reported to give even better performance[24]. Optimum pressures and concentrations for such gases and mixtures have not yet been ascertained reliably and in non-uniform fields reduction of the electric strength of the gas, when the pressure increases above a certain limit, is known to occur[25].

It cannot be said that any major developments in the design of generators for nuclear physics work have been reported since 1940, although many workers have entered the field and constructed machines incorporating small improvements. Probably application of experience gained in these machines, and in the development of compact generators for x-ray purposes, will lead to substantially better performance in machines designed after 1946. *Table I* compares the published performance of certain generators built before that date with the early machines, and also with a recent new design proposed by MCKIBBEN[26]. A useful review of electrostatic generators has recently been made by VAN DE GRAAFF and TRUMP[27].

Table I. Generator Characteristics

	Generator Characteristics					
Designer	*Tuve*	*Herb*	*Williams*	*von Ardenne*	*Danforth*	*McKibben*
Insulating gas and pressure	*Air, 1 atm*	*Air+CCl_2F_2, 7 atm*	*Air, 6 atm*	*Air, 1 atm*	*N_2+CCl_2F_2, 5 atm*	*SF_6, 17 atm*
Diameter of H.V. Electrode	80″	30″	108″	66″	24″	48″
Number of gas gaps, and total lengths to ground	*One, 99″*	*One, 18″*	*One, 54″*	*One, 66″*	*One, 10″*	*Five, 48″*
Length of insulating column to ground	70″	132″	250″	110″	60″	240″
Material of solid insulation	*Resin, fabric base*	*Resin, fabric base*	*Porcelain*	*Resin, paper base*	*Resin, fabric base*	*Glass-bonded mica*
Max voltage and limiting factor	1·3 *Mv (belt)*	2·6 *Mv (belt)*	3·5 *Mv (tube)*	1·1 *Mv (gas gap)*	1·75 *Mv (tube)*	*Estimated* 12 *Mv*
Total width of belt and belt speed	40″, 7,200 *ft/min* (?)	26″, 2,700 *ft/min*	72″, 2,700 *ft/min*	16″, 2,400 *ft/min*	14″, 3,800 *ft/min*	30″, 5,200 *ft/min*
Belt material	*Paper*	*Rubberized fabric*	*Woven cotton*	*Rubber*	*Woven cotton*	*Probably woven cotton*
Tube diameter and length per section	8″ *ext* 4″ *int* 64″ *long*	5″ *ext* 2½″ *long*	13″ *ext* 3½″ *int* 4″ *long*	12″ *ext* 3″ *int* 30″ *long*	12″ *ext* 4″ *int* 3⅛″ *long*	8″ *int* ½″ *long*
Tube material	*Pyrex glass*	*Porcelain with wax seals*	*Porcelain with wax seals*	*Porcelain with wax seals*	*Porcelain with wax seals*	*Glass-bonded mica with plastic adhesive seal*
Ion source	*Hot cathode arc*	*Hot cathode arc*	*Hot cathode arc*	*Hot cathode arc with magnetic field*	*Capillary hot cathode arc*	*Not published*
Target current	½—12μ*A* H^+	< 3μ*A* H^+	*Not published*	17μ*A* H^+	$\frac{1}{10}$—2μ*A* H^+	*No estimate*
Method of stabilizing	*Manual*	*Corona point current fed back to spray*	*Corona point current fed back to spray*	*Not published*	*Manual*	*Possibly electron beam*
Stability obtained	±20 *kv*	±10 *kv*	± 30 *kv*	*Not published*	± 5 *kv*	*No estimate*

ACCELERATING TUBES

Accelerating tubes for D.C. generators present special problems in focusing, electrical breakdown, and vacuum requirements. The usual practice in the lower field strength range has been to use a few cylindrical glass or porcelain sections of large diameter, inside which coaxial metal cylinders are fitted (*Figure 4*). The potentials of these cylinders are held at controllable values by connecting them to appropriate points in the rectifier circuit, or across appropriate sections of a resistance or corona point potential divider. Such an electrode system has a focusing action depending upon the dimensions and relative potentials. It also serves to control the field distribution over the surface of the insulating, vacuum tight material from which the tube is constructed. Such tubes are described in detail in the literature[10, 13, 28].

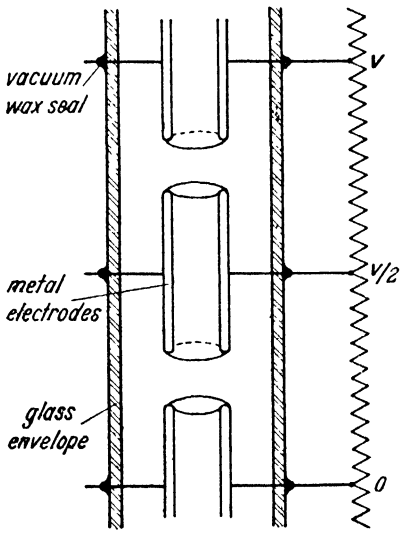


Figure 4. Construction of low voltage accelerating tube

At field strengths above about 300 kv per foot, however, such simple construction begins to fail on account of electrical breakdown inside the vacuum. This problem becomes more serious with increase of field strength and total voltage. In generators operating at above 500 kv/ft or 2·5 Mv, the tube is likely to be the factor limiting the output voltage. The vacuum requirements also become more stringent on the larger machines, since more ions are formed in the tube by the accelerated particles. This not only gives an additional current load, but also, in positive particle accelerators, gives rise to a serious output of x-rays from reverse electrons striking conductors at the high voltage end of the tube. Special screening may then be required to protect the health of operating staff and to reduce the background radiation in the vicinity of the experimental apparatus. Focusing in the tube, however, becomes less important at high voltages, as the particles are travelling too fast to have time to move far sideways under the influence of transverse forces.

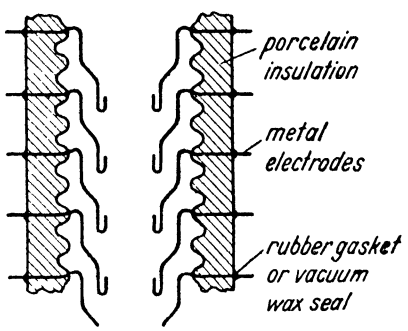


Figure 5. Section of high voltage accelerating tube

The modern accelerating tube for use in electrostatic generators is subdivided into many sections, usually less than 4 inches long and some times as short as $\frac{3}{8}$ inches in length (*Figure 5*). These sections are usually porcelain,

but various glasses have been tried, and glass-bonded mica composition (*Mycroy, Micalex*) has also been tested and is proposed for one of the newest generators. The original cylindrical electrodes have sometimes been replaced by re-entrant, overlapping spinnings. Plane circular orifices have also been used, particularly in generators accelerating electrons. The material of the electrodes, too, has been varied; steel, stainless steel, covar, and aluminium have been used, though the latter has not yet progressed beyond the experimental stage. There has also been a number of variations in the vacuum seals used between electrodes and insulating sections. Vacuum wax, rubber gaskets, covar-glass seals, and plastic adhesive seals have been tried. Finally, different designers have adopted different standards in respect of desirable pumping speeds, and diameters of tubes vary accordingly [21, 26, 27, 29, 30].

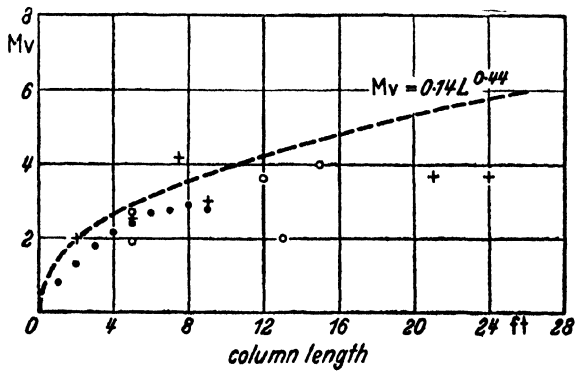


Figure 6. Electrostatic generator performance
• *Harwell*, + *U.S.A. Tube Ltd.*, ◦ *other U.S.A.*

This wide variation in tube materials and geometry reflects existing uncertainty about the nature of the electrical breakdown in an evacuated system. *Figure 6* shows a plot of the voltage limit of certain generators as a function of tube length. The empirical curve was extrapolated from results[31] for breakdown between metal electrodes *in vacuo* at voltages below 1 Mv, the highest for which experimental data have been published. Other work on vacuum breakdown (flash arcs) at still lower voltages is even more difficult to apply to this range of voltages, though much more has been published [32–34]. The non-linearity of the relationship between voltage performance and length is shown by *Figure 7*, which gives the voltage withstood by a two section tube plotted against diameter of the orifice in a metal diaphragm inserted between the two sections. Such experiments accord with the view[31] that vacuum breakdown occurs by virtue of a particle exchange between the electrode surfaces, which can become divergent if the product of the re-emission coefficients exceeds unity. These coefficients are likely to depend both upon the energy of the incident particle and on the electrode surface

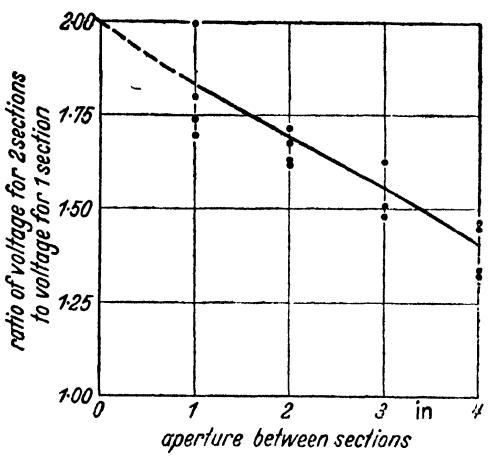


Figure 7. Performance of two 20 inch copper-glass sections

field strength on account of its effect on the potential barrier. Such a combination gives a non-linear relationship between voltage and length of the general kind observed in practice.

Experiments with voltages up to a few hundred kilovolts show that breakdown *in vacuo* between electrodes spaced by insulation occurs across the insulating surface, at voltages less than can be withstood by the electrodes separated only by the residual gas, and dependent upon the material of insulation. A report by McKibben[35] gives examples. When a number of sections are used in series, to form a tube, the insulation material may still determine the breakdown voltage. On the other hand, a non-linear increase of breakdown voltage with gap length between electrodes without insulating spacing may predominate, and give rise to failure at a lower voltage, independent of the insulation material. This is particularly likely to occur where the electrodes are shaped so that the surface of each insulating section is almost completely screened from the others, for then the voltage that can be withstood across the insulator surface by a number of insulating sections in series cannot be much less than that number multiplied by the voltage each section can withstand when tested alone. Such a tube is almost certain to fail from electrode mechanisms largely independent of the insulating surface.

The variations in vacuum technique found in the literature[27,30,35] similarly emphasize the difficulties of obtaining vacuum seals that will operate reliably under the influence of external pressure from compressed gas insulation, and in the large numbers required in a sub-divided tube (there may be 1,000 seals in one tube). The pressure required in the tube is usually set by the reverse electron current in the case of positive ion accelerators, but it cannot be allowed to exceed about 10^{-4} mm. Above this gas discharge in the tube soon occurs, while below it electrical breakdown seems little influenced by residual gas. Even when satisfactory vacuum tightness has been achieved, a high pumping speed has to be retained for the whole tube, in positive ion accelerators, as the ions admitted for acceleration are always accompanied by neutral gas which would build up a pressure if it were not pumped away quickly. Thus the long tubes necessitated by considerations of electrical strength often have to be made with the greatest possible diameter. This in turn requires that attention be given to mechanical strength under external compression, particularly where high pressure gas surround is used. It is advisable, therefore, to treat the mechanical, as well as the electrical, design of the accelerating tube as a fundamental factor in the layout of any modern D.C. accelerator.

SOURCES

Although in nuclear physics applications D.C. generators are usually required to provide positive ion beams, there are certain experiments which involve the use of γ-rays or electrons. In these circumstances the particle source

is provided by a hot filament assembly of the kind developed in X-ray technology. Such a cathode system using 0·010 inch diameter tungsten wire has recently been described by VAN DE GRAAFF[36]. No very serious design problems arise with the currents normally available from high voltage equipment.

Sources of positive ions, however, are less easily obtained, and although recent developments promise some improvement, it must be said that so far none of the various types used is satisfactory in all respects. The ions must always be produced by collisions between electrons and neutral gas atoms, and this results in their being accompanied by more or less neutral gas. A first requirement is therefore that this gas flow shall be slow enough to allow the pressure in the accelerating tube to be kept sufficiently low. A second requirement is usually that the ions produced by the source shall be largely of one particular kind *e.g.* H^+ as opposed to H_2^+ in proton sources. Frequently there is the further restriction that the ions are to be of substantially uniform energy.

Early ion sources consisted of discharge tubes using perforated cathodes of the canal ray type[37]. Voltages of the order of 50 kv are required to run this type of discharge, and the ions therefore have an energy spread of this order. Relatively large currents can, however, be produced; 100—200 μa of beam are available[9,38], of which around 50 per cent may be the protons or deuterons required. Reduction of the energy spread was first achieved by the use of hot cathode sources giving low voltage arcs [39, 40]. These have since been developed further by concentrating the discharge into a small volume by a constriction or capillary, the ions being extracted through a small diameter canal in a probe kept at a negative voltage with respect to its surroundings [41–44, 48]. The high current density in such discharge provides a good ratio of ions to neutral gas molecules, and beams of up to a few milliamps have been reported in laboratory tests though only 5—20 per cent of this is protons,

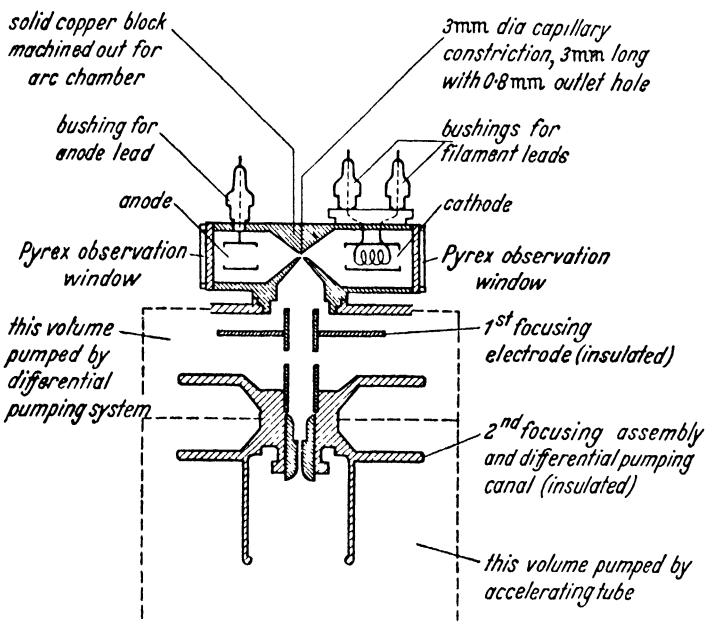


Figure 8. Capillary arc ion source (with hot cathode)

and the gas leakage rates of 20—30 cc/hr at N.T.P are still too high for use with some accelerating tubes. The best performance reported at a recent conference in the United States for this type of source actually operating in a high voltage electrostatic generator was 20 μa of resolved current at the target. *Figure 8* shows the layout of such a source.

Further improvement in performance has been claimed for the use of hot cathode discharges combined with magnetic fields[45, 46] and essentially non-metallic media for containing the discharge[47]. The latter appears to reduce the re-combination of atomic gas, and gives a greater proton percentage (60—100 per cent). A discharge which is almost completely free from metal and carries a high current density can be obtained by the use of radio frequency (RF) fields; ion sources using this principle have recently been described. A magnetic field may be required for best performance. RF sources have been reported[49, 50] to give 200—300 μa of resolved beam with gas consumption of 10—20 cc/hr at N.T.P but their use with electrostatic generators has not yet been described. *Figure 9* shows the layout of an RF ion source.

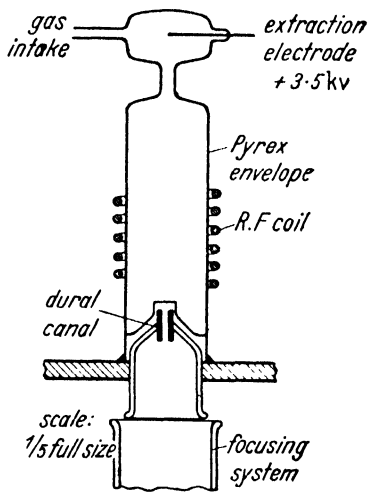


Figure 9. Radiofrequency ion source

While it is probably from the use of RF discharges that marked improvements in ion source performance can be expected, the extra equipment required to generate the RF power must be regarded as a disadvantage, and it seems that for the time being the hot cathode source will remain in more general use. Very recently cold cathode sources using axial magnetic fields on the principle of the Penning ion gauge have been reported to give good results. A development of great interest would be the successful production of a source of doubly ionized helium ions. Although this has been attempted, nothing has been produced so far which can be used in normal equipment for this purpose.

VOLTAGE CONTROL, MEASUREMENT AND STABILIZATION

Since the great advantage of D.C. accelerators lies in the precise control of particle energy which they can provide, voltage control and stabilization is a matter of fundamental importance in their design. This is particularly true for electrostatic generators, the output of which is inherently free from major fluctuations, and also at a voltage high enough to be of great interest in the exploration of nuclear energy levels.

The voltage of an electrostatic generator is determined by the condition that the current supplied by the belt shall equal that removed from the

electrode by the particle beam and various leakage currents. For machines operating at atmospheric pressure it is convenient to saturate the belt with charge, and to control the voltage by an adjustable corona point held near the electrode. Machines operating under gas pressure are more usually controlled by variation of the belt charging current through change in exciter voltage. In either case, manual operation of the control enables the voltage to be held to within about 1 per cent of a fixed value in respect of long period drift.

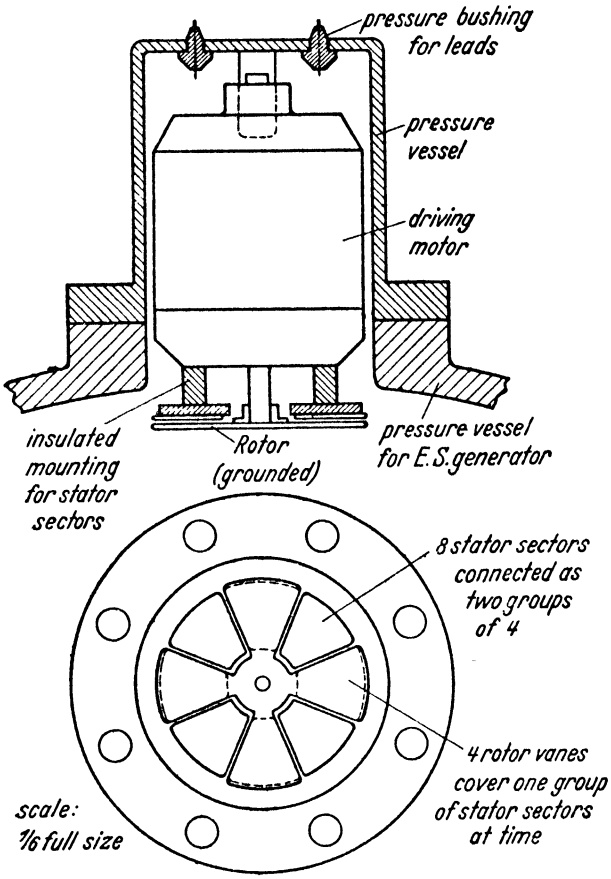


Figure 10. Generating voltmeter for pressure insulated electrostatic generator

The voltage is usually measured in the first instance by means of a generating voltmeter (*Figure 10*) in which a rotating vane system alternately exposes a set of conductors to the field from the high voltage electrode and shields them from it[23, 51]. The resulting alternating current gives a measure of the field strength, and the voltage can be deduced by calibration. This system has an accuracy of about ± 5 per cent provided the generator is not near breakdown voltage; special methods[52, 53] can improve this to a relative accuracy up to 0·1 per cent. More accurate determinations of particle energy require deflection of the particles themselves by magnetic or electric fields[54, 55]. Such analysers have been constructed to give absolute calibrations, and from their use the energies at which certain nuclear reactions occur have been established very precisely and can be used as calibration points. Useful reactions given by HERB[56] are:

Li (p n)	1·8823—1·8817 Mv	(*threshold*)
F (p γ)	0·8734—0·8735 Mv	(*resonance*)
Al (p γ)	0·9936—0·9930 Mv	(*resonance*)

The results given are for two successive separate determinations, to indicate the accuracy.

When voltage precision of this order is required, manual control of the generator voltage becomes inadequate as there are variations in voltage

produced by irregularities in belt surface, variations in corona *etc* which result in small but rapid fluctuations in particle energy. The effect of such variations on experiments is avoided by the use of analysers, of the kind already mentioned, which only pass particles through their slit systems when the particle energy lies within narrow limits. It can also sometimes be eliminated by arranging that the experimental equipment (counter system) is only sensitive when the output of the generating voltmeter lies between certain values[53]. Both these systems, however, reduce the effective beam intensity by an amount depending on the extent of the energy variations of the particles. It is therefore always desirable to restrict these fluctuations as far as possible, by automatic voltage governing systems. These are actuated by the energy analyser or generating voltmeter output and are arranged to correct the generator voltage, by various control systems, much more quickly than can be done by manual operation. The simplest control method is again by variation of exciter voltage. Versions of this system were described in 1938 and subsequent years[23, 29, 53, 55]. Although the speed of operation is much greater than with manual control, it is limited by the time taken by the belt to convey a change in spray current to the high voltage electrode. This delay, of the order of $\frac{1}{5}$ to $\frac{1}{10}$ sec, not only prevents the control of fluctuations of shorter duration, but also tends to limit the reduction in magnitude of slower changes that can be achieved by automatic control, for such governor systems constitute feedback servo systems, which ' hunt ' if the magnification (improvement of stability) increases from unity, with decreasing frequency of a sinusoidal disturbance, at a rate greater than inversely proportional to frequency.

To improve the precision of control and include the faster fluctuations of voltage, systems operating more rapidly than the exciter voltage control must be used. A corona point at variable potential, or with a grid control of variable potential, provides a great reduction in the time lag between control action and its effect[57]; similar variation of the generator load by a variable electron beam passing from negative to positive electrode[54] gives even faster response. Very rapid response should also be possible with systems of control in which the high voltage electrode potential is varied in a transitory manner by variation in voltage of a shield surrounding it, or of a point at the bottom of the accelerating column. It might also be possible to make small corrections by varying the voltage of the target with respect to earth. Provided that the inherent fluctuations are kept reasonably small by appropriate design, the new control methods give promise of further improvement of energy definition from the limit of around 1 kev at 2 Mev already reached to perhaps one fifth of this. Definition much beyond this is likely to be considerably more difficult, and probably of less importance, owing to the influence of target thickness, surface films, and thermal motion of the target nuclei.

REFERENCES

Rectifier Sets

[1] MITCHELL, R. G. *Wireless Engineer* 22 (1945) 474
[2] MÜLLER, H. *Arch. Techn. Messung* 95 (1939) 243
[3] VAN GEEL, W. C. *Philips Tech. Rev.* 4 (1939) 104
[4] PLOOS VAN AMSTEL, J. J. A. *ibid* 9 (1947) 267
[5] VAN DER TUUK, J. H. *ibid* 8 (1946) 199
[6] IMHOF, A. *International Conference on Large High-Tension Systems* (*C.I.G.R.E.*), 10*th Session* 1 (1939) 114, *Bull. Assoc. Suisse Elect.* 36 (1945) 333
[7] BENNETT, W. H. *J. appl. Phys.* 18 (1947) 479
[8] BOUWERS, A., *Elektrische Höchstspannungen.* Berlin, 1939
[9] BURCHAM, W. E. *Nature, Lond.* 160 (1947) 316
[10] GRAY, L. H. *Brit. J. Radiol.* 13 (1940) 82
[11] REYVAL, J. *Rev. Gen. Elec.* 50 (1941) 294

Electrostatic Generators

[12] VAN DE GRAAFF, R. J. *Phys. Rev.* 38 (1931) 1919; 43 (1933) 149
[13] TUVE, M. A. *et al ibid.* 48 (1935) 315
[14] VOELRATH, R. E. *ibid* 42 (1932) 298
[15] PAUTHENIER, M. *Rev. Gen. Elec.* 45 (1939) 583
[16] CHAUMAT, H. *Bull. Soc. Franc. Elect.* 3 (1933) 907
[17] MOREL, R. *Ann. Univ. Grenoble* 23 (1948) 155
[18] BARTON, H. A. *et al Phys. Rev.* 42 (1932) 901
[19] TRUMP, J. G. and VAN DE GRAAFF, R. J. *ibid.* 55 (1936) 1160
[20] VAN DE GRAAFF, R. J., *ibid* 49 (1936) 761
[21] HERB, R. G. *et al Rev. sci. Instr.* 6 (1935) 261; *Phys. Rev.* 51 (1937) 75
[22] — — *Phys. Rev.* 58 (1940) 579
[23] PARKINSON, D. B. *et al ibid* 53 (1938) 642
[24] BUECHNER, W. W. *et al ibid* 69 (1946) 692
[25] POLLOCK, H. C. and COOPER, F. S. *ibid* 56 (1939) 170
[26] MCKIBBEN, J. L. *U. S. Atomic Energy Commission Report. A.E.C.D.* 2038, 1948
[27] VAN DE GRAAFF, R. J. *et al Rep. Prog. Phys.* 11 (1947) 1

Accelerating Tubes

[28] VON ARDENNE, M. *Z. Phys.* 121 (1943) 236
[29] WILLIAMS, J. H. *Rev. sci. Instrum.* 13 (1942) 202
[30] DANFORTH, W. E. *et al Phys. Rev.* 73 (1948) 1413
[31] TRUMP, J. G. and VAN DE GRAAFF, R. J. *J. appl. Phys.* 18 (1947) 327
[32] HULL, A. W. and BURGER, E. E. *Phys. Rev.* 31 (1928) 1121
[33] GOSSLING, B. S. *J. Inst. Elect. Engrs.* 71 (1932) 460
[34] JACOB, L. *High Voltage Physics* p 80, *London*, 1934
[35] MCKIBBEN, J. L. *U. S. Atomic Energy Commission Report. A.E.C.D.* 2039, 1948

Sources

[36] BUECHNER, W. W. *et al Rev. sci. Instrum.* 18 (1947) 754
[37] OLIPHANT, M. L. E. and LORD RUTHERFORD. *Proc. roy. Soc. A* 141 (1933) 259
[38] HUBER. *Helv. Phys. Acta* 14 (1942) 45
[39] LAMAR, E. S. and LUHR, O. *Phys. Rev.* 44 (1933) 947
[40] — — *ibid* 46 (1934) 87
[41] TUVE, M. A. *et al ibid* 48 (1935) 241
[42] LAMAR, E. S. *et al ibid* 48 (1935) 886
[43] ZINN, W. H. *ibid* 52 (1937) 655
[44] ALLISON, S. K. *Rev. Sci. Instrum.* 19 (1948) 291
[45] VON ARDENNE, M. *Phys. Z.* 43 (1942) 91
[46] FINKLESTEIN, A. T. *Rev. sci. Instrum.* 11 (1940) 94
[47] LAMAR, E. S. *et al Phys. Rev.* 51 (1937) 936
[48] — and BUECHNER, W. W. *J. appl. Phys.* 18 (1947) 22
[49] THONEMAN, P. C. *et al Proc. Phys. Soc.* 61 (1948) 483
[50] RUTHERGLEN, J. G. and COLE, J. F. I. *Nature, Lond.* 160 (1947) 545

Stabilization

[51] TRUMP, J. G. *et al Rev. sci. Instrum.* 11 (1940) 54
[52] HAXBY, R. O. *et al Phys. Rev.* 58 (1940) 1035
[53] BROSTRÖM, K. J. and HUUS, T. *ibid.* 71 (1947) 661
[54] BENNETT, W. E. *et al ibid.* 70 (1946) 882
[55] HANSON, A. O. *Rev. sci. Instrum.* 15 (1944) 57
[56] HERB, R. G. *et al Phys. Rev.* 75 (1949) 246
[57] MCKIBBEN, J. L. *et al ibid* 70 (1946) 117

3

PHOTOGRAPHIC EMULSION TECHNIQUE

J. Rotblat

THE RECENT YEARS have seen an enormous development of the photographic emulsion technique, which has now become one of the most popular and valuable tools in the study of problems in nuclear physics and cosmic ray research. The number of its applications to other branches of science is also increasing rapidly. Since most of these developments took place during the last few years, the reviewing of recent progress becomes almost equivalent to the writing of a monograph on the subject. This is, of course, impossible within the limits of a short article, hence the somewhat sketchy treatment of some problems. For the same reason the list of references has had to be curtailed; during the last two years alone over two hundred papers have been published dealing with this subject.

There is still no monograph on the emulsion technique, but its principles and applications are beautifully explained and illustrated in POWELL and OCCHIALINI's book[1]. The earlier developments are dealt with in a summary article by SHAPIRO[2], and some general aspects of the technique are given in the review article by YAGODA[3] and in papers by DEMERS[4] and WEBB[5]. YAGODA[3a] has also recently published a book which, although dealing mainly with the tracks of α-particles, contains much useful information on the emulsion technique in general as well as an exhaustive bibliography.

HISTORICAL REVIEW

The use of photographic plates for the detection of nuclear particles dates back to the beginning of the science of radioactivity. In fact BECQUEREL discovered radioactivity by observing the blackening of photographic plates caused by the radiations from uranium salts. This method of detecting radiations, however, soon gave place to the electroscope and ionization chamber techniques which proved to be much more quantitative. The development of nuclear physics and the growing interest in the observation of single particles has brought to the forefront of detecting instruments the cloud chamber and particle counters with the associated electronic devices, and it was not until recent years that the emulsion technique began to compete with them as a method of studying individual particles.

The possibility of detecting individual particles by means of a photographic emulsion was first investigated in 1910 by KINOSHITA[6], who worked

under RUTHERFORD in Manchester. Using a microscope and counting the number of silver grains he has shown that a single α-particle is capable of rendering a halide grain developable. In the following year REINGANUM[7] observed for the first time the track of an α-particle in the emulsion as a row of several grains. There was little progress after this until 1925 when BLAU[8, 9] in Vienna, later joined by WAMBACHER[10], began a series of investigations on the use of photographic emulsions for the detection of protons and for the study of nuclear disintegrations. By sensitizing the emulsion with an organic dye, pinakryptol yellow, they managed to record tracks of protons; long tracks of fast protons were observed using thick emulsions, following a suggestion by MYSSOWSKY and TSCHISHOW[11]. Further improvements in the properties of emulsions resulted from the work of JDANOFF[12] (sometimes spelt Zhdanow) and the introduction by Ilford of special emulsions, first the *R* plates and then the Half-Tone plates, in which tracks of protons of an energy of some millions of electronvolts could be recorded. Other emulsions developed for this purpose were the Kodak fine grain α-plates and the Agfa *K*. Using these plates a number of investigators, notably TAYLOR[13] in England, and WILKINS[14] in the United States, have applied the emulsion technique to various problems in nuclear physics and cosmic ray research. For a complete bibliography of earlier publications see SHAPIRO[2].

By 1939 the photographic emulsion technique was already recognized as a useful tool for the investigation of nuclear and cosmic ray phenomena, but it was considered to be only a qualitative method and of limited applications. Even the users of the technique thought it to be incapable of producing accurate results in the measurements of energies; it was generally believed to be a tedious method and subject to large personal errors. This situation changed radically when POWELL began his systematic investigations on the technique[15-19]. He first proved that under proper experimental conditions the energy of a particle can be measured accurately from the length of its track in the emulsion, and that this applies not only to protons or α-particles, but that even the energy of neutrons can be determined with a high degree of accuracy. He has further shown that if suitable optical equipment is employed the nervous strain on the observer and the personal error can be greatly reduced. In a series of papers dealing with applications to nuclear physics and cosmic rays Powell has established the emulsion technique as a quantitative and versatile method capable of giving results of high precision and reproducibility.

The war period somewhat retarded the development of the technique, although photographic emulsions had been employed in the study of several problems connected with the atomic bomb project, but further work started immediately the war ended. The results of the pre-war work had indicated the improvements required; the main factors limiting the value of the technique were the wide gaps between grains, which made it difficult to determine

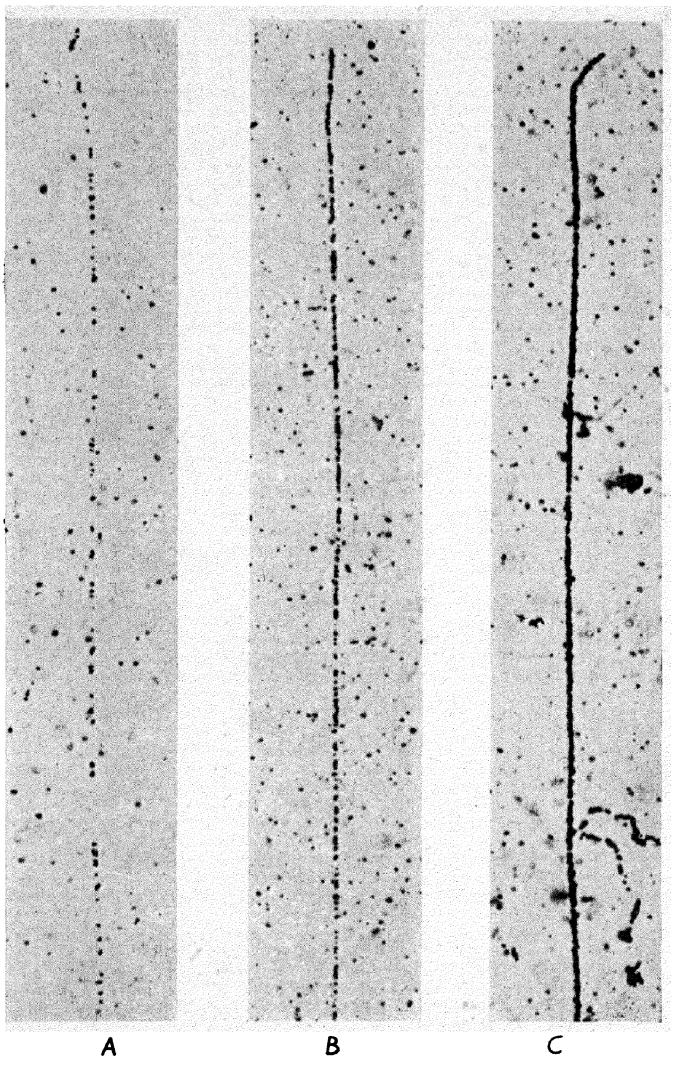


Figure 1. Tracks of protons in different emulsions:
A Ilford Half-Tone, B Ilford C 2,
C Kodak NT4 (by courtesy of Professor Powell)

(To face p. 39)

the exact length of a track, and the low sensitivity which, coupled with a strong background fog of individual grains, made it impossible to observe tracks of particles of a low ionizing power. Obviously emulsions were required with a smaller grain size and grain spacing and with a higher sensitivity to ionizing particles. Such emulsions were produced simultaneously in Canada and in England. In Canada DEMERS[20], starting from the earlier emulsions described by JDANOFF[12], developed several new emulsions which had all the desired characteristics. A more systematic effort was made in England, where Ilford, at the instigation of POWELL[21] and others, developed a new emulsion, the Concentrated Half-Tone, which had a much greater ratio of silver halide to gelatin than the Half-Tone and in which, therefore, the grain spacing was so much reduced that tracks of protons of several Mev appeared as almost continuous lines.

Further work in England was stimulated by the setting up by the Cabinet Advisory Committee on Atomic Energy of a special Panel to coordinate and promote the development of the emulsion technique. On the recommendation of the Panel contracts were placed by the Ministry of Supply with Ilford, and later also with Kodak, for development work according to a programme outlined by the Panel. As a result of this a new series of emulsions called 'Nuclear Research Emulsions' has been produced by Ilford, which offers a whole range of sensitivities and grain sizes to meet various demands. The magnitude of the improvement achieved can be judged from the micro-photograph in *Figure 1*, on which tracks of protons of the same energy are shown, recorded in a Half-Tone emulsion *A* and in an Ilford *C2* Nuclear Research Emulsion *B*.

Although the recording in these emulsions of heavily ionizing particles was nearly perfect there was a demand for an emulsion capable of recording particles of low ionizing power, and consequently most of the further effort was put into developing very sensitive emulsions. The climax came in 1948 when Kodak produced the first emulsion, *NT4*, which is sensitive to electrons at minimum ionization and thus capable of recording any charged particle of any energy (BERRIMAN[22]). The greater sensitivity of this emulsion is evident from the third track *C* in *Figure 1* which was taken under conditions similar to *A* and *B*. This development greatly extended the field of applications and opened up new and far reaching possibilities.

The full value of the photographic emulsion technique has become evident during the last two years, mainly as a result of the brilliant discoveries, by Powell and his school, of mesons of different masses and of a number of new phenomena in cosmic rays and nuclear physics. The technique has not only established itself as an important tool of general use in nuclear physics, but it has helped to open entirely new fields of work and has revealed phenomena which would have been otherwise impossible to detect.

EMULSIONS FOR NUCLEAR RESEARCH

General characteristics of emulsions—The mechanism of the formation of developable grains along the track of an ionizing particle has been studied by DEMERS[4], CUER[23] and WEBB[5]. Although the processes involved are of a somewhat different nature from those in light photography there are no fundamental differences, and the mechanism of latent image formation, as given in the theory of GURNEY and MOTT[24] (see also BERG[25]), can be applied to ionizing particles as well. The requirements in nuclear physics call, however, for emulsions with properties differing considerably from those used in ordinary photography.

The ideal detecting device in nuclear physics should make possible not only the detection of each particle, but also its identification and accurate determination of its charge, mass, energy and momentum. On this basis the main requirements of an emulsion for nuclear physics work may be roughly defined as, *1* tracks should be produced by all charged particles; *2* the tracks should be well defined and stand out above the fog background, which should be reduced to a minimum; *3* tracks of particles of different charges and masses should have different appearances, which will enable their identification.

There are several characteristic properties of emulsions which can be adjusted in order to meet these requirements. The most important of these are the concentration of silver halide, the mean grain size, the mean grain spacing and the sensitivity. The latter property is not easily defined quantitatively. It is usually described as the probability that a silver halide grain struck by an ionizing particle will become developable. This probability will be determined by two factors, the amount of energy spent by the particle in the grain, which depends on the charge and velocity of the ionizing particle, and the sensitivity proper, which depends on the distribution of the sensitivity specks and on the treatment of the emulsion during its manufacture. If the probability of producing a latent image in the grain is too low the gaps between the grains in a track will become so wide that it will be impossible to recognize the grains from those of the background fog. In a given emulsion this will happen with particles of a sufficiently high velocity. This maximum velocity of a singly charged particle can, therefore, be used as a term defining the sensitivity; the latter could also be expressed as the reciprocal of the specific energy loss of the particle (DEMERS[4], CUER[23]).

The various parameters characterizing the emulsion are not independent. It has been shown by JDANOFF[12], and confirmed by DEMERS[4], that the average density of grains, which is the reciprocal of the grain spacing, is given by the formula $n=3CP/2\rho d$ where C is the concentration of the silver halide, ρ its density, d the mean diameter of the grain and P the probability that a grain struck by the particle will be rendered developable. It is also known that P is a function of d; namely, within limits, the sensitivity is roughly proportional to the cube of the grain diameter (KODAK[26]).

These interdependencies make it difficult to produce an emulsion to serve all purposes. For the recording of particles of a very high velocity the sensitivity should be increased to such an extent that even a particle of an energy corresponding to the minimum ionization will render developable each grain through which it passes. For this purpose emulsions with sufficiently large grains would have to be used. On the other hand, for recording particles of very low energies, the grains and their spacing should be so small that even a particle of very short range will give a track of several grains. Although the manufacturers have means of treating emulsions to increase the sensitivity of grains of a given size, this can be done only within relatively narrow limits.

In order to obtain a track of a well defined length the grain spacing should be as small as possible; according to the above formula this can be achieved either by decreasing the grain size, increasing the sensitivity or increasing the concentration of silver halide. There are, however, limits to each of these factors. The dependence between grain size and sensitivity has already been mentioned. Increasing the silver halide concentration gives rise to scattering of the track of the particle, which makes the measurement of its length difficult, and leads to a large shrinkage of the emulsion at processing.

Discrimination between various particles and the determination of their direction of motion can be achieved either by measuring the grain density along the track or by observing the small angle scattering. The first method requires a sufficiently large grain spacing so that the individual grains will be resolved, while the second calls for a high concentration of silver halide so that the scattering will be more frequent.

Apart from these requirements the emulsion should be sufficiently thick so that even long tracks will be fully contained in it. It should be of a uniform composition and of uniform thickness; it should have a stable latent image, good adhesion to the glass and not be distorted on processing.

Properties of available emulsions—From the discussion in the previous section it is clear that no single emulsion can meet all requirements, hence several types of emulsions are produced by the manufacturers and for each experiment the appropriate type has to be chosen.

The main series of emulsions produced by Ilford have approximately the same concentration of silver halide, but differ in grain size and sensitivity. Each type is designated by a letter and a number, which originally were supposed to indicate the grain size (decreasing in alphabetical order), and sensitivity (increasing with the number). The subsequent introduction of intermediate types has, however, upset this nomenclature. Emulsion *D1* has the finest grain and the lowest sensitivity. It is most suitable for recording very heavy ionizing particles, like fission fragments; α-particles will be recorded with grains well separated, while protons will not be recorded at all. In the *E1* type, which has a slightly coarser grain, protons of several Mev produce tracks in which the individual grains are resolved, while α-particles of the

same range give tracks of a practically continuous character. This emulsion is, therefore, useful when a discrimination between protons and α-particles is desired. Type *C2*, which has a higher sensitivity than *E1*, is a good all purpose emulsion for recording tracks of particles of heavy and medium mass. Type *B2* has the coarsest grain and a slightly higher sensitivity than *C2*. The most sensitive Ilford emulsion is *G5*, which has a grain size slightly greater than *C2*. It is sufficiently sensitive to record particles of minimum ionization, and therefore is sensitive to all charged particles at all energies.

Kodak have three main types of emulsions. Type *NT1a* corresponds roughly to Ilford's *E1*. Type *NT2a* has a higher sensitivity and is capable of recording electrons up to 100 kev. The highest sensitivity is that of the *NT4* emulsion, which is suitable for recording singly charged particles at the minimum ionization. On the other hand it has a poor discriminating power, and continuous tracks are obtained even with particles of relatively low ionization (BROWN *et al* [27]).

In the United States Eastman Kodak produce four types of emulsions: *NTA* (corresponding to *NT1a*), *NTB* (roughly equivalent to *C2*), *NTC* (roughly equivalent to *D1*) and *NTB3*, a sensitive emulsion, in which electrons up to 400 kev can be recorded.

Figures 2 and *3* show photographs of tracks produced by various particles in some of these emulsions. The characteristics of the main types of emulsions are summarized in *Table I*. The grain diameters of the Ilford emulsions were

Table I. Characteristics of photographic emulsions used in nuclear physics

Emulsion	Ilford					Kodak (England)			Eastman Kodak (U.S.A.)			
	D1	*E1*	*C2*	*B2*	*G5*	*NT1a*	*NT2a*	*NT4*	*NTC*	*NTA*	*NTB*	*NTB3*
Mean grain diameter (microns)	0·12	0·14	0·16	0·21	0·18	0·19 ± 0·04	0·22 ± 0·04	0·39 ± 0·04	0·1 – 0·3	0·2 – 0·3	0·2 – 0·3	0·2 – 0·3
Highest velocity detectable $\beta = \mu/c$		0·2	0·31	0·46	*all*	0·2	0·55	*all*		0·15	0·49	0·83
Highest detectable energy of electrons (Mev)	—	—	0·03	0·07	*all*	—	0·1	*all*	—	—	0·08	0·4
Highest detectable energy of μ *mesons (Mev)*	—	2	5·5	0·14	*all*	2	20	*all*	—	1	16	85
Highest detectable energy of protons (Mev)	—	20	50	120	*all*	20	200	*all*	—	10	150	750
Highest detectable energy of deuterons (Mev)	—	40	100	240	*all*	40	400	*all*	—	20	300	1,500
Highest detectable energy of α*-particles (Mev)*	*Low energy*	500	1,500	*all*	*all*	500	*all*	*all*	*Low energy*	250	*all*	*all*
Highest detectable energy of fission fragments	*all*	*all*	*all*	*all*	*all*	*all*	*all*	*all*	*all*	*all*	*all*	*all*

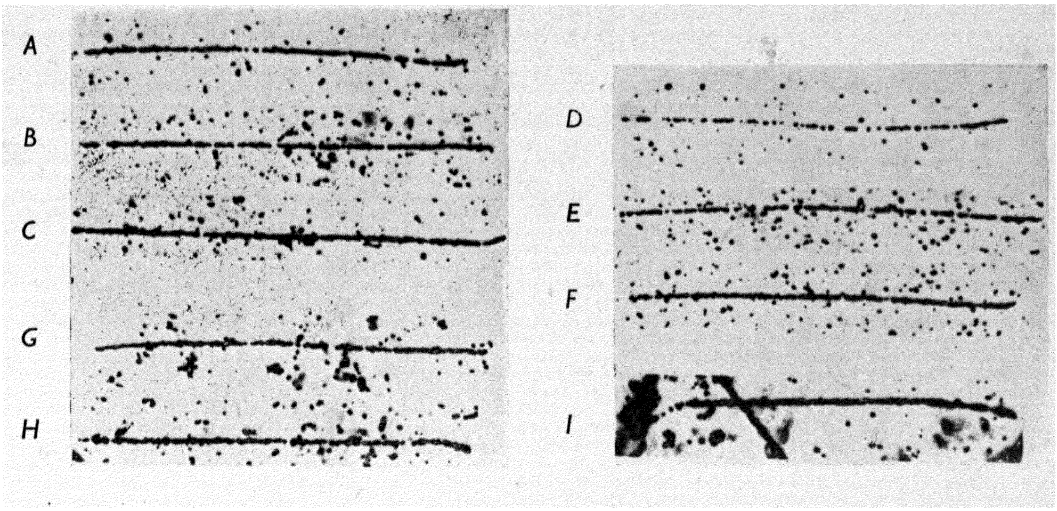


Figure 2. Tracks of various particles of about 50 μ *range in various emulsions:*

A, B, C *proton, deuteron and* α*-particle in Ilford C2 emulsions*
D, E, F *proton, deuteron and* α*-particle in Ilford E1 emulsions*
G, H *proton and deuteron in Kodak NT2a emulsion*
I *α-particle and electron in Kodak NT4 emulsion.*

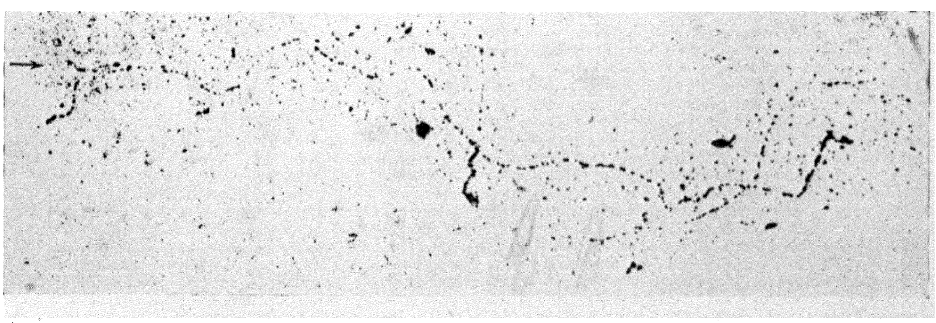


Figure 3. Track of electron about 300 μ *long; Kodak NT4 emulsion (by courtesy of Messrs Kodak Ltd.).*

(To face p. 42)

measured by KNOWLES and DEMERS[28], who, however, do not give the spread of these values; for the *NT2a* and *NT4* emulsions measurements were made from electron microscope photographs, the remaining values were given by the manufacturers. The wide limits indicate variations in grain size, both within one emulsion and from batch to batch. All these are grain sizes of the undeveloped emulsion; after processing the grains appear larger, the increase depending on the degree of development.

The highest observable velocities below the minimum ionization value given in the table apply to singly charged particles. These values, as well as those of the highest energies observable, are given for orientation purposes only, since the limits depend considerably on the background of grains due to fog and other causes. The best check as to whether a plate is sensitive to particles at minimum ionization is by observing the very long and straight tracks from cosmic rays (BROWN[27]). The grain density of tracks of particles at minimum ionization is 300 to 400 grains per mm in *NT4* emulsion.

There is little information on the lowest energies observable. DEMERS[4] recorded 200 kev protons in his fine grain emulsions, and BLUM[29] claims to have observed tracks of electrons of less than 10 kev.

The composition of all British emulsions is very nearly the same. When absolutely dry the concentration of silver halide is 86 per cent by weight. The Eastman Kodak emulsion has a silver halide content of 81 per cent, except for the *NTC*, where it is only 65 per cent. The atomic composition of the dry emulsions is given in *Table II.*

Table II. Compositions of dry emulsions

		*Ilford**	*Kodak (England)*		*Eastman Kodak (U.S.A.)*†	
	gm/cc	*No. of atoms per cc* ($\times 10^{22}$)	*gm/cc*	*No. of atoms per cc* ($\times 10^{22}$)	*gm/cc*	*No. of atoms per cc* ($\times 10^{22}$)
H	0·049	2·93	0·038	2·39	0·043	2·64
C	0·30	1·51	0·27	1·43	0·34	1·60
N	0·073	0·31	0·080	0·36	0·11	0·49
O	0·20	0·75	0·16	0·65	0·17	0·68
S	0·011	0·02	—		—	
Br	1·465	1·15	1·44	1·13	1·22	0·96
Ag	2·025	1·17	1·97	1·14	1·70	0·99
I	0·057	0·03	0·036	0·02	0·054	0·027

* In the *G5* emulsion the iodine content is reduced to 0·026 gm/cc and the bromine content increased to 1·496.

† *NTA*, *NTB* and *NTB3* emulsions.

Normally the emulsions contain some water and consequently the composition will vary with conditions of humidity. *Table III* gives amounts of moisture contained in the emulsion at several values of relative humidity.

Table III. Moisture content of emulsions

Relative humidity per cent	*Moisture content by weight at 20° C (%)*		
	Ilford	*Kodak (England)*	*Eastman Kodak (U.S.A.)*
30	2·0	1·3	
50	2·65	2·6	2·2
70	3·7	3·5	4·0

The composition of emulsions is likely to vary from batch to batch and for very accurate measurements of range each batch should be calibrated. The quality of emulsions is, however, improving steadily and errors due to lack of uniformity, either in composition or in thickness, are gradually decreasing.

The refractive index is assumed to be that of the gelatin *i.e.* between 1·50 and 1·53.

The standard thicknesses of emulsions are 50, 100 and 200 microns, but thicker emulsions up to 1,000μ have been used. The normal coating is on glass plates, 1·25 to 1·40 mm thick, but emulsions are available as films without glass support. Some emulsions are provided with a super coating of gelatin, about 0·5μ thick, for protection against scratching. In experiments in which particles enter from the surface, this coating will reduce the range by an amount depending on the angle of dip (MAUER[30]).

Plates are available in various sizes, although Kodak standardize on 1 inch × 3 inch. Narrow plates should be avoided if possible, since distortion of the emulsion may occur in them during processing when the strains set up at coating are relieved.

Loading and sandwiching—For some work it is desirable to introduce into the emulsions elements not normally present there. Thus emulsions impregnated with lithium or boron can be used as detectors of slow neutrons. Impregnation with deuterium is very useful for the investigation of various nuclear processes involving deuterons *e.g.* photodisintegration, scattering. Loading with uranium is valuable for the study of fission processes.

Emulsions loaded with lithium, beryllium*, boron and bismuth are manufactured by Ilford. The concentration of these elements in the emulsion is the maximum compatible with uniform loading. YAGODA and KAPLAN[31] included

* Loading with beryllium has recently been discontinued owing to its toxic properties.

lithium and boron simultaneously by impregnating the emulsion with a solution of lithium borate. Deuterium was initially loaded in the form of calcium nitrate containing heavy water of crystallization (GIBSON *et al*[32]), or simply by soaking in heavy water (GOLDHABER[33]), but the possibility of exchanging with water from the atmosphere made the keeping properties of such emulsions very poor. In order to increase the uptake of deuterium, WÄFFLER and YOUNIS[34] saturated emulsions with heavy water and, without drying, exposed them in watertight containers; the swelling of the gelatin and fading of the latent image lead, however, to complications in interpreting the results. More satisfactory was the loading with a stable compound of deuterium, hexadeutero-diacetin, which has been successfully carried out by Ilford. Plates impregnated with uranium have been used by many workers (LARK-HOROVITZ[35], CUER *et al*[36], PERFILOV[37], BORST *et al*[38], GREEN *et al*[39], BRODA[40]). The normal procedure is to soak the plate with uranyl acetate or ammonium uranate in diluted acetic acid. BRODA[40] made a study of the rate of uptake of uranium in emulsions as a function of various parameters, like impregnation time, concentration of the uranyl ion, *p*H of the solution *etc.* He found that over a wide range of concentrations the uptake of uranium is a linear function of the concentration of the uranyl ion.

In work involving bathing plates in a solution, a correction has to be made for the change of the stopping power of the wet emulsion. POWELL[21] found a 20 per cent decrease in the stopping power of the wet emulsion, due to its swelling (see also GOLDHABER[33]). On the other hand soaking with alcohol increases the stopping power, probably due to drying of the emulsion (WESTÖÖ[41]).

Related to loading is the sandwich technique in which thin layers of various materials are interposed between layers of emulsion. DEMERS[42] was the first to use very thin layers of ammonium uranate suspension to investigate the fission process. PERKINS used emulsions sandwiched in layers of plain gelatin and in this way separated the disintegrations produced by cosmic rays in light elements from those in the halide. A typical sandwich consisted of four layers of emulsion 30 μ thick separated by three thin layers of plain gelatin (HARDING[43]). Layers of lead phosphate (HODGSON *et al*[44]) and foils of heavy elements have also been used. PICCIOTTO[45] placed a drop of solution containing the material to be investigated *e.g.* $Sm_2(SO_4)_3$, between two layers of emulsion, thus ensuring that all tracks were observed while not upsetting the composition and properties of the emulsion.

Fading of the latent image—It has been known from early work (BLAU[46], LAUDA[47]) that the latent image produced in the emulsion by the passage of a charged particle is not stable. If an exposed emulsion is left for a certain time before developing it the number of grains in the track gradually decreases. This effect became more noticeable in recent years, due to the greater

accuracy of the technique and to the use of grain counting as a method of determining the mass of particles. The latent image fading is very serious for work in cosmic rays, where exposures lasting several months are frequently made, and it has led to considerable errors in the determination of masses by means of grain counting (OCCHIALINI[48], LATTES *et al*[49]).

The factors influencing latent image fading have been the subject of much study (CHEKA[50], COPPENS[51], LAMB and BROWN[52], LA PALME and DEMERS[53], YAGODA and KAPLAN[54], MATHER[55]) and a most thorough investigation was made by ALBOUY and FARAGGI[56, 57]. They have established that the rate of fading increases exponentially with temperature and with the amount of water contained in the emulsion. If the plate is kept in an atmosphere of oxygen the fading is much faster than in air, whereas there is practically no fading in nitrogen, particularly when it is dry, and in vacuum. Impregnation with materials which increase the *p*H of the emulsion (borax, Na_2CO_3) decreases fading, while acids increase it. The latent image seems to be the more stable the larger the grain size and the sensitivity; indeed, the *NT4* emulsion shows very little fading[27]. Within the same emulsion the rate of fading increases with the energy of the particle, so that fading is usually most pronounced at the start of the track. This fact has been made use of by FARAGGI[58] to determine the point of origin of tracks of two particles flying away in opposite directions, such as those which occur in disintegrations produced by slow particles.

The pronounced effect of humidity, and particularly of the presence of hydrogen peroxide, on the rate of fading has led YAGODA and KAPLAN[54] to the belief that fading is caused by the action of hydrogen peroxide produced in the emulsion by the radiations themselves, but this explanation appears unlikely when one calculates the quantities of hydrogen peroxide produced. Much more feasible is the explanation of the mechanism of fading suggested by ALBOUY and FARAGGI[56, 57]. According to them the fading is caused by the oxidation of silver grains by the oxygen from the air in the presence of water, according to the formula $2Ag+O+H_2O \rightarrow 2Ag^+ + 2OH^-$. It is known (BERG[59]) that oxidation reduces the efficiency of the sensitivity centres of the grain. A medium of a high *p*H retards the oxidation or enhances the action of the sensitivity specks. All observed facts fit in with this explanation.

The knowledge of factors influencing fading will greatly help to eliminate this effect. Good results are obtained by drying off the water from the emulsion and adding to it a plasticizer (glycerin) to prevent it from breaking up.

Desensitization and eradication of background—In an emulsion of a given sensitivity a higher degree of discrimination between various particles can be achieved by desensitizing the emulsion. This method has been employed by PERFILOV[60], POWELL *et al*[21], and GREEN and LIVESEY[61] to observe tracks of

fission fragments in the presence of a high flux of neutrons, which give rise to proton recoil tracks. An oxidizing agent, such as chromic acid or potassium permanganate, can be employed for this purpose. By using an appropriate concentration of the oxidizing agent the sensitivity of the emulsion to protons can be greatly reduced, while affecting only little the recording of α-particles. Actually, the loading of emulsions with a solution of uranyl acetate of an appropriate strength has by itself a sufficient desensitizing effect to eliminate the proton tracks (GREEN and LIVESEY[61]).

This desensitizing effect has to be taken into account whenever loading is employed. All substances which lower the *p*H value of the emulsion will have a desensitizing action. An increase of the *p*H value, obtained for example by loading with borax, has an intensifying action (PICCIOTTO[62]).

The latent image fading and desensitizing effect of oxidizing agents can be made use of for the eradication of background tracks. If an emulsion is left for some time it accumulates a background fog of developable but unexposed grains, as well as many tracks due to cosmic rays and to radioactive contaminations. This problem has become acute with the development of the electron sensitive emulsions, which become very quickly contaminated with tracks; the storage of such plates is therefore a very difficult problem, although, according to DILWORTH[63], keeping the plates at a temperature of −87°C, using solid carbon dioxide and acetone, reduces the sensitivity of the emulsion to less than 25 per cent.

In order to obtain emulsions free from unwanted tracks EVANS and GEORGE[64] obtained liquid emulsions from the manufacturers and coated the plates in their underground laboratory just before performing the experiment.

LIEBERMANN and BARSCHALL[65] have suggested a way to eradicate the background fog by the use of an oxidizing agent (potassium permanganate), which reduces the developable grains into free silver and then into a soluble silver salt. DE FELICE[66] used this method to remove the background of tracks, but it is not clear to what extent this process will affect the properties of the emulsion. DEMERS[4] removed fog, without much affecting the sensitivity, by treatment with chromic trioxide. He concludes from this that there is a chemical difference between fog centres and the active centres due to ionization events. YAGODA and KAPLAN[67] were able to obliterate completely the background by keeping the emulsion for four hours over 3 per cent hydrogen peroxide at 25° C. After dessication the sensitivity was restored and the emulsion could be used for the normal exposure (see also WIENER and YAGODA[68]).

Processing—This is a very important part of the emulsion technique and unless properly carried out it may lead to serious errors or loss of significant results. A variation of the acidity or the temperature of the developer may considerably alter the size of the developed grain or even prevent the developing of tracks of some particles. STEVENS[69] and VAN DEN GRINTEN[70] have

employed this dependence on the *p*H value of the developer as a means of discrimination between tracks of various particles.

The processing of emulsions up to 100 μ thick does not present any special difficulties. The makers supply details, but most laboratories use techniques based on their own experience. A typical procedure is as follows:

1 *Development*—Develop for 20 to 40 minutes at 18°C in Ilford *ID19* or Kodak *D19B* developer diluted to one third concentration.

2 *Stop Bath*—Rinse and bathe for 10 minutes in 2 per cent acetic acid.

3 *Fixation*—Fix at 18°C in a solution made up of two parts of saturated hypo, one part acid hardener (*stock solution F53*) and eight parts water. Fixation should continue for some time after the plate is cleared.

4 *Washing*—Wash in running water for several hours.

Most workers recommend keeping the plate in motion during the whole processing. Special rocking devices are used in some laboratories (POWELL and OCCHIALINI[1]) to produce laminar flow of the solution over the surface of the emulsion.

Processing thicker emulsions is more difficult and up till recently this was the main factor limiting the thickness of emulsions used. Owing to the slow penetration of the developer into the emulsion, grains at the top of the emulsion are developed to a much higher degree than those at the bottom, causing considerable differences in the grain density of a track dipping into the emulsion.

Two procedures have been recommended to overcome this difficulty. The first, the so-called temperature development (DILWORTH *et al*[71]), makes use of the fact that the permeation of the developer has a lower temperature coefficient than that of development. Consequently if the emulsion is soaked with the developer at a low temperature, the developing action is practically nil, but the whole emulsion is uniformly impregnated with the solution. When the plate is subsequently warmed up the development action takes place equally throughout the depth of the emulsion, giving a uniform rate of development. By means of this method emulsions up to 1,000 μ thick have been developed satisfactorily. The usual procedure is to soak the plate with the developer at 5°C, raise the temperature to 20° for the time of development, check further development in a stop bath again at 5°, start fixation at this temperature and raise it gradually to 20°C. All changes of temperature and *p*H must be very gradual in order to avoid reticulation and peeling of the emulsion (WILSON and VANESLOW[72]). Some workers recommend pre-soaking of the emulsion before developing, but WILSON and VANESLOW[72] find no advantage in this, in fact they claim that it causes additional background.

In the second method (BLAU and DE FELICE[73]) two baths are used in development. The first contains the developing agents but without the alkali, so that no developing action takes place in it; as in the temperature method

this stage serves only for the uniform diffusion of the developer into the emulsion. The actual development takes place in the second bath, to which the alkali is added.

The fixing of thick emulsions may take a long time. According to PURSLOW[74] the time needed for fixation is proportional to the square of the thickness. A considerable reduction of the fixation time can be achieved by agitating the solution with nitrogen (WILSON and VANESLOW[72]).

Shrinkage—One disadvantage of the concentrated emulsions is the large shrinkage resulting from the removal of silver halide during fixation. Owing to the high ratio of silver halide to gelatin this loss causes a considerable reduction in the thickness of the emulsion, over 60 per cent as compared to 10 per cent in the old Half-Tone emulsions. The ratio of the thickness of the emulsion during exposure to that after processing is called the shrinkage factor S. Provided that the emulsions in the given batch are all of uniform thickness the shrinkage factor can be determined by measuring the thickness of the emulsion after processing and comparing it with that of an unprocessed strip. In case of exposures in vacuum a correction has to be made for the small shrinkage before exposure due to the loss of water from the emulsion. Measurements with various emulsions of standard composition show that the shrinkage factor $S=2{\cdot}7\pm0{\cdot}2$, the limits at average humidity and including measurements on emulsions from different batches (ROTBLAT and TAI[75]). For lithium loaded emulsions S may go up to 3·2. Changing the conditions of processing leads to a change in S by less than 10 per cent.

When precision measurements of the range are to be made it is important to know the shrinkage factor accurately, since the angle of dip of the track in the shrunk emulsion will be smaller than the angle of dip of the particle when passing through the plate. For such work it is important to know whether the shrinkage is uniform throughout the depth and whether the same correction can be applied to all angles of dip. ROTBLAT and TAI[75] have studied this problem in emulsions impregnated with lithium and found that although the shrinkage is uniform, the reduction of the angle of dip is not uniform for all particles; tracks of heavily ionizing particles with a large angle of dip show a smaller apparent shrinkage than those with a smaller angle. This is probably due to the fact that in tracks in which the grains are touching the displacement of the grains at shrinkage is hampered to a certain extent. Thus while in most cases it is permissible to correct for the shrinkage simply by multiplying the depth measurement by the shrinkage factor, this does not apply to angles of dip larger than 25 to 30° for heavily ionizing particles.

OPTICAL EQUIPMENT

Universal microscopes—POWELL[17] was the first to emphasize the importance of the optical equipment for accurate results and for relieving the nervous strain on the observer. This is still true even with the new concentrated

emulsions, although the contrast of the track is so good that there is no longer any special fatigue and observers have been known to examine tracks all day long without any signs of strain.

Although several types of projection microscopes are now in use, which make possible the viewing of tracks on a screen, the chief instrument is still the ordinary microscope for the individual observer. The main requirements of such a microscope are high optical precision in both the sub-stage condenser and the objective, small depth of focus, flatness of field of view, large working distance, accurate depth gauge, precise motion of the mechanical stage, a protractor for angle measurement and eyepiece graticules. Built in illumination is desirable, and the adjustment of sub-stage illumination is important if the full resolving power is to be achieved. Some observers recommend dark field illumination though its advantages are dubious. A binocular microscope with inclined eyepieces is recommended for the comfort of the observer. When using such a microscope it should be remembered that the magnification depends on the interocular distance of the eyepieces; in some microscopes it depends also on the setting of the depth gauge.

A small depth of focus is essential for the measurement of the angle of dip of the track, since this angle is determined by focusing on the first and last grain and reading the difference on the depth gauge; the refractive index of the emulsion has to be taken into account in this measurement. It is an advantage to use oil-immersion objectives, mainly because of their high power, but also because the refractive index of the oil is very close to that of the emulsion.

Cooke, Troughton & Simms have recently modified the *M.4000* binocular microscope to meet the special requirements for emulsion work, in accordance with the specification of the Photographic Emulsion Panel. A photograph of this microscope is shown in *Figure 4*. Its main feature is the precision design of the mechanical stage which is fitted with micrometer movements in the *X* and *Y* directions. The micrometer heads are graduated every 5 micron, but it is possible to read the position of the stage with an accuracy of 2 micron; the length of a track can thus be obtained by reading it directly on the micrometers. The absence of backlash makes it possible to return to any point on the plate, if its coordinates have been noted. The depth gauge is graduated in one micron divisions which can also be interpolated. One of the eyepieces is equipped with a protractor by means of which the angle of a track with a given direction can be read with an accuracy of 15 minute of arc. Special eyepiece graticules are provided with scales reading directly in microns for given objectives and eyepieces.

The magnification employed depends largely on the type of investigation. The great improvement in the qualities of emulsion makes possible the use of smaller magnifications, which is advantageous when large areas of plate have

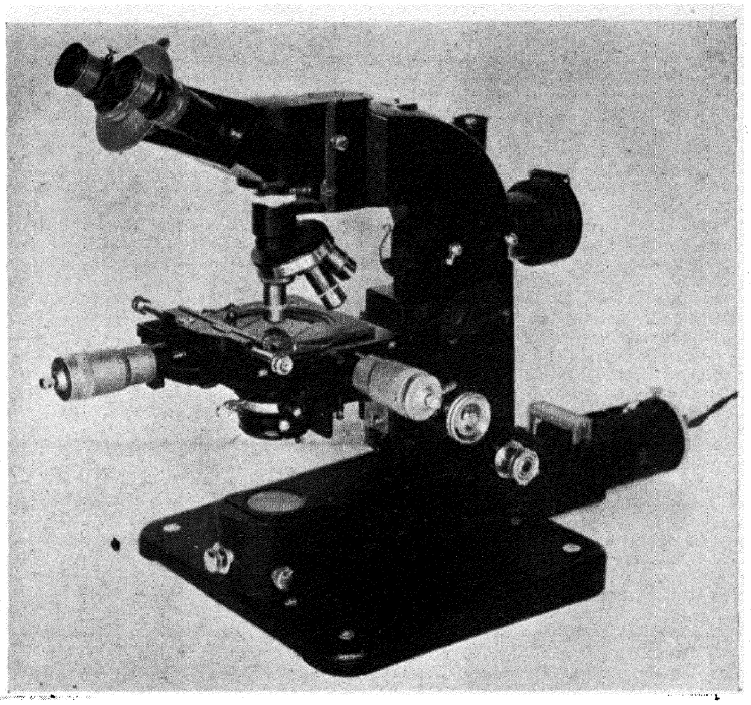


Figure 4. Microscope for nuclear research emulsions (type M.4005, Cooke, Troughton and Simms)

(To face p. 50)

to be scanned. POWELL has used an overall magnification of 90 for work with *NT4* emulsions[27]. For finer details higher magnifications have to be used. The choice of optics is often also dictated by the mean number of tracks per field of view; for comfortable work this number should not be less than one fifth or greater than twenty.

One disadvantage of a high power objective is its very short working distance. For example, the 2·2 mm apochromatic objective (numerical aperture n.a. 1·32, magnification × 80) has a working distance of only 0·12 mm which, taking shrinkage into account, allows its use for emulsions only up to 250μ thick. Cooke, Troughton & Simms have recently succeeded in increasing the working distance of their 3·75 mm oil-immersion fluorite objective (n.a. 0·95, ×45) to 1·5 mm, without worsening its optical properties. Thus even the thickest emulsions produced at present can be viewed at a high magnification. If the glass backing is thin it is even possible to examine the emulsion from the other side.

Another disadvantage of the highly corrected apochromatic objective is the curvature of the field of view, which means that a track parallel to the surface will not have all grains in focus at the same time. This has to be taken into account in measurements of the angle of dip, which have to be made either on the same spot of the field of view or on grains equidistant from the centre (CHAMPION and POWELL[76]).

When tracks of the same angle relative to a fixed direction are to be measured it is convenient to rotate the plate until the tracks are parallel to the X or Y movement. POWELL has designed a special turntable for this purpose[77]; its frame can be clamped to the mechanical stage and the table rotated through the desired angle. Such a turntable is shown in *Figure 4*. The scanning is then done simply by using the stage motion.

Projection microscopes—When large areas of a plate are to be examined in the search for some rare event, as in cosmic ray work, and in order to avoid the tediousness of prolonged looking through the eyepiece, a projection microscope is useful. Another of its advantages is the possibility of obtaining a facsimile, or of direct printing, of the desired tracks. Several such projection microscopes are available commercially as, for example, the Leitz Panphot, or the Vickers' Projection Microscope, made by Cooke, Troughton & Simms.

OCCHIALINI and PAYNE[78] have converted an ordinary microscope into a projection microscope with automatic scanning. A mercury vapour lamp is used and the image projected on to a vertical screen. By means of a small motor with differential gearing the mechanical stage is made to move slowly, so that the image of the emulsion passes across the screen. In order to observe events throughout the depth of the emulsion the stage motion is coupled with a rotation of the fine focusing adjustment in such a way that a focusing cycle over the whole depth is obtained for each field of view; the speed of

focusing is about 5 to 10 micron per second over depths from 10 to 400 micron. All the observer has to do is to watch the screen until an event worthy of recording is observed, when the scanning can be stopped by remote control.

Reflecting microscopes—For work with particles of very high energies, of ranges reaching up to several cm in glass, stacks of plates are used and the passage of a particle through the consecutive emulsions is studied. In magnetic deflection experiments two plates are arranged with the emulsions facing each other with a gap between. For such applications it is desirable to be able to observe the tracks through large thicknesses of glass plates. While this is obviously impossible with the normal microscope it can be achieved by means of the reflecting microscope in which mirrors are used instead of lenses. BURCH[79] described the construction of such a microscope, in which aspherical mirrors were used to increase the numerical aperture. BATES and OCCHIALINI[80] used this microscope for the observation of tracks in a sandwich of the type described above. The performance of this microscope was found to be about equal to that of a high power oil-immersion objective, with the added advantage of a very large working distance of about 20 mm. The reflecting microscope may become an important tool in the photographic emulsion technique, but the very high technical skill required for making the mirrors makes it unlikely that it will be mass produced. A simple optical system which can be used in conjunction with a conventional microscope and which gives a working distance of 7 mm at n.a. 0·75 is described by DYSON[81].

Photomicrographs—The photographing of tracks viewed through the microscope is an important part of the emulsion technique. With a projection microscope this can be done by direct printing. For normal microscopes a camera attachment has to be used; in the *M.4005* type a special fitting is provided which makes it possible to attach a 35 mm miniature camera.

In most cases the track does not lie in one plane and only part of it is in focus at one instant. A series of photographs has to be taken to bring the successive sections into focus. All prints are then aligned and rephotographed. When the tracks are longer than the field of view a ' mosaic ' is prepared from a number of photographs of consecutive fields of view. These are rephotographed so that the whole event is constructed as though it lay in one plane. An example of a mosaic composed of over sixty photographs is shown in *Figure 16*. MORRISON and MORTON[82] describe a simple projection system for taking photomicrographs which enables one to obtain a considerable length of track image on a single film. BARBOUR[83] has designed a tilting stage, which makes it possible to bring the whole length of a track in a given field of view into the focal plane, and thus to be obtained on one photograph.

Densitometers—The determination of the density of ionization by means of grain counting is possible only when the individual grains are resolved.

With particles of higher ionizing power 'clogging' is observed, the tracks forming a continuous line. A measure of the rate of energy loss can then be obtained by photometric determination of the density of the track, by means of a photomultiplier. The equivalence of densitometric measurements with grain counting was proved by CURTIS and OSBORNE[84]. Devices which make possible the automatic measurement of track densities have been used by DEMERS and MATHIEU[85] and by HOUGH[86]. The output of the photomultiplier is coupled to a cathode ray oscillograph on which the absorption of light by the tracks is observed.

METHODS OF TRACK ANALYSIS

Measurement of length and orientation of track—In order to determine the length of a track two measurements are necessary: of the length of the projection l of the track on the focal plane of the objective (*Figure 5*) and of the angle of dip β. The length l is read either on the eyepiece scale, which has to be calibrated, or directly on the micrometer heads of the mechanical stage; the stage is moved so that the beginning and the end of the track are in turn brought to a fixed point on the eyepiece scale. If the track shows bends due to scattering, the length of each section has to be measured separately by rotating the eyepiece scale to a direction parallel to the track. The angle of dip is obtained either by focusing the microscope on the first and last grains, which gives the vertical component of the whole track h, or by measuring the difference in depth of the first few grains[76]. For accurate measurements the bends in the vertical direction have also to be taken into account. The observed value of h (or β) has to be corrected for the shrinkage factor S, and for the refractive index. If the thickness of the processed emulsion is determined by means of the microscope under the same conditions as the track measurements, the refractive index is already included in the measurement of the shrinkage factor. The range of the particle in the emulsion will then be given by $R=(l^2+S^2h^2)^{\frac{1}{2}}=l(1+S^2\tan^2\beta)^{\frac{1}{2}}$

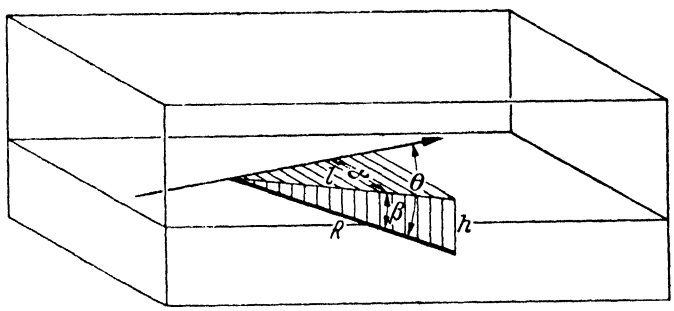


Figure 5. Orientation of track in emulsion

Often it is required to determine the orientation of the track relative to a given direction parallel to the surface of the emulsion. This angle θ (*Figure 5*) is given by $\cos\theta=\cos\alpha\cos\beta$, where α is the angle between the projection of the track and the specified direction. The angle α can be measured by means of

the angular protractor in the eyepiece by rotating it until the fiducial line in the eyepiece scale is parallel to the track.

Range-energy relation—The energy of a particle can be determined from its range if the relation between them is known. In the old Half-Tone emulsions, in which the silver halide content was very low, it could be assumed that the stopping power of the emulsion relative to air was constant for all energies; the known range-energy relation for air could therefore be used, once the emulsion was calibrated for one energy value (POWELL)[19]. The new emulsions have such a high silver halide content that this assumption is no longer valid and the stopping power of the emulsion has to be determined for various energies. From the known composition of the emulsion and the stopping powers of the individual elements the stopping power of the emulsion can be calculated. Such calculations have been carried out by CUER[87] and WEBB[5]. Since, however, the formulae contain some factors which are not well known it is preferable to use an experimental range-energy curve.

The range-energy relation for Ilford *B1* emulsions, for protons and α-particles up to 13 Mev, has been determined by LATTES, FOWLER and CUER[88, 89], who measured the ranges in the emulsions of particles produced in several nuclear transmutations. Since the Q values for these reactions are known one can calculate the ranges of these particles in air and hence the stopping power for the given energy. BRADNER *et al*[90] have extended the range-energy calibration for protons in *C2* emulsions to 40 Mev. The ranges of several α-particles from natural radioactive elements have also been measured and used for calibration purposes (TSIEN *et al*[91], GREEN and GIBSON[92], COTTON[93]). Another method of determining the range-energy curve was used by ROTBLAT[94], who measured the ranges of protons and α-particles scattered elastically by deuterons of known energy through various angles. Since the relationship between the energy of the scattered particles and the angle of scattering is known one obtains in this way directly the energies of the particles for the various ranges measured.

Results of measurements with *C2*, *E1*, *G5* and *NT2a* emulsions have shown no significant differences in their stopping powers[94]. PECK[95], however, who measured ranges of protons in *NTB* emulsions obtained results differing very considerably from the above. He suggests that small differences in composition and humidity may have a large effect on the range-energy relationship, but it seems rather likely that his results contained a systematic error.

The range-energy relationship for electrons in *NT2a* plates was measured by ROSS and ZAJAC[96], HERZ[97] and BLUM[29], and in *NT4* plates by ZAJAC[102], using monochromatic beams of β-rays or photoelectrons from x-rays. Owing to the tortuous shape of electron tracks the accuracy of these measurements is not as high as for heavier particles.

In *Figure 6* are given the experimental range-energy curves for protons and α-particles up to 13 Mev. These results apply to plates exposed in vacuum ; for exposures in air and under average conditions of humidity the ranges have to be increased by about 3 to 4 per cent. The same curves extrapolated to higher energies are shown on a logarithmic scale in *Figure 7*, which gives also curves for several other particles. Some of these curves are based on experimental results and some are calculated. As will be shown later the relation between energy and range can be approximately expressed by the formula $E = KZ^{2n}M^{1-n}R^n$, where Z and M are the charge and mass of the particle and K is a constant. The exponent n is not constant, but the logarithmic curves are nearly linear at high velocities. For this region LATTES *et al*[98] give an empirical relationship for singly charged particles,

$$E = 0{\cdot}262M^{0{\cdot}425}R^{0{\cdot}575}$$

where M is expressed in units of the proton mass, R is in microns and E in Mev.

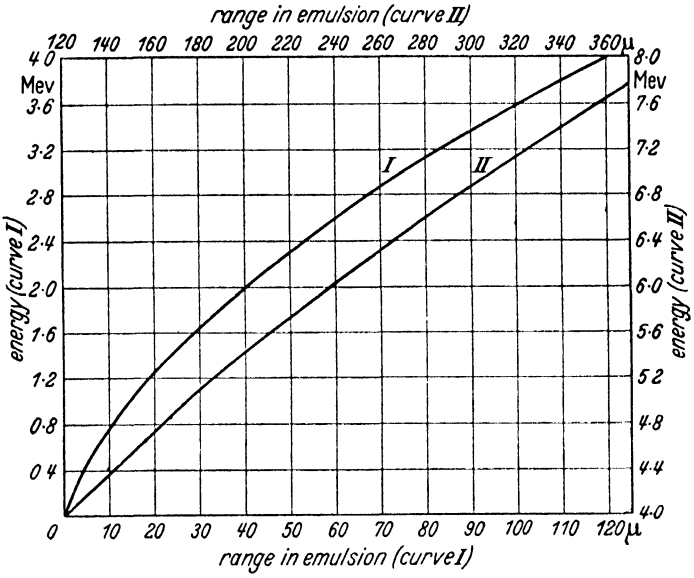


Figure 6a. Range-energy curves for protons ; Ilford and Kodak emulsions

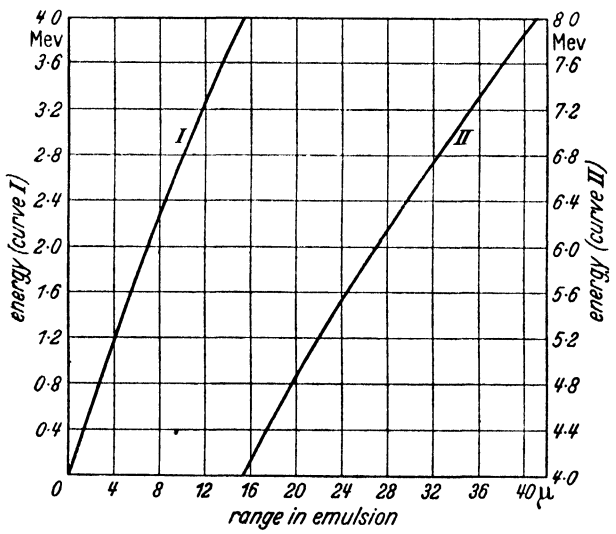


Figure 6b. Range-energy curves for α-particles; Ilford and Kodak emulsions

For lower energies, where the logarithmic curve cannot be approximated to a straight line, one can calculate the range of a particle (Z, M) of energy E by means of the formula $R_{Z,M}(E) = (M/Z^2)R_H(E/M)$ where Z and M are expressed in proton units and $R_H(E/M)$ is the range of a proton of energy E/M. This relation is not accurate for particles other than singly charged owing to the capture and loss of electrons near the end of the range.

Straggling—The ranges in the emulsion of particles of a given energy show fluctuations similar to those in air, but owing to the discontinuous character of the track, the small number of grains and their finite size, the straggling in the emulsion is usually greater than in air. The straggling γ can be determined from the distribution of the ranges of tracks produced by a homogeneous group of particles, namely

$$\gamma = \left(\frac{\pi}{2}\right)^{\frac{1}{2}} \left[\frac{\Sigma_N (R - R_0)^2}{N}\right]^{\frac{1}{2}}$$

where R_0 is the average range of the particle and N the total number of tracks in the group. Another way of expressing straggling is to give the half width value $2\Delta R$ *i.e.* the width of the distribution curve at half its maximum height.

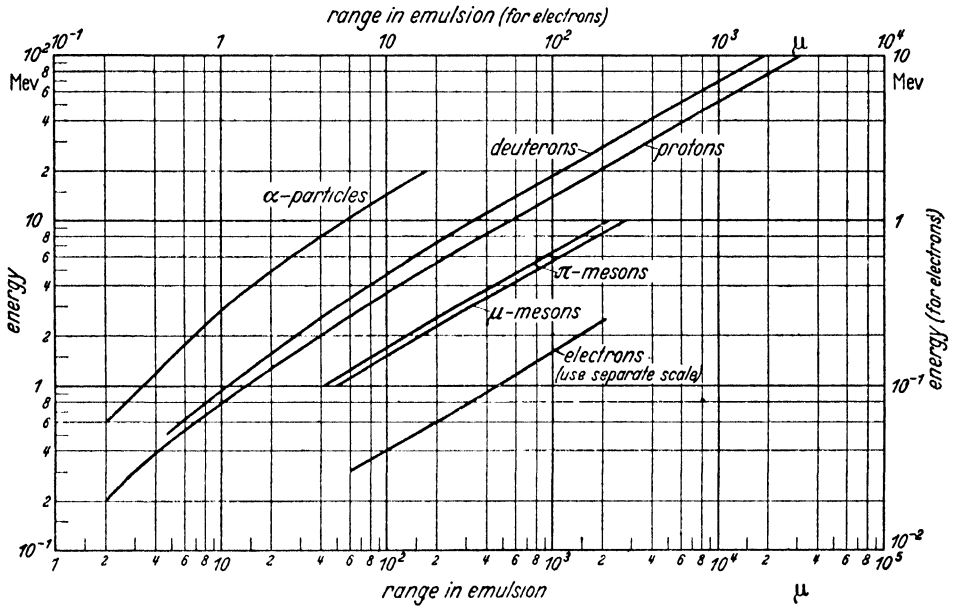


Figure 7. Range-energy curves for various particles

If the distribution of ranges follows a Gaussian law it is easy to show that

$$\Delta R = 2\gamma(\ln 2)^{\frac{1}{2}}\pi^{-\frac{1}{2}} = 0{\cdot}94\gamma$$

Usually the straggling is expressed as a percentage of the range $\Delta R/R$, or of energy $\Delta E/E = n\Delta R/R$ where n is the range-energy exponent mentioned above (n is nearly $\frac{1}{2}$ at high energies). These expressions determine the resolution of range or energy obtainable in the emulsion.

The straggling of various particles has been measured by POWELL *et al*[21], DEMERS[4], LATTES *et al*[89] and ROTBLAT[94] and calculated by CUER[99].

Figure 8 shows the variation of the percentage straggling with energy for protons and α-particles from 0·4 to 8 Mev (ROTBLAT[94]). For comparison the corresponding curve for air is also given (LIVINGSTON and BETHE[100]).

Measurement of grain density—The density of grains of a given track is a measure of the rate of loss of energy of the particle in the emulsion. The relationship between the energy loss and the grain density is not a simple one, since the phenomena of space charge and recombination of ions will tend to reduce the relative sensitivity of the emulsion at very high specific ionizations. Various formulae expressing this dependence have been suggested by DEMERS[4] and BLAU[101]; the experimental results of ZAJAC[102] agree better with Demers' formula. In general we can write

$$dN/dR=f_1(dE/dR)$$

where dN/dR is the number of grains per unit range of track and dE/dR is the rate of energy loss. Experimental curves for this relation in *NT4* emulsions are given by BROWN *et al*[27].

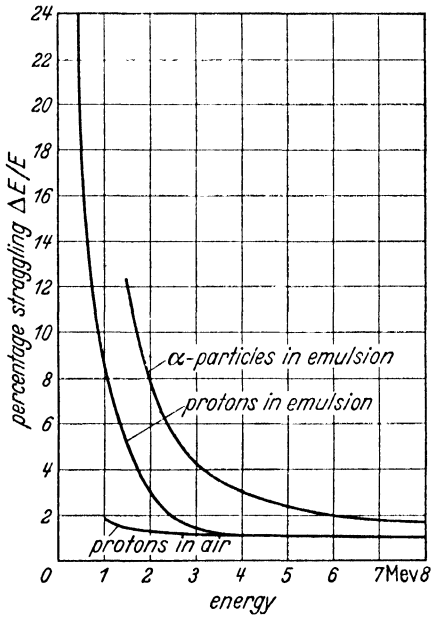


Figure 8. Energy straggling for proton and α-particle tracks in emulsions

Assuming that the loss of energy in the emulsion is governed by a process similar to the ionization in air, the specific energy loss is independent of the mass of the particle and dependent only on its charge and velocity. We can then write

$$dE/dR=Z^2 f_2(v)=Z^2 f_3(E/M)$$

On integration this gives

$$E=M f(RZ^2/M)$$

If we assume

$$f(RZ^2/M)=K(RZ^2/M)^n$$

we obtain the range-energy relation quoted above.

From the relation between grain density and energy loss we obtain similarly an expression for the number of grains in a track; for singly charged particles the number is $N=M F(R/M)$. This shows that the total number of grains in the track of a given particle depends on its mass. If, therefore, the grain density is plotted as a function of the residual range, different curves will be obtained for particles of different masses. Thus the mass of the particle can be determined from the measurement of the grain density coupled with range measurement.

The usual procedure is to count the number of grains in successive equal intervals along the trajectory of the particle. *Figure 9* shows the results of such measurement by LATTES *et al*[124] for α-particles, tritons, protons and π and μ mesons, in Ilford *C2* boron loaded emulsions. The logarithm of the number

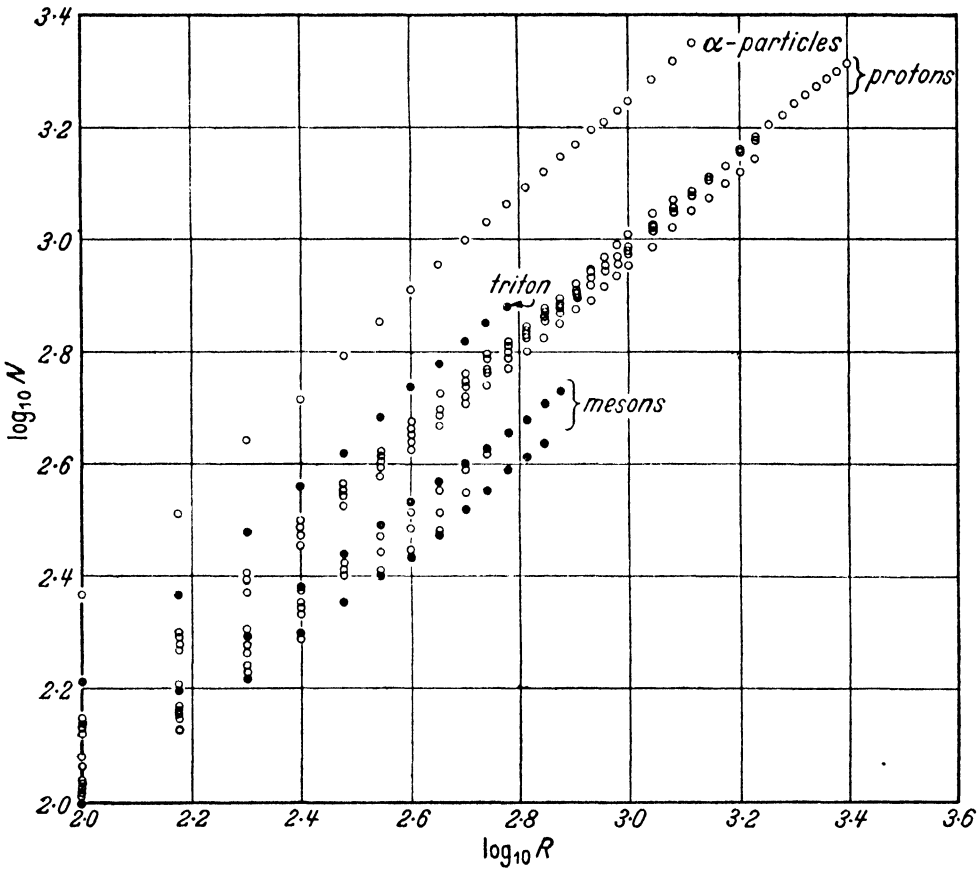


Figure 9. Variation of grain density N with residual range R for various particles, in Ilford C2 boron loaded emulsion. One scale division $=0{\cdot}85\mu$

of grains is here plotted against the logarithm of the corresponding range. As is seen the points lie very closely on a straight line over most of the range. We can, therefore, put

$$F(R/M)=K(R/M)^m \text{ and } N=KM^{1-m}R^m$$

An empirical formula for the number of grains in a section of the track of residual range R is given by LATTES *et al*[98] for *C2* boron loaded emulsions:

$$N=76\times M^{0.289}R^{0.711}$$

where M is again expressed in units of the proton mass and R is in microns. On the basis of this relationship and assuming that all π and μ mesons observed were singly charged, the ratio of their masses was determined (LATTES *et al*[98]).

Instead of the N-R curves one can use the relationship between the specific grain density dN/dR and the residual range. From the previous considerations we can deduce the expression

$$dN/dR = \phi(R/M)$$

which shows that if we plot dN/dR against R, for various singly charged particles, then the residual ranges corresponding to the same grain density will be in the same ratio as their masses (LATTES *et al*[98], BLAU[101]).

These methods of measuring masses are liable to systematic errors. Owing to the latent image fading the grain density of tracks produced at various times will differ considerably even for particles of the same mass. Another source of error is introduced by the non-uniform distribution of grains of silver halide in the gelatin. In some emulsions, 'islands' are observed in which the silver halide concentration is much higher or lower than the average. The variation of the degree of development with depth and the fore-shortening of tracks of large angles of dip will also affect the grain density of tracks at various depths in the emulsion. For these reasons the determinations of mass made by this method gave initially large errors. Recently, however, the improvements in the qualities of emulsions and methods of development have made it possible to use grain counting as an accurate and quantitative method of measuring the mass of a particle[27].

Small angle scattering—A charged particle traversing the emulsion will suffer frequent small angle deflections as a result of the Coulomb interaction at collisions with nuclei in the emulsion. The track will, therefore, not be a straight line but curved. Since the average angle of scattering will depend, among other factors, on the mass of the particle the observation of this angle, combined with range or grain density measurement, can be used as a method to determine the mass. This method was first suggested by BOSE and CHOUDHURI[103] and was employed recently by PERKINS[104], LATTIMORE[105], GOLDSCHMIDT-CLERMONT *et al*[106] and VAN DEN GRINTEN[107].

The theory of small angle scattering was given by WILLIAMS[108]. According to him the individual values of the angles of deflection show nearly a Gaussian distribution and the mean square scattering angle of a particle of velocity v and momentum p in passing through a thickness x of a medium of atomic number z is

$$(\Theta^2)_{av} = \frac{4\pi e^4 z^2 N x}{p^2 v^2} \ln\left(\frac{\Theta_{max}}{\Theta_{min}}\right)$$

where N is the number of atoms per cc in the medium, $\Theta_{min} = mcz^{\frac{1}{3}}/181p$ (m is the electron mass) and Θ_{max} is the smallest angle which can be recognized as a single deflection[105].

This formula shows that the average angle of deflection is approximately inversely proportional to the energy. Deflections will therefore occur with

increasing frequency towards the end of the track. By noting the frequency of deviations the direction of flight of the particle can thus be found.

As seen from the above formula the average deviation depends on the velocity of the particle, and therefore for a given residual range the mean angle of scattering will be different for particles of various masses. For each type of particle a curve can be drawn giving the relation between the angle of scattering and the residual range. A comparison of the experimental values with these curves enables the mass of the particle to be determined. Alternatively, curves can be drawn for the angle of scattering as a function of grain density (BOSE and CHOUDHURI[103]).

The usual method to determine the small angle scattering is to use a scanning projection microscope and make drawings of each track on the screen. The track can then be divided into a series of segments and the changes in direction between the segments or the angle between consecutive chords can be measured. Another method suggested by GOUDSMIT and SCOTT [109, 110] is to measure the difference between the actual length of a given portion of a track and the straight line joining its ends.

In the case of 'reulativistic particles' from cosmic rays the measurement of small angle scattering is greatly facilitated and the precision of results much improved by making use of the micrometer fitting to the stage of the *M.4005* microscope: the deflection of the track for every 100μ of lengt is read on the eyepiece scale (POWELL*).

Magnetic field deflection—One shortcoming of the emulsion technique, as compared with the cloud chamber, is that it is normally impossible to perform magnetic deflection experiments. Owing to the shortness of the track one would have to apply fields of the order of millions of gauss in order to be able to observe the radii of curvature. In addition, the small angle Coulomb scattering would greatly reduce the accuracy of such experiments. The use of the reflecting microscope, coupled with the sandwich method of arranging emulsions, has, however, opened the possibility of applying magnetic field measurements to the emulsion technique as well.

POWELL and ROSENBLUM[111] and BARBOUR[112] have used this method for the determination of the mass of mesons. Two plates are placed between the poles of an electromagnet, with the emulsions facing each other and separated by an air gap of several millimetre. A charged particle entering the gap from one emulsion will describe a spiral path in the air gap before entering the second emulsion. If the track of the particle in both emulsions can be identified, then from the observed change in the direction of motion while traversing the air gap, and from the distance between the points of exit and entry, the value of $H\rho$ and therefore the momentum of the particle can be calculated. If the particle comes to rest in the second emulsion the

* Private communication

observed range gives its velocity. Hence the mass of the particle can be determined. This method can, of course, also be used to determine the sign of the charge of the particle, simply by observing the direction of the deflection in the magnetic field.

The main experimental difficulty is the identification of the track in passing from one emulsion to the other. To help in the juxtaposition of the plates, POWELL and ROSENBLUM[111] used a grid of dots produced by means of an exposure to x-rays. The matching of the tracks can be checked by observing the angle of dip and the grain density at the points of exit and entry. In Powell's experiment the tracks were viewed by means of a reflecting microscope; BARBOUR[112] used plates coated on very thin glass and could thus work with an ordinary microscope.

According to FRANZINETTI[113] the mass of a particle can be determined by this method with an accuracy of about 5 per cent, which compares very well with the accuracy obtained in the cloud chamber.

Determination of charge—The determination of mass by the methods described up to now can be applied directly to singly charged particles, protons, mesons and electrons. It is possible to judge whether the particle carries a single charge by observing the grain density towards the end of the track. This is a characteristic quantity for a given emulsion. If the density is higher than this the particle carries more charges and the problem is then to determine the charge in addition to the mass.

The problem became of importance recently with the discovery, from experiments with free balloons, that the cosmic rays at very high altitudes contain heavy elements of atomic numbers reaching 50 (FREIER *et al*[114, 115], BRADT and PETERS[116]). Very long tracks of such nuclei, of energies of the order of 100,000 Mev, have been observed. Some of these pass right through a whole stack of photographic plates, giving a range in glass of over 20 cm (KAPLAN *et al*[117]).

The identification of these particles is simplified by the fact that at such high energies the atoms are completely stripped of electrons. These particles are therefore bare nuclei during most of their flight. Since the ratio of neutrons to protons is very nearly one for most light elements, it is justifiable to assume $M/Z=2$, where the mass and charge are relative to those of the proton.

If the appearance of the track is such that individual grains can be observed, the method of grain counting, coupled with the measurement of the range, can be used to determine the mass and, therefore, the charge, much in the same way as described earlier (BRADT and PETERS[116]). Most of these tracks, however, have a ' solid ' appearance and other means have to be used for their identification.

Two methods have been developed for this purpose. The first is based on the counting of the number of δ-rays, the secondary electrons ejected by the heavy particle from the atoms through which it passes. The emission of δ-rays can be seen in the photomicrograph in *Figure 15* which shows on the left side a track of a particle of $Z=19$. The use of emulsions sensitive to electrons makes the observation of δ-rays much easier (COSYNS *et al*[118]). The number of secondary electrons produced by a particle of charge Z and velocity $\beta(=v/c)$ has been calculated by MOTT[121]. According to his formula the number of δ-rays, with energies lying between certain limits, produced per unit of length is given by $N_\delta = KZ^2/\beta^2$, where K is a factor depending on the energy limits of the observed δ-rays and on the density of electrons in the emulsion. This factor can be determined by counting δ-rays produced by α-particles of a known energy. In order to determine the value of β the range of the track R has to be measured. Since the range is a known function of β and Z, curves can be drawn of N_δ against R for various values of Z. From these curves the value of Z of the particle can be found (BRADT and PETERS[116]). A more quantitative method has been worked out by SÖRENSEN[119], who measured the number of δ-rays in successive equal intervals along the track of a particle. If the number of δ-rays per given length of track is plotted against the residual range, the resulting distribution has a maximum for a certain value of β, the height of this maximum being proportional to the square of the charge of the particle. By comparing with the maximum obtained for α-particles the charge can be determined without ambiguity. *Figure 10* shows tracks of helium, lithium, beryllium and boron nuclei, on which the increasing number of δ-rays can easily be seen.

The second method is based on the observation of the thinning down of the track near the end of its range. The tracks of very heavy particles appear as very thick lines. This is partly due to the buckling of the column of silver grains during development, which occurs if there are too many developable grains, and partly to the large number of secondary electrons ejected. As the particle slows down, the specific ionization and the number of secondaries increases and therefore the track becomes thicker. But when the speed of the nucleus has been reduced to a value of the same order of magnitude as that of the electrons in the various atomic shells the nucleus will begin to capture electrons, thus reducing its effective charge and consequently the thickness of the track. The track of a highly charged particle will therefore show a maximum thickness at a certain distance from the end of the range (HEITLER *et al*[16]). The ' thin down ' length obviously depends strongly on the charge of the particle and this dependence can be calculated theoretically (FREIER *et al*[115]). The observation of the ' thin down ' length thus makes possible the determination of the charge (FREIER *et al*[115], BRADT and PETERS[116], HODGSON and PERKINS[44]).

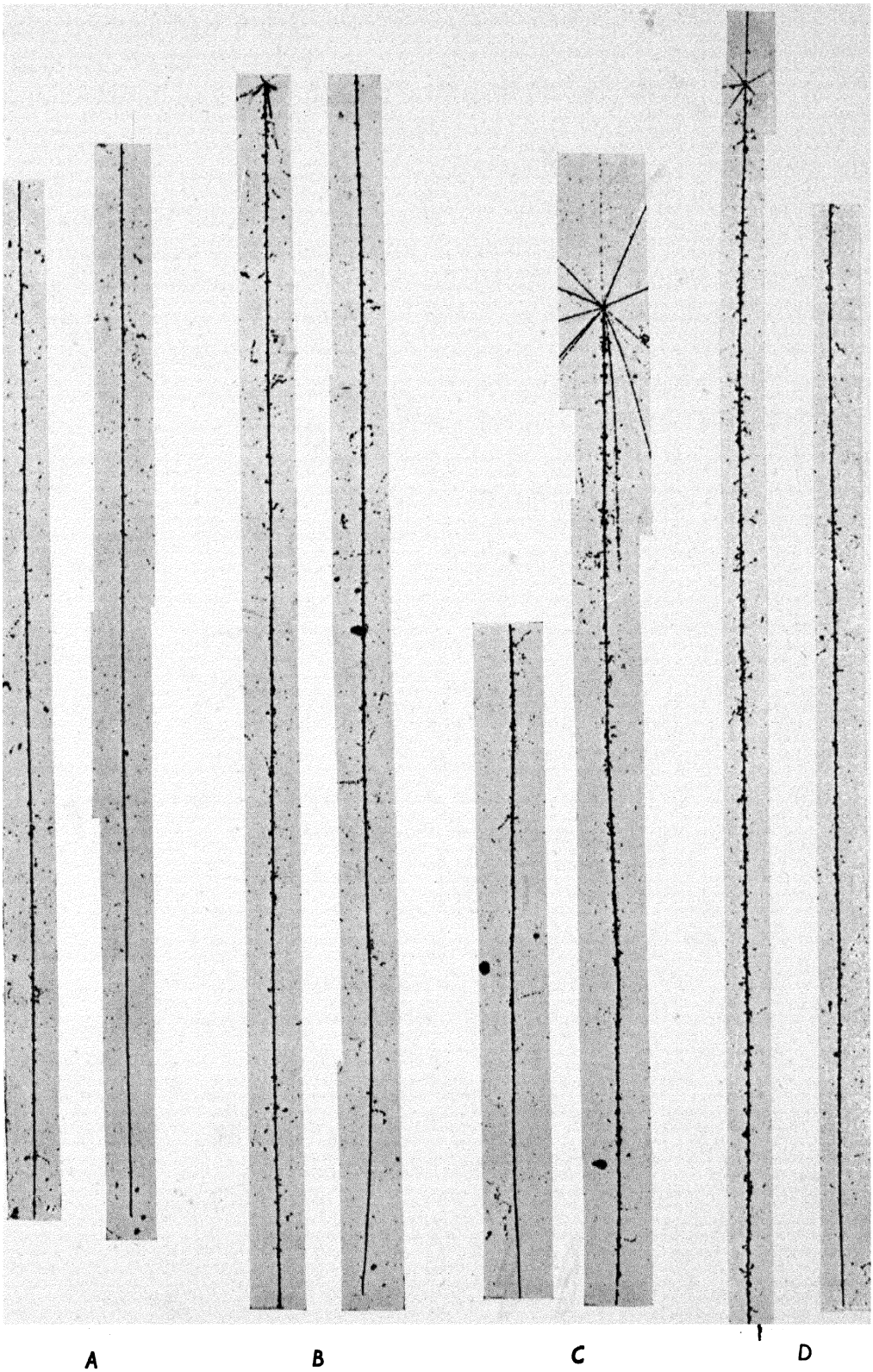


Figure 10. Tracks of A *helium,* B *lithium,* C *beryllium,* D *boron nuclei of very high energy, showing* δ*-rays (by courtesy of Professor Powell)*

(*To face p. 62*)

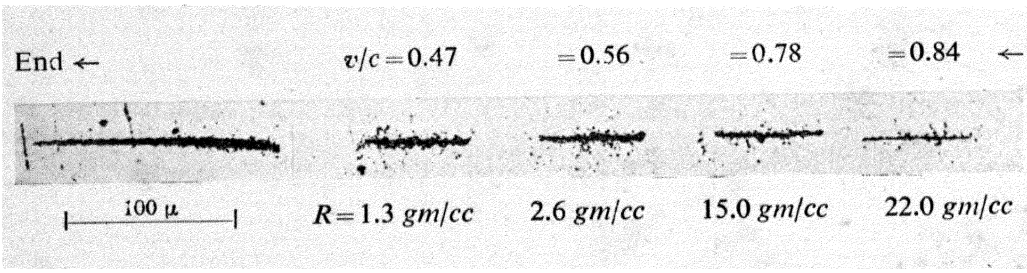


Figure 11. Track of iron nucleus of energy 62,000 *Mev showing thinning down effect The various sections are fragments of the track in each emulsion of the stack (by courtesy of Professor Peters)*

(To face p. 63)

The photomicrograph in *Figure 11* (BRADT and PETERS[120]) shows the thinning down of a track of an iron nucleus ($Z=26$) which has passed through 23 plates and had an initial energy of 62,000 Mev.

Angular distributions and energy spectra—For many applications in nuclear physics it is important to determine the angular distribution of particles or their energy spectrum. For this purpose the number of observed tracks in various angle or energy intervals is plotted against the angle or energy. While the actual measurement of angles, or the counting of tracks of a given length, does not represent any difficulties there are limitations to the accuracy of such results. For angular distributions an error will be introduced at large angles of dip, due to the uncertainty of the shrinkage factor correction and to the probability of such a track escaping observation altogether. In energy distributions a serious limitation results from the small thickness of the emulsion. Tracks of large angles of dip, or long tracks even at small angles of dip, will run out of the emulsion, making it impossible to measure their range and thus to determine the group of energy to which they belong.

In order to obtain the true energy spectrum a correction has to be made for the escape from the emulsion. Formulae giving this correction for various cases have been calculated by RICHARDS[122], CHAMPION and POWELL[76], GIBSON and LIVESEY[123], GREEN and LIVESEY[61] and LATTES *et al*[124]. In these calculations it has been assumed that the track is straight. Actually the small angle multiple scattering, which is so pronounced in the concentrated emulsions, makes the probability of escape much greater. POWELL and OCCHIALINI[125] have shown that the ignoring of the Coulomb scattering introduces a serious error in the energy distributions. Although the effect of scattering on the escape correction can be calculated, it is much sounder experimentally to minimize the fraction of escaping particles by working with the thickest possible emulsion, when distributions involving long tracks are to be determined.

APPLICATIONS

Applications to nuclear physics—The photographic emulsion technique has been applied in a very great variety of problems in nuclear physics. It has been used to determine energy spectra, to measure cross sections, to estimate half-lives, as a detector of very weak activities, or of particles in α- and β-ray spectrometers, and as a method of measuring γ-ray energies and neutron fluxes. Among these applications there are some to which the emulsion technique is particularly suitable because of the continuous sensitivity of the emulsion, the small space it occupies, and the simplicity of the technique.

One of the main uses of emulsions in nuclear physics is the investigation of the scattering of, and disintegrations by, charged particles. A beam of

mono-energetic particles is made to impinge on a foil or to collide with atoms of a gas filling a chamber. The particles, elastically and inelastically scattered through various angles, as well as the charged particles resulting from disintegrations emitted in various directions, enter a photographic plate at a small angle of incidence, leaving in it tracks of their paths. A scattering camera, in which particles scattered or emitted through a range of angles from 10° to 170° can be recorded in one experiment, has been described by POWELL (CHADWICK *et al*[77], GUGGENHEIMER *et al* [126], HEITLER *et al*[127], MAY *et al*[128]) and others (RUBIN[129], ROSEN *et al*[130], MARTIN *et al*[131]). For each angle of observation one can plot a histogram of the number of tracks against their length, and in this way obtain the energy spectrum of the particles emitted at a given angle with the original direction of the beam. An example of such a histogram obtained by BURROWS * is given in *Figure 12*, which shows the observations, at an angle of 75°, of the scattering and disintegration products of oxygen bombarded with 7·7 Mev deuterons. An analysis of the histogram shows that the groups 1, 2, 3, 5, 6 and 7, are due to protons emitted in the reaction $O^{16}(d,p)O^{17}$, in which the O^{17} nucleus was left in various states of excitation. Group 4 is due to deuterons elastically scattered from the oxygen nucleus, and groups 8 and 9 to α-particles from the $O^{16}(d,\alpha)N^{14}$ reaction, with the nitrogen nucleus formed in its ground and first excited state. Thus, from one exposure evidence can be obtained of the existence of many nuclear energy states and their energy values accurately measured. By plotting the number of particles from a given group against the angle of emission one can determine the angular distribution, or the probability that particles resulting from a given reaction will be emitted in a given direction. The

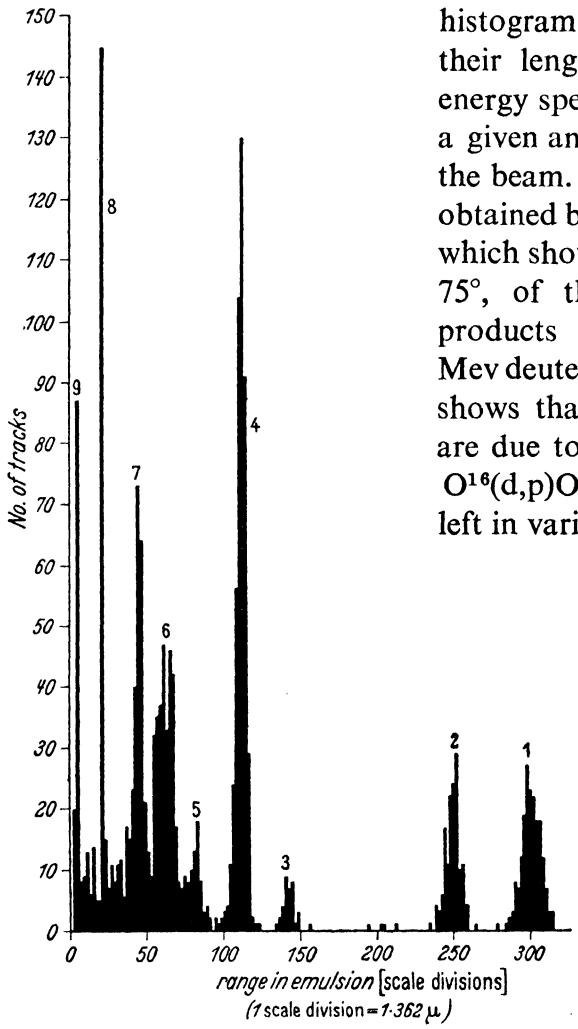


Figure 12. Histogram of scattering and disintegration products of oxygen bombarded by 7·7 Mev deuterons at 75°

* Unpublished results

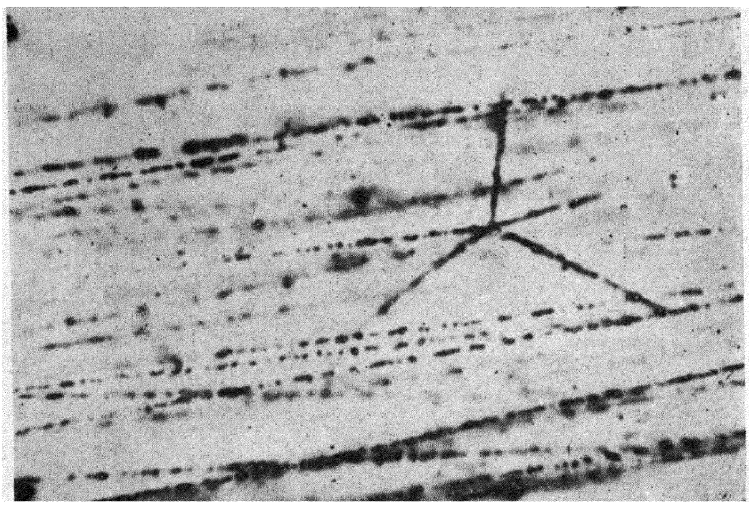


Figure 13. Tracks of four α-particles resulting from the disintegration of nitrogen by deuterons

(*To face p. 65*)

knowledge of such distributions is of great theoretical value. The main advantage of this method is the enormous wealth of information which can be obtained with an exposure lasting only a few hours. Compared with other methods it is extremely economical in the time which it occupies the cyclotron or other accelerators of particles.

The possibility of recording lengths and orientations of all products of a disintegration simultaneously makes possible the verification of the laws of conservation of energy and momentum in nuclear reactions. An example of this is given in *Figure 13*, which shows the disintegration of a nitrogen nucleus by a 9 Mev deuteron into four α-particles. Here the photographic plate was placed in the beam of deuterons and the disintegrated nitrogen nucleus was one of the constituents of the emulsion. By measuring the length of track of each α-particle and its orientation relative to the direction of the deuteron it was possible to establish that both the energy and momenta are conserved (FOWLER, BURROWS and CURRY[132]). The satisfactory results obtained in such experiments justify the use of this method for the determination of the energy and momenta of neutral particles, which may be emitted in some reactions, and which do not leave a track in the emulsion (LATTES and OCCHIALINI[133]).

Although neutrons are not detected directly they can be observed by means of the recoils or disintegrations which they produce in the emulsion. In the case of fast neutrons the tracks of proton recoils are observed which result from collisions of neutrons with hydrogen atoms in the emulsion. The energy of the recoil proton is related to that of the neutron by the formula

$$E_p = E_n \cos^2\theta$$

where θ is the angle between them. If, therefore, one measures the length of the proton track and its orientation relative to the direction of the neutron beam, the energy of the neutron can be calculated. This method has been applied by many investigators (POWELL[17, 19], RICHARDS[122], GIBSON and LIVESEY[123], LIVESEY and WILKINSON[134], PECK[135], GREEN[136], GROSSKREUTZ[137]) to the determination of energy spectra of neutrons produced in various reactions. When plotting such spectra, a correction has to be made for the variation with energy of the proton-neutron scattering cross section. KEEPIN and ROBERTS[138] used emulsions loaded with lithium enriched with Li^6 and determined the energy of fast neutrons by measuring ranges and angles of α-particles and tritons resulting from the disintegration of Li^6. Slow neutrons can be detected either *via* the protons emitted from the nitrogen in the emulsion in the N^{14} (n,p) reaction (CUER[139,140]) or by using plates loaded with lithium, boron or uranium.

The fission process and particularly the emission of α-particles accompanying some cases of fission of uranium has been the subject of study of many people (MYSSOWSKY and JDANOFF[141], DEMERS[42], GREEN[61], TSIEN[142,143], WOLLAN[144]). By observing the point of origin of the track of the α-particle in relation to the fission fragments it was concluded that the interval of time

between fission and emission of the α-particles is less than 2×10^{-14} sec (DEMERS[42]). The emission of α-particles was also observed in the photofission of uranium (TITTERTON and GOWARD[145]).

The development of emulsions sensitive to particles of low ionizing power has greatly increased the scope of applications of the photographic emulsion technique to work with very high energy particles produced in synchrocyclotrons and other accelerators. The first artificial production of mesons in the 184 inch synchrocyclotron at Berkeley was recorded in a photographic emulsion (GARDNER and LATTES[146,147], OCCHIALINI and POWELL[148]) and more recently the production of mesons by means of 335 Mev γ-rays in the Berkeley synchrotron (MCMILLAN and PETERSON[149]).

Applications to cosmic rays—The most striking successes of the emulsion technique have been achieved in the study of cosmic rays. The great advantage of the photographic plate is that it can be put at the top of a mountain and left there for events to be recorded automatically, or it can be sent up in balloons to very great heights. The production of emulsions sensitive to particles at minimum ionization has removed the last shortcoming of this technique and now it is possible to obtain a full record of all phenomena due to charged particles in cosmic rays.

The outstanding discovery during the last few years was that of the π meson, of mass 276 electron masses (OCCHIALINI and POWELL[48], LATTES *et al*[49], POWELL[150]). The photograph in *Figure 14* shows a π meson decaying into a μ meson which, in turn, decays into an electron. The possible existence of another still heavier meson of about 1,000 electron masses has been suggested by several authors (BROWN *et al*[27], YAGODA *et al*[151], WAGNER and COOPER[152]) but the evidence is, as yet, inconclusive.

The discovery of π mesons has brought out another spectacular advantage of the emulsion technique, namely its application to the study of phenomena which take place in a very short time (OCCHIALINI and POWELL[153]). A particle of a given energy is brought to rest in the emulsion in a time several thousand times shorter than in a gas. Thus a very short-lived particle, which moving in a gas would decay in flight, may in the emulsion come to rest before its decay, making it thus possible to observe the effects it produces at the end of its range. By observing the distance travelled by the particle before decaying an estimate can be made of its lifetime. The order of magnitude of lifetimes measurable by this method is very short; a particle of an energy of several Mev will have a time of flight of only 10^{-12} second. By means of such methods it was possible to establish that the mean life of a π meson was 6×10^{-9} second (CAMERINI *et al* [154]).

Apart from the discovery of mesons the photographic plates have revealed many new phenomena which take place in cosmic rays. The stars produced by

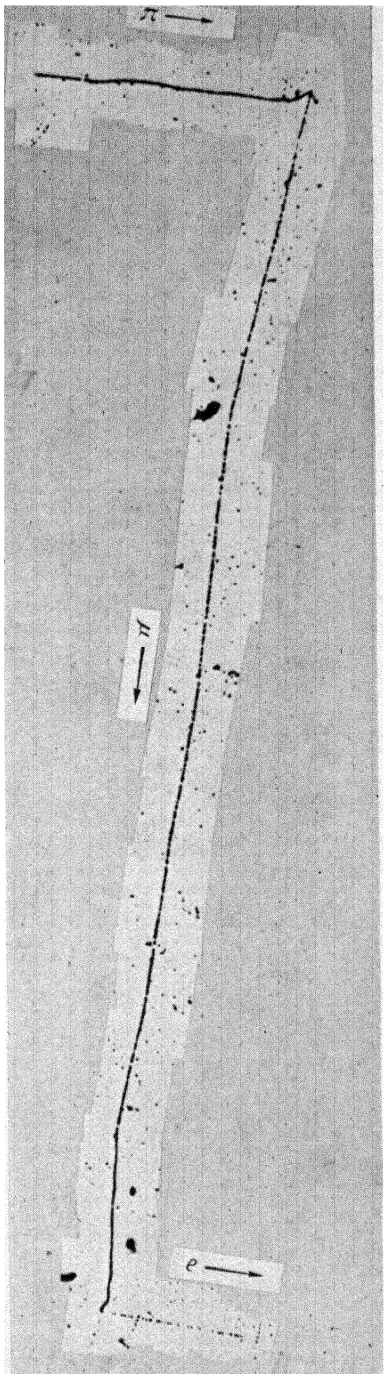


Figure 14. Track of π meson decaying into a μ meson and then into an electron (by courtesy of Professor Powell)

(To face p. 66)

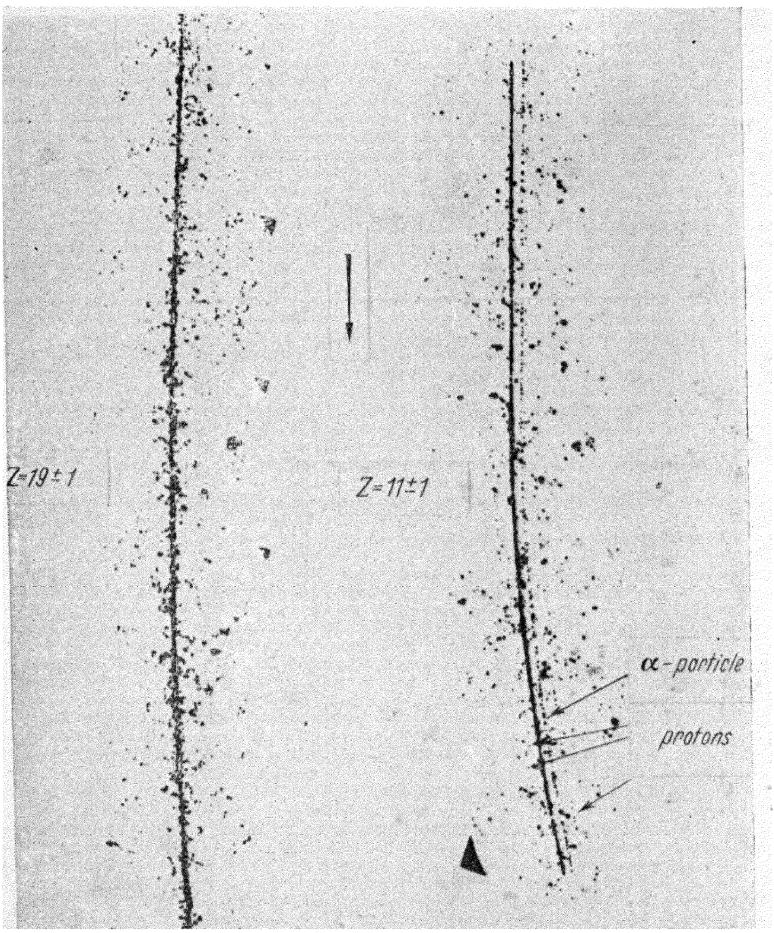


Figure 15. Narrow shower, on the right, produced by the disintegration of a potassium nucleus, left (by courtesy of Professor Peters)

(*To face p. 67*)

cosmic rays (OCCHIALINI and POWELL[155]), which are due to disintegrations of nuclei of atoms in the emulsion, have been the subject of much study, particularly by PERKINS[104, 156-158] and his colleagues (HARDING *et al*[159, 160]) who investigated the energy and angular distribution of the particles in stars. In most cases the distribution can be explained by the evaporation theory of nuclear reactions, although in some cases localized ' boiling off ' of particles has been established (HARDING *et al*[159], THOMSON[161]). The nature of the primary radiation responsible for the production of the stars is still not established (GEORGE and JASON[162], THOMSON[163], PERKINS[164]).

An interesting conclusion from these experiments can be drawn about the ranges of nuclear forces. It has been suggested by BAGGE[165] and ROSENFELD[166] that the energy distribution of the evaporated particles depends in a critical manner on the range of nuclear forces. HARDING *et al*[159] found in this way a value of 2×10^{-13} cm for the range of nuclear forces in good agreement with results from other fields.

The primary cosmic rays, consisting of heavy nuclei, observed at altitudes up to 140,000 ft were found to undergo various types of collisions with nuclei (BRADT and PETERS[167], BROWN *et al*[168], LEPRINCE-RINGUET *et al*[169], PICKUP and VOYVODIC[170], HORNBOSTEL and SALANT[171], OSBORNE and FELD[172]). In some cases such a particle may pass right through the target nucleus with an undiminished charge and almost undeflected, ejecting only a few nucleons from it. In other cases the colliding nucleus may be completely destroyed in a large nuclear explosion. Finally cases have been observed when part of the nucleus was sheared off in the collision and the remainder of it, partly dissociated into nucleons, proceeded with the original momentum. An example of such a narrow shower is shown in *Figure 15*, in which a nucleus of $Z=19$, the track of which is seen on the left part of the picture, was broken up in the glass between the two emulsions into a heavy fragment of charge 11, one α-particle and six protons[167]. Striking results were obtained with emulsions sensitive to particles at minimum ionization. Apart from tracks of heavily ionizing particles, most disintegrations contain many tracks of ' relativistic particles ' *i.e.* moving with velocities near that of light. Since their grain density is that of minimum ionization it is difficult to determine their masses; their characteristic feature is that they are emitted in fairly narrow bundles in the forward direction of the primary particle. A photomicrograph of such a star containing a shower of eleven relativistic particles is shown in *Figure 16*.

The study of these phenomena has only just begun and far reaching results may be expected soon from this field of application of the photographic emulsion.

Applications to geology and mineralogy—The use of the emulsion technique for the study of the distribution of radioactive elements in rocks has been described by CURIE[173] and others (POOLE and BREMNER[174], PICCIOTTO[175],

COPPENS[176]). A sample of rock is placed against a photographic plate for a suitable length of time and, after processing, examined for α-particle tracks. By prolonged exposures very small quantities of radioactive materials can be detected in this way. It is usually possible to observe and identify the tracks due to α-particles from the uranium and thorium series. By counting the number of single tracks and multiple stars from the successive disintegrations of members of these radioactive families it is possible to determine the period of formation of the rock.

CUER[177] used this method for the prospecting of uranium. The variation of the activity within various sections of the mineral, or from various faces of crystals, has also been studied (YAGODA[178], MATHER and KURIE[179]). A detailed account of the applications of nuclear emulsions in geology and mineralogy is given by YAGODA[3a].

Applications to health monitoring—The blackening produced by radiations in ordinary photographic emulsions is employed as a standard method of estimating doses of radiations received by people working with radioactive materials or near radiation producing instruments. The sensitivity of this method can be greatly increased by observing the tracks of individual particles. The most important application is the monitoring of dosages of slow and fast neutrons. The protons resulting from the slow neutron disintegration of nitrogen in the emulsion have been employed for this purpose (CHEKA[50]). Far better, however, is the use of emulsions impregnated with boron or lithium and the observation of the tracks of the particles from the $B^{10}(n,\alpha)$ and Li^6 (n,α) reactions (ROTBLAT[180], SHAPIRO and BARNES[181], TITTERTON[182]). The cross sections for these reactions are so high that it is possible to detect even a very low flux of thermal neutrons. With plates impregnated with boron a daily tolerance dose of slow neutrons will give about 100 tracks per field of view of 100 micron square; thus a result of a good statistical accuracy can be obtained in a short time.

One can also utilize for this purpose the fission tracks produced by slow neutrons in emulsions impregnated with uranium. It is not necessary to know the concentration of uranium since the neutron flux can be calculated directly from the observed ratio of α-particle tracks to fission tracks. Owing, however, to the continuous production of α-particle tracks such plates can be used only in experiments of short duration.

Applications to biology and medicine—One of the methods of using radioactive isotopes as tracers in investigations of biological and medical processes is the so-called radioautograph technique. In this method a sample of tissue containing a radioactive substance is placed against an ordinary photographic plate. The area of blackening of the plate indicates the distribution of the radioactive substance in the tissue. The scope of this technique can be greatly extended by using nuclear research emulsions for the observation of individual

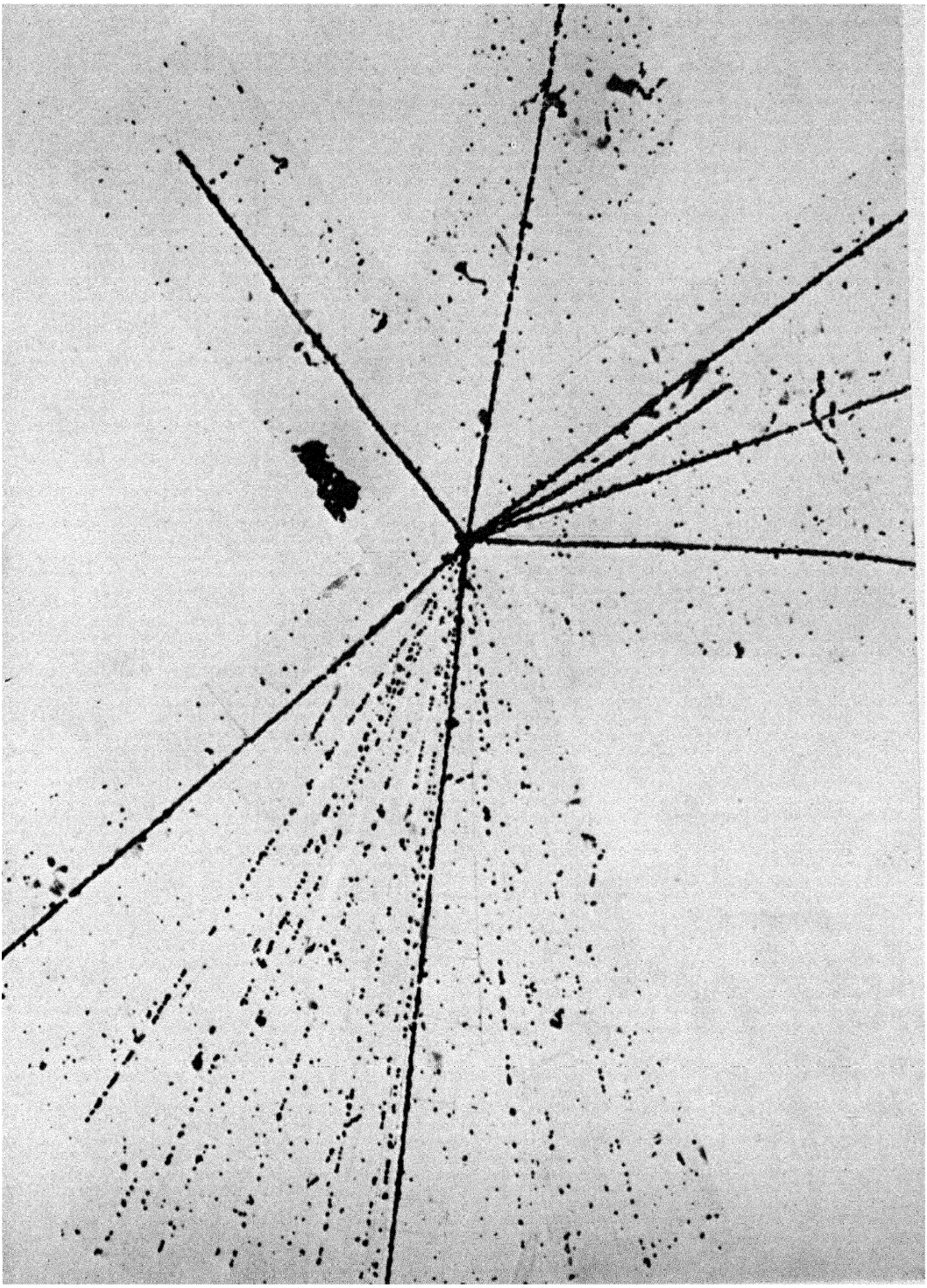


Figure 16. Cosmic ray disintegration of a nucleus containing a shower of eleven singly chargea particles moving with relativistic velocity (by courtesy of Professor Powell)

(To face p. 68)

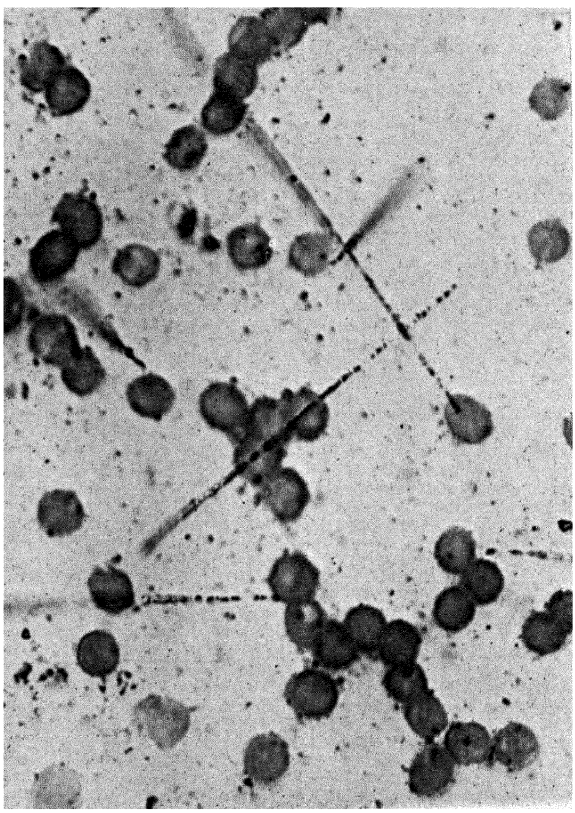


Figure 17. Radioautograph showing emission of α-particles from blood cells

(*To face p. 69*)

particles. In this way it is possible to locate the position of a radioactive atom with an accuracy of 0·1—0·2 micron, which makes this method of particular value to studies concerning cells (DEMERS and FREDETTE[183], ENDICOTT and YAGODA[184], ROTBLAT[185]).

One of the first applications of this method was the investigation of the distribution of lead in the organism (ANSELL and ROTBLAT[185]). Thorium B was injected into a rabbit and drops of blood taken at various time intervals were smeared over a photographic emulsion. When the plates were developed and stained, tracks of α-particles emitted from thorium C and C$'$ could be seen on the background of the blood cells. A photomicrograph of a field of view showing the tracks and cells is given in *Figure 17*. An analysis of the distribution of lengths and angles of the track makes it possible to decide whether the lead penetrated inside the cell or remained on its surface.

The development of electron sensitive emulsions opens the possibility of extending this method to practically all radioactive tracers, and this will undoubtedly prove to be of great value for the study of many problems in biological and medical research.

REFERENCES

1 POWELL, C. F. and OCCHIALINI, G. P. S. *Nuclear Physics in Photographs* Oxford, 1947
2 SHAPIRO, M. M. *Rev. Mod. Phys.* 13 (1941) 58
3 YAGODA, H. *Nucleonics* 2 (1948) 2
3a —*Radioactive Measurements with Nuclear Emulsions* New York, 1949
4 DEMERS, P. *Canad. J. Research* 25 (1947) 223
5 WEBB, J. H. *Phys. Rev.* 74 (1948) 511
6 KINOSHITA, S. *Proc. roy. Soc. A* 83 (1910) 432
7 REINGANUM, M. *Phys. Z.* 12 (1911) 1076
8 BLAU, M. *J. Phys. Rad.* 5 (1934) 61
9 —and WAMBACHER H. *Akad. Wiss. Wien.* 143 (1934) 285
10 WAMBACHER, H. *ibid* 140 (1931) 271
11 MYSSOWSKY, L. and TSCHISHOW, P. *Z. Phys.* 44 (1927) 408
12 JDANOFF, A. *J. Phys.* 6 (1935) 233
13 TAYLOR, H. J. *Proc. roy. Soc. A* 150 (1935) 382
14 WILKINS, T. R. *J. appl. Phys.* 11 (1940) 35
15 POWELL, C. F. and FERTEL, G. E. F. *Nature, Lond.* 144 (1939) 115
16 HEITLER, W., POWELL, C. F. and FERTEL, G. E. F. *ibid* 144 (1939) 283
17 POWELL, C. F. *ibid* 145 (1940) 155
18 —*Endeavour* 1 (1942) No. 4
19 —*Proc. roy. Soc. A* 181 (1943) 344
20 DEMERS, P. *Phys. Rev.* 70 (1946) 86
21 POWELL, C. F., OCCHIALINI, G. P. S., LIVESEY, D. L. and CHILTON, L. V. *J. Sci. Instrum.* 23 (1946) 102
22 BERRIMAN, R. W. *Nature, Lond.* 162 (1948) 992
23 CUER, P. *Sci. Ind. Photogr.* 18 (1947) 321, 353
24 GURNEY, R. W. and MOTT, N. F. *Proc. roy. Soc. A* 164 (1938) 151
25 BERG, W. F. *Rep. Prog. Phys.* 11 (1948) 248
26 KODAK Private Communication
27 BROWN, R., CAMERINI, U., FOWLER, P. H., MUIRHEAD, H., POWELL, C. F. and RITSON, D. M. *Nature, Lond.* 163 (1949) 47, 82
28 KNOWLES, W. and DEMERS, P. *Phys. Rev.* 72 (1947) 535
29 BLUM, J. *C. R. Acad. Sci., Paris* 228 (1949) 918
30 MAUER, P. B. and REYNOLDS, H. L. *Phys. Rev.* 73 (1948) 1131

[31] YAGODA, H. and KAPLAN, N. *Phys. Rev.* 75 (1949) 1328
[32] GIBSON, W. M., GREEN, L. L. and LIVESEY, D. L. *Nature, Lond.* 160 (1947) 534
[33] GOLDHABER, G. *Phys. Rev.* 74 (1948) 1725
[34] WÄFFLER, H. and YOUNIS, S. *Helv. Phys. Acta* 22 (1949) 414
[35] LARK-HOROVITZ, K. *Phys. Rev.* 59 (1941) 941
[36] CUER, P., MORAND, M. and COTTON, E. *Cahiers de Phys que* 22 (1944) 72
[37] PERFILOV, N. A. *Compt. Rend. Acad. Sci. URSS* 47 (1945) 623
[38] BORST, L. B. and FLOYD, J. J. *Phys. Rev.* 70 (1946) 107
[39] GREEN, L. L. and LIVESEY, D. L. *Nature, Lond.* 158 (1946) 272
[40] BRODA, E. *J. Sci. Instrum.* 24 (1947) 136
[41] WESTÖÖ, R. *Arkiv für Math. Astr. Fysik* 34B (1947) No. 22
[42] DEMERS, P. *Phys. Rev.* 70 (1946) 974
[43] HARDING, J. B., *Nature, Lond.* 163 (1949) 440
[44] HODGSON, P. E. and PERKINS, D. H. *ibid* 163 (1949) 439
[45] PICCIOTTO, E. *C. R. Acad. Sci., Paris* 228 (1949) 2020; 229 (1949) 117
[46] BLAU, M. *Akad. Wiss., Wien* 140 (1931) 623
[47] LAUDA, J. *ibid* 145 (1936) 707
[48] OCCHIALINI, G. P. S. and POWELL, C. F. *Nature, Lond.* 159 (1947) 186
[49] LATTES, C. M. G., MUIRHEAD, H., OCCHIALINI, G. P. S. and POWELL, C. F. *ibid* 159 (1947) 694
[50] CHEKA, J. S. *Phys. Rev.* 74 (1948) 127
[51] COPPENS, R. *C. R. Acad. Sci., Paris* 227 (1948) 61
[52] LAMB, W. A. and BROWN, F. W. *Phys. Rev.* 74 (1948) 104
[53] LA PALME, J. and DEMERS, P. *ibid* 72 (1947) 536
[54] YAGODA, H. and KAPLAN, N. *ibid* 71 (1947) 910
[55] MATHER, K. B. *ibid* 76 (1949) 487
[56] ALBOUY, G. and FARAGGI, H. *J. phys. Rad.* S8 (1949) 105
[57] — — *C. R. Acad. Sci., Paris* 228 (1949) 68
[58] FARAGGI, H. *ibid* 227 (1948) 527
[59] BERG, W. F. *Ann. Rep. Progr. Chem.* 39 (1942) 49
[60] PERFILOV, N. A. *Compt. Rend. Acad. Sci. URSS* 45 (1944) 7
[61] GREEN, L. L. and LIVESEY, D. L. *Phil. Trans. roy. Soc.* 241 (1948) 323
[62] PICCIOTTO, E. *C. R. Acad. Sci., Paris* 228 (1949) 173, 247
[63] DILWORTH, C. C. *Cosmic Radiation* p 157 London, 1949
[64] EVANS, J. and GEORGE, E. P. *Nature, Lond.* 164 (1949) 20
[65] LIEBERMANN, L. N. and BARSCHALL, H. H. *Rev. sci. Instrum.* 14 (1943) 89
[66] DE FELICE, J. A. *Phys. Rev.* 74 (1948) 1244
[67] YAGODA, H. and KAPLAN, N. *ibid* 73 (1948) 634
[68] WIENER, M. and YAGODA, H. *ibid* 76 (1949) 469
[69] STEVENS, G. W. W. *Nature, Lond.* 162 (1948) 526
[70] VAN DEN GRINTEN, W. *Phys. Rev.* 74 (1948) 1244
[71] DILWORTH, C. C., OCCHIALINI, G. P. S. and PAYNE, R. M. *Nature, Lond.* 162 (1948) 102
[72] WILSON, M. J. and VANESLOW, S. *Phys. Rev.* 75 (1949) 1144
[73] BLAU, M. and DE FELICE, J. A. *ibid* 74 (1948) 1198
[74] PURLSOW, E. T. Selo Physics Laboratory, Central Report File 1479 (1946) File No. 9/46
[75] ROTBLAT, J. and TAI, C. T. *Nature, Lond.* 164 (1949) 835
[76] CHAMPION, F. C. and POWELL, C. F. *Proc. roy. Soc. A* 183 (1944) 64
[77] CHADWICK, J., MAY, A. N., PICKAVANCE, T. G. and POWELL, C. F. *ibid* 183 (1944) 1
[78] OCCHIALINI, G. P. S. and PAYNE, R. M. Unpublished 1947
[79] BURCH, C. R. *Proc. phys. Soc.* 59 (1947) 41
[80] BATES, W. J. and OCCHIALINI, G. P. S. *Nature, Lond.* 161 (1948) 473
[81] DYSON, J. *Proc. phys. Soc. B* 62 (1949) 565
[82] MORRISON, A. and MORTON, F. *Rev. Sci. Instrum.* 20 (1949) 341
[83] BARBOUR, I. *ibid* 20 (1949) 530
[84] CURTIS, N. W. and OSBORNE, L. S. *Phys. Rev.* 75 (1949) 1327
[85] DEMERS, P. and MATHIEU, R. *ibid* 75 (1949) 1327
[86] HOUGH, P. V. C. *ibid* 76 (1949) 163
[87] CUER, P. *C. R. Acad. Sci., Paris* 223 (1946) 1121
[88] LATTES, C. M. G., FOWLER, P. H. and CUER, P. *Nature, Lond.* 159 (1947) 301
[89] — — — *Proc. phys. Soc.* 59 (1947) 883
[90] BRADNER, H., SMITH, F. H., BARKAS, W. H. and BISHOP, A. S. *Phys. Rev.* 77 (1950) 462
[91] TSIEN, S. T., CHASTEL, R., FARAGGI, H. and VIGNERON, L. *C. R. Acad. Sci., Paris* 223 (1946) 571

92 GREEN, L. L. and GIBSON, W. M. *Proc. phys. Soc.* 62 (1949) 296
93 COTTON, E. *C. R. Acad. Sci., Paris* 224 (1947) 823
94 ROTBLAT, J. *Nature, Lond.* 165 (1950) 387
95 PECK, R. A. *Phys. Rev.* 72 (1947) 1121
96 ROSS, M. A. S. and ZAJAC, B. *Nature, Lond.* 162 (1948) 923
97 HERZ, R. H. *Phys. Rev.* 75 (1949) 478
98 LATTES, C. M. G., OCCHIALINI, G. P. S. and POWELL, C. G. *Proc. phys. Soc.* 61 (1948) 173
99 CUER, P. *C. R. Acad. Sci., Paris* 224 (1947) 41
100 LIVINGSTON, M. S. and BETHE, H. A. *Rev. mod. Phys.* 9 (1937) 285
101 BLAU, M. *Phys. Rev.* 75 (1949) 279
102 ZAJAC, B. and ROSS, M. A. S. *Nature, Lond.* 164 (1949) 311
103 BOSE, D. M. and CHOUDHURI, B. *ibid* 148 (1941) 259
104 PERKINS, D. H. *ibid* 159 (1947) 126
105 LATTIMORE, S. *ibid* 161 (1948) 518
106 GOLDSCHMIDT-CLERMONT, Y., KING, D. T., MUIRHEAD, H. and RITSON, D. M. *Proc. phys. Soc.* 61 (1948) 183
107 VAN DEN GRINTEN, W. *Phys. Rev.* 76 (1949) 163
108 WILLIAMS, E. J. *Proc. roy. Soc. A* 169 (1938) 531
109 GOUDSMIT, S. A. and SCOTT, W. T. *Phys. Rev.* 74 (1948) 1537
110 SCOTT W. T. *ibid* 75 (1949) 1763
111 POWELL, C. F. and ROSENBLUM, S. *Nature, Lond.* 161 (1948) 473
112 BARBOUR, I. *Phys. Rev.* 74 (1948) 507, 76 (1949) 320
113 FRANZINETTI, C. *Cosmic Radiation* p 159 London, 1949
114 FREIER, P., LOFGREN, E. J., NEY, E. P., OPPENHEIMER, F., BRADT, H. L. and PETERS, B. *Phys. Rev.* 74 (1948) 213
115 — — — — *ibid* 74 (1948) 1818
116 BRADT, H. L. and PETERS, B. *ibid* 74 (1948) 1828
117 KAPLAN, M. F., PETERS, B. and BRADT, H. L. *ibid* 75 (1949) 1329
118 COSYNS, M., DILWORTH, C. C., OCCHIALINI, G. P. S. and SCHÖNBERG, M. *Nature, Lond.* 164 (1949) 129
119 SÖRENSEN, S. O. C. *Phil. Mag.* 40 (1949) 947
120 BRADT, H. L. and PETERS, B. *Phys. Rev.* 76 (1949) 156
121 MOTT, N. F. *Proc. roy. Soc. A* 124 (1929) 425
122 RICHARDS, H. T. *Phys. Rev.* 59 (1941) 796
123 GIBSON, W. M. and LIVESEY, D. L. *Proc. phys. Soc.* 60 (1948) 523
124 LATTES, C. M. G., OCCHIALINI, G. P. S. and POWELL, C. F. *Nature, Lond.* 160 (1947) 453, 486
125 POWELL, C. F. and OCCHIALINI, G. P. S. *Phys. Soc. Rep. Cambr. Conf.* p 150 1947
126 GUGGENHEIMER, K. M., HEITLER, H. and POWELL, C. F. *Proc. roy. Soc. A* 190 (1947) 196
127 HEITLER, H., MAY, A. N. and POWELL, C. F. *ibid* 190 (1947) 180
128 MAY, A. N. and POWELL, C. F. *ibid* 190 (1947) 170
129 RUBIN, S. *Phys. Rev.* 72 (1947) 1176
130 ROSEN, L., TALLMADGE, F. K. and WILLIAMS, J. H. *ibid* 76 (1949) 1283
131 MARTIN, L. H., DUNBAR, D. N. F., BOWER, J. C. and HIRST, F. *Nature, Lond.* 164 (1949) 310
132 FOWLER, P. H., BURROWS, H. B. and CURRY, W. J. J. *ibid* 159 (1947) 569
133 LATTES, C. M. G. and OCCHIALINI, G. P. S. *ibid* 159 (1947) 331
134 LIVESEY, D. L. and WILKINSON, D. H. *Proc. roy. Soc. A* 195 (1948) 123
135 PECK, R. A. *Phys. Rev.* 73 (1948) 947
136 GREEN, L. L. and GIBSON, W. M. *Proc. phys. Soc* 62 (1949) 407
137 GROSSKREUTZ, J. C. *Phys. Rev.* 76 (1949) 482
138 KEEPIN, G. R. and ROBERTS, J. H. *ibid* 76 (1949) 154
139 CUER, P. *J. Phys. Rad.* 8 (1947) 83
140 — MORAND, M., KING, T. and LOCQUEREUX, R. *C. R. Acad. Sci., Paris* 228 (1949) 557
141 MYSSOWSKY, L. and JDANOFF, A. *Nature, Lond.* 143 (1939) 794
142 TSIEN, S. T. *C. R. Acad. Sci., Paris* 224 (1947) 1056
143 — HO ZAH-WEI, VIGNERON, L. and CHASTEL, R. *Nature, Lond.* 159 (1947) 773
144 WOLLAN, E. O., MOAK, C. D. and SAWYER, R. B. *Phys. Rev.* 72 (1947) 447
145 TITTERTON, E. W. and GOWARD, F. K. *ibid* 76 (1949) 192
146 GARDNER, E. and LATTES, C. M. G. *Science* 107 (1948) 270
147 — and — *Phys. Rev.* 74 (1948) 1236
148 OCCHIALINI, G. P. S. and POWELL, C. F. *Nature, Lond.* 161 (1948) 551
149 MCMILLAN, E. M. and PETERSON, J. M. *Science* 109 (1949) 438

[150] POWELL, C. F. *J. Phys. Rad.* 9 (1948) 289
[151] YAGODA, H., KAPLAN, N. and CONNER, C. H. *Phys. Rev.* 76 (1949) 171
[152] WAGNER, N. and COOPER, D. *ibid* 76 (1949) 449
[153] OCCHIALINI, G. P. S. and POWELL, C. F. *Nature, Lond.* 162 (1948) 168
[154] CAMERINI, U., MUIRHEAD, H., POWELL, C. F. and RITSON, D. M. *ibid* 162 (1948) 433
[155] OCCHIALINI, G. P. S. and POWELL, C. F. *ibid* 159 (1947) 93
[156] PERKINS, D. H. *ibid* 160 (1947) 299
[157] — *ibid* 161 (1948) 486
[158] LEPRINCE-RINGUET, L., HEIDMAN, J., LI, T. T. and PERKINS, D. H. *ibid* 161 (1948) 844
[159] HARDING, J. B., LATTIMORE, S. and PERKINS, D. H. *Proc. roy. Soc. A* 196 (1949) 325
[160] — and PERKINS, D. H. *ibid* 164 (1949) 285
[161] THOMSON, G. P. *ibid* 196 (1949) 311
[162] GEORGE, E. P. and JASON, A. C. *Proc. phys. Soc.* 62 (1949) 243
[163] THOMSON, G. P. *Phil. Mag.* 40 (1949) 589
[164] PERKINS, D. H. *ibid* 40 (1949) 601
[165] BAGGE, E. *Phys. Z.* 21 (1944) 461
[166] ROSENFELD, L. *Nuclear Physics* p 154 Amsterdam, 1948
[167] BRADT, H. L. and PETERS, B. *Phys. Rev.* 75 (1949) 1779
[168] BROWN, R. H., CAMERINI, U., FOWLER, P. H., HEITLER, H., KING, D. T. and POWELL, C. F. *Phil. Mag.* 40 (1949) 862
[169] LEPRINCE-RINGUET, L., BOUSSER, F., FONG, H. T., JAUNEAU, L. and MORELLET, D. *C. R. Acad. Sci., Paris* 229 (1949) 163
[170] PICKUP, E. and VOYVODIC, L. *Phys. Rev.* 76 (1949) 446
[171] HORNBOSTEL, J. and SALANT, E. O. *ibid* 76 (1949) 468
[172] OSBORNE, L. S. and FELD, B. T. *ibid* 76 (1949) 468
[173] CURIE, I. *J. Phys. Rad.* 7 (1946) 313
[174] POOLE, J. H. J. and BREMNER, J. W. *Nature, Lond.* 161 (1948) 884 ; 163 (1949) 130
[175] PICCIOTTO, E. *Bull. soc. Belg. Geol.* 58 (1949) 75
[176] COPPENS, R. *C. R. Acad. Sci., Paris* 228 (1949) 177
[177] CUER, P. *Ann. Geophys.* 2 (1946) 147
[178] YAGODA, H. *Am. Mineral* 31 (1946) 462
[179] MATHER, K. B. and KURIE, F. N. D. *Phys. Rev.* 73 (1948) 1474
[180] ROTBLAT, J. *Nature, Lond.* 160 (1947) 493
[181] SHAPIRO, M. M. and BARNES, J. R. *Phys. Rev.* 73 (1948) 1243
[182] TITTERTON, E. W. *Nature, Lond.* 163 (1949) 990
[183] DEMERS, P. and FREDETTE, V. *ibid* 72 (1947) 538
[184] ENDICOTT, K. M. and YAGODA, H. *Proc. Soc. Expt. Biol. Med.* 64 (1947) 170
[185] ROTBLAT, J. *Brit. Science News* 2 (1949) 201

4

ELECTRONIC CIRCUITS FOR NUCLEAR DETECTORS

G. G. Scarrott

THE STUDY of the small pulses of electric current which are caused, for instance in an ionization chamber, by the passage of single nuclear fragments has become one of the chief methods of nuclear physics. Consequently the use of electronic valves, previously the prerogative of the communication engineer, has entered the nuclear laboratory. Valves are used not merely to amplify the very small primary pulses to an amplitude suitable for recording. They are also employed in discriminators which select pulses above a certain size or within certain size limits; in scalers which reduce (usually by a power of 2) the number of pulses which are to be recorded by the mechanical meter; in coincidence circuits which record those instances in which two pulses from two different detectors arrive within a very short time interval (*e.g.* 10^{-6} sec).

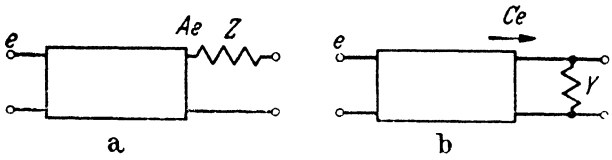
Valves are also employed in rectifiers for generating various auxiliary potentials, and in giving those potentials any desired degree of stability.

In this article are described the basic principles to which all these multifarious activities can be reduced, in particular the principle of positive and negative feedback. Positive feedback is the basis of all trigger circuits and scalers; negative feedback can be used to increase stability, both in amplifiers and power supplies. The article also contains a discussion of other circuit elements which are of importance in nuclear circuitry, such as diodes and delay lines, and of the methods for achieving a favourable signal/noise ratio. In the first part the basic circuit units will be described in some detail. The second part will be concerned with the use of these units in typical electronic research instruments. It is assumed that the reader is well acquainted with the properties of valves and the principles of voltage and power amplifiers.

BASIC CIRCUITS

The simplest way of using a valve is to connect it as a resistance coupled amplifier. Such an amplifier can be described in terms of the relation between input and output (usually non-linear) and its band-width. Many of the circuit units to be described can be considered to be derived from the simple valve amplifier by the use of feedback to suppress or exploit the non-linearity.

Feedback in general—Neglecting for the moment the effects of non-linearity and the small input admittance of a valve grid, a simple voltage amplifier can be represented as in *Figure 1*. The two ways of representing the output impedance as a constant voltage source in series with an impedance



A = voltage gain
Z = output impedance

C = current gain
Y = output admittance

Figure 1. Simple voltage amplifier. Current and voltage gain relationships: $YZ=1$, $A/Z=C$, $C/Y=A$

or a constant current source in shunt with an admittance are shown in *Figure 1*a and b respectively. There are two essentially different ways of deriving a feedback voltage from such an amplifier: it can be made proportional to the output voltage or to the output current as shown in *Figure 2*a and b.

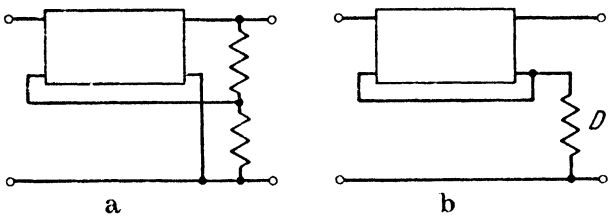
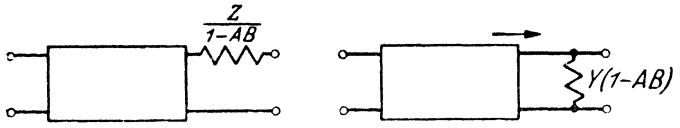


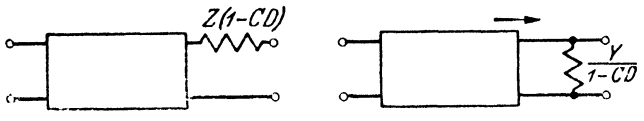
Figure 2. a *Voltage feedback utilizing voltage divider with ratio B of high impedance and* b *current feedback, impedance D negligible compared with output impedance of amplifier*

Analysis of these circuits shows that they can be represented by the equivalent simple amplifiers with parameters as in *Figure 3*. From the formal correspondence between the parameters for voltage and current feedback amplifiers



Voltage gain $= A/(1 - AB)$ *Current gain* $= C$

a



Voltage gain $= A$ *Current gain* $= C/(1 - CD)$

b

Figure 3. a *Equivalent circuits for Figure* 2a, *voltage feedback with feedback factor AB*

b *Equivalent circuits for Figure* 2b, *current feedback with feedback factor CD*

it is evident that the properties of any particular current feedback amplifier can be derived from those of an analogous voltage feedback amplifier by a process akin to inversion. Hence it is unnecessary to consider both kinds of feedback in detail and from now on we shall consider voltage feedback only.

Effect of feedback factor AB—In order to allow for the effects of non-linearity the analysis in the preceding paragraph can be considered to apply to small signals based on some mean operating point; the amplifier parameters A and Z are then differential coefficients which vary with this operating point, which may have been reached as a result of some preceding signal. Three distinct possibilities then arise depending on the value of the feedback factor AB.

$AB \ll -1$ —Here $1-AB \sim AB$, so that the voltage gain $\sim 1/B$. This is the well known case of negative feedback in which the effective gain of the system is determined mostly by the degeneration factor B in the feedback network. Thus, if an accurately linear amplifier is required the feedback network must be made of linear elements such as resistances or capacities to ensure that B is independent of signal amplitude. Limiting still occurs in a feedback amplifier at an amplitude such that A is reduced so far that the original condition $AB \ll -1$ no longer holds. In the operating range the non-linearity effect of variation in A is reduced approximately to $1/AB$ of what it would have been in the absence of feedback.

Since the gain of the system is about $1/B$ a variety of characteristics is available by appropriate choice of B. Thus if B is derived from a differentiating network the amplifier will produce an output which is approximately the time integral of the input signal, and *vice versa*. This is the essence of some time base circuits. Another possible feedback network can be made using a reference voltage. If the input terminals are short circuited the amplifier will then deliver an output nearly equal to the reference voltage. We then have a voltage stabilizer. In general any peculiarities (even non-linearity) introduced into the factor B will be faithfully inverted and introduced into the amplifier characteristic, provided always of course that $AB \ll -1$.

The output impedance in all the above cases is reduced approximately in the ratio AB.

$0 < AB < 1$ —In this case the voltage gain of the amplifier is higher than A, rising to an infinite value at $AB=1$. The output impedance is also larger than the value Z without feedback and also rises to infinity at $AB=1$. Hence the output approaches a constant current source with a finite transfer admittance C when the voltage gain is infinite. These expressions are strongly dependent on the variable and somewhat unpredictable amplifier parameters A and Z, so that the use of these properties is limited to those cases where it is desired to increase the gain of an amplifier but where the exact value of the increased gain is not important.

$AB > 1$ —Here the amplifier is clearly unstable since a small displacement from a supposed equilibrium value of the output voltage will cause a greater displacement. It follows that the amplifier will drive its operating point to one of the extreme positions where A has fallen to a value

which makes $AB<1$. This is the essential property of a trigger circuit and this result suggests that there are as many ways of making a trigger circuit as there are ways of putting positive feedback on to an amplifier.

NEGATIVE FEEDBACK AMPLIFIERS

In order to allow for the effect of phase changing elements such as stray capacities and coupling condensers it is useful to consider the signal to be sinusoidal. Then A and if necessary B can be written as complex functions of the frequency and plotted on the complex plane (Argand diagram); the curve so obtained is called a vector locus. The condition that the feedback should reduce the gain is then that $|1-AB|>1$. If $|1-AB|<1$ the gain is increased by the feedback and it can be shown that instability occurs when the vector locus of AB encloses the point 1,0. The vector locus of AB can be used to determine the frequency response curve since it enables the vector $1-AB$ to be readily evaluated, see *Figure 4*. It frequently occurs that the factor B is constant and independent of frequency, and in this case the

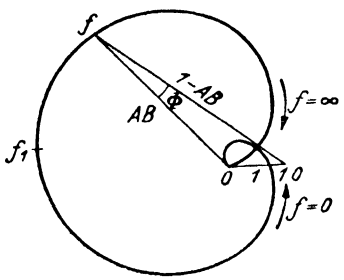


Figure 4. Frequency response curve

Voltage gain $= A/(1-AB)$

For constant B, gain $= \frac{1}{B} \cdot \frac{AB}{(1-AB)}$

Amplitude distortion = ratio of vectors AB and $1-AB$*, phase distortion =* ϕ

vector locus method is particularly convenient. It is evident from *Figure 4* that there are always extreme frequencies for which $|1-AB| \gg 1$. At such frequencies at best the gain is not stabilized by the feedback; and at the worst the gain might rise to a high value if the vector locus of AB approaches the point 1,0. By a similar argument the output impedance $Z/(1-AB)$ is not low at extreme frequencies.

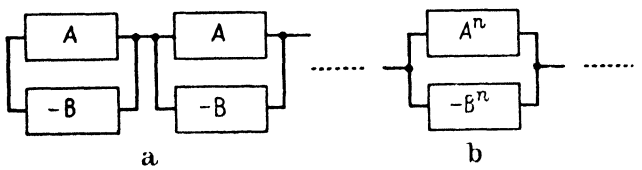


Figure 5. a *Total gain of n amplifiers of gain A and feedback loops* $-B$ *is* $[A/(1+AB)]^n = 1/(B^n + \text{terms in } A + A^{-n})$
b *For overall feedback total gain is* $A^n/[1+(AB)^n] = 1/(B^n + A^{-n})$, *less dependent on A than the former expression*

The question now arises whether in the design of a feedback amplifier with more than one valve it is preferable to use an individual feedback path for each valve or to use feedback loops enclosing more than one valve. From the point of view of gain stability the use of overall feedback is clearly preferable from the argument illustrated in *Figure 5*. If, however, the gain is

to be controlled over a wide frequency band the use of overall feedback involves difficulties owing to the fact that phase changes in A are roughly proportional to the number of valves in the amplifier. This usually limits the number of valves in a feedback loop to three.

Most feedback amplifiers are required to produce an output voltage which accurately reproduces to a different scale an input voltage. The use of voltage feedback automatically achieves this end but the same result can also be obtained by passing the current output from a current feedback amplifier through a load resistance as illustrated in *Figure 6*. There is no clear general preference in this matter. At first sight the low output impedance of the voltage feedback method might seem to be a decisive advantage. However, in those cases where the amplifier is required to drive a fixed small capacity load the low impedance output is chiefly needed at the high frequency end of the pass band. At these high frequencies the low output impedance is likely to be illusory. When the amplifier is expected to drive a large or variable capacity load the use of voltage feedback is usually preferable. Such a case occurs *e.g.* when the load is an unpredictable length of coupling cable.

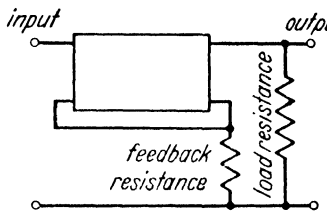


Figure 6. Use of current feedback with a load resistance to produce feedback controlled voltage gain

ACTUAL FEEDBACK CIRCUITS

The simplest feedback amplifier is the well known cathode follower illustrated with its principal parameters in *Figure 7*. The most useful properties of the

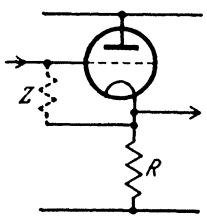


Figure 7. Cathode follower

$$\text{Gain} = \frac{G}{G + 1/R + 1/R_A} \sim 1,$$

$$\text{Output impedance} = \frac{1}{G + 1/R + 1/R_A} \sim 1/G.$$

Effective input impedance of Z between grid and cathode

$$= Z \cdot \frac{G + 1/R + 1/R_A}{1/R + 1/R_A} \sim \frac{Z\mu R}{(R + R_A)}$$

G = *mutual conductance* R_A = *anode impedance* μ = *amplification factor*

cathode follower are its low output impedance and high input impedance. The high input impedance property can be used as shown in *Figure 8* to reduce the effective capacity of a screened cable. In general the high input impedance and low output impedance properties of a cathode follower cannot be used together, as the exploitation of one of them destroys the other. For example if the low output impedance property is used it implies that a large current is being delivered from the output to a low impedance load. In this case the cathode does not follow the grid accurately and the high

input impedance property is lost. Conversely, if the circuit in *Figure 8* is used to exploit the high input impedance a signal voltage on the cathode caused by load current is coupled to the grid *via* the cable capacity. This reduces the current turned on for a given load signal voltage and consequently increases the output impedance. When a cathode follower is used for its low output impedance the mutual conductance is the only important parameter of the valve so that a high-slope triode should be used. The amplification factor should be high when the high input impedance property is desired, hence in this case a pentode can be used with profit. Furthermore, where a very large signal voltage has to be delivered the pentode connection has an advantage for the same reason that a pentode voltage amplifier will produce a larger output than a triode.

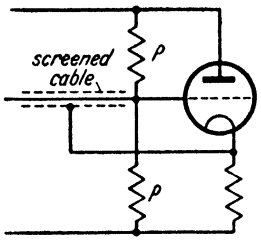


Figure 8. Cathode follower used to reduce effective capacity of screened cable. P, P is a high resistance potentiometer to determine D.C. conditions

The amplifier and feedback paths in a cathode follower are so short that no difficulty arises in ensuring stability and for the same reason the output impedance is low up to the highest frequencies normally encountered.

If a cathode follower is used to transmit large pulses of short duration the low impedance output may be illusory if the current required from it into the capacity load on the downward part of the pulse is greater than the current already flowing in the valve. For this reason a cathode follower will reproduce the leading edge of a large positive pulse better than a large negative one.

When the type of valve and its operating conditions have been chosen the best way to achieve these is usually as shown in *Figure 8*. The essential point of the method shown is that the large cathode resistance of a cathode follower can also be used to render accurately determinate the D.C. operating conditions in spite of unpredictable variations in valve characteristics.

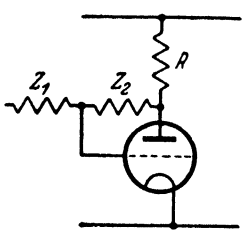


Figure 9. Anode follower. Assuming valve is a pentode with very high anode impedance $(Z_1 + Z_2) \gg R$, *and* $Z_2/Z_1 \ll GR$

$$\text{Gain} = \frac{GRZ_2}{(GRZ_1 + Z_1 + Z_2)} \sim \frac{Z_2}{Z_1}$$

$$\text{Output impedance} = \frac{R(Z_1 + Z_2)}{(GRZ_1 + Z_1 + Z_2)} \sim \frac{(Z_1 + Z_2)}{GZ_1}$$

$$\text{Input impedance} = Z_1 + \frac{Z_2}{(1 + GR)} \sim Z_1$$

Another way of putting negative feedback on a single valve amplifier is depicted in *Figure 9*, often called an anode follower. In this circuit the grid is driven by a voltage obtained by combining the input and output

voltages *via* Z_1 and Z_2 so that this is an example of voltage feedback. The parameters can be readily deduced and are given in *Figure 9*. With the usual condition that $AB \gg 1$, the gain of such an amplifier is controlled mainly by the impedances Z_1 and Z_2. If a voltage amplifier of constant gain is required the ratio Z_1/Z_2 must be independent of frequency so that Z_1 and Z_2 must be composed of similar combinations of elements. Some typical combinations are shown in *Figure 10*. If Z_1 and Z_2 are made with dissimilar elements the amplifier applies to the input signal an operation determined by Z_1 and Z_2 *e.g.* integrating and differentiating circuits are shown in *Figure 11*. The valve operating conditions in this anode feedback type of amplifier can be realized by the use of the conventional cathode biasing resistor or by making the feedback D.C. coupled with the aid of a negative line (see *Figure 10*).

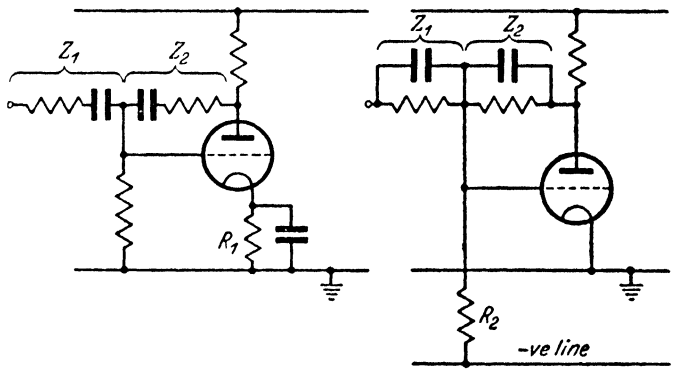


Figure 10. Negative feedback with single valve amplifier and constant gain. Resistances R_1, R_2 specify D.C. conditions

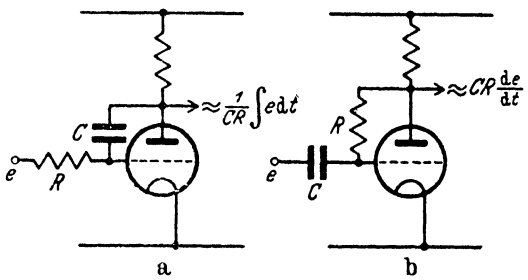


Figure 11. Feedback amplifiers a *integrating,* b *differentiating*

By the use of current feedback as described on page 77 applied to a single valve amplifier the circuit of *Figure 12* results. This method of stabilizing the gain of a single valve is widely used on account of its simplicity but should not be used when the high output impedance is a disadvantage. As in the case of the cathode follower the feedback resistance can be used to stabilize the D.C. operating conditions.

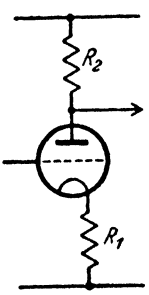


Figure 12. Single valve with current feedback

i *For pentode with screen coupled cathode, voltage gain* $= GR_2/(1 + GR_1)$, *output impedance* $= R_2$

ii *For pentode with screen at fixed potential, voltage gain* $\sim GR_2/(1 + G\rho R_1)$ *where* ρ = *cathode/anode current* $\sim$ 1·3 *for most RF pentodes*

iii *For triode, voltage gain* $= \dfrac{GR_2}{1 + GR_1 + (R_1 + R_2)/R_A}$

If a transformer can be used (that depends on the frequency band over

which the amplifier has to operate) the polarity of the output signal can always be chosen irrespective of the number of valves in the amplifier to make the application of the negative feedback possible. Although transformers are often used in this way in audio frequency amplifiers they are rarely used in pulse amplifiers on account of the large band-width required.

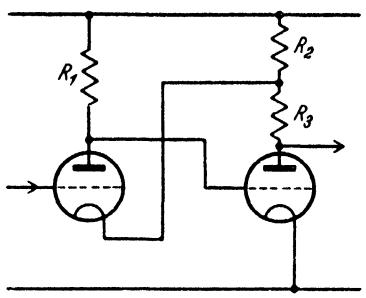
A feedback amplifier with two valves in the loop can be constructed as in *Figure 13*. This is clearly an example of voltage feedback but in this

Figure 13. Two valves with voltage feedback, both pentodes, with $R_3 \gg R_2$

$$\text{Current gain} = \frac{G\{R_2 + GR_1(R_2 + R_3)\}}{(R_2 + R_3 + GR_2R_3)} \sim \frac{G^2R_1}{(1 + GR_2)}$$

$$\text{Output impedance} = \frac{(R_2 + R_3 + GR_2R_3)}{(1 + GR_2 + G^2R_1R_2)} \sim \frac{R_3(1 + GR_2)}{G^2R_1R_2}$$

$$\text{Voltage gain} = \frac{G\{R_2 + GR_1(R_2 + R_3)\}}{(1 + GR_2 + G^2R_1R_2)} \sim \frac{R_3}{R_2}$$



case the simple analysis of page 74 cannot be applied directly since the cathode of the first valve into which the feedback voltage is fed has a large input admittance. The simplest way to analyse such a circuit is to deduce the current gain and output impedance. The current gain can be readily calculated since there is no voltage feedback with the output short circuited. The output impedance is also easily determined by writing down the output current resulting from a postulated change of V in the output voltage. The voltage gain is then the product of these two values. As an amplifier this circuit is of limited value since the D.C. conditions for the valve requires either a low impedance negative line or a blocking condenser in the feedback path. The former is not always available and the use of a blocking condenser in the feedback path is liable to raise difficulties in a wide band amplifier.

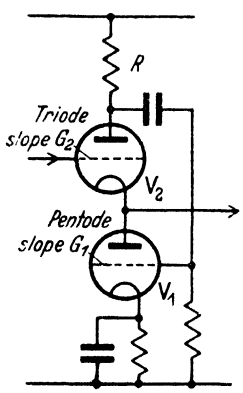


Figure 14. White cathode follower

$$\text{Output impedance} = \frac{1}{G_1(1 + G_2R)}$$

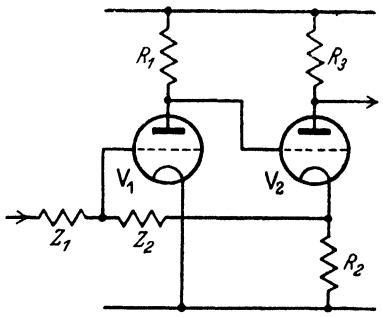
$$\text{Voltage gain} = \frac{\mu_2}{(\mu_2 + 1)}$$

where μ_2 = *amplification factor*

When the feedback ratio is made unity the White cathode follower results in which the difficulties mentioned do not arise. This circuit (*Figure 14*) is very useful; it has a lower output impedance and a higher input impedance than a normal cathode follower and it has a large available output current in both directions. The D.C. operating conditions for the White cathode follower are controlled entirely by the choice of the self bias resistance of the lower of the two valves, (V_1 in *Figure 14*).

Another way of putting negative feedback over two valves is depicted in *Figure 15*. This is effectively a current feedback method as described on page 77 and therefore suffers from the limitations mentioned therein. No

Figure 15. Current feedback over two valves, both pentodes, with screen of second coupled to cathode



$$\text{Voltage gain} = \frac{GR_1R_3Z_2}{(R_2 + 1/G)(Z_1 + Z_2) + GR_1R_2Z_1}$$

$$\sim \frac{R_3Z_2}{R_2Z_1} \text{ if } GR_1 \gg \left(R_2 + \frac{1}{G}\right)$$

$$\text{Output impedance} \sim R_3$$

difficulty arises with this method in the realization of the D.C. operating conditions of the valves.

If we take the output from the cathode of V_2 in *Figure 15* and connect the two valves in series as shown in *Figure 16*, an anode feedback analogue

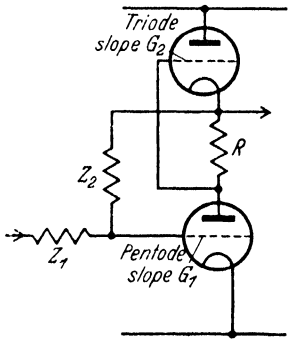


Figure 16. Anode feedback amplifier with large available output current in both directions

$$\text{Current gain} = \frac{Z_2}{Z_1 + Z_2} G_1 (1 + G_2R)$$

$$\text{Output impedance} = 1 \Big/ \left\{ \frac{Z_1G_1}{Z_1 + Z_2} (1 + G_2R) + \frac{1}{R_A} \right\}$$

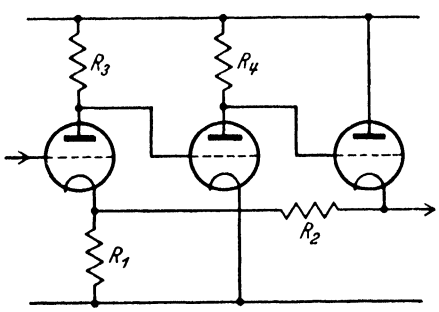
$$\text{Voltage gain} = 1 \Big/ \left\{ \frac{Z_1}{Z_2} + \frac{(Z_1 + Z_2)}{Z_2G_1R_A(1 + G_2R)} \right\}$$

$$\sim Z_2/Z_1 \text{ if } G_1R_A(1 + G_2R) \gg 1 + Z_2/Z_1$$

of the White cathode follower results which has similar useful properties without, of course, the high input impedance of the White cathode follower.

Since a three valve amplifier produces an output of the same sign as

Figure 17. Three valve feedback amplifier with voltage feedback via cathodes



For identical pentodes, if

$$\frac{R_3GR_4}{(R_1 + 1/G)} \gg \frac{R_2}{R_1}$$

$$\text{Voltage gain} \sim \frac{(R_1 + R_2)}{R_1}$$

$$\text{Output impedance} \sim \frac{(R_1 + R_2)}{R_1G^2R_3R_4}$$

a single valve it is to be expected that negative feedback can be applied over three valves by methods similar to those used for one valve. Thus the three valve unit in *Figure 17* is somewhat analogous to the cathode follower, that

in *Figure 18* to a cathode feedback amplifier and *Figure 19* to an anode feedback amplifier. The circuit in *Figure 17* is probably the most useful of the three on account of its low output impedance, high input impedance and

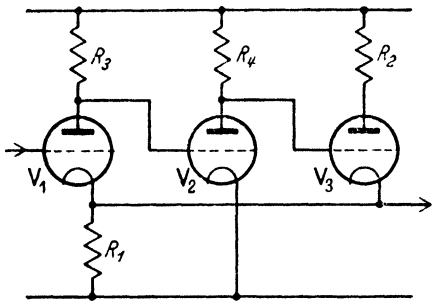


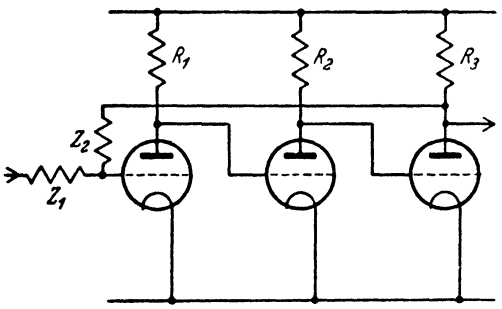
Figure 18. Three valve feedback amplifier with current feedback via cathodes. ρ is ratio of anode to cathode current in V_3.

For identical pentodes, with V_3 screen coupled to cathode and $G^3R_1R_3R_4 \gg 1$
Voltage gain ~ R_2/R_1
Output impedance ~ R_2
With V_3 screen not coupled to V_3 cathode, voltage gain ~ $R_2\rho/R_1$

simple feedback network. It has, however, a small disadvantage in that the use of the last valve as a cathode follower implies that the possible gain of the three valve unit is less than that of the circuits of *Figures 18* and *19*. This

Figure 19. Three valve feedback amplifie with anode voltage feedback

For identical pentodes, if $G^3R_1R_2R_3 \gg (Z_1 + Z_2)/Z_1$
Voltage gain ~ Z_2/Z_1
Output impedance ~ $Z_2/Z_1G^3R_1R_2$



lower gain is, of course, compensated by a higher effective band-width. Owing to the presence of several phase changing elements in the feedback loop these three valve units are liable to have a poor transient response (see page 76) unless precautions are taken in the design to avoid this. These precautions are shown in *Figure 20*. All that is required is that the time constants C_3R_3

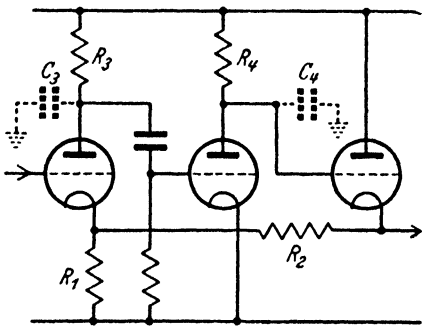


Figure 20. Three valve circuit designed to avoid poor transient response

Feedback factor $AB \sim G^2R_1R_3R_4/R_2$
Criterion to avoid peak at HF end of response curve: $C_3R_3/C_4R_4 \sim AB$ or $1/AB$
LF peak can be avoided by omitting the second coupling condenser as shown

and C_4R_4 in the feedback loop should be very dissimilar in order that the total attenuation should be large at the frequency for which the total phase change reaches 180°. The exact criterion for the ratio of the time constants

has been worked out by ELMORE and the result is given in *Figure 20*. These results imply that it is usually impracticable to use a feedback factor greater than about 20. For many purposes, however, this factor is large enough to ensure adequate stability of gain.

TRIGGER CIRCUITS

As explained earlier, a trigger circuit can be considered as an amplifier with large positive feedback which can be stable only at the ends of the non-linear amplifier characteristic where the feedback factor AB has fallen to a value less than unity. This analysis is completely valid only if both the amplifier and the positive feedback are directly coupled, in which case the circuit clearly has two stable positions, one at each end of the amplifier characteristic. If there is an A.C. coupling in the feedback loop two possible kinds of behaviour are distinguishable depending on the steady potential supplied to the resistance component of the A.C. coupling. Thus if we suppose the amplifier to be D.C. coupled and the positive feedback A.C. coupled as in *Figure 21*, making one A.C. coupling in the loop, then the potential V determines the behaviour of the circuit. If V is such that the amplifier is normally biased to a saturated low gain part of its characteristic then the complete circuit is evidently permanently stable in that position. It can however be triggered to the other low gain part of the amplifier characteristic where it is stable for a limited time depending on the feedback time constant CR. Hence a circuit with one A.C. coupling and the amplifier normally biased off has one stable position and one temporarily stable position with a characteristic resetting time from one to the other.

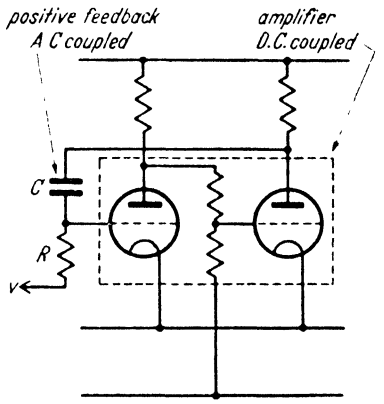


Figure 21. Trigger circuit with no A.C. coupling

If the potential V in *Figure 21* is chosen to bring the amplifier on the high gain part of its characteristic the circuit cannot be permanently stable in any position. It will drive itself as described on page 75 to a saturated low gain position of the amplifier where it can remain for a period determined by the time constant CR. At the end of this period the circuit will again become unstable and drive itself to the other low gain position of the amplifier where a similar process takes place. In this case therefore the circuit alternates between the two stable states and is of course the well known multivibrator.

If more than one A.C. coupling is included in the feedback loop the properties of the circuit are substantially the same as those of a circuit with a single A.C. coupling: that with the shortest time constant.

The foregoing analysis is applicable to all trigger circuits and the more detailed consideration which follows is concerned with the various methods of putting positive feedback on well known amplifier circuits.

If we consider first a conventional single valve amplifier brief reflection shows that positive feedback is possible only if the sign changing property of a transformer is used. It follows that a trigger circuit made in this way cannot have two stable positions, since the transformer constitutes one A.C. coupling in the feedback loop. The D.C. conditions of the valve then determine whether the circuit is an oscillating multivibrator or a self resetting trigger circuit. In the latter case transformer mutual inductance and terminating impedances determine the resetting time. This time can be made very short by appropriate design of the transformer and the resulting circuit is the well known blocking oscillator often used as a generator of short pulses. There are two possible ways of connecting the transformer based on the two possible ways of using a valve *i.e.* as a grounded cathode (the conventional way) or a grounded grid amplifier.

Another way of making a single valve trigger circuit is shown in *Figure 22.* If in an ordinary pentode we use the suppressor as the controlling electrode and the screen as the controlled electrode, leaving the other electrodes at fixed potentials an amplifier results in which the sign of the output signal voltage (from the screen) is the same as the sign of the input signal. Thus positive feedback can be applied to such an amplifier merely by coupling the screen to the suppressor. All three types of trigger circuit described above can be made in this way depending on the bias conditions and type of feedback coupling. This type of trigger circuit is often called a ' transitron '.

A great variety of two valve trigger circuits are possible. This arises from the fact that it is very easy to apply positive feedback to a two valve amplifier. Furthermore, since non-linearity is no disadvantage in an amplifier used for a trigger circuit, any of the five electrodes in a pentode valve can be used as an active electrode. Thus the simplest way of listing the various forms of two valve trigger circuits is in terms of the possible ways of coupling two valves together. The methods in common use are as follows:

1 anode to control grid coupling
2 anode to screen coupling
3 anode to suppressor coupling
4 screen to control grid coupling
5 cathode to cathode coupling.

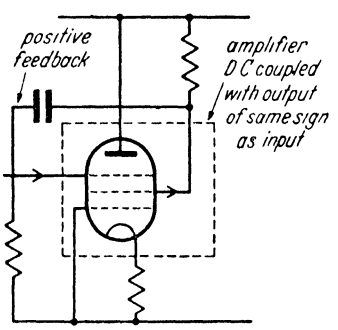


Figure 22. Transitron trigger circuit

To make a trigger circuit the two valves must be coupled in both directions (making a positive feedback loop) using any of these methods. All these pairs

of electrodes may be A.C. or D.C. coupled and the properties of the resulting trigger circuit may be deduced from the bias conditions and type of coupling as shown above. In the design of a trigger circuit to solve any specific problem the types of cross coupling used would be chosen to suit the speed and sensitivity required and to leave appropriate electrodes vacant for external connections.

As an example consider the design of a two valve trigger circuit for use as an amplitude discriminator. Such a device might be required to generate a standard pulse whenever a positive control potential exceeds a pre-set value. Evidently the trigger pair should have a vacant sensitive grid available to which the control voltage can be connected. Since any of the active electrodes can be used for the output pulse the only other relevant consideration is that the trigger should operate as fast as possible. The anode current of a pentode under any normal operating conditions is much larger than the screen current, so that it is clearly preferable for high speed that the anode should be used for one of the cross couplings. One control grid can be left vacant by using the cathodes for the other cross coupling, so that the resulting circuit appears as in *Figure 23.* This cathode coupled trigger circuit is commonly known as a Schmitt circuit after the originator. In this device no resetting time was specified, so that both the cross couplings are made D.C. couplings. The trigger resets when the control potential falls to a value rather below the critical triggering value. The difference between the operating and resetting control voltages can be called the back lash and is of great value as will be shown in the section on discriminators.

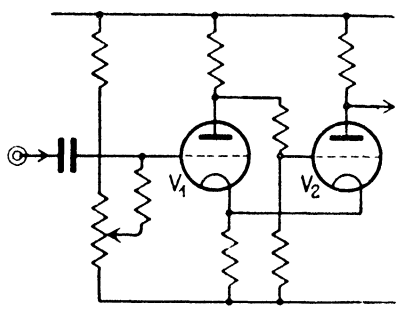


Figure 23. Schmitt circuit used as amplitude discriminator

It would be tedious to attempt a full discussion of the properties of all the trigger pairs obtained by the use of the various forms of cross coupling. Instead the same information may be put in terms of operating characteristics and general methods of obtaining them.

Speed of triggering—The speed of the triggering process is clearly related to the high frequency response of the amplifier on which the trigger circuit is based and on the amount of positive feedback. Hence a pair of pentodes used as such (with the screens and suppressors at fixed potential) is faster than a pair of triodes. Furthermore the current that can be momentarily turned on in a valve by driving it into grid current is many times greater than the current that can be turned off, since the latter is limited by the steady state dissipation of the valve. It follows that the anode that is going negative during the triggering does so much more rapidly than the one that

is going positive. This property is not possessed by a cathode coupled pair since the common cathode resistor limits the current that can be turned on to a value similar to that which is being turned off in the other valve. Hence for the highest speed high band-width factor pentodes should be used with anode to grid cross couplings. If electrodes other than the anode and control grid are used for triggering the speed is always reduced. For example if a screen is used as an anode the effective mutual conductance of the valve is reduced to about a quarter of the value for the anode and in addition the valve is effectively a triode, so that the band-width is considerably reduced.

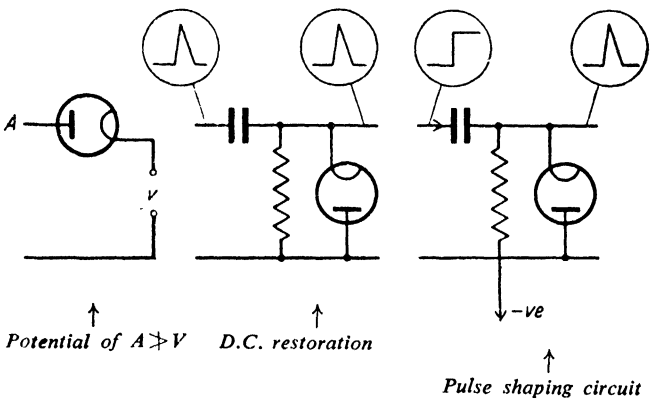


Figure 24. Diode potential stop

Back lash—The meaning of back lash in a cathode coupled pair has already been described. The value of the back lash is controlled by the amount of positive feedback used. Thus if a large anode load is used in V_1 in *Figure 24* the positive feedback factor and the back lash are large.

Sensitivity—If a trigger circuit is expected to be immediately self resetting on removal of the operating signal the minimum triggering signal must be greater than the back lash. In many cases trigger circuits are required to be self resetting after a time lag or can be reset by a separate signal. Under these circumstances the maximum usable sensitivity is limited solely by the long term stability of valve characteristics to a value of about $\frac{1}{4}$ volt minimum triggering signal.

USE OF DIODES

In addition to the well known use of the diode as a power rectifier it is very useful as a circuit element. In the following discussion the diode is assumed to be a perfect conductor in one direction and a perfect insulator in the other. This is of course not quite true. The type of diode in common use as a circuit element has an impedance of some 200 ohm in the conducting direction and a capacity of about 3 pF in the reverse direction. In addition the non-linear portion of the characteristic between the conducting and non-conducting segments occupies about $\frac{1}{4}$ volt instead of zero as in the hypothetical perfect diode.

Diode potential stop—If a diode is connected as in *Figure 24* it acts as a potential stop *i.e.* the potential of point A in *Figure 24* cannot rise above *V*.

If the diode is reversed the potential of A cannot drop below *V*. Two typical applications are depicted in *Figure 24*. D.C. restoration is used to ensure that the passage of a pulse does not affect the base line potential at the receiving end of an A.C. coupling. The other circuit shown in *Figure 24* is used to generate a triangular pulse of well defined duration from a square pulse.

Diode current stop—If a current from a high impedance source is passed through a diode in the conducting direction we have a current stop. Here the diode behaves as a low impedance to currents up to the value of the biasing current but becomes a high impedance to greater currents. A typical circuit using a diode in this way is shown in *Figure 25*. The amplifier valve with a current biased diode in its cathode has large negative cathode feedback as soon as the driving signal exceeds the value at which the valve cathode current is equal to the diode biasing current. Hence, such an amplifier ceases to amplify but cannot run into grid current when overdriven.

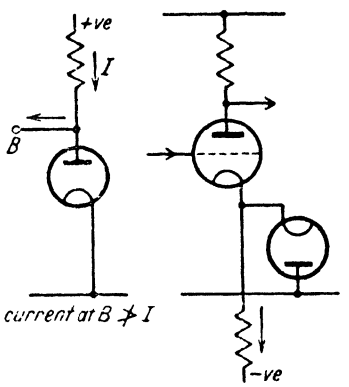


Figure 25. Diode current stop

Diode as a coupling element—It is often required to feed a signal into a trigger circuit in such a way that the operation of the trigger circuit cannot feed a signal back to the source. *Figure 26* shows a diode used to fulfil this requirement. With correct choice of D.C. conditions the diode can be made conducting for the passage of the triggering signal, but the operation of the trigger merely applies a voltage to the diode in the non-conducting direction.

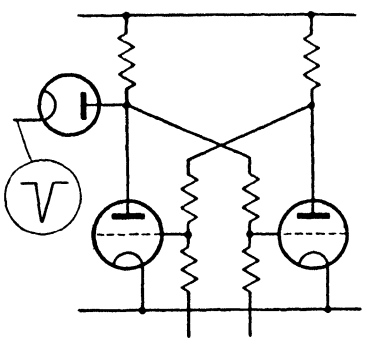


Figure 26. Diode coupling element

Diode coincidence circuits—By the use of two diodes it is possible to make a circuit which produces an output pulse only if its two input terminals are simultaneously excited by input pulses. This coincidence circuit is shown in *Figure 27*. Each diode acts as a potential stop which vetoes all signals allowed through by the other. Thus only if both vetoes are removed by simultaneous

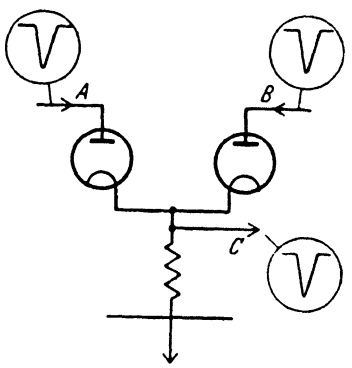


Figure 27. Diode coincidence circuit. Pulse occurs at C only if A and B are coincident

input pulses can an output pulse be produced. This coincidence circuit can be extended by adding more diodes to accommodate more than two input channels. It can also be made into a veto circuit if the D.C. conditions and sign of one of the input pulses are altered.

CATHODE COUPLED PAIRS

A cathode coupled pair (*Figure 28*) has two input terminals and two output terminals. The simplest way to analyse such an apparently complex network

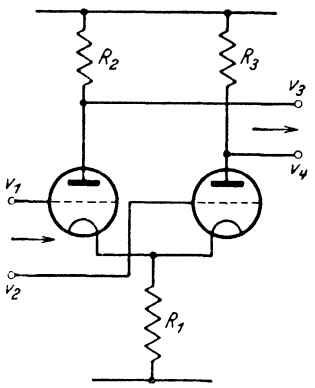


Figure 28. Cathode coupled pair

$$\text{If } \frac{v_1 + v_2}{2} = v_a \qquad \frac{v_1 - v_2}{2} = v_b$$

$$\frac{v_3 + v_4}{2} = v_c \qquad \frac{v_3 - v_4}{2} = v_d$$

In phase gain $v_c/v_a \sim R_2/2R_1$

Out of phase gain $v_d/v_b \sim G\,R_2\,R_A/(R_2 + R_A)$

Usually, out of phase gain $\gg$ *in phase gain*

is to resolve the input and output voltages into in phase and out of phase components. Then, neglecting the effect of non-linearity, a cathode coupled pair has a much higher gain for the out of phase components of the input voltages than for the in phase components. In the extreme case where the common cathode resistor is made very high or replaced by a constant current circuit the in phase gain approaches zero.

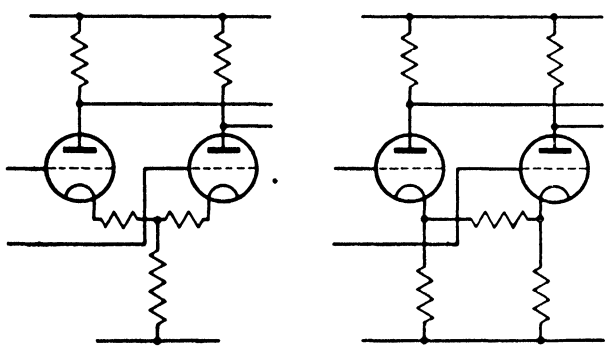


Figure 29. Cathode negative feedback applied to cathode coupled pairs

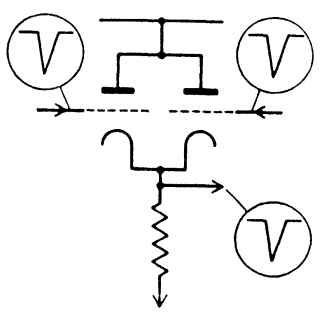


Figure 30. Cathode coupled triodes coincidence circuit

Cathode negative feedback can be applied to a cathode coupled pair by inserting the feedback resistors between the cathodes and the common cathode resistor (*Figure 30*). The resultant T network can be converted to an equivalent Π network yielding an alternative way of making a cathode coupled pair with feedback. The first method is preferable in those cases

where a constant current circuit is used as a common cathode resistor. The second method is sometimes convenient when the negative feedback is required to be adjustable as a form of gain control.

Cathode coupled pairs are particularly useful in D.C. amplifiers. One of the difficulties in the design of the first stage of a D.C. amplifier arises from the fact that random variations in the valve heater voltage cause corresponding variations in the mean electron emission energy from the cathode. This variation, which may amount to a fraction of a volt, is equivalent to a variation in the effective grid potential in addition to that due to the signal. The drift in a D.C. amplifier which results from this effect can be reduced by using a cathode coupled pair, since any change in the emission energy which is common to the two valves has no effect on the output.

Cathode coupled pairs are also of great value in the later stages of D.C. amplifier. Both the input terminals of such a pair (the two grids) present a high impedance to the input signal and can therefore be operated from a high impedance source such as the output of a preceding stage. In addition, since the in phase gain per stage is small, a drift in the H.T. voltage has small effect on the operating conditions of late stages of a D.C. amplifier made with cathode coupled pairs.

If one of the grids of a cathode coupled pair is earthed and the other used as an input terminal for an ordinary unbalanced signal an amplifier results in which the output signal can be of the same sign as the input signal (by using the appropriate anode as the output terminal). For some purposes, notably in pulse forming circuits, such an amplifier is very useful. Negative feedback can be applied to the unused grid of the pair when accurate gain stabilization is required.

The non-linearity of a cathode coupled pair can be usefully exploited in the trigger circuit described on page 85 and in the coincidence and gate circuit shown in *Figure 30*. In the latter, if the two grids are maintained at different potentials, the common cathode must be at a potential somewhat higher than that of the higher grid. Thus its action is very similar to that of a diode coincidence circuit of *Figure 27* with the important difference that no current is taken by the input terminals of the circuit.

DELAY LINES

Artificial delay lines are often used as circuit elements and should ideally delay a signal without causing any distortion. To approximate this ideal a delay line is usually designed as a low pass filter with, however, special attention paid to the phase characteristic at the expense of the attenuation outside the pass band which is of course of no interest. The simplest delay line would be a constant K type low pass filter. In such a filter the phase

shift per section at the cut off frequency f is π radians. It follows that the time delay per section is $1/2f$ seconds at the cut off frequency. If the time delay for any other frequency in the pass band were calculated in this way from the phase characteristic it would be found to vary with frequency over a range of some 30 per cent. A signal with components lying entirely in the pass band of the filter would therefore be delivered slightly distorted and delayed. The delay time would not be accurately determinate owing to the distortion. If the delay line is designed as a filter with a cut off frequency about 50 per cent higher than the highest component of the signal the distortion becomes quite small since most of the variation of delay time with frequency occurs in the top third of the pass band. The delay per section then becomes $1/3f$ where f is the filter cut off frequency.

'*M derived*' *delay lines*—The process of '*M* derivation' often applied to constant *K* type filters to improve the stop band attenuation and image impedance characteristics can also be applied (with a different value of *M*) to a delay line to make the time delay nearly independent of frequency in the pass band. For this purpose a series derived section with *M* about 1·7 is easily realizable in the form of T sections with mutual inductance coupling between the series inductances as shown in *Figure 31*. Such a section has an

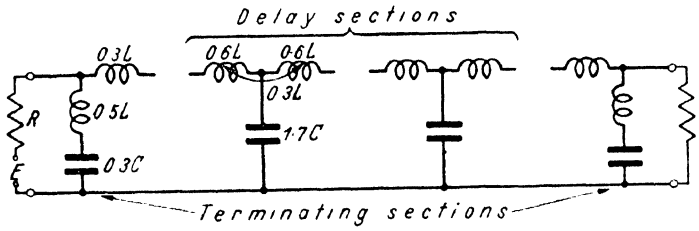


Figure 31. Lowpass filter designed to give constant delay in passband with terminating half sections to give good matching
R = image impedance
f = cut-off frequency
L = R/πf
C = 1/πfR
delay = 1/2f per section

image impedance which is not at all constant in the pass band. This fault can be readily cured by the use of conventional series *M* derived half sections with $M=0{\cdot}6$ as terminal matching sections.

The shunt condensers in a delay line must be large compared with the stray capacities if the performance is to be predictable. This sets a limit to the choice of image impedance in terms of the highest signal frequency. Thus a delay line with a cut off frequency of 10 Mc/s cannot be made with an image impedance greater than about 1,000 ohm. A lower impedance than this would be preferable. The limiting value of image impedance is inversely proportional to the cut off frequency.

Delay lines are often used for pulse shaping. When used in this way a delay line pulse shaper produces an output which can be expressed as $f(t)-f(t-T)$ where $f(t)$ is the input to the circuit and T is determined by the delay line. Thus if $f(t)$ is a step function the output would be a square wave.

There are two ways of using a delay line to do this (*Figure 32*). The first uses a deliberately mismatched line to produce a reflection. In this method the time T in the foregoing expression is twice the delay of the line. The second method uses a delay line directly so that in this case T is just the delay of the line. Other methods may be derived from these by inversion. A third method which is derived in this way from the first is shown in *Figure 32*.

In general a delay line must be matched at least at one end. For a line used as a delay network it would not matter which end. Thus if the line is matched at the receiving end, no reflections take place and the correct operation is immediately obvious. If the line is matched at the transmitting end the signal is sent on the line with half amplitude but doubles itself by reflection at the open circuited receiving end. The reflected wave is completely absorbed by the matched termination at the transmitting end so that the net effect is independent of which end is matched. When high fidelity is important it is sometimes desirable to match a delay line at both ends. A small mismatch is then not so important since reflections will be attenuated twice before they can cause any distortion.

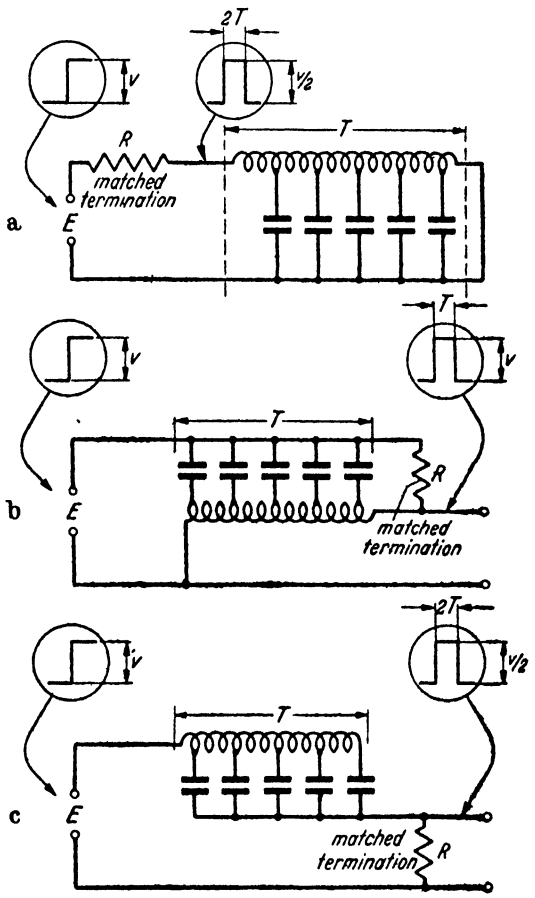


Figure 32. Delay line pulse shapers: a *shorted delay line pulse shaper with matched termination,* b *another type of circuit,* c *matched termination open circuited delay line pulse shaper obtained by inverting* a

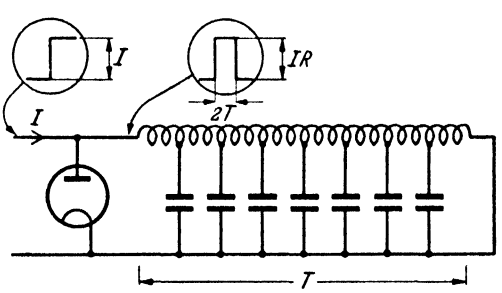


Figure 33. Shorted delay line with diode termination: R is image impedance of line

In certain circumstances it is possible to terminate a pulse shaping delay line with a diode as shown in *Figure 33*. This circuit is entirely analogous with that in *Figure 32*a but has the advantage that for a given current input the output voltage pulse has twice the amplitude of that produced by the corresponding

resistance matched circuit. After a pulse has been produced by a diode terminated line the circuit is not immediately available to generate another since the line is left in a charged condition. Owing to this effect the diode termination cannot be used if the interval between pulses is less than about ten times the pulse duration.

AMPLIFIERS FOR IONIZATION CHAMBERS AND PROPORTIONAL COUNTERS

There are two distinct types of amplifier used with ionization chambers. Either a direct coupled amplifier can be used to measure the mean ionization current or an A.C. coupled amplifier may be used to detect the individual pulses of ionization caused by individual incident particles. In both it is evidently desirable that the amplifier gain should be as stable as possible and that random fluctuations in the output due to effects such as valve noise should be as small as possible.

D.C. amplifiers—The signal from an ionization chamber takes the form of a very small current being delivered from an extremely high source impedance. To operate an electronic amplifier this current signal is converted into a voltage by using a high resistance load as shown in *Figure 34*. Most of the random fluctuations in the output of this type of amplifier arise from the cathode of the valve as described on page 89. The zero drift due to this effect can be minimized by increasing the signal voltage (using a high load resistor) and reducing the equivalent cathode drift voltage. This can be done by using a cathode coupled balanced circuit (page 88) and a stable source of cathode heating power. It is clear from *Figure 34* that any grid current passed by the valve would be indistinguishable from signal current and so would cause an additional zero drift. For this reason the first stage is often made with a special valve (an electrometer valve) in which care is taken in the valve design to achieve a stable cathode, small grid current, and high insulation resistance on the grid. To stabilize the gain of a D.C. amplifier negative feedback can be used in a variety of ways of which a typical sample is shown in *Figure 35*. The application of negative feedback does not affect the zero drift. The drift can be considered to be due to a very low frequency noise voltage effectively in series with the grid circuit. No circuit trickery can therefore distinguish between the signal voltage and the drift voltage.

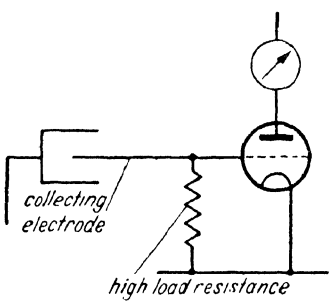


Figure 34. D.C. amplifier for use with ionization chamber

Pulse amplifiers—A high voltage gain (10^5) is usually necessary in a pulse amplifier for use with an ionization chamber. Accordingly several stages are required and it is usually convenient to house the first few of these stages in a separate box (the head amplifier or pre-amplifier) which is mounted as close as possible to the chamber (*Figure 36*). This arrangement has several advantages:

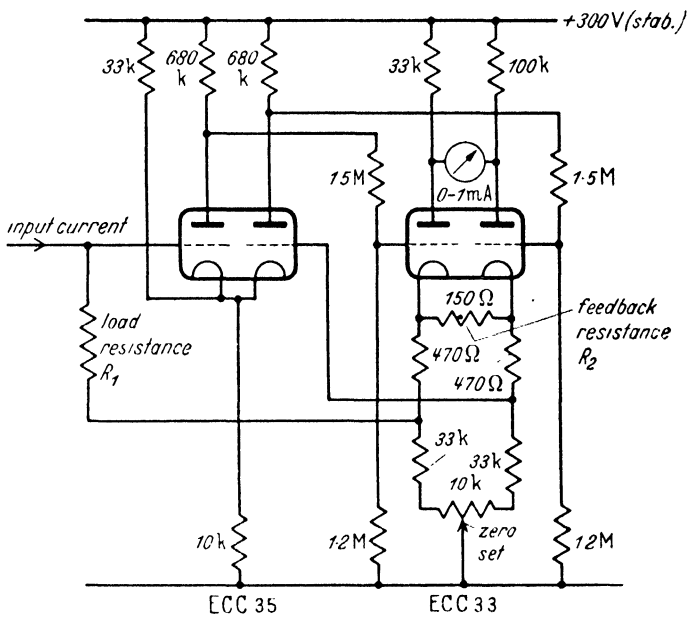


Figure 35. Typical D.C. amplifier with cathode coupled pair input circuit to reduce cathode drift and negative feedback to stabilize gain: current gain $\sim R_1/R_2$

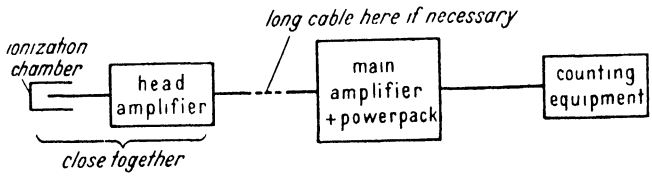


Figure 36. Usual arrangement of pulse amplifier for ionization chamber

1 the lead from the chamber to the head amplifier has the smallest possible capacity and the least chance of picking up extraneous signals

2 the longer lead from the head amplifier to the main amplifier carries a signal at comparatively high level and so reduces the chance of picking up unofficial signals

3 the physical separation of the head and main amplifiers reduces the interaction between them which can (and often does) lead to instability.

Dealing now with the electronic design of the amplifier as a whole the first question to be settled is the frequency pass band. It is therefore relevant to consider the spectra of the signal and the noise.

The signal from an ionization chamber is a step function pulse of charge with a somewhat sloping front (*Figure 37*). The time occupied by the sloping front varies from one pulse to another with a fairly well defined maximum value depending on the ionization chamber. The amplifier output pulse produced by this signal must be accurately proportional in amplitude to the input (independent of input pulse rise time) but can be of any pulse shape.

This implies that the amplifier pass band can be of any width in the frequency range in which the energy spectrum of the input pulse is independent of the pulse rise time.

The duration of the output pulse is inversely proportional to the effective band width passed by the amplifier. This sets a lower limit to the pass band width in terms of the resolving time of the amplifier, which may be defined as the time from the beginning of a pulse to the instant when the disturbance has fallen to some small specified fraction of the maximum value.

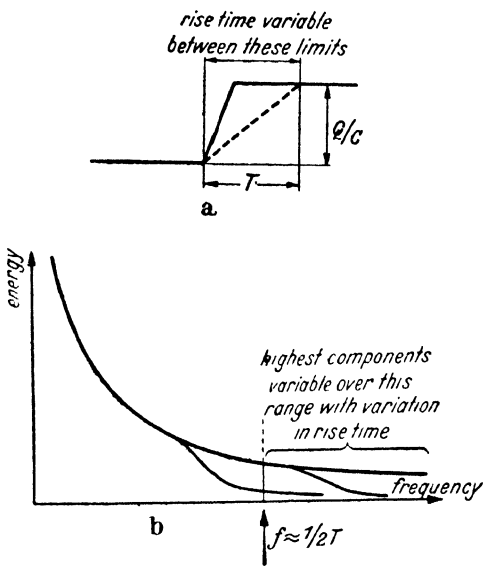


Figure 37. a *Input pulse slope (voltage wave state assuming very high resistance leak on chamber): Q is collected charge, usually electrons only, and C is capacity of chamber and amplifier input*
b *Spectrum of input pulse*

When all those sources of noise which may be considered to be due to obviously faulty design (such as ripple on the H.T. line) have been eliminated there remain the following sources the presence of which is inevitable:

1 shot noise in the valves

2 thermal agitation noise in the resistors

3 partition noise (in pentodes only).

In addition to these there are other sources which arise from the imperfections of valves:

4 grid current noise

5 flicker effect

6 microphonic noise.

Of these noise sources *1*, *2*, *3* and *4* have energy spectra which are flat over the whole frequency range, while *5* and *6* produce most of their noise in the lowest frequencies and have little effect above about 10 kc. To achieve the best signal/noise ratio the amplifier pass band must be chosen with a band width enough to give the required resolving time and a location in the spectrum which is as low as possible without running into excessive flicker and microphonic noise. It follows from the foregoing argument that short resolving time and high signal/noise ratio are incompatible.

Having determined the frequency pass band of the amplifier the position in the amplifier of the pass band determining elements must be settled. These pulse shaping elements, which constitute a crude sort of filter, restrict the noise contribution of all valves preceding them in the amplifier. The bandwidth restriction should therefore be placed somewhere in the middle of the amplifier where the signal is so large that the following valves do not contribute appreciably to the noise. If the pulse shaping elements are located too late in the amplifier they render the immediately preceding valves vulnerable to overloading by the components of the signal which are ultimately rejected. The pulse shaping circuit is therefore often placed between the head amplifier and the main amplifier where the signal level is such that neither of these deleterious effects can occur. The position of the attenuator (used as a gain control) is determined by similar considerations. All the valves of the amplifier which follow the attenuator receive a signal amplitude which is independent of the input pulse size, since the attenuator is naturally operated to keep the output stage of the amplifier approximately fully loaded. The total gain following the attenuator must therefore not be so great that valve noise intrudes. The attenuator cannot be placed too near the output end of the amplifier since in this case the stages immediately preceding the attenuator would be overloaded when a low gain setting is in use.

DETAILED DESIGN OF AMPLIFIER

Dealing now with the detailed design of a pulse amplifier it is reasonable to consider first the head amplifier. All the problems in the design of a head amplifier are concerned with achieving the maximum signal to noise ratio. Although all the valves and resistances in an amplifier contribute the various forms of noise described on page 94 in any intelligently designed amplifier the first valve and its grid leak are the most important sources of noise. The choice of a suitable valve and its operating conditions is therefore the first problem in the design of a head amplifier.

The thermal agitation noise produced by the first grid leak is partly shunted by the capacity of the chamber and the grid of the first valve. The effective noise produced by the grid leak under these circumstances can be most readily calculated by converting the parallel combination of grid leak and total input capacity into an equivalent series combination. The resistance component, which is a function of the frequency for which the transformation was carried out, is then the net source of noise according to the well known expression $V^2=4KTRdF$. As the grid leak is made larger the resistance component of the equivalent series combination becomes smaller so that the noise becomes smaller. The grid leak must therefore be made high to reduce the grid leak noise contribution. If the grid resistance is chosen high enough

to ensure that its equivalent noise resistance is appreciably less than that of the rest of the components in the amplifier pass band region there is no profit to be gained by increasing the grid leak still further.

The desirable value of grid leak chosen in this way depends on the chamber capacity and amplifier pass band and is usually 100MΩ or more. For this reason alone it is desirable that grid current in the first valve should be small since otherwise the D.C. operating conditions would be affected by the grid current. Furthermore there are random fluctuations in the grid current which constitute a source of noise. The magnitude of this grid current noise is dependent on the arithmetic sum of the positive and negative grid currents so that grid current noise is present even when the net grid current is zero. Since the grid current allowed in the first valve is considerably less than that specified in the valve manufacturers' tolerance limits, the most suitable first valve often has to be selected for low grid current.

To eliminate partition noise and to reduce shot noise the first valve should be a triode with a high slope, low input capacity and high amplification factor. Ideally if several valve types equally fulfilling this specification are available *i.e.* with equal ratios of slope to input capacity, the valve with input capacity most nearly approaching that of the chamber is preferable.

The choice of operating conditions for the first valve is made as a compromise between the desirable conditions for low shot noise and those for low grid current noise. A low value of grid bias leads to high slope, low shot noise, but high grid current and conversely.

Microphonic noise becomes troublesome only at comparatively low frequencies. If the pass band of the amplifier has to be chosen to include these frequencies *i.e.* if the input pulse rise time is long, the first stages of the amplifier must be mounted on a soft compliant support *e.g.* on rubber sponge. As a further precaution an anti-microphonic valve such as the *EF 37* with well supported grid structure can be used. Flicker noise also occurs mainly in the low frequencies but in this case very little can be done to reduce the effect.

It is usual to make the head amplifier with more than one valve so that the signal level at the beginning of the main amplifier is high enough to ensure freedom from noise troubles in the main amplifier. Negative feedback is commonly applied to the head amplifier and when this is done a convenient arrangement is the ring of three with cathode feedback (page 81). If the lead from the head amplifier to the main amplifier is long enough to make its quarter wave resonant frequency come near or in the pass band, a matched termination must be provided at one end usually the receiving end. The head amplifier then has to feed its signal into the characteristic impedance of the coupling line, about 90 ohm. If the coupling line is not matched, the impedance presented to the head amplifier output is a rather large capacity. In either case the output impedance from the head amplifier must be low.

There are comparatively few problems in the design of the main amplifier. Linearity and gain stability are obtained by the use of negative feedback over the largest possible groups of valves. Here again the three valve feedback unit (page 81) is useful. The pulse shaping elements are incorporated in the main amplifier and may be made either with resistance and condenser combinations (*Figure 38*) or with a delay line (page 91).

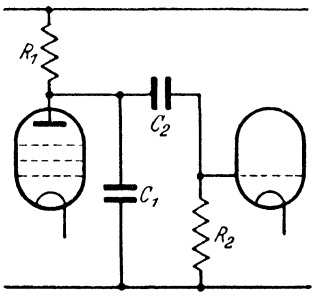


Figure 38. Typical resistance condenser pulse shaping circuit in the middle of an amplifier.

If required resolving time is T_r best signal/noise ratio is obtained with $T_1 = T_2 \sim T_r/3$ where $C_1R_1 = T_1$ and $C_2R_2 = T_2$

The output impedance of the main amplifier should be low to ensure that the output pulse is independent of the capacity load connected to the amplifier. The output stage of the main amplifier should be designed to recover as quickly as possible from the effects of an overloading signal. Such signals may occur frequently *e.g.* when small pulses are being counted in the presence of larger ones.

The worst effect of an overloading pulse is to charge the grid coupling condenser of the affected stage. Hence the cure is to avoid the use of a coupling condenser if possible or to reduce the flow of grid current by the use of an appropriate resistance (*Figure 39*). The output stage of the amplifier must

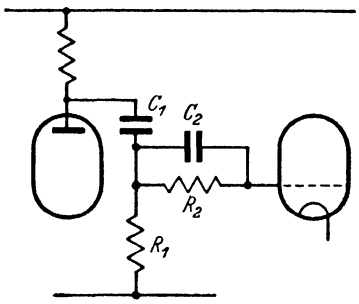


Figure 39. Coupling system to reduce effect of an overloading signal.

C_1R_1 is the normal coupling condenser and leak, R_2 is a high resistance $\sim$ 1M to reduce flow of grid current, C_2 is small condenser $\sim$ 50 pF to bypass R_2 for high frequencies

be able to produce a large steep fronted voltage pulse in the rather large capacity of the output cable so that the output impedance must be low and the available output current large. For this reason it is usual to make the output pulses of positive sign so that a cathode follower output can be used to satisfy these requirements.

AMPLITUDE DISCRIMINATORS

An amplitude discriminator must produce an output pulse, preferably of constant size and shape, whenever an input pulse is supplied of greater than

a known pre-set amplitude. Discriminators are used to determine the distribution of input pulse sizes or to distinguish between genuine pulses and noise. For the latter it is desirable that the discriminator should not be operated by noise pulses superimposed on a genuine pulse, since in that way two or more output pulses might be generated for one input pulse (*Figure 40*). There are two ways of avoiding this effect, by the use of back lash in a biased-off trigger circuit (page 85) or by introducing a dead time so that after an output pulse has been generated the discriminator cannot be operated again for a known pre-set time. It is inevitable that if the time spent by the input pulse over the discriminating level is too short the discriminator will not have time to operate. The effective discriminating level is therefore dependent on the input pulse length. The dependence must be made as small as possible.

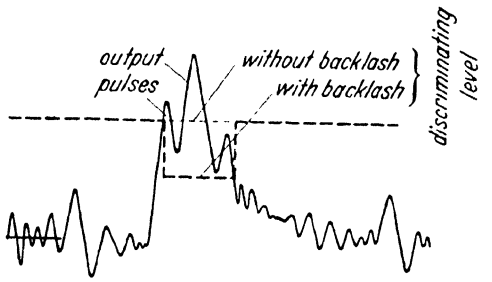


Figure 40. Illustrating the generation of false pulses by noise superimposed on a genuine pulse. Input signal with one input pulse and noise. A single discriminator would generate two output pulses

Another necessary property of a discriminator is that it must not be adversely affected by the receipt of input pulses considerably larger than the discriminating level. If, for example, the biased-off cathode coupled trigger circuit described earlier should pass grid current in the first valve when a large pulse is supplied then the effective bias would be increased for subsequent pulses.

Figure 41 shows a typical discriminator in which attention has been paid to all the problems mentioned in the preceding paragraph. The first three valves constitute a biased-off trigger circuit with about 4 volt back lash and with a discriminating level adjustable from 5 to 50 volt. In this trigger circuit the first valve is cathode coupled to the second in order that it can cathode follow for at least 50 volt beyond the triggering level without running into grid current. The second and third valves constitute the trigger circuit which is not cathode coupled so that the maximum speed of triggering may be achieved. By this means the dependence of the discriminating level on the input pulse is reduced. The amplitude discriminating trigger circuit is made effectively D.C. coupled by the use of long time constants in the cross couplings with D.C. restoration. The discriminating bias is thus determined by a single potentiometer chain across the stabilized H.T. line.

The dead time is introduced by the second trigger pair V_4 and V_5 which constitute an A.C. coupled self resetting trigger circuit with a characteristic relaxation time. This circuit is arranged so that it cannot be affected by

input trigger inpulses while it is in its temporarily stable state. It is also designed to recover its normal condition as quickly as possible after the elapse of the dead time so that if a triggering pulse arrives shortly after the end of the dead time the full dead time will again be imposed. The last valve in the discriminator is a pulse generator of the blocking oscillator type. This is arranged so that it can be triggered by the amplitude trigger circuit and vetoed by the dead time trigger circuit if the latter is required. The blocking oscillator is caused to block by the use of a diode instead of the conventional resistance capacity grid coupling circuit. This reduces the recovery time of the output pulse generator so that the minimum time between output pulses is about 2 microseconds. The output pulse is taken from the cathode and has a low source impedance so that the pulse height and shape is practically unaffected by the large capacity of an output cable.

The discriminator which has been described in the previous paragraph is rather elaborate and has been used to illustrate the methods by which the circuit units described in the first part of this article

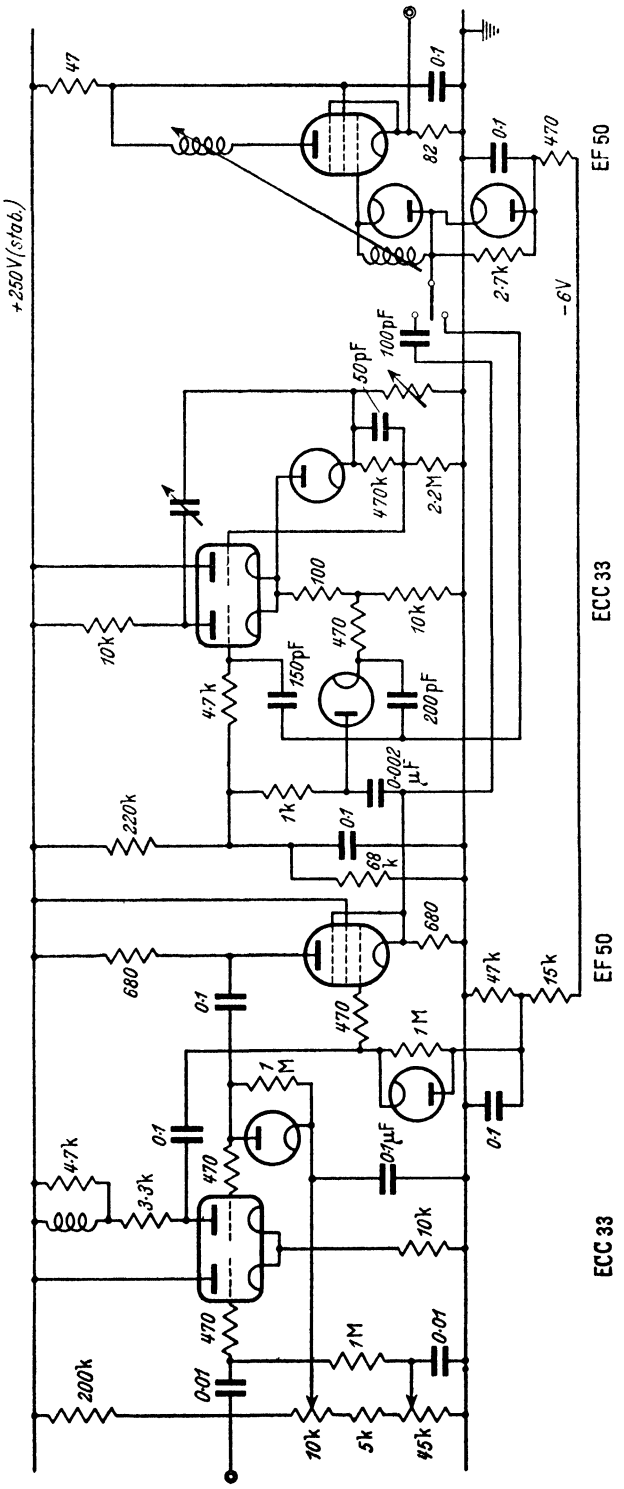


Figure 41. Typical amplitude discriminator

are used to solve a particular set of problems. It sometimes occurs that the conditions under which a discriminator will be used are restricted *e.g.* the input pulse rise time will always be greater than some specified value. In these cases a simpler discriminator circuit can often be used.

AMPLIFIERS FOR GEIGER COUNTERS

The output from a Geiger counter is a pulse of charge which therefore generates a voltage pulse inversely proportional to the capacity connected to the counter. The charge is usually of such a magnitude that a pulse of several volts amplitude is produced when the counter is lightly loaded with a capacity of about 20 or 30 pF. The purpose of a Geiger amplifier is primarily to isolate the counter from the capacity of the cable which leads to the scaling unit. To do this a simple isolating valve is put as close to the counter as possible. It is usually connected as a simple amplifier as shown in *Figure 42.*

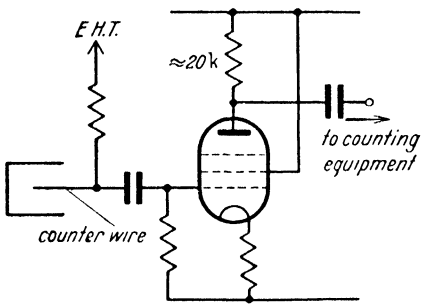


Figure 42. Simple amplifier commonly used with Geiger counters

Quenching circuits—When a counter is used which is not self quenching it must be externally quenched by reducing

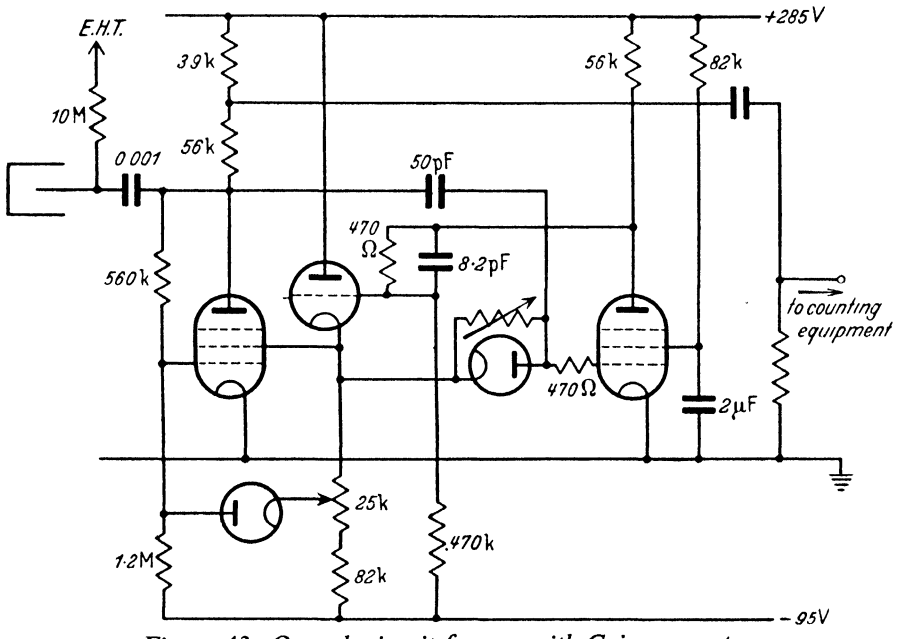


Figure 43. Quench circuit for use with Geiger counters

the E.H.T. supply by some 200 volts for a short period after each discharge. This can be done by a trigger circuit which is operated by the Geiger pulse

and which superimposes a negative square pulse of some 200 volt amplitude and 200 microsecond duration upon the supply to the Geiger counter (*Figure 43*).

COINCIDENCE CIRCUITS

The resolving time of a coincidence circuit may be defined as twice the longest time interval between input pulses which are counted as coincident. In order to render this time accurately determinate it is necessary to incorporate pulse shaping circuits as shown in the block diagram *Figure 44*. The pulse shaping units are designed to standardize the output pulses and care is taken to make the time delay between output and input pulses as small and constant as possible.

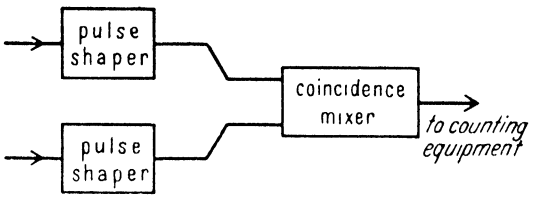


Figure 44. Block diagram of coincidence circuit

The detection of coincidences may be achieved by combining the shaped pulses by simple linear addition and feeding the resultant output into an amplitude discriminator (*Figure 45*). Alternatively the shaped pulses can be combined using non-linear elements such as diodes or triodes, when the output amplitude difference between coincident and non-coincident pulses is greatly increased and consequently the resolving time becomes less dependent on the discriminator setting.

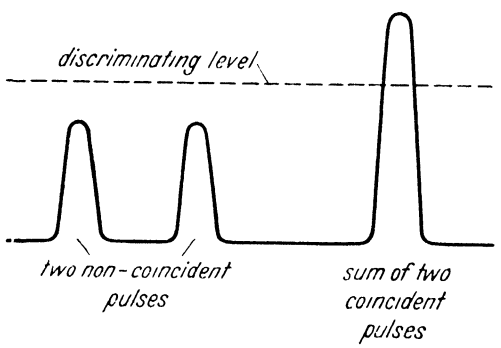
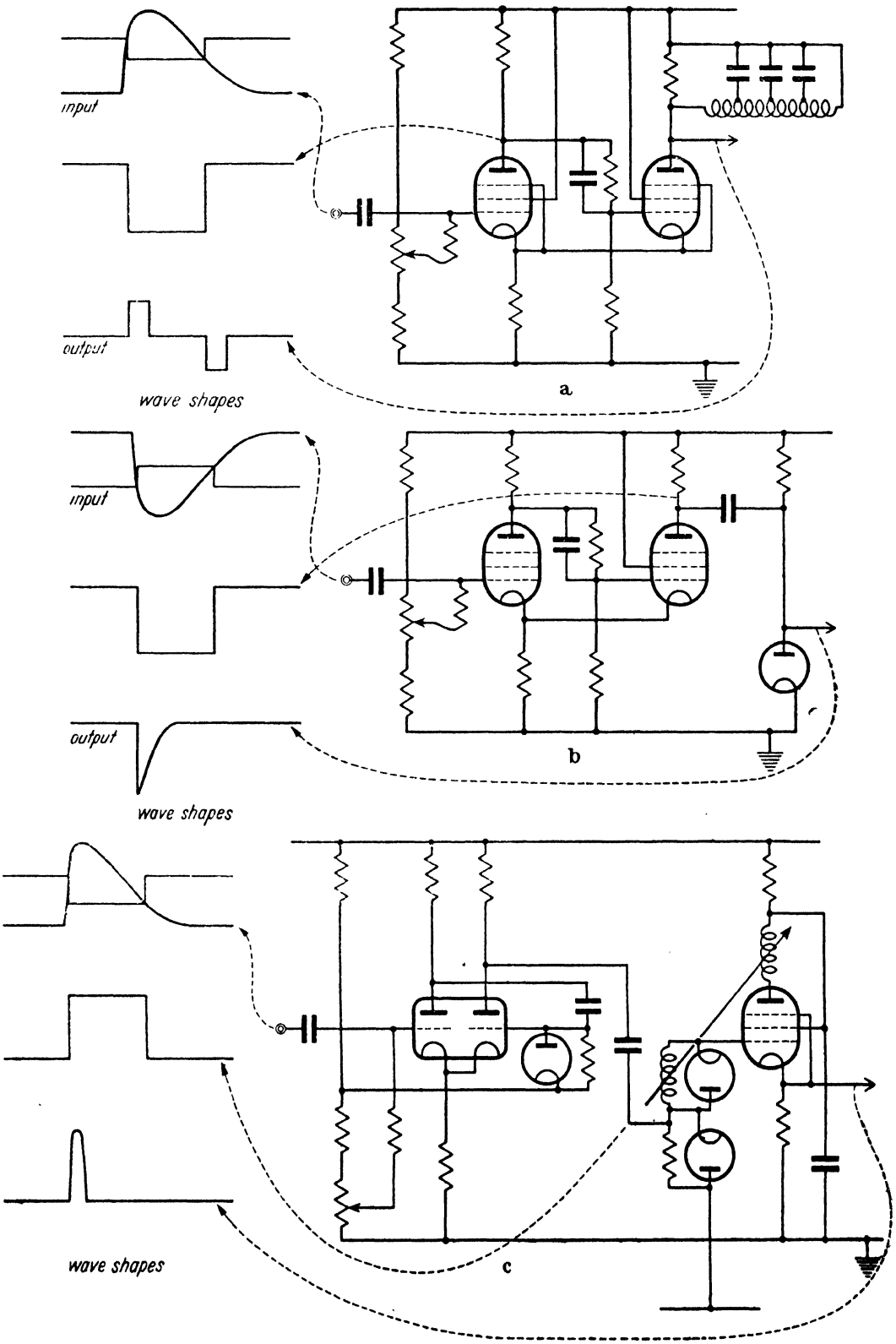


Figure 45. Use of simple discriminator for coincidence counting

Pulse shaping circuits—When a moderate resolving time (>0·5 microsecond) is required it is possible to use a trigger circuit for accurate pulse standardization. The input pulse is used to operate a trigger circuit which generates a square pulse of standard amplitude and of length determined by the length of the input pulse. The front edge of this pulse can then be used to generate a square pulse of known duration with the help of a delay line by any of the methods described on page 90. Alternatively the front edge can be converted into a short triangular pulse using the diode pulse shaping circuit described on page 87. A third method of generating a standard pulse makes use of a blocking oscillator. All three circuits are shown in *Figure 46*.

Figure 46. Typical pulse shapers for coincidence circuits: a *Trigger circuit and delay line pulse shaper;* b *Trigger circuit and diode pulse shaper;* c *blocking oscillator used as pulse shaper*



When a very short resolving time is required (<0·1 microsecond) it usually implies that the input pulses *e.g.* electron multiplier pulses, are already steeper than can be conveniently generated by electronic means. In these cases the pulses are merely shaped by a simple differentiating circuit or a delay line without the intervening trigger circuit.

Coincidence mixers—There are several types of non-linear combination circuit used to accentuate the difference between coincident and non-coincident pulses. The simplest is the diode circuit described on page 87. By appropriate connection of the diodes this circuit will operate with input pulses of either sign. If the shaped input pulses are negative the cathode coupled triode circuit can be used.

A third combination circuit utilizes the well known ' knee ' in pentode anode characteristics. The input negative pulses are fed to the control grids of two valves connected as shown in *Figure 47*. The common anode load

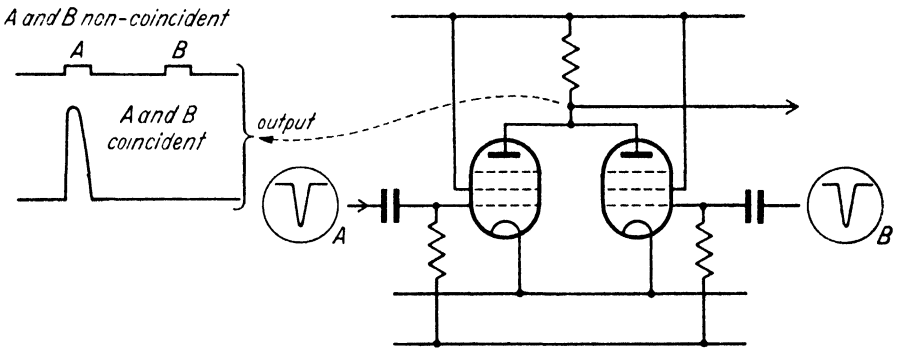


Figure 47. Non-linear coincidence mixer using knee in pentode characteristics

and D.C. conditions of the grids are so chosen that the anode operating potential is well below the ' knee ' of the anode characteristic even if one valve is removed. Thus the positive anode pulse resulting from a negative pulse fed into one grid is very small although if coincident pulses are fed into both grids the anode pulse is large.

Another combination circuit uses a pentode which is normally cut off from both the suppressor and control grids. Positive pulses supplied simultaneously to these grids will then cause a negative pulse to appear on the anode.

Veto circuits (anti-coincidence circuits)—A pulse fed into a veto channel is required to impose an over-riding veto on the output from the system *e.g.* a three channel system with input channels A B and C might have channels A and B arranged as a coincidence circuit with C applying a veto. This would mean that the system must produce an output pulse when simultaneous pulses arrive at A and B, provided that there is no pulse in channel C.

In this case the veto from channel C must operate even if the pulse in channel C is a trifle late due to a small delay in the operation of its counter. This can be ensured by putting a small delay t (approximately 1 microsecond) in channels A and B. Then to ensure that the veto is applied when the counters in channels A and B introduce a delay it is sufficient merely to arrange that

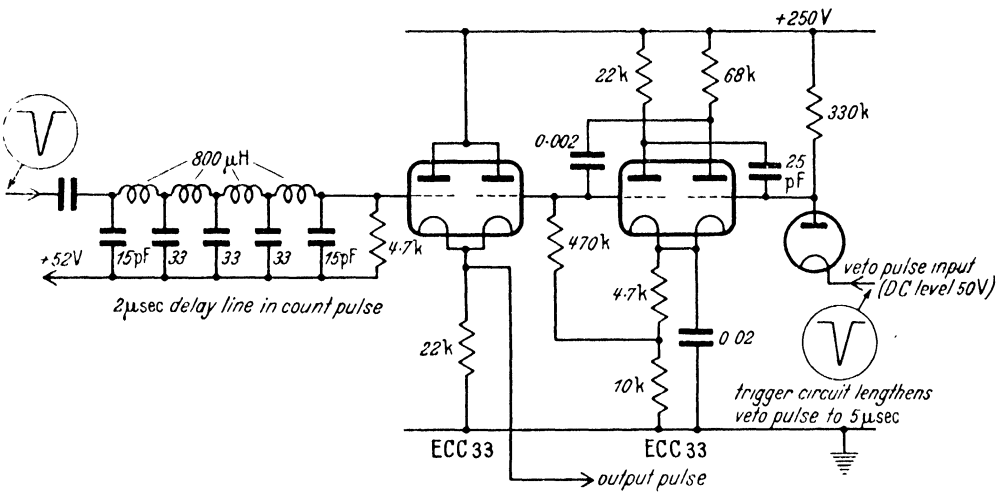


Figure 48. Typical veto circuit using double triode coincidence mixer

the pulse in channel C is longer than those in A and B by about $2t$. Any of the coincidence mixers can be used as a veto circuit by altering the D.C. conditions and sign of pulse of one of the inputs. A typical veto circuit using a cathode coupled triode mixer is shown in *Figure 48*.

GATE CIRCUITS

Sometimes a pulse *e.g.* from an ionization chamber, is required to be accepted and ultimately measured when and only when a signal pulse is received from some other source. Circuits which will do this are known as gate circuits. It is evident that a gate circuit is similar to a coincidence mixer with the important difference that the output pulse must be accurately proportional to the input pulse when the gate is open.

The diode and triode coincidence mixers fulfil this specification and of these the cathode coupled triode mixer is preferable since a high input impedance is presented by both the signal and gate input terminals. All gate circuits produce an output pulse from the gate signal. This effect is undesirable and is of the smallest magnitude from the double triode and double diode gate circuits.

Another gate circuit is made by using the control and suppressor grids of a pentode as the gate and signal inputs or *vice versa*. This arrangement is markedly inferior to the double triode gate both in linearity and in the magnitude of the undesired output gate signal.

SCALERS

Binary scalers—The counting of pulses is usually done ultimately by some form of mechanical register such as a Post Office call meter. When the mean pulse rate is too high to operate a mechanical register directly a scaler is interposed between the source of pulses and the register. The simplest scaler is the scale of two illustrated in *Figure 49*. It is a D.C. coupled symmetrical

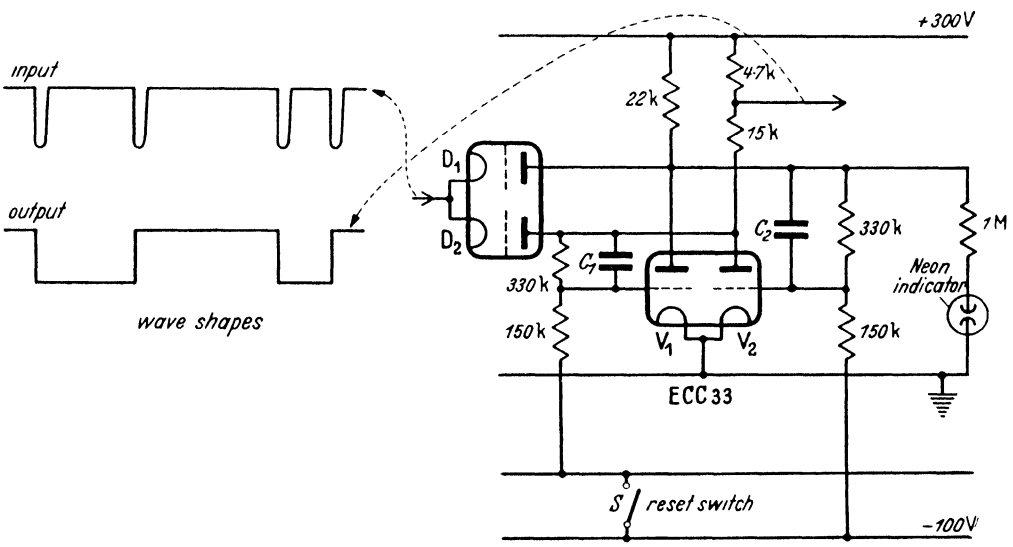


Figure 49. Typical scale of two circuit

trigger circuit which therefore has two stable positions. The triggering pulses are fed simultaneously into corresponding points on the trigger circuit *e.g.* the two anodes. The arrangement shown will operate equally well from either the downward portions of an input square wave or the negative pulses obtained by differentiating such a wave.

If we suppose that initially V_1 is conducting and V_2 cut off, then diode D_1 is cut off and D_2 has no volts across it. A negative input pulse is passed by D_2 and condenser C_1 to the grid of V_1 and thereby initiates the triggering action to the other state of the circuit. It is evident that the circuit must be stable in either position even when the input signal potential is at the lower value of its square wave form, but must be triggered by the downward portion of the square wave. This is achieved by the inclusion of two small condensers C_1 and C_2 which effectively remember the preceding state of the circuit and thus contain the data to determine the next state. The action of the circuit when fed with negative pulses instead of a square wave is very similar. When fed with negative pulses the circuit therefore delivers square waves which can be used to drive another similar circuit. The second stage will trigger from

the downward parts of the square wave produced by the first stage *i.e.* on every second input pulse. If n such stages are interposed between the source of pulses and the mechanical register then the mean pulse rate fed to the latter is $1/2^n$ of the mean input pulse rate. Hence if m counts are recorded on the mechanical register the number of input pulses must be $m \times 2^n$ plus the number stored in the scaling circuit.

The number stored can be deduced from the final position of the scaling stages. Each stage has two possible positions, one of which signifies 0 and the other 1. A resetting arrangement ensures that all the stages of the scaler are initially in their 0 position. Then if the final positions of the stages are written in order with the first stage on the right, the resulting number, composed of noughts and ones, is the expression, in binary notation, of the number stored in the scaler. For instance 10011 means $1 \times 16 + 0 \times 8 + 0 \times 4 + 1 \times 2 + 1 \times 1 = 19$.

The position of a typical stage of the scaler can be indicated by a small neon lamp as shown in *Figure 49*. A commonly used method of resetting is also shown. If the switch S (common to all stages) is temporarily opened then the trigger circuit has but one stable position, the 0 position. If pentodes are used there are several ways of making a symmetrical D.C. coupled trigger circuit, any of which can be used to make a scale of two stage where the operation would be similar to that of the triode trigger pair described.

An important parameter of a scaling stage is its resolving time which may be defined as the shortest interval between two pulses which can be correctly counted. The lower limit to the resolving time is set by the time constant of the condensers C_1 and C_2 with their associated grid coupling resistor chains. If the incoming pulses are regarded as infinitely sharp the lowest practicable value for C_1 and C_2 is determined by the input capacity of the valves used. The grid D.C. coupling resistors effectively reduce the anode loads of the valves so that the ultimate lower limit for the coupling resistors is determined by the slope of the valves used and by the voltage of the negative line. It follows that the shortest resolving time is achieved by the use of a high negative line voltage and a pair of pentodes with a high band width factor. In this way a resolving time of about 0·3 microsecond can be obtained, and about 1 microsecond using a pair of triodes.

Ring scales of ten—The interpretation of the result yielded by a scaler operating on the binary system is rather inconvenient. To avoid this trouble several types of scale of ten are in use. Of these the simplest is probably the ring type using ten trigger pairs (*Figure 50*). These can each have two states,

say A and B. The trigger pairs are interconnected cyclically in such a way that if the nth stage is reset from its B to its A state then the $n+1$th stage will be triggered from its A to its B state. All the pairs are fed asymmetrically with input pulses from a common busbar, the connections being so arranged that a pair in the B state is triggered to the A state by an input pulse but a pair in the A state is unaffected. The initial state of the ring is determined by the resetting button with one of the trigger pairs (representing zero) in the B state and all the others in the A state. The first input pulse resets the zero pair to the A state and therefore triggers the next pair (representing 1) to the B state. Thus the electrical pattern on the ring circuit rotates by one tenth of a revolution for every input pulse received. A pulse can be derived from

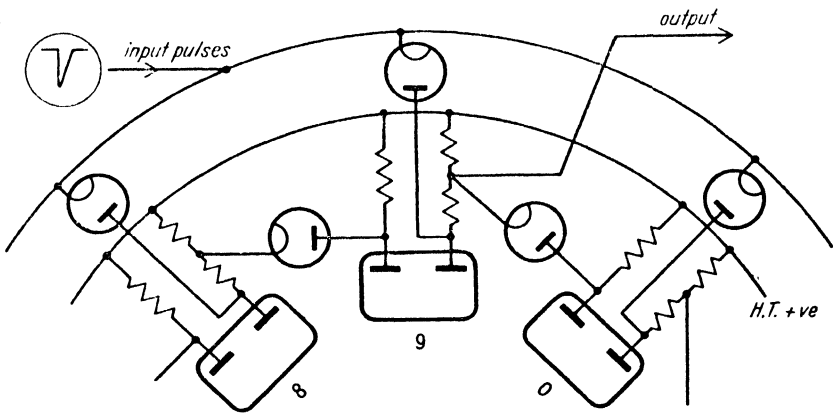


Figure 50. Typical ring type decade scaler

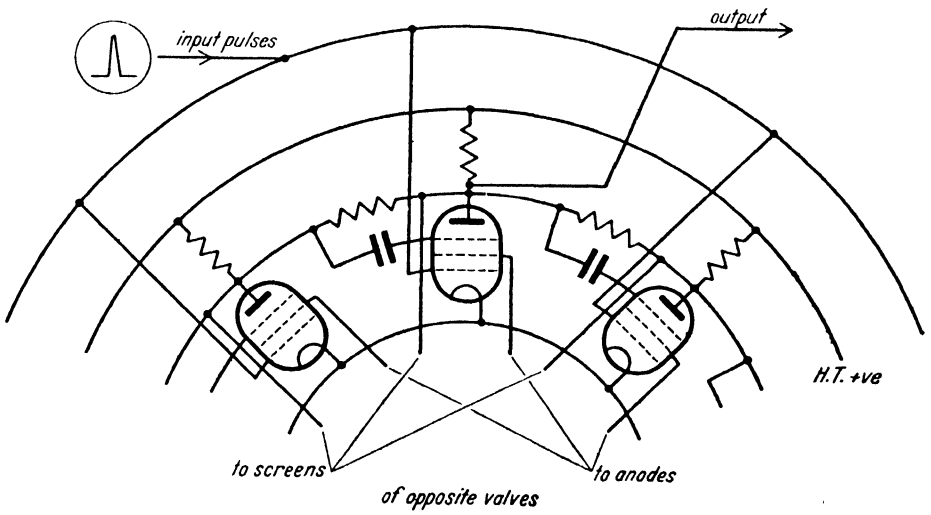


Figure 51. Regener ring decade scaler circuit

the resetting of the trigger pair representing nine and used to operate an identical ring of ten pairs. In this way a scale of a hundred or a thousand can be made.

Another ring type scaler which is rather more economical in valves is the Regener ring using five trigger pairs to make a scale of ten, *Figure 51.*

The ten valves in this circuit are arranged in a ring and diametrically cross connected to make five diametral trigger circuits. All adjacent anodes are connected circumferentially by resistances the value of which are chosen as follows. If, of three adjacent valves, the first and last are in the non-conducting state then the D.C. conditions of the trigger pair comprising the middle valve and its diametral partner must be so altered by the circumferential resistances that the middle valve can be only in its non-conducting state. This condition sets an upper limit to the value of the circumferential resistances. If the first and last valves are in opposite states *e.g.* conducting and non-conducting, then the middle valve trigger circuit must retain its normal two stable positions. This condition sets a lower limit to the value of the circumferential resistances. The only stable position of a ring circuit interconnected in this way is with five adjacent valves conducting and the other five cut off. There are evidently ten possible positions of this electrical pattern on the ring circuit corresponding to the ten digits 0 to 9. This pattern is made to advance by one tenth of a revolution per input pulse in the following way. The ring consists of ten pentodes with direct anode-to-screen diametral cross couplings, leaving the control and suppressor grids unused. Positive pulses applied to the control grids of all the valves will then cause negative pulses on the five anodes at high potential but negligible pulses on the five low potential anodes. Each anode is coupled by a resistance capacity coupling to the suppressor of the next valve in the ring. Then four of the valves with high anode potential will receive negative pulses on their suppressor grids. These valves will be unaffected since they are already in the state with negligible anode current. One of the valves with high anode current will also receive a negative pulse on its suppressor and consequently will trigger with its diametral partner to its other stable state. The net result of an input pulse is therefore that the electrical pattern has moved on by one valve in the direction of the anode to suppressor couplings.

A third type of ring circuit similar to the Regener ring can be made using ten triodes (five double triodes) arranged in a ring with opposite valves connected as D.C. coupled trigger pairs, *Figure 52.* Additional resistors are connected between each anode and the grid which is coupled to an adjacent anode *e.g.* from A_1 to G_7 in *Figure 52.* These resistances are chosen so that all the trigger circuits have the normal two stable positions but that if two neighbouring diametral pairs are in dissimilar positions then one of them, say the clockwise one, will be nearer to its critical triggering condition than the other. If then the ring is set into a condition with five adjacent valves conducting and the other five cut off, one of the pairs will be more readily triggered than the others. A suitable pulse fed into all ten cathodes will trigger the sensitive pair but will be ignored by the others. The electrical pattern is therefore made to rotate in a clockwise direction since the sensitive

pair is always on the clockwise edge of the five up five down pattern. Satisfactory discrimination between triggering of the edge of the pattern and of the rest of the pattern can be obtained by the use of the small diametrically connected condensers and an appropriate rate of rise of the input positive

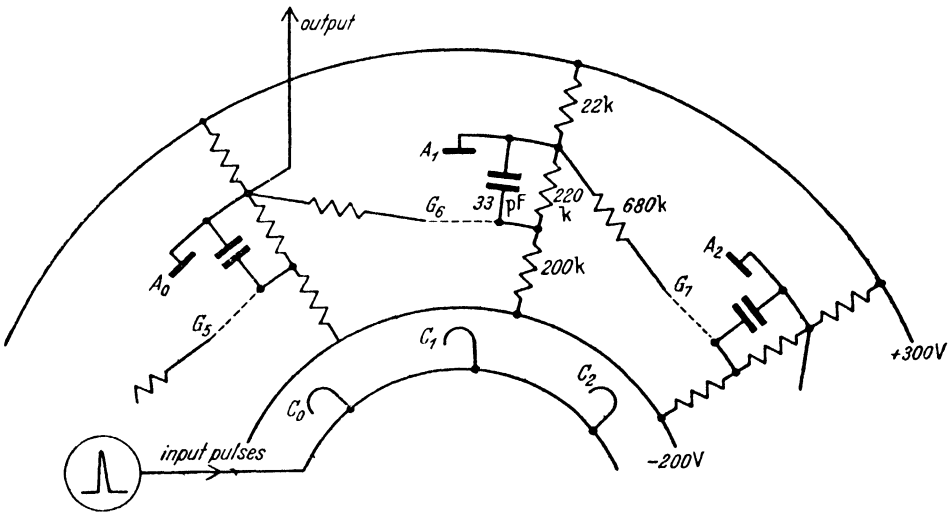


Figure 52. Regener ring decade scaler using triodes. All triodes one type ECC33. To simplify the diagram electrodes of valves are shown dissociated

pulse fed to the cathodes. A positive pulse fed to the cathodes of a D.C. coupled trigger circuit initiates the triggering process *via* the valve which is conducting. Since this valve is in grid current the positive cathode pulse does not have much effect unless its rate of rise is greater than the rate of rise of the grid when the available grid current is all diverted into the cross coupling condenser. In the ring circuit four of the trigger pairs have their ' on ' valves with about twice the grid current of the ' on ' valve in the remaining pair. The rate of rise of the input cathode pulse can therefore be chosen to trigger the sensitive pair but leave the others unaffected.

To indicate the position of these ring circuits neon indicator lamps are used connected to the anodes of the ring *via* high resistances. In this way any valve which is cut off lights its associated neon lamp. The pattern of lights then indicates the position of the ring.

Other scales of ten—There are two other scales of ten in use, each in effect derived by the combination of a conventional scale of two and a scale of five.

A scale of five can be made by the use of a form of ring circuit with five valves with their cathodes connected together. Each grid is D.C. coupled by a resistance mixing circuit to all the other anodes and so receives a potential which is the average of the other anodes. By appropriate choice of circuit constants such an arrangement can be made so that the only stable condition is with one valve conducting and the other four cut off. There are thus five stable positions. Each anode is connected cyclically *via* a condenser to the

next grid. Hence a positive pulse applied to the cathodes causes a positive pulse to appear on the grid of the next valve in the sequence. Each pulse therefore causes the next valve to become conducting. A scale of ten can therefore be made by feeding this ring of five from a conventional scale of two.

An ingenious way to make a scale of five is shown in *Figure 53*. The symbols in binary notation for the numbers 0 to 5 are as follows: 000=0; 001=1; 010=2; 011=3; 100=4; 101=5. A scale of five can therefore

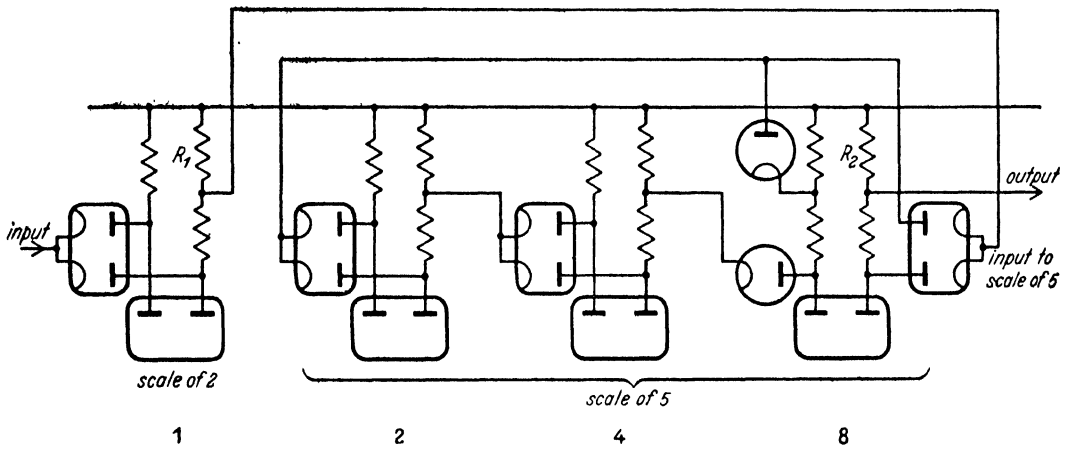


Figure 53. Decade scaler derived from binary scaler. R_2 should be 20 per cent greater than R_1

be made from a scale of eight by arranging to make the next pulse after four reset the ' four ' without adding one to the ' one ' stage. The requirement is therefore:

1 an input pulse must reset the ' four ' if it is in the four position but must not directly affect it if it is in the ' nought ' position

2 an input pulse must be fed directly to the ' one ' stage in the usual way unless the ' four ' stage is in the four position in which case the input pulse must be diverted

3 the ' one ', ' two ' and ' four ' stages must otherwise be connected in the usual way for a binary scaler.

All these requirements are met by the system of diodes shown in *Figure 53*. The input square waves are provided by the output of a conventional scale of two so that the complete circuit comprising four trigger pairs and five double diodes makes a scale of ten.

Meter driving stage—At the end of a scaler it is necessary to use a pulse lengthening circuit to provide a long enough pulse to drive the mechanical register. If a large scaling factor (100 or more) precedes the register the arrival

of pulses at the register is almost uniform so that a simple self-resetting trigger pair is all that is necessary.

If the scaling factor is small, say 2 or 4, an appreciable reduction in counting losses can be achieved by making the output circuit operate in two stages as shown in *Figure 54.* When triggered by an input pulse a long powerful pulse is supplied to the mechanical register and then the circuit is insensitive to further triggering pulses for a time slightly longer than the dead time of the mechanical register. If a pulse then arrives too soon after its predecessor it is ignored but no extra dead time is added. A circuit of this type fed with pulses at an indigestible rate counts at the maximum speed of which it is capable. A simple pulse lengthening circuit under the same circumstances will not count at all.

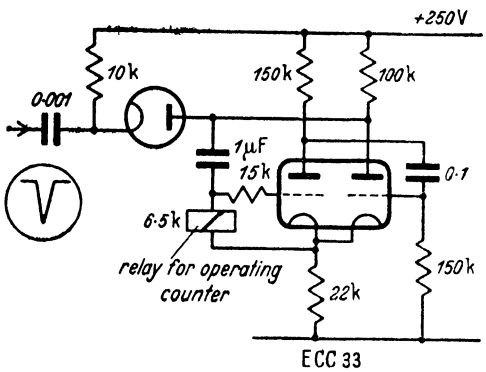


Figure 54. Mechanical counter driving circuit with dead time after each operation

Integrating scalers—For moderate counting rates it is possible to make a scaler by converting the input pulses into constant pulses of charge. These charge pulses can then be used to charge a condenser. The condenser is discharged when it has received a pre-set number of input pulses, say 10. Then the number of times that the condenser has to be discharged in a given period is one tenth of the total number of pulses received during that period. Owing to the comparatively long time required to discharge the condenser it is not possible to make this type of scaler operate at extremely high rates.

PULSE RATE METERS

To indicate the mean rate of arrival of pulses a rate meter can be used. The usual mode of operation of such a device is illustrated in *Figure 55.* The incoming pulses are first standardized to a constant height and duration and the mean current of the standardized pulses is then read on a suitable meter. For a given mean input pulse rate the best accuracy possible is limited by the time constant of

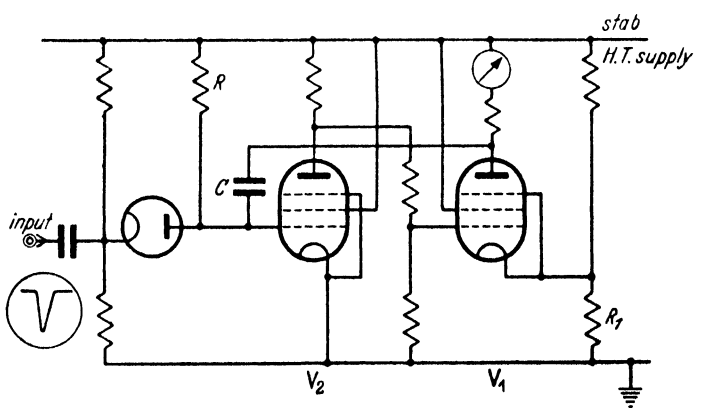


Figure 55. Typical pulse rate meter circuit

the indicating meter circuits. For high pulse rates (say greater than 10^5 per second) this is no disadvantage since in the time constant of an ordinary moving coil meter (about half a second) sufficient pulses can arrive to give a statistical accuracy at least as good as the intrinsic accuracy of the meter. At low pulse rates it is necessary to increase the time constant of the indicating meter artificially to obtain a reasonable overall accuracy. For pulse rates less than about ten a second it is not convenient to use a rate meter since if the time constant of the meter is made long enough to give a good statistical accuracy it becomes inconvenient to read. A typical design for a pulse rate meter is shown in *Figure 55*. In this circuit V_1 and V_2 constitute a trigger pair in which V_1 is normally non-conducting. When the circuit is triggered the current passed by V_1 is accurately standardized by the large cathode feedback resistance R_1. The time during which V_1 remains conducting is also accurately standardized by the time constant CR. Thus the mean current passed by V_1 and indicated by the meter is proportional to the mean pulse rate. The scale of the rate meter is slightly non-linear since if the input pulse rate is high some of the pulses will be ignored.

STABILIZERS

Voltage stabilizers—As mentioned earlier a voltage stabilizer can be considered to be a D.C. amplifier with negative feedback *via* a reference voltage as shown in *Figure 56*. The output impedance of such a stabilizer can be

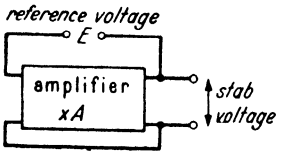


Figure 56. Block diagram for simple voltage stabilizer. If amplifier output impedance is Z and voltage gain is A, stabilizer output impedance is ~ Z/A

written down directly from the expression for a negative feedback amplifier. It is clear that the D.C. amplifier should have a high gain and low output impedance to be suitable for use as a stabilizer. The most common stabilizer circuit is the well known two valve arrangement shown in *Figure 57*. These two valves are used as voltage amplifier and cathode follower output to give high voltage gain and low output impedance respectively. The reference voltage can be provided either by a neon voltage regulator or by a dry H.T. battery.

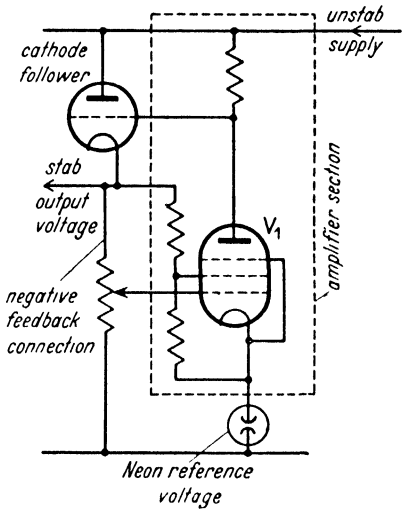


Figure 57. Simple voltage stabilizer

To improve the performance of the simple two valve stabilizer the amplifier gain can be increased by the use of positive feedback as shown in *Figure 58*. The positive feedback must be put over the amplifier alone and must not

include the output cathode follower stage since the output impedance of an amplifier with positive voltage feedback is increased in the same ratio as the gain. The use of a cathode coupled pair as an amplifier (*Figure 58*) renders the application of positive feedback very easy and in addition ensures that the reference voltage does not have to supply any current. It does so in the simpler circuit (*Figure 57*) to the detriment of its performance as a constant reference voltage.

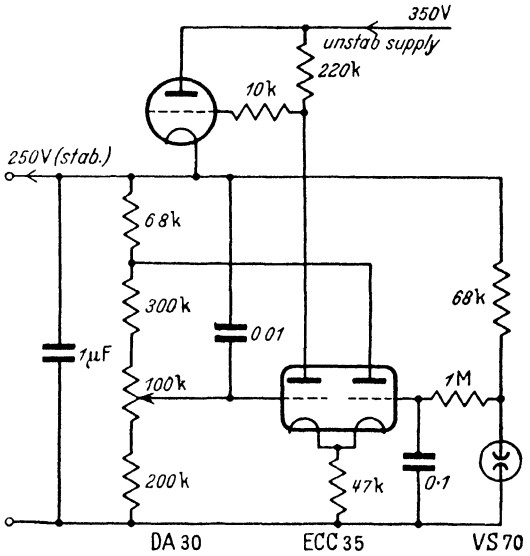


Figure 58. Voltage stabilizer with positive feedback

E.H.T. voltage stabilizers— For proportional counters and Geiger counters a high voltage (about 2kv) is required with high stability. The arrangement of *Figure 57* is not directly applicable to the production of such high stabilized voltages since the amplifier valve V_1 has approximately the full stabilized voltage across it. The most satisfactory arrangement is probably a stabilizer of the same type as that of *Figure 58* adapted to supply a small current at high voltage. A typical stabilizer designed in this way to supply 5ma at 2kv is shown in *Figure 59*. Brief study of this circuit shows how the use of a cathode coupled pair as an amplifier makes it possible to avoid over running the voltage rating of the amplifier valve.

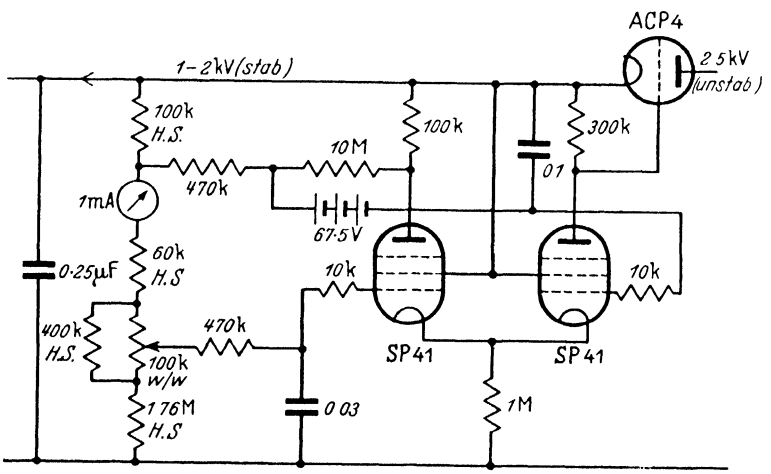


Figure 59. Voltage stabilizer with positive feedback suitable for high voltage supply

Current stabilizers — A current stabilizer results if current feedback is applied to a D.C. amplifier *via* a reference voltage (*Figure 60*). Current stabilizers are usually required to stabilize the current in a deflecting magnet, in which case the current to be controlled is often inconveniently

large. The D.C. amplifier represented in *Figure 60* may then be a complex device the output stage of which might be a large generator. The feedback loop therefore contains several elements with long time constants and consequently the chief difficulty in the design of such current stabilizers is the problem of preventing hunting. The methods of doing this cannot be dealt with in detail here but are based in principle on the methods described earlier (page 82) for preventing oscillation in feedback amplifiers.

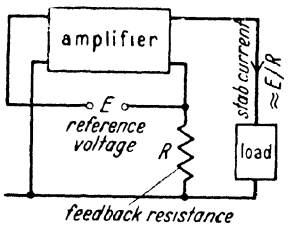


Figure 60. Block diagram of current stabilizer

GLOSSARY

Resistance R in ohms of an electrical element is defined as $R=e/i$ where e is the potential difference across the element in volts and i is the current through it in amperes.

Conductance is the reciprocal of resistance.

Impedance Z is a generalization of the concept of resistance to include all linear elements *i.e.* condensers, inductances, resistances and combinations thereof. It is defined as follows:

$$\text{Let } e=\text{real part } e_0 \exp(j\omega t)$$
$$i=\text{real part } i_0 \exp(j\omega t)$$

e and i are then both sine waves of frequency $\omega/2\pi$; e_0 and i_0 are in general complex. The impedance, defined by analogy as $Z=e_0/i_0$, is then also complex. To avoid confusion, $\sqrt{(-1)}$ is written as j.

Admittance Y is the reciprocal of impedance.

With these definitions the impedance of a resistor, inductance and condenser is written R, $j\omega L$, and $1/j\omega C$ respectively. The impedance of a series combination is the sum of the impedances of the components. Similarly the admittance of a parallel combination is the sum of the admittances of the components.

Argand diagram Complex quantities such as e_0, i_0, Y and Z can be represented in the complex plane by points where abscissae and ordinates are specified by the real and imaginary parts respectively. The resulting figure is known as an Argand diagram. The straight line joining the representative point on the Argand diagram to the origin is often called the vector representation of the quantity.

Inversion If two impedances Z and Z' are such that $ZZ'=R^2$ where R is a real constant for all values of ω, Z is said to be the inverse of Z' and *vice versa*. The inverse of the series combination of Z_1 and Z_2 is the parallel combination of Z_1' and Z_2' where $Z_1Z_1'=Z_2Z_2'=R^2$.

Pass band The pass band of an amplifier or filter is the range of frequencies over which the gain of the amplifier is large or the loss of a filter is small. The exact definition of the width of the pass band (band-width) is somewhat arbitrary. Most commonly the edges of the pass band are defined as those frequencies for which the output voltage is $1/\sqrt{2}$ of the value in the middle of the pass band.

Band-width factor of a valve is defined as $G/2\pi C$ where G is the mutual conductance of the valve in amperes per volt and C is the sum of the input and output capacities of the valve in farads.

5

THEORY OF BETA-DECAY

T. H. R. Skyrme

SINCE the publication of KONOPINSKI's general review[1] of β-ray theory much experimental work of increased accuracy has been done. Some difficulties have disappeared, some new ones have come and gone, others it seems have come to stay, of which the most remarkable is the ubiquity of the 'allowed' spectrum. In this review we have not attempted to digest all this mass of evidence, but have referred only to those experiments which are significant for the general theory. On the other hand we have tried to summarize, or refer to, most of the fruitful developments in β-ray theory, both in general concepts and in analyses of particular problems which are amenable to experiment. The list of references is intended to be reasonably complete only for theoretical papers.

FACTS AND HYPOTHESES

The main facts of β-decay that any theory must explain are

a Most unstable nuclei decay by emitting an electron (or positron) with a corresponding increase (or decrease) of one unit of nuclear charge. Although β-particles may be accompanied by γ-rays, often no such radiation is observed. The possibility that β-particles are different from electrons is discussed by CRANE[2]. An experiment confirming the identification has been made by GOLDHABER[3].

b The β-rays have a continuous energy spectrum, usually of the same characteristic shape, with a maximum energy equal, within experimental error, to the available energy difference between the parent and daughter nuclei.

c So far as knowledge goes, the initial and final nuclei differ in spin by an integral multiple of $\hbar$, and have the same statistics, although the electron has a spin $\frac{1}{2}\hbar$.

d The lifetimes of different β-active nuclei differ considerably, and that of a given nucleus is correlated partially to the maximum energy in the way first noticed by SARGENT[4].

The neutrino hypothesis—The apparent failure observed here in the laws of conservation of energy and angular momentum is customarily explained by

Pauli's neutrino hypothesis, which postulates that an uncharged particle with spin $\frac{1}{2}\hbar$ and small or zero mass is emitted simultaneously with the β-particle.

This hypothesis, the consequences of which were first evaluated by FERMI[5], is fundamental in all β-ray theory; unfortunately its very nature precludes any direct test, and our faith in it must rest on rather indirect evidence.

Literally this is true of any elementary particle, but it is especially true of the neutrino because we can identify only one event for each particle. Cross sections for inverse β-processes are extremely small[6]. Double β-decay however may involve the same neutrino twice.

The most general consequence of the neutrino hypothesis which can be tested comes from the conservation of linear momentum. It predicts that if the momenta and energies of the electron and the recoiling nucleus are measured for the same event, the apparent defects of momentum and energy should be related as for a single particle, that is, $\Delta E = c\Delta p$, if the neutrino have no rest mass. The ideal experiment of this type, in which the magnitudes and directions of both momenta are measured, has not yet been made. However, several less complete experiments have shown that there is an apparent loss of momentum which is compatible with the neutrino hypothesis. CRANE and HALPERN[7] measured in a cloud chamber the magnitudes of both momenta for Cl^{38} and showed that high energy recoils were associated as often with low energy as with high energy electrons. Li^8, where the unstable daughter nucleus Be^8 breaks up quickly into two α-particles, has been studied recently[8]; the best measured quantity was the mean square recoil momentum, and its value was certainly different from that expected if there were no neutrino. These and other experiments concerned with the neutrino have been reviewed in detail by CRANE[2].

As well as confirming the conservation of momentum, recoil experiments can give the angular correlation between the electron and the neutrino, which may be important for discriminating between different forms of interaction; we shall discuss this later (p 131, 132).

We must consider next how this decay process is to be represented mathematically. First it is assumed that neutrinos are described by an uncharged quantized field of the Dirac electron type, because no other way of describing relativistic particles of spin $\frac{1}{2}$ is known. As with the electron field, we must assume in a sensible theory that all the states of negative energy are filled in the 'vacuum' and then 'holes' among them will describe anti-particles, analogous to positrons, except that, as the neutrinos have no charge, 'anti-neutrinos' will be indistinguishable physically from neutrinos. So long as we deal with only one event in the history of each neutrino* it makes no difference whether that event be described as the emission of a neutrino or the absorption of an anti-neutrino, and because it is more convenient

* This includes all β-ray phenomena except double β-decay.

formally the emission of an electron is usually associated with the absorption of an anti-neutrino and *vice versa*, so that the number of light particles, or ' leptons ', is conserved.

The nucleus is supposed to consist of protons and neutrons only, so that decay with the emission of a negative β-particle involves the simultaneous change of a nuclear neutron into a proton and of an anti-neutrino, plucked from the vacuum, into an electron. This may be described phenomenologically by adding to the Hamiltonian of the system an interaction term, coupling the nucleon system to the electron-neutrino field. We shall examine in the following sections the possible forms of this term and the detailed theories of β-decay to which they lead. We should then expect that just one of these possible hypotheses explained all the experimental facts about lifetimes, spin changes, spectral shapes *etc.*

It now appears rather doubtful whether this hope can be fulfilled, but even if it could the achievement would not give a completely satisfying picture of β-decay. An interaction involving the wave functions of four particles at the same point in space, with a very small coupling constant, does not commend itself as an elementary process. YUKAWA's original suggestion[9], that β-decay is an indirect process in which, for instance, a neutron in the nucleus changes over into a proton and emits a negative meson which then decays into an electron and neutrino, gives a qualitatively attractive ' explanation ' in terms of simpler processes, but the necessary properties of such a meson have not been correlated quantitatively with those of any of the mesons yet observed. This question is discussed in detail in the last section.

All the theories discussed here are based on formalisms that are generalizations of that used for describing the electromagnetic field and its interaction with charged particles. Recent developments in the theory of quantum electrodynamics[10] have shown that, while the equations can be so manipulated as to describe radiation processes in correct detail, there is yet some fact or principle lacking which makes the theory not finally acceptable. For the former reason we might expect that, *a fortiori* because the coupling is so small, an analogous theory of β-decay should also describe β-processes correctly. If, however, experimental evidence should become clearly contradictory to any such theory we shall have to seek a different description of particle transformations, or perhaps to say that the difficulties not overcome in electrodynamics are more important where particle transformations are involved.

PHENOMENOLOGICAL THEORY—ALLOWED TRANSITIONS

FERMI[5] first formulated mathematically the neutrino hypothesis of β-decay by direct analogy with radiation theory; soon afterwards other similar theoretical possibilities were suggested and discussed by GAMOW and TELLER[11],

and by KONOPINSKI and UHLENBECK[12]. It will be convenient to use at first the language of quantised field theory[13] for all the four particle fields, in a discussion of the theoretical possibilities. The β-interaction is described, it is assumed, by the addition of a small term H_β to the Hamiltonian of the system, so that, according to standard perturbation theory, the probability per unit time of a transition from a state a to a state b of the unperturbed system is equal to

$$(2\pi/\hbar)|(b|H_\beta|a)|^2\,\delta(E_a - E_b) \qquad \ldots\ldots (1)$$

where $(b|H_\beta|a)$ is the matrix element of H_β between states a and b, and the δ-function expresses the conservation of energy. This matrix element must be different from zero only when the states a and b differ by the interchange of a proton and a neutron, and therefore must be bilinear in the pairs of field operators $\psi_N(x)$ and $\psi_P^*(x)$, $\psi_n(x)$ and $\psi_e^*(x)$ or their conjugates, where $\psi_f(x)$, $\psi_f^*(x)$ are the absorption and emission field operators of the four fields f, denoted by the obvious abbreviations N, P, n, e.

If H_β does not contain any derivatives of the field operators its form is restricted, by the requirement of Lorentz invariance, to a linear combination of five elementary interactions. The possible forms of H_β must be derived from possible invariant forms of action principle, and restrictions on the forms of any terms of H_β that contain field derivatives are less easily determined, and it is partly for this reason that such terms have not been considered much (some general forms were considered by HOYLE[14]), but latterly and principally because any simple hypothesis in which these terms are important such as that of KONOPINSKI and UHLENBECK[12] predicts spectral shapes and energy lifetime relations that disagree with good experimental evidence[1]. More complicated hypotheses that involve field derivatives significantly may be constructed to overcome any finite set of these objections, but until such expressions are found to result naturally from other theory it is better first to examine the detailed consequences of the simplest hypotheses, which do indeed show considerable agreement with experiment.

The possible forms of an H_β which do not involve field derivatives are included in the formula

$$H_\beta = \sum_{i=0}^{4}\left(G_i\int J_i(x)dx + G_i^*\int J_i^*(x)dx\right) \qquad \ldots\ldots (2)$$

where $J_i(x)$ are five independent quadrilinear invariants of the fields; five elementary types of interaction are

$$J_0 = (\psi_P\beta\psi_N)\,(\psi_e^*\beta\psi_n) \qquad \text{'scalar'}$$

$$J_1 = (\psi_P\psi_N)\,(\psi_e^*\psi_n) - (\psi_P\alpha\psi_N)\,(\psi_e^*\alpha\psi_n) \qquad \text{'vector'}$$

$$J_2 = (\psi_P^*\beta\sigma\psi_N)\,(\psi_e^*\beta\sigma\psi_n) + (\psi_P\beta\alpha\psi_N)\,(\psi_e^*\beta\alpha\psi_n) \qquad \text{'tensor'}$$

$$J_3 = (\psi_P^*\sigma\psi_N)\,(\psi_e^*\sigma\psi_n) - (\psi_P^*\gamma_5\psi_N)\,(\psi_e^*\gamma_5\psi_n) \qquad \text{'pseudo-vector or axial vector'}$$

$$J_4 = (\psi_P^*\beta\gamma_5\psi_N)\,(\psi_e^*\beta\gamma_5\psi_n) \qquad \text{'pseudo-scalar'}$$

where α, β *etc* are the usual Dirac matrices; these form a convenient basis because they are correlated to distinctive selection rules (see p 123).

The states of the nucleus are described more conveniently by the coordinates $\boldsymbol{x}_i$, σ_i, τ_i (space, four-component spin and charge) of the individual nucleons than by the states of the quantized nuclear fields.

The matrix elements of the nuclear fields may then be written in terms of the coordinate wave functions $\psi(\boldsymbol{x}_i,\sigma_i,\tau_i)$ according to a standard formula[13],

$$(b\Big|\int \psi_P^*(\boldsymbol{x})F(\boldsymbol{x})\psi_N(\boldsymbol{x})d\boldsymbol{x}\Big|a)$$

$$= \sum_{\sigma_i,\sigma_i'}\sum_{\tau_i,\tau_i'}\int\ldots\int\psi_b^*(\boldsymbol{x}_i,\sigma_i,\tau_i)\sum_{r=1}^{N}\left[F_{\sigma_r\sigma_r'}(\boldsymbol{x}_r)Q_r\right]\psi_a(\boldsymbol{x}_i,\sigma_i',\tau_i')d\boldsymbol{x}_1\ldots d\boldsymbol{x}_N$$

where $F_{\sigma,\sigma'}(\boldsymbol{x})$ is any spin matrix and function of $\boldsymbol{x}$, and Q_r is the operator that, acting on the r-th particle, converts it from a neutron to a proton, or gives zero if it already is a proton.

The wave function of the neutrino involved will be a plane wave since it has no other interactions, and plane waves may also be used for the electrons if the nucleus is not too heavy nor the energy too small. Then the matrix element of $\psi_e^*(\boldsymbol{x})\rho\psi_n(\boldsymbol{x})$, equal to $u_e^*(\boldsymbol{x})\rho u_n(\boldsymbol{x})$, where $u_e^*(\boldsymbol{x})$, $u_n(\boldsymbol{x})$ are the spinor wave functions of the emitted electron and absorbed neutrino, becomes $(u_e^*\rho u_n)e^{i\boldsymbol{k}.\boldsymbol{x}}$, where u_e^*, u_n are spinors and $\boldsymbol{k}=\boldsymbol{k}_e-\boldsymbol{k}_n$ is the momentum given to the light particles.

Therefore the matrix element of H_β may be written

$$(b|H_\beta|a) = \sum_t g_t M_t(\boldsymbol{k})\,(u_e^*\rho_t u_n) \qquad \ldots\ldots(3)$$

where the ρ_t are the various operators β, α *etc*, the g_t are constants (corresponding with G_i) and the nuclear matrix element

$$M_t(\boldsymbol{k}) = \sum_{\sigma_i\sigma_i'}\sum_{\tau_i\tau_i'}\int\psi_b^*(\boldsymbol{x},\sigma,\tau)\left\{\sum_{r=1}^{N}(\rho_t)_{\sigma_r\sigma_r'}Q_r e^{i\boldsymbol{k}.\boldsymbol{x}}\right\}\psi_a(\boldsymbol{x},\sigma,\tau)d\boldsymbol{x} \qquad \ldots\ldots(4)$$

Now $\boldsymbol{k}.\boldsymbol{x}\ll 1$, because the wavelengths of the light particles are much longer than the nuclear radius (for all usual β-decay energies), so we may replace $M_t(\boldsymbol{k})$ by $M_t(0)$ if this does not vanish. Then

$$|(b|H_\beta|a)|^2 = \sum_{t,t'} g_t g_{t'}^* M_t M_{t'}^* (u_e^*\rho_t u_n)(u_n^*\rho_{t'}^* u_e)$$

measures the probability of one particular mode of decay. Summation over

the uninteresting spins of the light particles can be made by the usual method of Dirac and Casimir

$$\sum_{Spins}(u_e^*\rho_t u_n)(u_n^*\rho_{t'}^* u_e) = \tfrac{1}{4}\,trace\left\{\rho_t\left(1-\frac{\boldsymbol{a}.\boldsymbol{k}_n+\beta\kappa_n}{\sqrt{\boldsymbol{k}_n^2+\kappa_n^2}}\right)\rho_{t'}^*\left(1+\frac{\boldsymbol{a}.\boldsymbol{k}_e+\beta\kappa_e}{\sqrt{\boldsymbol{k}_e^2+\kappa_e^2}}\right)\right\} \quad \ldots.(5)$$

where $\kappa_r = m_r c/\hbar$ are the reciprocal Compton wavelengths of the particles. Finally, when an average is made over the directions of the momentum, most cross terms disappear, giving

$$\text{Av}\sum_{Spins}|(b|H_\beta|a)|^2 = A + B(m_e c^2/E_e) + C(m_n c^2/E_n) + D(m_e m_n c^4/E_e E_n)$$

where E_e and E_n are the total energy of the electron and neutrino (including rest mass), and B,C,D are not greater than A in absolute value. B and C involve cross terms between adjacent interactions; their signs are changed in the case of positron emission.

Let E_0 be the total energy available to the light particles, that is, the difference of the nuclear energy levels. Then the possible states in which the electron leaves with an energy between E and $(E+dE)$ have a total statistical weight

$$\left(\frac{1}{8\pi^3}\right)^2\int\int d\boldsymbol{k}_e d\boldsymbol{k}_n \delta(E-\sqrt{\boldsymbol{k}_e^2+1})\;\delta(E+E_n-E_0)\,dE =$$

$$= \frac{1}{4\pi^4}E(E^2-1)^{\frac{1}{2}}(E_0-E)\{(E_0-E)^2-m^2{}_n\}^{\frac{1}{2}}dE$$

where, as in many subsequent expressions, units have been chosen so that $c=\hbar=m_e=1$, and the unit of energy is thus the electron's rest mass. The probability of such a decay is

$$2\pi\Sigma|(b|H_\beta|a)|^2 = (1/2\pi^3)\{A + B/E + (C + D/E)\,m_n/(E_0-E)\}\times$$

$$\times E(E^2-1)^{\frac{1}{2}}(E_0-E)\{(E_0-E)^2-m^2{}_n\}^{\frac{1}{2}}dE \quad \ldots.(6)$$

This formula, which gives the shape of the electrons' spectrum, must be corrected for the effect of the nuclear Coulomb field before comparing it with experiment. If Coulomb wave functions had been used throughout, the decay probability would have been multiplied by the relative electron density at the nucleus. This formula was first given by FERMI[5]; the last factor was included by later writers, *e.g.* MARSHAK[15]. Numerical values have been given in a convenient graphical form by BLEULER and ZÜNTI[16]. For the present case the Coulomb field factor is

$$F^{\mp}(Z,E) = \{2!/\Gamma(1+2s_0)\}^2\,(2pR)^{2(s_0-1)}\,e^{\pm\pi\alpha ZE/p}|\Gamma(s_0+i\alpha ZE/p)|^2\left\{\frac{1+s_0}{2}\right\} \quad \ldots.(7)$$

where $s_0=(1-\alpha^2Z^2)^{\frac{1}{2}}$, α is the fine structure constant $e^2/\hbar c$, Z is the nuclear

charge, R the nuclear radius and $p=(E^2-1)^{\frac{1}{2}}$ is the electron momentum. The minus/plus sign refers to electrons/positrons respectively.

Experimental comparison is usually made by drawing a Fermi or Kurie plot of $K(E)=[N(E)/E(E^2-1)^{\frac{1}{2}}F(Z,E)]^{\frac{1}{2}}$ as a function of E, where $N(E)$ describes the observed electron spectrum. If the neutrino mass is zero and $B=0$ this quantity should be proportional to E_0-E; if the mass of the neutrino is not zero $K(E)$ should deviate from linearity near the upper end point $E=E_0-m_\nu$. Also the maximum energy of the β-particles will be less than the energy difference E_0, which may be known from other data. But it has been pointed out by KOFOED-HANSEN[17] that the usual method of finding the end point by extrapolation only gives E_0 and not the true maximum energy of the electrons, except when E_0 is very small, so that the neutrino mass can in general only be determined by examining the spectral shape. This difficulty is less serious with H^3, from the upper limit[18] of which HUGHES and EGGLER[19] have deduced that the mass of the neutrino must be less than 25 kev. In later experiments[20, 20A] an even lower limit of 4 kev at most was found. The new higher value of the upper limit removes also much of the difficulty with the short lifetime of H^3, which was used by KONOPINSKI[21] as an argument for a finite neutrino mass. The problem of determining the neutrino's mass is discussed by FRANK[22].

Recent measurements[23–25] of spectra that are believed to belong to allowed transitions (and others) have usually shown good agreement with the theoretical curve. Recent experiments by BACKUS[26] and by COOK and LANGER[27–30] seemed to show a definite deviation from theory at low energies, which could not be explained by theory[31–33]. The experiments on Cu^{64} have been repeated by ALBERT and WU[34] using thinner and more uniform sources. They find that under these improved experimental conditions with allowance also for the effect of atomic screening of the Coulomb field of the nucleus[35], the experimental spectrum agrees very nearly with theoretical expectation, with the remaining deviation probably due to instrumental error.

This first comparison shows good agreement between detailed theory and experiment, and in addition shows that

a the neutrino mass is very small, probably zero; certainly $m_\nu<0{\cdot}01m_e$

b the cross terms which give rise to the coefficient B are unimportant.

It also supports the hypothesis that velocity dependent terms in H_β are small, for if not these would have to be of a rather special form to yield this same spectral shape. It does not discriminate between the different forms of the G_i compatible with b; in particular any one of the five standard interactions by itself is possible.

A second important deduction from the formula 6 is the total probability of β-decay. If we put $m_n=0$ and $B=0$ we obtain a formula for the decay constant λ_{ab}, the reciprocal of the mean lifetime,

$$\lambda_{ab} = (1/2\pi^3)\Sigma_t |g_t M_t|^2 \int_1^{E_0} F(Z,E)E(E^2-1)^{\frac{1}{2}}(E_0-E)^2 dE = \Sigma_t |g_t M_t|^2 f(E_0) \ldots . (8)$$

This formula applies to a transition between two definite nuclear states. The total decay constant for any nuclear species is found by summing over all the magnetic sub-states of the final nucleus, and is, of course, independent of the initial sub-state. This introduces a statistical weight factor that, for the same values of the matrix elements M_t, may be different according to the direction in which the decay takes place [15,36,37]. The matrix elements M_t cannot be calculated for any decay except that of the free neutron, but we can place upper limits upon them. Certainly $|M_t|<1$, because $|\rho_t| = 1$ and the wave functions are normalized to unity, so $\lambda_{ab}<G^2 f(E_0)$, where $G^2=\Sigma|g_t|^2$. Then if t be the lifetime of a β-active nucleus, $sft<1/G^2$: where s is a statistical weight factor depending on the nuclear spins and the possible spin change in β-decay. If no spin change is allowed $s = 1$; if there may be a change of one unit, then, for example, in the decay of He^6 (assumed spin 0) to Li^6 (spin 1), since there are three accessible final states from one possible initial state, $s = 3$.

The observed values of ft for different nuclei vary by a factor of more than 10^{16}. Almost without exception these values exceed a lower limit that is equal to the nearly constant value of ft for the mirror nuclei (the light positron emitters $Z^{2z-1}\rightarrow(Z-1)^{2z-1}$). He^6 appears to decay unexpectedly rapidly, but this may largely be explained by the s-factor if a spin change of one unit be allowed; H^3 used to be a grave exception but recent determinations of the end point [20, 20A] have removed most of the discrepancy. These facts indicate a value for G^2, the 'constant of β-decay', roughly equal to 10^{-23}, in units of $(\hbar^3/m^2c)^2$; the lifetime of the neutron[38] is not yet known accurately enough to fix the value of the constant.

That such a definite lower limit appears to exist, in particular that the mirror nuclei, with greatly varying disintegration energies, have a nearly constant ft value, is further evidence that H_β does not contain important velocity dependent terms, for these must, in general, give decay constants that increase rapidly with the decay energy. There seems to be a systematic variation of ft values[1, 34] through the periodic table, which may largely be due to the decrease in the value of the matrix elements as Z increases, for there will be less overlapping of the wave functions of very complex systems, and there are large irregular fluctuations which are discussed in the next section.

FORBIDDEN TRANSITIONS

The great variation of the ft values cannot be explained in terms of random fluctuations in the values of the matrix elements M_t alone, but there are good

reasons why often $M_t = 0$ and then the approximation used in replacing $M_t(\boldsymbol{k})$ by M_t is no longer justified; this will happen when the change in nuclear spin is greater than that allowed by ρ_t or when the parity change is unsuitable. A theoretical separation of allowed and forbidden transitions may then be made as follows.

We first neglect the Coulomb interaction; then the exponential $e^{i\boldsymbol{k}.\boldsymbol{x}}$ involved in $M_t(\boldsymbol{k})$ may be expanded in a series of spherical harmonics, and the first terms which give a non-zero contribution to $M_t(\boldsymbol{k})$ will involve the n-th harmonic, if n be the excess of the nuclear spin change (or the $(n+1)$-th if the parity change be unfavourable), and $M_t(\boldsymbol{k})$ will be smaller by a factor $(kR)^n$ than the ' usual value ' of M_t. Furthermore while M_t may be nearly equal to unity if $\rho_t = 1, \beta, \sigma$ or $\beta\sigma$, it will be smaller by a factor of the order v/c (where v is an average nuclear velocity), when $\rho_t = \alpha, \beta\alpha, \gamma_5$ or $\beta\gamma_5$, since these operators involve the ' small ' components of the spinor wave functions.

A transition is 'allowed' if the spin and parity change permit the principal matrix elements M_t to be different from zero, although in particular cases they may be small for other reasons. There is no parity change unless the interaction is of the purely pseudo-scalar type involving only $\rho = \beta\gamma_5$. A transition is ' first forbidden ' if only the small matrix elements M_t involving α, $\beta\alpha$ or γ_5 are non-zero or if for the principal matrix elements the first contribution to $M_t(\boldsymbol{k})$ comes from the first harmonic. It is 'second forbidden ' if the next harmonics are involved, and so on.

This classification must be distinguished from the experimental ones, whereby the degree of forbiddenness is related to the *ft* value, or to the shape of the electron spectrum. A satisfactory theory of β-decay should of course relate these to the theoretical classification with due allowance for the fact that the matrix elements cannot be evaluated exactly.

Selection rules—If, as is usually supposed, H_β is of a simple unmixed type involving only one of the interactions J_i, the theoretical classification may be expressed in terms of definite selection rules concerning spin and parity changes. For example, in the case of the vector interaction J_1, an allowed transition involves the scalar operator 1 which permits no spin or parity change, which may be symbolized by $\Delta J=0$, (+); a first forbidden transition involves α or $1.\boldsymbol{x}$, both of which are vectors, so that $\Delta J=0$, 1, (*not* $0\leftrightarrow 0$), (−). In this way the following table of selection rules may be constructed.

Table I. Selection Rules for Spin and Parity Changes

Interaction	*Allowed*	*First Forbidden*	*Second Forbidden*
J_0	$\Delta J=0$, (+)	$\Delta J=0$, 1 (*not* $0\leftrightarrow 0$), (−)	$\Delta J=1$, 2 (*not* $0\leftrightarrow 1$), (+
J_1	$\Delta J=0$, (+)	$\Delta J=0$, 1 (*not* $0\leftrightarrow 0$), (−)	$\Delta J=1$, 2, (+)
J_2	$\Delta J=0$, 1 (*not* $0\leftrightarrow 0$), (+)	$\Delta J=0$, 1, 2, (−)	$\Delta J=2$, 3, and $0\leftrightarrow 0$, (+)
J_3	$\Delta J=0$, 1 (*not* $0\leftrightarrow 0$), (+)	$\Delta J=0$, 1, 2, (−)	$\Delta J=2$, 3, (+)
J_4	$\Delta J=0$, (−)	$\Delta J=0$, 1 (*not* $0\leftrightarrow 0$), (+)	$\Delta J=1$, 2 (*not* $0\leftrightarrow 1$), (−)

Certain spin and parity changes are completely forbidden: $(0\leftrightarrow 0)$, $(-)$ for J_0 and J_1 and $(0\leftrightarrow 0)$, $(+)$ for J_3 and J_4; also $(0\leftrightarrow 1)$, $(+)$ for J_0 and $(0\leftrightarrow 1)$, $(-)$ for J_4. A detailed analysis of the various matrix elements is given by KONOPINSKI [40].

The spin relation rules associated with J_0, J_1 and J_4 are usually known as FERMI selection rules[5]; those with J_2 and J_3 as GAMOW-TELLER rules[11]. The differences within these two groups appear only in the second forbidden transitions.

Spectral shape—If we may use plane waves for the electron, the nuclear matrix element $M_t(\boldsymbol{k})$ may be expanded in a power series in $\boldsymbol{k}$, so that $(b|H_\beta|a)$ is given by formula 3 as a function of $\boldsymbol{k}$ and the spinors u_e, u_n; the spectral shape and total decay constant come by integrations over the momenta and spins. We can also carry out these integrations first in the following way, in which we may also introduce the effect of the Coulomb field.

We may write

$$(b|H_\beta|a) = \Sigma_t g_t \int I_t(\boldsymbol{x})[u_e^*(\boldsymbol{x})\rho_t u_n(\boldsymbol{x})]\,d\boldsymbol{x}$$

where $I_t(\boldsymbol{x}) = \psi_b^*(\boldsymbol{x})\rho_t Q\psi_a(\boldsymbol{x})$ and the various coordinates have been abbreviated into one symbol $\boldsymbol{x}$. Then the total probability of emission of an electron with energy between E and $E+dE$ is

$$P(E)dE = (1/2\pi^3)\,E\,(E^2-1)^{\frac{1}{2}}(E_0-E)^2 \sum_{t\,t'} g_t\,g_{t'}^* \times$$

$$\times \int\int I_t(\boldsymbol{x})I_{t'}^*(\boldsymbol{x}')\left[\mathrm{Av}\sum_{Spins} u_e^*(\boldsymbol{x})\rho_t u_n(\boldsymbol{x})u_n^*(\boldsymbol{x}')\rho_{t'}^* u_e(\boldsymbol{x}')\right]d\boldsymbol{x}d\boldsymbol{x}'$$

The expression in brackets may be expanded as a power series in $\boldsymbol{x}$ and $\boldsymbol{x}'$, by the formula

$$\mathrm{Av}\sum_{Spins}\left[u_e^*(\boldsymbol{x})\rho_t u_n(\boldsymbol{x})u_n^*(\boldsymbol{x}')\rho_{t'}^* u_e(\boldsymbol{x}')\right] = \tfrac{1}{4}\,\mathrm{trace}\,[\rho_t\theta_n(E_0-E,\boldsymbol{x},\boldsymbol{x}')\rho_{t'}^*\theta_e(E,\boldsymbol{x}',\boldsymbol{x})]$$

where $\theta_r = \mathrm{Av}\sum_{Spins} u_r(\boldsymbol{x})u_r^*(\boldsymbol{x}')$ is calculated from the wave functions. If plane waves are used for these

$$\theta_n = \frac{\sin t}{t} + \frac{i\,\boldsymbol{\alpha}.(\boldsymbol{x}-\boldsymbol{x}')}{|\boldsymbol{x}-\boldsymbol{x}'|}\frac{d}{dt}\left(\frac{\sin t}{t}\right) \quad \text{where} \quad t = (E_0-E)|\boldsymbol{x}-\boldsymbol{x}'|$$

$$= 1-\tfrac{1}{3}i(E_0-E)\,\boldsymbol{\alpha}.(\boldsymbol{x}-\boldsymbol{x}') - \tfrac{1}{6}(E_0-E)^2|\boldsymbol{x}-\boldsymbol{x}'|^2+ \quad \ldots.$$

and similarly

$$\theta_e = 1+\beta/E-\tfrac{1}{3}i\{(E^2-1)/E\}(\boldsymbol{\alpha}.\boldsymbol{x}-\boldsymbol{x}') - \tfrac{1}{6}(1+\beta/E)(E^2-1)|\boldsymbol{x}-\boldsymbol{x}'|^2+\ldots.$$

If Coulomb wave functions are used for the electrons we find similarly

$$\theta_e = F_0\left[\left(1+\frac{\beta s_0}{E}\right)\left(\frac{1+s_0}{2}\right)-\frac{i\alpha.x}{|x|}\left(1+\frac{\beta s_0}{E}\right)\left(\frac{\alpha Z}{2}\ |x|\ \frac{1+s_0}{2}\ \frac{E-\beta}{1+2s_0}\right)+\right.$$

$$+\frac{i\alpha.x'}{|x'|}\left(1-\frac{\beta s_0}{E}\right)\left(\frac{\alpha Z}{2}+|x'|\ \frac{1+s_0}{2}\ \frac{E+\beta}{1+2s_0}\right)+\frac{x.x'-i[\sigma_1 x_1 x']}{|x|\,|x'|}\times$$

$$\left.\times\left(1-\frac{\beta s_0}{E}\right)\left(\frac{1-s_0}{2}+\frac{\alpha Z}{2}\ \frac{E+\beta}{1+2s_0}\ (|x|+|x'|)+|x||x'|\ \frac{1+s_0}{2}\left\{\frac{E+\beta}{1+2s_0}\right\}^2\right)\right]$$

$$+\frac{(E^2-1)F_1}{9}\left[(2x.x'+i[\sigma,x,x'])\left(1+\frac{\beta s_1}{E}\right)\left(\frac{2+s_1}{4}\right)+\ldots\ldots\right]$$

where

$$F_n=\left(\frac{(2n+2)!}{n!\,\Gamma(1+2s_n)}\right)^2(2pR)^{2(s_n-n-1)}\,e^{\pi\alpha ZE/p}\,|\Gamma(s_n+i\alpha ZE/p)|^2$$

$$s_n=[(n+1)^2-\alpha^2Z^2]^{\frac{1}{2}}$$

$$\alpha=e^2/\hbar c$$

Z and R are the nuclear charge and radius and $p=(E^2-1)^{\frac{1}{2}}$ is the electron's momentum. The leading term of this expression gives rise to the function $F(Z,E)$ introduced in the previous section.

Detailed calculations of the shape of forbidden spectra for some typical cases have been made by KONOPINSKI and UHLENBECK[40], and MARSHAK[15, 41,42] has calculated the shapes and lifetimes expected for some interesting highly forbidden transitions. The general features of these spectra can be seen from the formulae above. Near the upper limit of the spectrum $E \sim E_0$, $\theta_n \sim 1$ *i.e.* the neutrino must come out in an s-wave and the first contributing term of θ_e will vary with energy as $(E^2-1)^n$ where n is the degree of forbiddenness, because the electron must carry off all the excess angular momentum, so that there should be relatively more electrons near the upper end point in a forbidden than in an allowed spectrum. There is generally a similar rise toward the lower limit $E \sim 1$ for a similar reason (though for certain types of interaction and for large Z this may be masked) so that relative to an allowed spectrum a forbidden one generally has a minimum near the centre and rises towards the ends. Once-forbidden transitions involving the ' small ' matrix elements only will, however, have the allowed shape.

When Z is large the phenomena are somewhat different[40]. For θ_e contains as coefficients of the harmonics terms of the order αZ as well as those of the order pR, and for large Z the former may be the more important. Consequently, for large Z,

a The decay constant for first forbidden transitions may be smaller than that allowed for only by the factor $(\alpha Z)^2$ instead of $(E^2-1)R^2$. This is in fact the case except when $\Delta J = 2$; then the αZ terms drop out[40].

b A first forbidden spectrum should be of roughly the same shape as an allowed one, except when $\Delta J = 2$.

c A second forbidden spectrum, except when $\Delta J = 3$, should differ roughly by a correction factor $(E_0-E)^2$, since the greatest part of the matrix element comes from the product of (α^2Z^2) terms in θ_e with $(E_0-E)^2$ terms in θ_n.

Experimental evidence—If the nuclear spin and parity changes are known a theoretical lower limit to the lifetime can be derived by giving all the nuclear matrix elements their maximum possible values for such a transition, and if the observed lifetimes be shorter than this lower limit for a particular form of interaction that form must be ruled out. (The constant involved in each type of interaction is determined by those decays of light nuclei that can safely be assumed to be ' well allowed '.) MARSHAK[15, 42] and GREULING[36] have made such calculations for the nuclei Be^{10}, C^{14}, P^{32}, K^{40}, Rb^{87}, Lu^{176} and RaE, for most of which the spin changes are known experimentally. Both authors conclude that the experimental lifetimes are explained best by a tensor form of interaction (GAMOW-TELLER selection rules), but that a vector interaction or possibly pseudo-vector are not ruled out conclusively; scalar or pseudo-scalar forms lead to definite disagreement.

The evidence on forbidden transitions from the lifetimes of the naturally radioactive elements has recently been reviewed by FEATHER and RICHARDSON[43], who have published a revised Sargent diagram of these elements, taking into account that, for large Z, first forbidden transitions may have probabilities smaller only by the factor $(\alpha Z)^2$. They introduce a new line in the diagram corresponding with such transitions, and classify as second forbidden most of the transitions formerly considered first forbidden. This new interpretation agrees well with the facts known about spin and parity changes. They draw also a special line corresponding with forbidden $0\leftrightarrow 0$, $(+)$ transitions to explain the disintegrations $ThB\rightarrow ThC\rightarrow ThC'$ (ground state to ground state). These decays furnished the original evidence[11] for the GAMOW-TELLER rules, but their former interpretation led to difficulties with the parity changes which are removed by the new one. This special class of transitions is forbidden (but not completely forbidden) only with the tensor interaction.

The evidence from the lifetimes of light nuclei is discussed in the next section. GAMOW-TELLER selection rules can explain more facts than FERMI rules, but difficulties remain on either hypothesis.

The shape of the electron spectrum provides a better test of the theory as it is less dependent on the values of the matrix elements and is independent of them if only one matrix element is involved. Experimentally, the only spectrum known to differ significantly from the allowed shape * is that of RaE; both its shape and the lifetime of RaE are explained by theory[36] if the transition is second forbidden (tensor or vector interaction), and this assignment agrees with that of FEATHER[43].

That other measured spectra of forbidden transitions, such as P^{32}, K^{40}, and more recently Be^{10}, have the allowed shape is difficult to understand, and if the facts are confirmed will necessitate some revision of theoretical ideas about forbidden β-decays.

LIGHT NUCLEI

WIGNER has used his theory[44, 45] of the energy levels in light nuclei to derive further approximate selection rules for β-decay, from the approximate quantum numbers of his theory additional to the only true quantum numbers, spin and parity. In Wigner's second approximation the Hamiltonian of the nucleus is assumed to be independent of charge, so that the energy levels are grouped into charge multiplets (split in fact by the charge dependent forces), characterized by a total charge quantum number T. If FERMI selection rules are true, an allowed transition involves essentially the matrix element of the operator ΣQ_r; this operator commutes with T and can therefore have non-zero matrix elements only for transitions within a charge multiplet. But in this approximation the only neighbouring isobars that belong to the same charge multiplet are the mirror nuclei, where the decay should therefore be most allowed. This is indeed largely true, but fails to explain why He^6, C^{10} and others should decay equally rapidly.

For this reason, *inter alia*, GAMOW-TELLER rules are preferable, because the operator involved permits transitions between different charge multiplets. In Wigner's first approximation, where the Hamiltonian is assumed independent of both spin and charge, the GAMOW-TELLER operator allows transitions between states of the same super-multiplet. Indeed we can in this approximation calculate these matrix elements exactly because the spin and charge dependence of the nuclear states is known. This removes the difficulty associated with He^6, C^{10} *etc* but does not explain all the facts of the decay of light nuclei.

These theories predict also that there is no parity change for allowed transitions since all the states of a super-multiplet have the same parity. This would rule out the pseudo-scalar form of interaction.

* Note added in Proof—Since this article was written several papers[90] have appeared reporting spectra which show the 'forbidden shape', so it appears that the allowed spectrum is not so ubiquitous as thought at first.

The mystery of the long lifetime of Be^{10} has now been solved[46] by the discovery that B^{10} has spin 3, and that C^{10} decays to an excited state of B^{10}, while Be^{10} goes directly to the ground state. Thus the ground state of B^{10} does not belong to the same super-multiplet as Be^{10}, so that the spin dependent nuclear forces are at least large enough to cause this inversion which is however not very great, amounting to only about 5 per cent of the binding energy. It is still hard to understand the long lifetime of C^{14}, which is known[47] to have spin 0, and decays to N^{14} with spin 1. In the opposite direction the decay of B^{12} to C^{12} is unexpectedly rapid if the decay does go to the ground state of C^{12} which should belong to a super-multiplet different from that of B^{12}.

K-CAPTURE

The closed states for electrons in the nuclear Coulomb field are usually unimportant for β-decay, because the vacant orbits are too far from the nucleus. Even for H^3, where there is little spare energy, and a vacant K-orbit, direct decay to an atom of He^3 is only 1—2 per cent as probable as emission into the continuous spectrum. This phenomenon has been studied by DAUDEL *et al*[48].

On the other hand it is very probable, at least in heavy nuclei, that atomic electrons are captured instead of positrons emitted (capture of negative energy electrons). Indeed only the former may be possible if there is not enough energy available. If E_c be the total energy of the captured electron, E_n that of the emitted neutrino, and E_0 the change in nuclear energy level, the energy balance requires

$$E_0 + E_c = E_n$$

so that the electron may be captured if only $E_0 > -E_c$, while positron emission requires $E_0 > 1$. Usually the capture of K electrons is most important since their density at the nucleus is greatest, but if E_0 is nearly equal to, or less than, $-E_k$, L-capture may become important, and so on.

The matrix element for the absorption of an electron from the closed state u_c and the emission of a neutrino into a state u_n^* is

$$\Sigma g_t \int I_t(x)[u_n^*(x)\rho_t u_c(x)]dx \sim \Sigma g_t M_t[u_n^*\rho_t u_c(R)]$$

for an allowed transition, neglecting the momenta of the light particles and evaluating the electron wave function at the nuclear radius according to the usual convention. The total probability of the capture of the electron is then

$$\lambda_c = \sum_n 2\pi\delta(E_0 + E_c - E_n) \sum_{t,t'} g_t g_{t'}^* M_t M_{t'}^* (u_n^*\rho_t u_c(R) u_c^*(R)\rho_{t'}^* u_n)$$

$$= (1/2\pi) \sum_{t,t'} g_t g_{t'}^* M_t M_{t'}^* \left\{ u_c^*(R)\rho_t\rho_{t'}^* u_c(R) \right\} (E_0 + E_c)^2$$

For an unmixed form of interaction only the terms with $t = t'$ enter, so

$$\lambda_c = (1/2\pi) \sum_t |g_t M_t|^2 (E_0 + E_c)^2 |u_c(R)|^2$$

and if we insert the wave functions of the two K-orbits we obtain the total decay constant for K-capture

$$\lambda_k = (2/\pi^2) \sum_t |g_t M_t|^2 (E_0 + s_0)^2 \ (2\alpha ZR)^{2(s_0-1)} (\alpha Z)^3 / \Gamma(1 + 2s_0) \ldots . \quad (9)$$

where the symbols have the same meaning as before (p 120, 121).

The energy E_0 is not usually known as the neutrino is not observed, but λ_k will usually be overestimated by putting $E_0 = 1$; if E_0 is much larger there will be positron emission. Then the observed lifetimes of K-capturers exceed the minimum lifetime calculated from this formula with a scatter similar to that of β-emitters. This confirms that the mechanism of K-capture is similar to that of β-emission.

Relation to positron emission—If positron emission is also possible the corresponding decay constant is

$$\lambda_+ = (1/2\pi^3) \sum_t |g_t M_t|^2 \int_1^{E_0} E(E^2 - 1)^{\frac{1}{2}} (E_0 - E)^2 F^+(Z,E) dE \ldots . \quad (10)$$

The ratio λ_+/λ_k depends only upon E_0 and Z; it is large only when E_0 is large and Z is small, so that positrons can escape through the potential barrier, and in fact there are rather few positron emitters with $Z > 40$. Some numerical values are given by MØLLER[49, 50].

When both K-capture and positron emission are possible and lead to the same nuclear level, a measurement of their ratio gives a useful test of the theory. However, K-capture can conveniently be observed only when it leads to an excited level which subsequently emits a γ-ray, and the only measurement[51] that refers surely to an allowed transition is on the decay of Cd^{107}, where the experimental value of λ_+/λ_k agrees well with the theoretical value of 0·003. DEUTSCH[52] has measured the ratio for the positron emitters V^{48}, Mn^{52}, Co^{58} and finds good agreement with the theoretical formula for allowed transitions, but these decays are probably forbidden so the comparison is not very significant; agreement with the expected ratio for forbidden transitions is less good.

Forbidden transitions—An electron capture process may apparently be forbidden, that is, have a very long lifetime, if E_0 is very nearly equal to $-E_k$, just as may an ordinary β-decay if $(E_0 - 1)$ is small, only here the cause cannot easily be identified. It may also be forbidden, like a β-decay, by spin or parity selection rules; K-capture is allowed or forbidden according to the same selection rules as a β-decay, and the decay constant is reduced by the same factors $(E_0 + E_k)^2 R^2$ or $\alpha^2 Z^2$.

Detailed calculations of the expected lifetimes of some longlived *K*-capturers have been made by MARSHAK[15]. Unfortunately the experimental data on these decays are too meagre for useful comparison with theory.

Effect of atomic binding—In a light element the value of $\sum_c |u_c|^2$ at the nucleus will be changed by ionization or by chemical combination of the atoms. Attempts to detect this effect in the case of Be^7 have been made by DAUDEL and co-workers[53] who found a small effect that lay however within experimental error, and by SEGRÈ and WIEGAND[54, 55], who found a very small difference ($0{\cdot}03 \pm 0{\cdot}018$ per cent) between the lifetime of beryllium metal and beryllium oxide. The effect is unexpectedly small, but rather detailed knowledge of molecular binding would be needed to give a reliable theoretical estimate.

DOUBLE BETA-DECAY

If two stable isobars that differ by two charge units are separated by an unstable one it is possible for one of the former to decay into the other by a double β-transition that passes through a virtual state of the intermediate nucleus. The matrix element for this process involves G^2 and is therefore very small; it does however depend greatly on the assumptions made about the neutrino and anti-neutrino (p 116), and herein lies its principal interest.

If the emission of an electron can only be accompanied by the emission of a neutrino, two neutrinos will be emitted in the double β-decay, along with the two electrons, and all four particles must share the available energy. But if the electron emission may be accompanied by either the emission or the absorption of a neutrino, the neutrino emitted with the first electron may be absorbed when the second electron is emitted. Then since energy is conserved only between initial and final states, this neutrino may have any momentum, limited only by a reduction in the matrix element when its wavelength becomes comparable with nuclear dimensions. In the second case the volume of phase space accessible for the intermediate states is much greater than in the first and consequently the probability of the double β-decay process is considerably greater on this hypothesis.

A quantitative statement of these considerations leads to a crude numerical estimate. In the first case the matrix element for the emission of a particular set of particles is of the form

$$(GM)^2/\Delta$$

where Δ is an energy denominator of the size of the nuclear energy difference; if $\boldsymbol{k}_e$, $\boldsymbol{k}_e'$, $\boldsymbol{k}_n$, $\boldsymbol{k}_n'$, be the momenta of the four particles, the total decay probability is proportional to

$$\int\int\int\int \frac{(GM)^4}{\Delta^2}\delta(E_e + E' + E_n + E_n' - E_0)d\boldsymbol{k}_e d\boldsymbol{k}_e' d\boldsymbol{k}_n d\boldsymbol{k}_n'$$

while on the second hypothesis the matrix element is of the form

$$\int \frac{(GM)^2}{|\boldsymbol{k}_n|} d\boldsymbol{k}_n$$

since the neutrino energy is the main contributor to the energy denominator, and therefore the decay probability is proportional to

$$\int\int\left(\int \frac{(GM)^2}{|\boldsymbol{k}_n|^2} d\boldsymbol{k}_n\right)^2 \delta(E_e + E_e' - E_0) d\boldsymbol{k}_e d\boldsymbol{k}_e'$$

Here the $\boldsymbol{k}_n$ integration will effectively be cut off at $|\boldsymbol{k}_n| = 1/R$ by a reduction in M, therefore the ratio of the decay probabilities in the two cases will contain a factor $(\lambda/R)^4$ where λ is a mean wavelength of the emitted particles.

The first calculations of double β-decay on the usual neutrino hypothesis were made by GOEPPERT-MAYER[56]. Detailed calculations on the basis of MAJORANA's symmetrical theory (identifying the neutrino with the anti-neutrino) have been made by FURRY[57] for various types of β-interaction. He finds that the probability of double β-decay would indeed be increased by a large factor, of the order 10^{10}, as estimated above, except for the scalar interaction where there is a strong cancellation of the matrix elements. These reduced lifetimes, of the order 10^{15} years are not too long to be detected experimentally, and FIREMAN[58] claims to have detected this decay for Sn^{124} with a lifetime between 0·4 and 0·9 $\times$ 10^{16} years. This effect, if it be real, supports the neutrino hypothesis, with the symmetric neutrino theory, in a convincing way, by showing that a neutrino can be a cause as well as an effect.

ANGULAR CORRELATIONS

The probability of the emission of the electron and neutrino into two particular states depends upon the size of $(u_e^* \rho_t u_n)$, which varies with their relative directions and spins and with the form of the operator ρ_t. The consequent angular correlation between the particles is the only simple phenomenon that can differentiate, from the evidence of allowed transitions, between the possible forms of H_β.

Electron-neutrino correlation—The probability that electron and neutrino be emitted with definite momenta is determined entirely by the expression 5

$$\sum_{Spins} (u_e^* \rho_t u_n)(u_n^* \rho_{t'}^* u_e) = \tfrac{1}{4}\, trace \left\{ \rho_t (1 + \boldsymbol{\alpha}.\boldsymbol{v}_n) \rho_{t'}^* (1 + \boldsymbol{\alpha}.\boldsymbol{v}_e + \beta/E) \right\} \quad \ldots (5)$$

where $\boldsymbol{v}_n$, $\boldsymbol{v}_e$ are the velocities of the emitted particles in units of c. If now we average over directions of these keeping fixed only the angle between them this expression becomes

$$\tfrac{1}{4}\, trace \left\{ \rho_{t'}^* (1 + \beta/E) \rho_t + \tfrac{1}{3} (\rho_{t'}^* \boldsymbol{\alpha} \rho_t . \boldsymbol{\alpha}) v_e \cos\theta \right\}$$

For the operators that occur in an allowed transition of an unmixed type this is equal to $\delta_{tt'}W(\theta)$ with

$$W(\theta) = 1 + av_e \cos\theta \qquad \ldots . (11)$$

which is therefore the correlation function sought[59-61]. For the five elementary interactions $J_0 \ldots . J_4$ the constant a has the values -1, $+1$, $+\frac{1}{3}$, $-\frac{1}{3}$, -1 respectively, so that only the scalar and pseudo-scalar interactions are indistinguishable among unmixed forms.

This angular correlation is the same for positrons as electrons, and is independent of the Coulomb field of the nucleus.

Calculations of the correlations expected in the forbidden transitions have been made by HAMILTON[60]. A general feature noticed by him is that electron and neutrino are preferentially emitted in the same direction in all highly forbidden transitions, because the matrix element $M_t(\boldsymbol{k})$ will be large when $\boldsymbol{k}$ is large and $\boldsymbol{k}$ is the sum of the momenta of the emitted particles, so that the correlation function will contain powers of $(1 + \cos\theta)$.

Nuclear recoil—In most recoil experiments only the magnitude of the recoil momentum is measured, and the angular correlation has to be deduced from the spectrum of recoil energies. The spectra predicted by various types of interaction have been calculated by KOFOED-HANSEN[62]. Their form is rather insensitive to the value of a in the correlation function, so that an experimental accuracy of a few per cent is needed to distinguish between the different possibilities.

Experiments of this type[2], have been made by JACOBSEN and KOFOED-HANSEN[87,88] on Kr^{88} and by CHRISTIE, COHEN, FOWLER, and LAURITSEN[8] (see p 116) on Li^8. While these showed that momentum was not conserved without a neutrino, they were not sufficiently refined to discriminate reliably between different angular distributions.

A more sensitive type of experiment measures the spectrum of nuclei that recoil at a definite angle with the direction of the emitted electron. SHERWIN[63] has made such experiments, using a time-of-flight technique, on P^{32} and Y^{90}. His results were fitted best by a $(1 - v\cos\theta)$ correlation function or even by $(1 - v\cos\theta)^2$, though such a form is not expected theoretically. ALLEN, PANETH and MORRISH[64] measured the spectrum of He^6 recoils using a radioactive gas to avoid surface effects which may have influenced Sherwin's experiment. Their results, based on recoils at 180° and 162° to the electron's direction, indicate that $a<0$, favouring $a = -\frac{1}{3}$ (pseudo-vector interaction). This is in agreement with the fact that GAMOW-TELLER selection rules are needed to explain the short life of He^6.

RADIATION EFFECTS

The interaction of the charged particles with the electromagnetic field affects β-decay mainly through the change in electron density at the nucleus, embodied in the function $F(Z,E,)$ introduced on p 120; these effects will now be considered in more detail.

Static interaction—The electromagnetic interactions may be divided in the customary way[65] into static, or Coulomb, interactions between the charged particles, and their interactions with the transverse radiation field of real photons. The protons in the nucleus are so much heavier and smaller than the electrons that they may be regarded almost as a fixed point charge in the field of which the electrons move, and this may be taken into account by using for the ejected electrons their wave functions in a central Coulomb field instead of plane waves. However, a small difficulty arises here because these wave functions, solutions of Dirac's equation, diverge at the origin of the central field.

For a single neutron which decays into a proton and emits an electron (and neutrino) the radiation interactions may be considered in more detail by regarding them as small perturbations simultaneously with the β-interaction. Then the divergent parts of the radiation corrections may be eliminated according to the prescriptions of the new quantum electrodynamics[10], and the remainder contribute corrections to the matrix element for β-decay of the relative order of magnitude $(e^2/\hbar c)\log(M_p/m_e)$. When β-decay occurs within a many-particle nucleus there will be a small correction of this same magnitude due to the nucleon that is actually transformed, while the Coulomb attractions of the other protons are roughly equivalent to a central field at some mean distance R. Since $F(Z,E)$ is rather insensitive to R, only a small error will be made if, as Fermi originally suggested, R be taken equal to the nuclear radius; moreover the shape of the spectrum is independent of the value of R assumed.

A different source of error in $F(Z,E)$ arises from the screening of the nucleus by the atomic electrons, and this is important for small energies of the β-particles, comparable with mean atomic binding energies. This screening reduces the height of the potential barrier against positrons and therefore increases the probability of their emission. According to a recent calculation by LONGMIRE and BROWN[35], using the Thomas-Fermi model, the probability of electron emission is increased also. They find the function $F_c(Z,E)$, corrected for screening

$$F_c^{\mp}(Z,E) = F^{\mp}(Z,E \mp D_0) \times (E - mc^2/E \mp D_0 - mc^2)^{\frac{1}{2}} \quad \ldots . (12)$$

where the minus/plus sign refers to electrons/positrons, and

$$D_0 \sim 1{\cdot}13\, Z^{4/3}\,(e^2/\hbar c)^2 mc^2$$

γ-ray emission—The γ-rays, or conversion electrons, observed ' in coincidence ' with β-rays are generally the radiation emitted by the nucleus after a beta transition to an excited level. The width of the excited state is so small that the γ-ray emission is quite independent of the β-decay, except for the inherited angular momentum of the state, which may cause some angular correlation between the β and γ-rays. This, however, cannot be interpreted simply, because the unobserved neutrino takes away part of the angular momentum.

γ-ray emission which is really simultaneous with a β-ray and shares the available energy with it is a rather rare event. This event occurs when the radioactive nucleus emits a neutrino and a ' virtual ' electron, with the wrong energy for escape, that then radiates a photon so that the three particles together have the correct decay energy. The radiative step introduces a factor $(e^2/\hbar c)$ into the probability of the event, which is therefore rather rare compared with ordinary β-decay. *Bremsstrahlung* in the Coulomb field of the nucleus is negligible in comparison as its probability is smaller by a further factor $(Ze^2/\hbar c)^2$.

Detailed calculations have been made by BLOCH[66] for ordinary β-decay, and by MØLLER[49] and by MORRISON and SCHIFF[67] for the case of *K*-capture. In the former case the probability $P(E,k,\theta)\ \sin\theta\ d\theta$ for emitting an electron with energy E and a photon with energy k, with an angle θ between them is, for an allowed transition

$$P(E,k,\theta) = \frac{e^2}{4\pi^4}\,|GM|^2\,\frac{(E_0-E-k)^2}{k}\times\frac{v}{(1-v\cos\theta)^2}\times$$
$$\times\left\{k^2(1-v\cos\theta)+E(E+k)\,v^2\sin^2\theta\right\}$$

where $v=(E^2-1)^{\frac{1}{2}}/E$ is the electron's velocity; at high energies, $(v\sim 1)$, the electron and photon prefer to be emitted in the same direction. The second term exhibits the usual infra-red catastrophe ($1/k$ divergence for soft photons), but if we disregard this term (which appears reasonable for small electron energies because of the factor v^2), integration of the first term gives for the total probability of emitting an electron with energy E, together with a photon

$$P_\gamma(E) = (e^2/48\pi^4)\,|GM|^2\,(E_0-E)^4\log(1+v)/(1-v)$$

which, for small electron energies, bears to the ordinary probability of β-decay the ratio

$$P_\gamma(E)/P(E) = (e^2/12\pi)\,(E_0-E)^2 \qquad \ldots.(13)$$

Similarly for *K*-capture there is found for the ratio of decay with emission of a photon to ordinary *K*-capture $P_{k\gamma}/P_k = (e^2/12\pi)(E_0+E_k)^2$ .... (14)

It is very hard to observe this weak continuous γ-radiation accompanying β-emission as it is masked by other effects, but in the *K*-capture case only the associated X-radiation will interfere. BRADT *et al*[68] has observed this radiation

accompanying K-capture in Fe^{55}, and finds an intensity of 2×10^{-5} quanta per decay, which agrees with the formula above if $(E_0 + E_k)^2 \sim 0{\cdot}1$, which may be reasonable in view of the long life of the nucleus.

Radiation and virtual states—It is possible also for a β- and γ-ray to be emitted simultaneously if the β-decay go to an excited state of the second nucleus above the level of the first state (a virtual transition in which energy is not conserved) which then decays by emitting a photon, so that the electron and photon share the available energy. Ordinarily this phenomenon will be so much less probable than a direct β-decay to the final state that it will not be observed, but if the direct decay be highly forbidden (certain types of transition are completely forbidden for all except the tensor interaction (p 124)), simultaneous β- and γ-emission may be an easier alternative. LONGMIRE[69] has discussed these alternatives to completely forbidden transitions, and estimates that in the most favourable cases the lifetimes would be 10^6—10^7 years. For the differential probability of emitting an electron of energy E and a γ-ray of energy k he gives

$$P(E,k) \propto \frac{k^{2s-1}}{(E_1-k)^2} E(E^2-1)^{\frac{1}{2}}(E_0-E-k)^2 \qquad \ldots . (15)$$

if the β-transition be allowed, and the γ-transition be electric dipole ($s = 1$), or magnetic dipole ($s = 2$). In the resonance denominator E_1 is the excitation energy of the virtual level.

In the second step the photon also might be internally converted by the emitted electron, which would then emerge alone; as the energy of the electron in the first transition would then be unlimited, the matrix element for the whole process could then be rather greater than if both electron and photon were emitted.

MESON THEORY

YUKAWA[9] first suggested that β-decay might be the result of a two-step process in which a nucleon emits a virtual meson (with insufficient energy to leave the nucleus) which then decays into an electron and neutrino before being re-absorbed by a nucleon. This mechanism would relate the constant of β-decay to two somewhat simpler constants: the nucleon's 'meson charge', which is related to the strength of nuclear forces, and the lifetime of the meson for decay into electron and neutrino.

This attractive hypothesis has not yet, however, been correlated successfully with the properties of any observed meson. To the first idea, formed when there was only one meson, that the ordinary cosmic ray meson was responsible for both nuclear forces and β-decay, there was the objection that the observed lifetime of 2×10^{-6} seconds, together with the roughly known strength of nuclear forces, was too long to explain the value of the β-decay

constant G. This identification has been abandoned since it has been found that this β meson interacts only weakly with nuclei[70], and does not itself decay into an electron and neutrino, but probably into three particles, so that its own decay is analogous to an ordinary β-decay. This latter comparison can indeed be substantiated quantitatively[71], and if it is significant would indicate that some steps in the β-decay process were not connected only with nucleons.

The next idea, that π mesons were responsible for β-decay, must also be rejected, it seems, because the observations[72] on the π meson do not allow it to have a short enough lifetime for disintegration into electron and neutrino, if indeed it does decay at all in this way, to explain β-decay[73].

To save a meson theory of β-decay some hitherto unobserved meson must therefore be postulated. If it interact strongly with nuclei and decay rather slowly into an electron and neutrino it is likely soon to be discovered, associated with nuclear reactions of great energy, but if it be coupled weakly with the nuclei, and itself decay rapidly, it will only be manifest through its association with β-processes.

Various meson theories of β-decay have been proposed and we shall analyse here the relations between the properties of the mesons and the effective form of β-interaction that they produce[74–79].

Meson fields of integral spin—Since all four particles involved in β-decay have spin $\frac{1}{2}$ it is most simple to assume that the mesons involved have spin 0 or 1, and are linked exchangewise with the pairs of heavy particles and of light ones. The mesons obviously cannot link directly a heavy particle to a light particle, otherwise the former would decay spontaneously to the latter.

There are four possible meson fields of this type[80], usually known by the transformation properties of their potentials as scalar, vector, pseudo-vector and pseudo-scalar fields. Each type may be coupled in two formally different ways with either pair of particle fields, one involving the meson potentials and the other their derivatives, the meson field strengths. In the usual formulation some terms of direct β-interaction appear when the Hamiltonian is formed, which cannot be eliminated as they are not invariant in form and which, moreover, are different according to whether the meson fields or potentials are taken as independent variables[80].

These ambiguities do not arise if the equations of motion of the fields are taken as starting point, and if it is assumed, as is natural on such a meson theory, that these equations do not contain any terms of direct β-coupling. In the case of the scalar or pseudo-scalar fields the type of coupling with the free light particle fields is immaterial[74, 81] (in the lowest significant order). If the coupling with the nucleons be through their scalar or pseudo-scalar invariant respectively *i.e.* coupling with the meson potentials, the effective

β-interaction will be of the simple forms J_0 or J_4, but if the nucleons be coupled through their vector or pseudo-vector covariants the β-coupling involves field derivatives. Thus for the scalar field with vector nuclear coupling

$$H_\beta \propto \int \left[\operatorname{div}(\psi_P^* \alpha \psi_N) - iE_0 \psi_P^* \psi_N \right] (\psi_e^* \beta \psi_n) d\boldsymbol{x}$$

The behaviour of the other two fields is similar though more complicated. Here again, if the nucleons are coupled directly to the meson potentials the effective β-interaction is of the simple types J_1 or J_3 in the vector and pseudo-vector cases respectively, but if the nucleons are coupled to the meson field quantities (tensor coupling) the β-coupling again involves derivatives.

Thus each type of field gives rise to one unmixed type of β-interaction with the same name and to more complicated velocity dependent forms, which must be ruled out from considerations of spectral shape and energy-lifetime relations.

In each case a relation is obtained between the nuclear coupling constant g, the meson's lifetime τ and the constant of β-decay. These relations lead to the inequality

$$\tau \leqslant 2 \times 10^4 (g^2/4\pi\hbar c)(M_e/M_m)^5 \qquad \ldots . (16)$$

where M_e/M_m is the mass ratio of electron to meson. Except for rather special values of the coupling constants there is approximate equality.

Meson pair theories—It is possible also to construct meson theories of nuclear forces [82], and of β-decay[83], in which pairs of spin $\frac{1}{2}$ mesons interact with the other particles. For the explanation of β-decay and of charge exchange forces, one of this pair must be charged and the other uncharged. The mesons may be linked to the other particles through any of their five covariants, and these will lead to a simple form of β-interaction of one of the five corresponding forms J_i, and to nuclear forces governed by a similar form of interaction. However, the summation over intermediate states here gives rise to strong divergences, and until these can be eliminated in a satisfactory way the theory cannot be maintained quantitatively. This divergency would not appear if the neutral meson of the pair were itself the neutrino, and if the charged meson were directly linked to the electron field so that meson to electron decay can occur only as a virtual process.

Effects of an indirect β-interaction—The β-interaction resulting from a meson theory may be represented only approximately by a point interaction of the four participating fields. In truth the interaction is distributed over a region of a size determined by the meson's Compton wavelength $\lambda\!\!\!^{-}_m$. Although this may be comparable with nuclear dimensions, it is always small compared with the wavelengths $\lambda\!\!\!^{-}_e$ of the light particles, unless the meson be very light,

so that the corrections to the point interaction are only of the relative order of magnitude $(\lambda\!\!\!^{-}_m/\lambda\!\!\!^{-}_e)^2$. This is small even compared with the ratio of forbidden to allowed matrix elements, so that these corrections should not make any observable difference to spectral shapes or to the expectations of forbidden transitions.

Neither should there be any new radiation effects. The nuclear Coulomb field may affect the production of charged mesons, but there will be a compensating effect in their disintegration which will leave unchanged the effect of the Coulomb field on β-decay, though this is true only so long as the meson's momentum is small compared with its rest mass. The meson is much less likely to radiate photons than the electron to which it decays because of its greater mass.

We may conclude that since it is difficult to decide by experiment even the form of H_β it will be much harder to decide whether this is a direct interaction or the result of a meson intermediary.

REFERENCES

We have not repeated all the references given by KONOPINSKI in his review. Further references to the literature on the neutrino hypothesis are given by CRANE[2].

[1] KONOPINSKI, E. J. *Rev. mod. Phys.* 15 (1943) 209
[2] CRANE, H. R. *ibid* 20 (1948) 278
[3] GOLDHABER, M. and SCHARFF-GOLDHABER, G. *Phys. Rev.* 73 (1948) 1472
[4] SARGENT, B. W. *Proc. roy. Soc. A* 139 (1933) 659
[5] FERMI, E. *Z. Phys.* 88 (1934) 161
[6] BETHE, H. A. and BACHER, R. F. *Rev. mod. Phys.* 8 (1936) 82
[7] CRANE, H. R. and HALPERN, J. *Phys. Rev.* 53 (1938) 789; 56 (1939) 232
[8] CHRISTY, R. F., COHEN, E. R., FOWLER, W. A. and LAURITSEN, T. *ibid* 72 (1947) 698
[9] YUKAWA, H. *Proc. math. phys. Soc. Jap.* 17 (1935) 48
[10] SCHWINGER, J. *Phys. Rev.* 74 (1948) 1439
[11] GAMOW, G. and TELLER, E. *ibid* 49 (1936) 895
[12] KONOPINSKI, E. J. and UHLENBECK, G. E. *ibid* 48 (1935) 7
[13] WENTZEL, G. *Einführung in die Quantumtheorie der Wellenfelder* (1943)
[14] HOYLE, F. *Proc. Cam. phil. Soc.* 33 (1937) 277
[15] MARSHAK, R. E. *Phys. Rev.* 61 (1942) 388, 431
[16] BLEULER, E. and ZÜNTI, W. *Helv. phys. Acta* 19 (1946) 375
[17] KOFOED-HANSEN, O. *Phys. Rev.* 71 (1947) 451
[18] NOVICK, A. *ibid* 72 (1947) 972
[19] HUGHES, D. J. and EGGLER, C. *ibid* 73 (1948) 809, 1242
[20] CURRAN, S. C., ANGUS, J. and COCKROFT, A. L. *Phil. Mag.* 11 (1949) 53
[20A] HANNA, G. C. and PONTECORVO, B. *Phys. Rev.* 75 (1949) 983
[21] KONOPINSKI, E. J. *ibid* 72 (1947) 518
[22] FRANK, F. C. *Proc. phys. Soc.* 59 (1947) 408
[23] LAWSON, J. L. and CORK, J. M. *Phys. Rev.* 57 (1940) 983
[24] TOWNSEND, A. A. *Proc. roy. Soc. A* 177 (1940) 357
[25] PEACOCK, W. C. *Phys. Rev.* 72 (1947) 1049
[26] BACKUS, J. *ibid* 68 (1945) 59
[27] COOK, C. S. and LANGER, L. M. *ibid* 73 (1948) 601 1219
[28] — — *ibid* 74 (1948) 227
[29] — — and PRICE, H. C. *ibid* 73 (1948) 1935
[30] — — — and SAMPSON, M. B. *ibid* 74 (1948) 502
[31] LEWIS, H. and BOHM, D. *ibid* 69 (1946) 129
[32] COOPER, E. P. *ibid* 74 (1948) 1565
[33] CRANBERG, L. and HALPERN, J. *ibid* 73 (1948) 59, 1269
[34] ALBERT, C. S. and WU, R. D. *ibid* 75 (1949) 315
[35] LONGMIRE, C. and BROWN, H. *ibid* 75 (1949) 264

[36] GREULING, E. *Phys. Rev.* 61 (1942) 568
[37] STRACHAN, C. *Proc. phys. Soc.* 61 (1948) 481
[38] SNELL, A. H. and MILLER, L. C. *Phys. Rev.* 74 (1948) 1217
[39] NORDHEIM, L. W. and YOST, F. L. *ibid* 51 (1937) 942
[40] KONOPINSKI, E. J. and UHLENBECK, G. E. *ibid* 60 (1941) 308
[41] MARSHAK, R. E. *ibid* 70 (1946) 980
[42] — *ibid* 75 (1949) 513
[43] FEATHER, N. and RICHARDSON, H. O. W. *Proc. phys. Soc.* 61 (1948) 452
[44] WIGNER, E. P. *Phys. Rev.* 51 (1937) 106
[45] — *ibid* 56 (1939) 519
[46] GORDY, W., RING, H. and BURG, A. B. *ibid* 74 (1948) 1191
[47] JENKINS, F. A. *ibid* 74 (1948) 355
[48] DAUDEL, R., JEAN, M. and LECOIN, M. *J. Phys. Rad.* 8 (1947) 238
[49] MØLLER, C. *Phys. Z. Sowjet* 11 (1937) 9
[50] — *Phys. Rev.* 51 (1937) 84
[51] BRADT, H. L., GUGELOT, P. C., HUBER, P., MEDICUS, H., PREISWERK, P. and SCHERRER, P. *Helv. Phys. Acta* 18 (1945) 351
[52] DEUTSCH, M. *Phys. Rev.* 67 (1945) 313
[53] BOUCHEZ, R., DAUDEL, R., DAUDEL, P. and MUXART, R. *J. Phys. Rad.* 8 (1947) 336
[54] SEGRÈ, E. *Phys. Rev.* 71 (1947) 274
[55] — and WIEGAND, C. E. *ibid* 75 (1949) 39
[56] GOEPPERT-MAYER, M. *ibid* 48 (1935) 512
[57] FURRY, W. H. *ibid* 56 (1939) 1184
[58] FIREMAN, E. L. *ibid* 75 (1949) 323
[59] BLOCH, F. and MØLLER, C. *Nature, Lond.* 136 (1935) 912
[60] HAMILTON, D. R. *Phys. Rev.* 71 (1947) 456
[61] YANG, C. N. *ibid* 74 (1948) 764
[62] KOFOED-HANSEN, O. *ibid* 74 (1948) 1785
[63] SHERWIN, C. W. *ibid* 73 (1947) 216, 1173, 1219
[64] ALLEN, J. S., PANETH, H. R. and MORRISH, A. H. *ibid* 75 (1949) 570
[65] HEITLER, W. *Quantum Theory of Radiation* Oxford, 1944
[66] BLOCH, F. *Phys. Rev.* 50 (1936) 472
[67] MORRISON, P., and SCHIFF, L. I., *ibid* 58 (1940) 24
[68] BRADT, H. L., GUGELOT, P. C., HUBER, P., MEDICUS, H., PREISWERK, P., SCHERRER, P. and STEFFEN, R. *Helv. phys. Acta* 19 (1946) 222
[69] LONGMIRE, C. L. *Phys. Rev.* 75 (1949) 15
[70] CONVERSI, M., PANCINI, E. and PICCIONI, O. *ibid* 71 (1947) 209
[71] HOROWITZ, J. J., KOFOED-HANSEN, O. and LINDHARD, J. *ibid* 74 (1948) 713
[72] GARDNER, E. and LATTES, C. M. G. *Science* 107 (1948) 270
[73] MARSHAK, R. E. *Phys. Rev.* 75 (1949) 700
[74] YUKAWA H. and SAKATA, S. *Proc. math. phys. Soc. Jap.* 17 (1935) 467
[75] SAKATA, S. *Phys. Rev.* 58 (1940) 576
[76] BETHE, H. A. *ibid* 57 (1940) 260, 988
[77] NELSON, E. C. *ibid* 60 (1941) 830
[78] ROZENTAL, S. *Kgl. Dansk. Vid. Selskab.* (M-F) 18 (1940) No. 7 and 23 (1945) No. 11
[79] — *Phys. Rev.* 60 (1941) 612
[80] KEMMER, N. *Proc. roy. Soc. A* 166 (1938) 127
[81] DYSON, F. J. *Phys. Rev.* 73 (1948) 929
[82] MARSHAK, R. E. *ibid* 57 (1940) 1101
[83] — and BETHE, H. A. *ibid* 72 (1947) 506
[84] PRIMAKOFF, H. *ibid* 74 (1948) 110
[85] ROSEN, L. *ibid* 73 (1948) 1272
[86] FALKOFF, D. L. and UHLENBECK, G. E. *ibid* 73 (1948) 649
[87] JACOBSEN, J. C. and KOFOED-HANSEN, O. *Kgl. Dansk. Vid. Selskab.* 23 (1945) No. 12
[88] — — *Phys. Rev.* 73 (1948) 675
[89] WANG, C. S. and FALKOFF, D. L. *ibid* 73 (1948) 1220
[90] BRADEN, C. H., SLACK, L. and SHULL, F. B. *ibid* 75 (1949) 1964, 1965
JENSEN, E. N. and LASLETT, L. J. *ibid* 75 (1949) 1949
SHULL, F. B. and FEENBERG, E. *ibid* 75 (1949) 1768
SIEGBAHN, K. *Ark. Mat. Astr. Fys.* 34B (1946) No. 4
LANGER, L. M. and PRICE, H. C., JNR *Phys. Rev.* 75 (1949) 1109
— — *ibid* 76 (1949) 641
OSOBA, J. S. *ibid* 76 (1949) 345
MITCHELL, A. C. G. and PEACOCK, C. L. *ibid* 75 (1949) 1272
SAXON, D. and RICHARDS, J. *ibid* 76 (1949) 982

6

SPECTROSCOPY OF BETA- AND GAMMA-RAYS

P. E. Cavanagh

BETA-SPECTROSCOPY is primarily concerned with the study of the continuous energy distribution of electrons emitted by radioactive nuclei, and the measurement of the energies and intensities of groups of well defined energy arising from the internal conversion of nuclear γ-rays. It is also concerned with the investigation of the energies and intensities of nuclear γ-rays through the study of secondary electrons produced by the interaction of the γ-rays with matter.

The first analysis of the β-ray spectra of the natural radioactive elements was done by a magnetic deflection method using photographic recording[1]. No attempt was made to focus the electrons, and although roughly monoenergetic groups were detected it was not realized that they were superimposed on a continuous background. An important improvement was the introduction of the semicircular focusing magnetic spectrometer by DANYSZ[2] in 1911. The development of its use by RUTHERFORD, ELLIS, MEITNER and others showed that the spectra consisted of sharp lines superimposed on a continuous background. ELLIS found that the lines could be arranged in groups such that the energy differences were equal to the X-ray level differences for the atom resulting from the radioactive process, and hence deduced that they arose from the ejection of electrons from the various electronic shells by γ-rays, emitted subsequent to the radioactive transformation.

Investigation of the continuous spectra of nuclear β-particles soon revealed this as a most puzzling phenomenon. At first the distribution in velocities was thought to arise from variable energy losses of the nuclear electrons, by collision processes in emerging from the source material. Therefore it was expected that if they were completely absorbed in material enclosing the source the thermal energy developed would correspond to the maximum β-ray energy. The calorimeter experiments of ELLIS[3], and of MEITNER and ORTHMANN[4], with radium E, chosen because it emits no nuclear γ-rays to obscure the result, showed conclusively that the thermal energy developed corresponds to the average β-ray energy. On the other hand, by

comparing the energies liberated in, for instance, the two alternative chains ThC—β—ThC′—α—ThD and ThC—α—ThC″—β—ThD, one found that the energy to be considered must be the maximum energy. These two results imply that energy is either not conserved, or escapes in some undetectable form. Similar difficulties arose in regard to spin. It was known that isobaric nuclei had the same spin, or spins differing by integral multiples of $\hbar$ ($=h/2\pi$), and also that they had the same statistics. However it was known that the free electron had spin $\hbar/2$, and obeyed Fermi statistics.

These considerations led PAULI to postulate the existence of a neutral particle with mass considerably less than that of the electron, of spin $\hbar/2$, and zero magnetic moment. Such a particle, if emitted in the β-process, would not contribute to the thermal energy in the calorimeter experiments because of its extremely low interaction with matter. Recent experiments on the recoil of nuclei in the β-process[5] provide fairly convincing evidence that a second particle is indeed emitted. FERMI[6] developed a theory of β-decay based on the neutrino hypothesis which explained the main features of the experimental results. A subsequent modification by KONOPINSKI and UHLENBECK[7], designed to give better agreement with the early and rather inaccurate experimental results, has since been abandoned. About that time SARGENT[8] published plots of the logarithm of the half-life against the logarithm of the maximum energy, for the natural β-emitters, and found that the points lay roughly on a series of parallel lines. Points lying on one of these lines were taken to correspond to transitions having the same order of forbiddenness. FERMI found that there were selection rules which depended upon considerations of angular momenta and parity. More general forms of the theory have been put forward by KONOPINSKI and UHLENBECK[9], WIGNER[10], and others, and an alternative set of selection rules was formulated by GAMOW and TELLER[11].

Much of the recent interest in β-spectroscopy has been in comparing the experimentally derived electron distributions with theory. In general a β-spectrum will be the resultant of several partial spectra, corresponding to β-ray transitions to various excited states of the product nucleus. The excited states will drop to the ground state with the emission of γ-radiation, usually in a very short time of roughly the order of 10^{-13} seconds. Thus the β-ray and corresponding γ-ray will be effectively coincident in time. This may be used as a means of identifying primary β-rays corresponding to γ-rays of particular energy, and in favourable circumstances enables the primary β-spectra to be plotted. The coincidence technique, and also the necessity of examining weak artificially produced radioactive sources, demands the use of a spectrometer with a much greater transmission than the semicircular focusing instrument. The first really effective instrument to satisfy this need was the short magnetic lens spectrometer, developed[17] at the Massachusetts Institute of Technology in 1940. This has a transmission

of the order of ten times that of the semicircular focusing instrument, though the best resolving power is about three or four times less than that normally attainable with the latter. The short lens spectrometer has been used very successfully in the study of artificially produced radioactive isotopes, and has become very popular. Recently the need has been felt for an instrument of high transmission which yet has a good resolving power, specially for the study of internally converted γ-rays of light nuclei. This object has been achieved in the design and construction of the double focusing spectrometer[15]. This instrument has a transmission rather better than that obtainable with the magnetic lens, together with a resolution comparable with that of the semicircular focusing instrument. A number of other spectrometers of various designs have been proposed and will be described. Only three of these would seem to offer real advantages over the magnetic lens instrument.

Throughout the history of β-ray spectroscopy other and simpler methods have been used in the study of β- and γ-spectra, notably simple absorption and coincidence absorption techniques. It is desirable before studying any source with a spectrometer, first to investigate it by these methods, which can often be made to give quite accurate results. Hence a discussion of these techniques will be given later in this article.

SPECTROMETERS

References to various types of spectrometer are scattered through the literature, and it was thought desirable to describe and give a first order theory of the better known instruments. Probably the most useful way in which the performance of a particular instrument may be estimated is by a determination of the transmission-resolution ratio as a function of the source area. Here the transmission is the percentage of all electrons of a particular momentum, emitted by the source, which are brought to a focus and recorded. The resolution is measured by the half width of the curve obtained for monokinetic electrons, expressed as a percentage difference in momentum (see *Figure 1*). The performance figure for optimum intensity, using a source of finite area, is usually very considerably less than the value for a point source, and also usually more difficult to estimate.

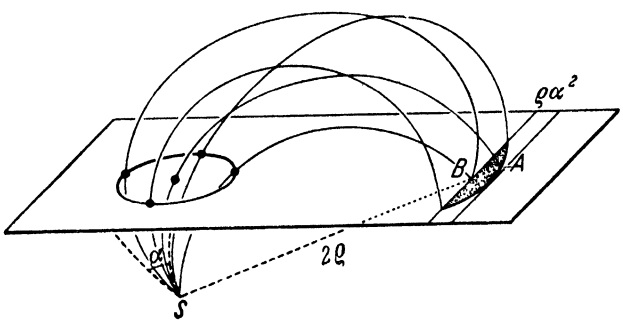


Figure 1. Electron trajectories in the semicircular focusing spectrometer

Semicircular focusing spectrometer—Although the semicircular focusing instrument has been outmoded, as far as performance is concerned, by later instruments it is still in general use, and the theory will be given rather fully, as illustrating the principles underlying spectrometer design and performance. The electrons are focused in a uniform magnetic field applied at right angles to the plane of the trajectories. The source is deposited on a wire a fraction of a millimetre in diameter and a few millimetres long, or as a narrow strip on a thin foil. A bundle of trajectories is selected by the defining slit, and further baffles of material of low atomic number are placed so as to prevent electron scattering from the walls of the vacuum chamber.

Two main types of detection are employed, the photographic plate and the Geiger counter. The photographic plate method has the advantage that electrons with a wide range of momenta may be recorded simultaneously. On the other hand the plate is relatively insensitive for electrons, and is non-linear, so it is difficult to make quantitative intensity measurements. These objections may be overcome by the use of the recently introduced photographic plates which are capable of detecting individual electrons. The Geiger counter method suffers from the disadvantage of utilizing only a narrow range of momentum at a time, and has a lower resolution, but each electron falling on the counter slit is recorded separately, and quantitative measurements are possible. Most recent spectrometers of this type utilize permanent magnets of the *Alnico* type, with coils so that the magnet may be energized to a particular field. The field is measured directly by rotating coil or disk methods. Fields of the order of several thousand oersted are easily obtainable with such magnets and are extremely stable.

The theory of the instrument has been worked out by Li[12]; the final integrals have to be evaluated numerically. However we can formulate a simple first-order theory which will be accurate enough for most purposes. Suppose initially that the source is infinitely narrow. A trajectory passing through the centre of the defining slit in a plane perpendicular to the applied magnetic field describes a circle of radius ρ cm given by: $H\rho=pc/e$, where H is the magnetic field in oersteds, p the relativistic momentum in c.g.s units, e and c the electronic charge and the velocity of light. Consider the diameter SA and the intersection with it of a trajectory making an initial angle α with the median. Then if the point of intersection is B, from *Figure 1* and elementary geometrical considerations

$$AB=2\rho\,(1-\cos\alpha)\simeq\rho\alpha^2, \text{ for small } \alpha$$

The position of B is independent of the sign of α, and this has the consequence that the spectral line is asymmetric, with a sharp rising front edge, called the head of the line, and a trailing edge at the back. The width of the line under the conditions stated is $\rho\alpha^2$ where α is the semi-angle of the defining aperture.

So far we have confined ourselves to a consideration of trajectories in the plane perpendicular to the magnetic field. Let us now consider trajectories which make small angles with this plane. Then by taking the component of the momentum in this plane one can show that the equation above still holds. Hence electrons emitted from the source within a cone of half-angle α will be focused within a strip of width $\rho\alpha^2$. The useful solid angle or transmission of the instrument is equal to $\alpha^2/4$ of a complete sphere. The source length is also limited to $2\rho\alpha$ as a result of these considerations. If the source has a finite width s this will contribute directly to the width of the line.

The relative change in momentum required, with a fixed value of the magnetic field, to shift the line by its width is given by

$$dp/p=d\rho/\rho=(s+\rho\alpha^2)/\rho=s/\rho+\alpha^2$$

So the resolution of the instrument is

$$R=\tfrac{1}{2}(s/\rho+\alpha^2)$$

where the factor $\frac{1}{2}$ comes from the definition of the resolution through the half-width.

This is so for a photographic plate detector. For Geiger counter detection the electron must pass through a slit of width w, and the resolving power becomes

$$R=\tfrac{1}{2}[(s+w)/\rho+\alpha^2]$$

It can easily be shown that the peak intensity of the line will be greatest for a source width $s=\rho\alpha^2$, and that for this value of s the spectral line has roughly the shape of an isosceles triangle. The counter window should preferably have the same width as the source. Under these circumstances the peak intensity is three quarters of what it would be with a wide counter slit. The average transmission over the source is $3\alpha^2/16$, the resolving power is $3\alpha^2/2$, the transmission-resolution ratio for this spectrometer (the efficiency) has an optimum value of about $\frac{1}{8}$. The optimum source area is $2\rho^2\alpha^3$, so the peak intensity is $\frac{1}{4}\rho^2\alpha^5$ for a source emitting one electron per second and per sq cm.

As the radius of curvature increases the transmission and resolution remain constant, provided that all dimensions are scaled equally. However the optimum source area is proportional to ρ^2 and this is important, especially for low energy work, because a large source area means that the source material may be thin, so as to avoid scattering and absorption, and still give an adequate intensity. This is, of course, true for all types of spectrometers.

A usual working resolution for this type of instrument is 1 per cent, and the corresponding transmission is about 0·1 per cent. A radius of curvature of 10 cm is a fairly average value. Together with the condition for 1 per cent resolution, this makes the optimum source area about 0·1 sq cm. The semicircular focusing spectrometer has usually been employed as an

instrument of high resolution (1 per cent or better), but there seems to be no obvious reason why it should not be employed with a considerably worse resolution, say 5 per cent with corresponding increases in transmission and source area.

Solenoid spectrometer—The first to use the focusing in a uniform longitudinal magnetic field was TRICKER[13]. The method was developed by WITCHER[14], who showed that the best focus for electrons emitted from a point source on the axis of the instrument is on a ring perpendicular to the axis. He constructed a spectrometer of 100 cm length, using ring focusing, and worked with a mean angle of emission, with respect to the field, of 18°. Typical figures obtained for the performance were 1 per cent transmission, with 5 per cent resolution. Thus the performance under these circumstances is similar to that of the short magnetic lens, except that it was possible to use a source of as much as 2 cm diameter, and hence of an area about sixteen times that employed in the short lens spectrometer, for the same performance. Recently it has been pointed out by FRANKEL[15] and PERSICO[16] that Witcher was not using his spectrometer under the best conditions, and that in fact there is a mean angle of emission such that the performance of the instrument is at an optimum. This can be shown easily. Consider an electron emitted at an angle α to the field, then if r and z are cylindrical polar coordinates, with z along the field, the equation to the trajectory can easily be shown to be

$$r = k \sin\alpha . \sin(z/k\cos\alpha) \quad \text{where} \quad k = 2\rho/He$$

The change in r, which corresponds to a given fractional change in p or k, for fixed z and α, is given by

$$\frac{dk}{k} = \frac{dr}{k\sin\alpha . \cos\chi . (\tan\chi - \chi)} \quad \text{where} \quad \chi = z/k\cos\alpha$$

Now let us consider the way in which r changes with α for fixed k and z.

$$dr/d\alpha = k\cos\alpha\cos\chi(\tan\chi + \chi\tan^2\alpha)$$

If $\tan\chi + \chi\tan^2\alpha = 0$, $dr/d\alpha = 0$, and this means that electrons emitted over a small range of angles will be brought to a ring focus at a value of z given by this expression.

We are principally interested in that value of the change in α which will give rise to the same change in r as a given fractional change in k, because this will give us a measure of the resolution in terms of the transmission. We shall confine ourselves to a consideration of the optimum case, given by $\tan\chi + \chi\tan^2\alpha = 0$, but we need to go to the next approximation in the evaluation of Δr. Expanding in the usual way to the second order, and using the above condition, we find

$$\Delta r = k(\Delta\alpha)^2 \sin\alpha\cos\chi(\chi/2)(3\sec^2\alpha + \chi^2\tan^4\alpha)$$

but $|dk/k| = \Delta r/(k\sin\alpha\cos\chi . \chi\sec^2\alpha)$

Using the focusing condition we get the resolution

$$R = \left(\frac{\Delta\alpha}{2}\right)^2 \frac{3\sec^2\alpha + \chi^2\tan^4\alpha}{\sec^2\alpha}$$

The transmission $T = d\Omega/4\pi = \frac{1}{2}\sin\alpha.\ \Delta\alpha$

hence $R = T^2\,(3\sec^2\alpha + \chi^2\tan^4\alpha)/\tan^2\alpha$

We now require the minimum value of R for fixed T as α varies. This will give us the optimum value of α. After differentiating, and solving an elementary transcendental equation, we obtain $\alpha \simeq 45°$ as the optimum value. Since $\Delta r \sim (\Delta\alpha)^2$, the spectral line has a 'head' similar to that for the semicircular focusing instrument. The resolving power is therefore a factor of two better than that given by the above formula. At the optimum $R \simeq 5T^2$.

This spectrometer is unique in that the resolution increases as the square of the transmission, which means that very high resolutions may be obtained for quite large values of the transmission. In a typical case $T = 5$ per cent and $R = 1{\cdot}25$ per cent.

The above analysis is correct for a point source. For a source of finite area, Persico finds that there is an optimum source diameter for luminosity (source area $\times$ transmission) for which

$$s/k \simeq \Delta\rho/\rho \simeq 25T^2$$

the optimum angle now being $\alpha = 40{\cdot}5°$

Here the resolution is five times worse for a given transmission, but it still competes favourably with the double focusing instrument, especially for high resolution.

For many applications this spectrometer will have the best performance of all. It takes considerably more power and copper for a given maximum focused energy than the short lens spectrometer, and has the further disadvantage that source and counter are in a high field region. This would make it difficult to use two such spectrometers back to back for coincidence work. These difficulties could be resolved by enclosing the solenoid in an iron box, and accepting the resulting non-linearity.

Magnetic lens spectrometer—This depends essentially on the same focusing principle as the last mentioned instrument, but here the magnetic field is more limited in space. As the name suggests the lens spectrometer consists essentially of a large coil which acts as a magnetic lens. The source and a Geiger counter are placed at opposite ends of an evacuated tube passing through the coil, and an annular bundle of electron trajectories is selected by a ring baffle. The electrons spiral in the longitudinal magnetic field, and are brought to a focus on the counter window. Other non-defining baffles may be used to reduce electron scattering from the walls of the tube, and a considerable

thickness of lead placed on the axis, to prevent direct γ-radiation from the source from affecting the counter. Typical dimensions for such an instrument are: inner and outer coil diameters 20 and 60 cm; length of coil 20 cm; source to counter distance 100 cm. The coil may be made to dissipate up to 5 kw, giving a maximum field strength of about 2,000 oersted, and focusing electrons up to 5 Mev in energy with a focal length of 25 cm. Circular sources of a few millimetres in diameter are used.

The theory of the instrument has been worked out by DEUTSCH, ELLIOTT and EVANS[17]. They find that the lens may be regarded as a simple optical lens except in regard to spherical aberration. The actual calculation of the latter involves laborious numerical integration of the equations of motion for electrons with different values of the initial constants. Although they outline the methods they prefer to determine the spherical aberration experimentally by measuring the variation in the apparent momentum of a monokinetic group of electrons defined by a narrow aperture, when the mean diameter is varied. Fortunately a fair approximation to the performance of the instrument may be obtained, even if the spherical aberration is neglected.

If a current i flows through the n turns of the focusing coil, then the focal length of the lens for electrons of a given momentum p is given by

$$f = c(p/ni)^2 \qquad \ldots.(1)$$

where c is a constant depending on the coil dimensions. The image and object distances u and v measured from the centre of the lens are connected with f by the well known thin lens formula

$$1/f = 1/u + 1/v \qquad \ldots.(2)$$

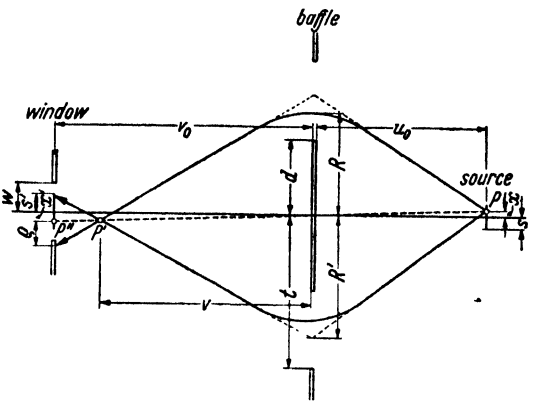


Figure 2a. Focusing in the lens spectrometer

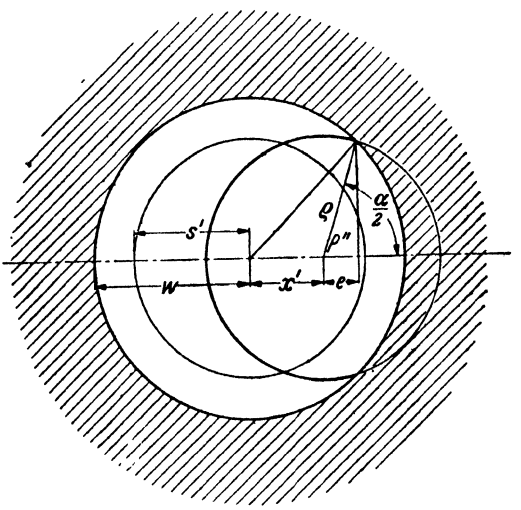


Figure 2b. Intersection of a bundle of electron paths with plane of window

The source and counter are commonly placed symmetrically with respect to the coil so that $u = v = v_0$. Consider now electrons of slightly wrong

momentum $p = p_0 = \Delta p$, which (see *Figure 2*a) are focused at the point P', after passing through the lens zone of radius R. The point P', at a distance $v_0 - v$ in front of the window W, does not necessarily lie in the plane of P and the axis. The rays will intersect the plane of the window in a circle of radius ρ. From similar triangles $\rho/R' = \overline{v_0 - v}/v$ and using the lens formulae $1/v_0 + 1/u_0 = 1/f_0$, *etc* we get

$$\rho = R'u_0(f_0 - f)/f(u_0 - f_0) \quad \ldots.(3)$$

where f is the focal length for electrons of momentum p, and f_0 that for electrons of momentum p_0 passing through R, and being focused at P'' in the plane of W (see *Figure 2*b). From geometrical optics we have $u_0/(u_0 - f_0) = m + 1$, where m is the magnification.

From equation 1

$$(f_0 - f)/f = (p_0/p)^2 - 1$$

$$\text{so that } \rho = R'(m + 1)\left\{(p_0/p)^2 - 1\right\} \quad \ldots.(4)$$

The fraction of this circle of confusion which falls on the window will be the fraction of the bundle of rays through P' which will be transmitted. From *Figure 2*b this fraction is given by

$$T_x = 1 - \alpha/2\pi = 1 - (1/\pi)\cos^{-1}\left\{\overline{w^2 - m^2x^2 - \rho^2}/2mx\rho\right\} \quad \ldots.(5)$$

Integrating over the surface of the source, and dividing by its area, we obtain

$$T_R = (1/\pi s^2)\int_0^s 2\pi x\, T_x dx$$

$$= 1 - (2/\pi s^2)\int_0^s x\cos^{-1}\left\{\overline{w^2 - m^2x^2 - \rho^2}/2mx\rho\right\} dx \quad \ldots.(6)$$

for the fraction of all electrons of momentum p leaving a uniform source of radius s, and passing through the lens zone of radius R, that will enter the counter through the window of radius s. If we consider a narrow lens zone, then we can make the approximation $(p_0/p)^2 - 1 = 2\Delta p/p_0$ so that

$$\rho = 2R'(m + 1)\,\Delta p/p_0 \quad \ldots.(7)$$

Now from *Figure 2*b it may be seen that all electrons passing the lens zone of radius R will enter the window if $\rho < |ms - w|$, and none will be transmitted if $\rho > |ms + w|$. If the maximum and minimum values of R' are d' and t' respectively, from equation 8 we find that the total spread in the momenta of the transmitted electrons is

$$\Delta p/p_0 = \pm (ms + w)/2d'(m + 1) \quad \ldots.(8)$$

while the spread in the range of complete transmission is

$$\Delta p/p_0 = \pm (ms - w)/2t'(m + 1) \quad \ldots.(9)$$

Equations 5, 8 and 9 strictly hold only for a narrow lens zone, and the extension to a zone of finite width requires a knowledge of the spherical aberration.

However, approximately, we may apply them directly to the lens spectrometer. If it is assumed that the source diameter is small, and that $w = ms$, then in the absence of spherical aberration all electrons of the given momentum leaving the source and passing through the defining slit will enter the window of the counter. Then the effective transmission is approximately

$$T = (t'^2 - d'^2)/4u_0^2$$

The resolving power is

$$R = ms/d'(m+1)$$

The efficiency is given by

$$T/R = [(t'^2 - d'^2)\, d'(m+1)]\ /(u_0^2 4ms)$$

Putting in typical values for $t' = 8{\cdot}75$, $d' = 6{\cdot}25$, $u_0 = 50$, $s = 0{\cdot}3$ all in centimetres, and $m = 1$, we have $T \simeq 0{\cdot}4$ per cent, $R \simeq 2{\cdot}5$ per cent, $T/R \simeq$ one sixth. A greater efficiency could be obtained by using smaller values of d', but spherical aberration then becomes more important, and shielding and scattering problems become more difficult. Another way of increasing the efficiency is by decreasing the source diameter, but this has obvious limitations, because even in this instance the source area is only 0·3 sq cm. The effect of spherical aberration will be to decrease the efficiency of the instrument by something of the order of 50 per cent, depending on the mean coil diameter, and the resolving power used. By decreasing u_0 by a factor of two, the efficiency increases to $\sim\frac{1}{3}$, making an allowance for spherical aberration, which is three times that of a semicircular focusing instrument of radius 10 cm, and utilizing approximately the same source area. However, this gain is limited to resolving powers of worse than 2 or 3 per cent, because spherical aberration limits the best practical resolution to about 1·5 per cent. Ring focusing which is used with the solenoid spectrometer may also be used to advantage with the short magnetic lens spectrometer. It increases the efficiency of the instrument by about a factor of two.

Apart from the increased efficiency, the magnetic lens spectrometer has the further advantage that it is a linear instrument, the magnetic field and hence the focused momentum being proportional to the current; also the source and counter are in relatively field free regions and are readily accessible.

Double focusing spectrometer—Although for many purposes the magnetic lens spectrometer has superseded the semicircular focusing instrument, there are applications in which the poor resolution of the former is a grave drawback, especially in the investigation of internal conversion and level schemes in light and medium nuclei, where the internal conversion coefficients are small (10^{-3}—10^{-4}). Recently a number of instruments capable of high resolving power, $\sim$0·3 per cent, and yet with an even greater transmission than the magnetic lens instrument, have been devised. Of these one of the

most promising appears to be that proposed originally by SVARTHOLM and SIEGBAHN[18]. This instrument, *Figure 3*, is based on the behaviour of the free oscillations of a charged particle in an axially symmetrical magnetic field,

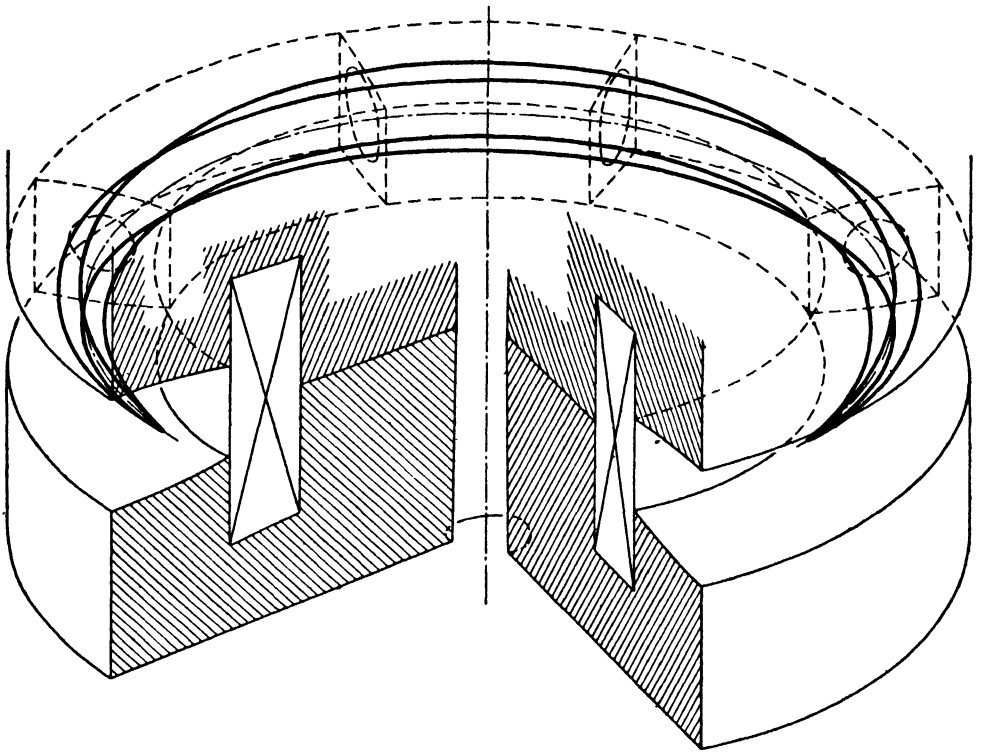


Figure 3. Diagram showing double focusing property of magnetic field (SVARTHOLM and SIEGBAHN[18])

varying with the radius, first established by KERST and SERBER[19]. If the magnetic field has the form

$$H = H_0(r_0/r)^n \quad 0<n<1$$

the angular frequencies of the radical and axial oscillations are given by

$$W_r = (1-n)^{\frac{1}{2}} W_0 \qquad W_a = n^{\frac{1}{2}} W_0$$

respectively, where W_0 is the orbital angular frequency given by $W_0 = eH/mc$, where m is the relativistic mass of the particle. If $n = \frac{1}{2}$ the radial and axial frequencies are equal, and for electrons diverging from a point source in such a field, the two oscillations will be in phase, and the electrons will be focused after half the oscillation period. Since the orbital frequency here is twice as great as the radial and axial frequencies, it is evident that the image point will be at an angular distance of $\sqrt{2}\,\pi$ or 254·6° from the object. When $n = \frac{1}{2}$ the field can be expanded in the following form

$$H = H_0 \left\{ 1 - \tfrac{1}{2}\left(\frac{r-r_0}{r_0}\right) + \tfrac{3}{8}\left(\frac{r-r_0}{r_0}\right)^2 - \ldots . \right\}$$

SHULL and DENNISON[20] have considered the more general expansion

$$H = H_0 \left\{ 1 - \alpha \left(\frac{r - r_0}{r_0} \right) + \beta \left(\frac{r - r_0}{r_0} \right)^2 - \ldots . \right\}$$

considering α and β as variable parameters. For double focusing *i.e.* focusing in the axial and radial directions, it is necessary that $\alpha = \frac{1}{2}$, so that the field to the first order is as $r^{-\frac{1}{2}}$. However β may be adjusted so as to eliminate either the second order radial aberration ($\beta = \frac{1}{8}$) or the second order axial aberration ($\beta = \frac{3}{8}$); ROSENBLUM[21] has suggested $\beta = \frac{1}{4}$ to give an image of minimum size. The performance of the instrument has been calculated in detail by SVARTHOLM and SIEGBAHN, and by SHULL and DENNISON[20]. The linear dispersion of the instrument is twice that of the semicircular focusing instrument for an equal radius of curvature. Moreover, it is easily possible to obtain a resolution of about 0·3 per cent together with a transmission of about 0·3 per cent. Thus the efficiency of the instrument is about unity, compared with one eighth for the semicircular focusing and one third for the magnetic lens instruments. The instrument can use source areas comparable with that of the semicircular focusing instrument, for the same resolution.

Instruments of this type have been constructed by SVARTHOLM and SIEGBAHN[18], by KURIE, OSOBA and SLACK[22] and by SHULL[23], and the experimental performance has borne out the theory very closely. The advantage of being able to get high resolutions and yet to maintain a good transmission is obvious. The instrument suffers from the disadvantages that pole pieces must be profiled to obtain the correct field distribution. Also, of course, in common with all instruments using iron, the momentum-current relation is non-linear. Furthermore, source and counter are placed in a high field region. However these disadvantages are not serious for many purposes, and the instrument does represent a real advance over the short magnetic lens instrument.

Radial inhomogeneous field semicircular focusing spectrometer—As we have shown earlier, for focusing in a uniform field, the trajectories on either side of the medial one are brought to a focus at a point nearer to the source than the latter. By arranging that the field at the medial trajectory is a maximum and falls off in the correct manner on either side this particular form of aberration may be eliminated, and a broad beam brought to a high order focus. The field distribution is given by

$$H = H_0 (1 - \tfrac{3}{4}\delta^2 + \tfrac{7}{8}\delta^3 - \tfrac{9}{16}\delta^4 + \tfrac{51}{320}\delta^5 + \ldots .)$$

where $\delta = (r - r_0)/r$, and r_0 is the radius of curvature of the medial trajectory. The angular width of the beam in the direction of the field is strictly limited, because although there is some focusing in this direction over half the beam, over the other half there is actual defocusing. A large spectrometer of this

type has been built by LANGER and COOK[24]. It uses an annular magnet and employs a mean radius of curvature of 40 cm, which has the advantage of making it possible to use the large source area of 1 sq cm. The efficiency of the instrument is about the same as that of the magnetic lens instrument, though the best resolution is much higher. It would appear to be more profitable to use a large magnet of this type for a double focusing instrument.

Four pole spectrograph and magnetic prism—This instrument was proposed by KORSUNSKY[25]. It is another attempt to improve the focusing in the plane perpendicular to the applied field. Two magnets with circular pole pieces are placed side by side. A source is placed at the outer edge of one magnet, and it can be shown that, for a particular value of the magnetic field and electron momentum, electrons from this source will emerge from the circular poles in a parallel beam, in the absence of the fringing field. The parallel beam will pass into the second magnet and be brought to a symmetrical focus. Again there is part focusing and part defocusing of the beam in the perpendicular direction, which necessitates a strict limitation of the beam in this direction. The calculated performance of the instrument is about the same as that of the magnetic lens instrument, but this neglects fringing fields which are almost certain to make it worse.

A similar principle has been utilized by SIDAY[26] in the design of a magnetic prism for very high resolutions. Since the calculations refer only to trajectories in the median plane it is not yet possible to see what effect non-median trajectories will have on the resolution.

Pair spectrometer—At high energies, ~ 5 Mev, and for materials of high atomic number, the most important interaction of γ-rays with matter is due to pair production. While it is possible to study the positrons alone this has the disadvantage, compared with the study of photoelectrons, that the positrons are distributed in a continuous spectrum. However, the pair spectrometer has been designed[27] in which positrons and electrons of a wide range of momenta are utilized for a single measurement. The instrument picks out and records those electron pairs which are emitted simultaneously, and for which the sum of the momenta is constant. In *Figure 4* a uniform magnetic field is applied perpendicular to the plane of the paper. An essentially parallel beam of γ-rays to be analysed falls on a thin radiator foil, placed perpendicular to the beam. Electron pairs are produced which for γ-rays of fairly high energy (>3 Mev) go very nearly in the forward direction. The positron and the electron may each fall into one of four counters placed in the plane of the radiator foil, that is at the position of semicircular focus. The counters are connected into coincidence circuits in pairs, and the coincidence outputs from pairs, such that the sum of the distances between them is constant, are paralleled *i.e.* all those coincidences arising from pairs, the sums

of radii of curvature of which are constant, are fed to the same recorder. The radius of curvature is proportional to the momentum, and it can be shown that at high energies if the sum of the momenta of the pair is constant

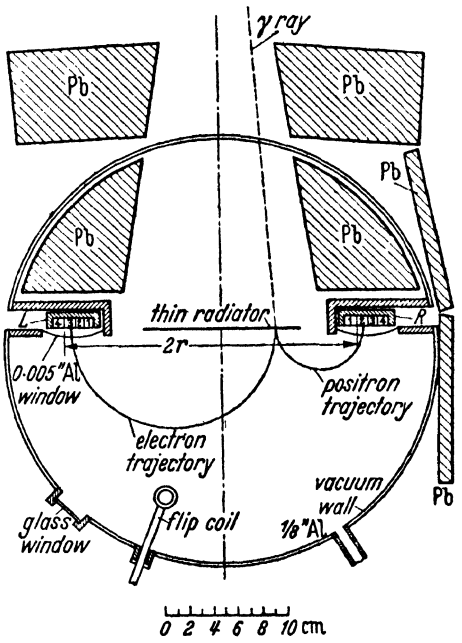


Figure 4. Diagram of spectrometer: horizontal section through the gap of the large magnet producing a magnetic field normal to the plane of the paper.

The vertical height of the gap is 4 in.

Coincidences are observed between any one of the four Geiger counters on the left, L and any one of the four on the right, R.

The γ-ray source (cyclotron target) was 60 cm from the radiator in the present experiments

the sum of the energies is constant also, and all the pairs are produced by γ-rays of the same energy. The quantum energy

$$k = E_+ + E_- = (p_+^2 + \mu^2)^{\frac{1}{2}} + (p_-^2 + \mu^2)^{\frac{1}{2}}$$

with p in energy units and $\mu = m_0c^2$. If $p_+ \gg \mu$ and $p_- \gg \mu$ this becomes

$$k=(p_+ + p_-)(1 + \mu^2/2p_+p_-)$$

The error term $\mu^2/2p_+p_-$ depend on the individual momenta, and hence on the place of origin of the pair, though only to the second order. For large values of the quantum energy this term will be small, and for energies $\sim$ 6 Mev it is completely negligible compared with other aberrations. The chief contribution to the magnitude of the resolving power is due to the finite width of the counter window; it is $w/2r$ where w is the window width, and $2r$ the distance between counters. For the constants of the spectrometer used by WALKER and MCDANIEL[27] *viz* $(2r)_{uv}$=24 cm and w=0·8 cm, the resolving power is 3·3 per cent. Other smaller terms which affect the resolution are due to *1* scattering of electrons in the walls separating the counters, *2* multiple scattering of electrons in the radiator, *3* angular divergence of the pair; *4* deviations from normal incidence of γ-rays striking the radiator far from its centre, and *5* energy loss of electrons within the radiator. Of these *2* and *5* place strict limitations on the thickness of radiator which may be used, of the order of a few thousandths of an inch of copper or aluminium for γ-rays of $\sim$ 6 Mev, and *2*, *3* and *4* are minimized by the

properties of semicircular focusing. In a typical set-up with the source some 60 cm from the radiator, Walker and McDaniel obtained one count for every 10^7 γ-rays emitted from the source for the 17·6 Mev γ-ray from the (Li,p) reaction, with a resolution of 6 per cent.

It is almost certain that this instrument will be used increasingly in connection with the study of proton and neutron capture processes, not only because it utilizes the conversion process which is most efficient at high energies, but also because a coincidence method effects an enormous reduction in the background rates which are encountered in the neighbourhood of accelerating machines or piles.

Focusing in a spherical electrostatic field—The focusing properties of various forms of magnetic field distributions have almost invariably been utilized in the design of β-ray spectrometers. It is interesting therefore to note that there is a form of electrostatic focusing which can compete with the best forms of magnetic focusing, especially in the low energy region. This is the focusing in a Coulomb electrostatic field. The focusing theory was first worked out by TEMPLE in 1937 (unpublished), and experimental use of this form of focusing has been made by PURCELL[28]. The performance of such an instrument, especially in the relativistic region, has been worked out by the author (unpublished).

Consider a point source of electrons in the field established between two concentric spherical conductors. Then for very low energies, all the electrons will be focused at a point diametrically opposite to the source. At higher energies, such that the relativistic change of mass with velocity becomes appreciable, point focusing no longer occurs, but rather focusing on a ring perpendicular to the source axis. The half angle which the ring subtends at the centre of the sphere is $\pi/\sqrt{(1 - v^2/c^2)}$. As the electron energy increases, the angle of the ring increases, until for very high energies there is no focusing of electrons emitted at differing tangential angles from the source, but nevertheless first order focusing still occurs because of the cylindrical symmetry of the system. Practically, it is necessary to investigate the focusing at angle π from the source, where a Geiger counter may be placed. The resolving power and the dispersion are not, as in the case of magnetic focusing, independent of the energy. In a typical case for spheres of mean diameter 1 m and separation 1·5 cm, the ratio transmission to resolving power is 1·6 at 0·2 Mev, and 0·7 at 2 Mev, for a point source. For a source of optimum area and other apparatus constants, such that the intensity is a maximum, the transmission is rather less than a half of its maximum value, but still compares favourably with the magnetic lens instrument. The instrument can be used with much better resolution than the latter, and in fact its overall performance is closely paralleled by the double focusing magnetic spectrometer. Disadvantages are in the difficulty of construction of the large spherical

conductors to the desired accuracy and concentricity, and also in the non-linear performance of the instrument. It should however be useful for work at low energies.

Focusing in the electrostatic field established between concentric cylinders has been used on a few occasions, but appears to have no advantages as compared with other instruments.

MEASUREMENT OF GAMMA-RAY ENERGIES

Absorption measurements—Absorption experiments with bad geometry (using poorly collimated γ-rays) are the simplest means of investigating γ-radiation when weak sources only are available. Under these circumstances a fairly accurate value of the γ-ray energy may be obtained for quantum energies up to 2-300 kev, because the secondaries are soft and easily absorbed, so that the effect of bad geometry is minimized. For higher quantum energies the secondary radiation is harder, and the bad geometry tends to decrease the absorption coefficient. In fact, the counting rate may actually rise, on interposing absorbers[29]. At higher energies, of the order of 5 Mev for lead, the absorption coefficient passes through a minimum value, where the Compton and pair production cross sections become about equal, the former decreasing and the latter increasing with quantum energy. Thus in this region absorption experiments give very inaccurate results.

Transition effect—This is a method developed by FEATHER[30] applicable to γ-rays of energies sufficiently low that the photoelectric cross section in materials of high atomic number is appreciable. γ-rays in traversing matter will reach equilibrium with their secondaries in a thickness of material of the order of the range of the secondaries. The equilibrium will, in general, depend on the atomic number of the material, and for γ-rays passing from one material to another there will be a transition region in which the equilibrium changes from that appropriate to the first to that appropriate to the second material. In essence the method consists in causing the γ-rays to eject photoelectrons from a layer of material of high atomic number, and measuring the range of these photoelectrons in material of low atomic number. The method may be applied at quantum energies as high as 1 Mev, but suffers from the usual limitations and inaccuracies of absorption methods.

Critical absorption—The energy of quanta in the x-ray region (say 1 kev to 80 kev) may be determined accurately by measuring the absorption in materials of different atomic number. The aim is to bracket the quantum energy by the *K*-absorption edges of materials of neighbouring atomic number, when it will be heavily absorbed in that material which has the lower *K* edge. Since the absorption coefficient alters by a factor of the order of

five in passing over an absorption edge, and varies fairly rapidly on either side, this method can be made to give quite accurate results.

Bothe method—This consists essentially of finding the maximum range of Compton electrons ejected by the γ-rays under consideration. The Compton electrons pass through two thin walled Geiger counters connected to a coincidence circuit, and absorbers are placed between the two counters. The coincidence rate is plotted against the thickness of absorber, and falls rapidly until the endpoint of the Compton electrons is approached. It then tails off into the background of accidental coincidences, γ-γ coincidences, and coincidences caused by scattered particles, which is usually of the order of 1 per cent of the counting rate for zero absorber. Since the absorption curve approaches the background very slowly, the endpoint is difficult to estimate to better than 5 per cent. To avoid this difficulty BLEULER and ZÜNTI[31] have made a semi-empirical determination of the absorber values required to reduce the coincidence counting rate by a factor of 2, 2^2.... 2^7. This enables a determination to be made of the quantum energy, provided only one γ-ray is present, from parts of the absorption curve away from the endpoint. Their results are valid for quantum energies less than 5 Mev, and are to some extent dependent on geometry. If a geometry similar to theirs is employed, it is possible in this way to determine the quantum energy to 2 or 3 per cent. The method has been extended to higher energies by FOWLER, LAURITSEN and LAURITSEN[32].

Cloud chamber and ion chamber measurements—Cloud chambers have been used extensively for determining γ-ray energies with weak sources, but have given very inaccurate results. The errors which are likely to arise in this type of work have only recently been fully appreciated.

A method which is applicable at high energies depends on the electrodisintegration of deuterium, the energy of the proton being measured with a high pressure ion chamber.

Spectrometer measurements—With the possible exception of the last, none of the foregoing methods is easily applicable when several γ-rays are present. In this case it is almost essential to use a spectrometer *i.e.* an instrument in which electrons of different energies are separated. The two effects most extensively used for the determination of γ-ray energies in the spectrometer are the Compton and photoelectric effects. Pair production has been studied in recent years, and will be increasingly important as a means of determining high quantum energies. To utilize the Compton effect the source is enclosed in a box of material of low atomic number sufficiently thick to stop all the primary electrons. The Compton electrons ejected from the box will be focused in the spectrometer and form a continuous spectrum, with a fairly sharply defined upper energy limit. Compton electrons due to lower energy

quanta will be superimposed, but the endpoints can still be determined provided the γ-ray is not too weak. The quantum energy E_γ is connected with the maximum electron energy E_e by the formula

$$E_e = E_\gamma/(1 + mc^2/2E_\gamma) \qquad \text{or} \qquad E_\gamma = \tfrac{1}{2}\,[E_e + (E_e^2 + 2E_e mc^2)^{\frac{1}{2}}]$$

where $mc^2 = 0{\cdot}511$ Mev.

A thin foil of material of high atomic number *e.g.* lead, may now be placed over the source box, and the photoelectrons ejected from it will form line spectra, which stand just clear of the Compton edge for all quantum energies except very low ones. Lines will appear due to electrons ejected from the K shell and the L shell, and for spectrometers of very high resolution even M electrons may be resolved. The quantum energies may be determined from the positions of the lines, after correcting for the effect of finite thickness of the radiator, by adding to their energies the binding energies of the electrons of the latter. This method can give results accurate to one per cent or better.

At high energies γ-rays are best investigated with a pair spectrometer, because the cross section for pair production increases with increasing quantum energy, whereas both the Compton and photoelectric cross sections decrease approximately inversely as the quantum energy in this region. A parallel beam of γ-rays falls on a thin radiator and ejects electron pairs from it. The electrons and positrons are separately focused in a uniform magnetic field into one of a number of counters, and those originating from the same γ-quantum are picked out by coincidence circuits and recorded, no matter from what part of the foil they are ejected. The sum of the energies of the positron and electron, including rest energies, then gives the quantum energy. The method has been applied very successfully by WALKER and MCDANIEL[27] in the study of the radiation emitted in the bombardment of lithium and fluorine by protons.

Determination of the relative intensities of γ-rays—Since γ-rays cannot be detected directly, but only by their effects on matter, a knowledge of the way in which these effects vary with quantum energy is necessary before the intensities of γ-rays with differing energies may be compared. The Compton effect in which the γ-quantum transfers part of its energy to a free electron in an elastic collision is probably the best understood, and the theory rests on the firmest basis. The cross section for this effect as a function of quantum energy is given by the KLEIN-NISHINA formula[33], which has been verified experimentally up to a few Mev by absorption experiments with good geometry and under conditions such that the photoelectric effect and pair production are relatively unimportant. The theory of the photoelectric effect has been treated by a large number of workers, and a good summary is given by HEITLER[34]. The results cannot be given in a closed mathematical form, valid over the whole range of the variables of quantum energy and atomic

number. However a Z^5 law holds over a large range of the latter. LATYSHEV[35], using a narrow aperture semicircular focusing spectrometer, has compared the photoelectric with the Compton cross section over the range of atomic numbers from copper to lead, and finds that a $Z^{4\cdot6 \pm 0\cdot25}$ law holds. With the spectrometer used in this way only a narrow range of angles, and therefore a narrow band of energies, of the Compton electrons is accepted, and the Compton spectrum becomes a rather broad line. The value of the cross section for the 2·62 Mev γ-rays from ThC″ in lead agreed accurately with that derived theoretically by HULME *et al*[36]. At high energies the photoelectric cross section is inversely proportional to the energy, but the range of the photoelectrons in the radiator increases approximately proportionally to the energy. If the thickness of the radiator is varied so as to correspond to a given percentage energy loss of the photoelectrons, the number emerging will be approximately independent of the energy. Thus it is possible to use the photoelectric effect for the study of γ-rays up to energies such that radiative losses begin to be important in the slowing down of electrons *i.e.* $\sim$ 10 Mev in lead. Latyshev has also performed similar experiments to verify the cross section for pair production derived by BETHE and HEITLER[37], with good agreement.

Theoretical cross sections cannot, however, be applied directly to derive relative intensities from measurements made, for instance, with the magnetic lens spectrometer. Allowance must be made for multiple scattering of electrons in the material of the radiator, and for the effects of angular distribution, if any. For photoelectrons emitted from a thick radiator a semi-empirical formula has been derived by DEUTSCH, ELLIOTT, and EVANS[17].

$$n_p = Ct_r\tau \left\{(kt_r/\beta^3\Delta p)^2 + 1\right\}^{-\frac{1}{2}}$$

where n_p is the measured line height, C the value which would be obtained if no absorption and scattering of electrons occurred, t_r is the radiator thickness, τ the photoelectric cross section, Δp is a measure of the momentum range transmitted, and k a constant.

For Compton electrons, provided that the distribution of source and scattering material is such that angular distribution effects are negligible and that an equilibrium thickness of radiator is used, the relative numbers ejected by γ-rays of differing energies will be given closely by the relative efficiencies of a Geiger counter, having a cathode of the same material as the radiator, providing this is of low atomic number. This has been measured over a range of energies by BRADT *et al*[38] using the coincidence method of calibration. A comparison of the number of electrons in the Compton partial spectra, if necessary extrapolating back on an energy similarity basis, will then give the relative intensities of the γ-rays. A comparison of these two methods gave results which agreed within about 25 per cent in a typical case.

MEASUREMENT OF SPIN CHANGES ASSOCIATED WITH GAMMA-RAY TRANSITIONS

Isomeric transitions—Equally important with the determination of the energy of a nuclear level is the spin to be associated with it. In general if the spin change associated with a given transition is large, the transition will be forbidden *i.e.* the lifetime of the excited nuclear state will be relatively long. It is well known that in the case of dipole and quadrupole transitions the nuclear lifetime is roughly of the order of 10^{-13} seconds. For higher multipole orders, and for low energies, the nuclear lifetime may be very long, possibly seconds, hours or even years. Many instances of such low lying states of long life have been reported in recent years, the so-called isomeric states of nuclei. A review of the recent experimental data, and its relation to the various theories which have been advanced, is given by WIEDENBECK[39]. Often a knowledge of the half-life and energy of the transition enables the spin change to be determined unambiguously. Frequently the γ-rays emitted in such transitions are very highly converted, and this leads to another method of determining the spin changes.

Internal conversion—The theory of internal conversion has been elaborated by a number of workers. Relativistic treatments have been given by HULME[40] for dipole radiation and the K and L shells, by TAYLOR and MOTT[41] for quadrupole radiation and the K shell; FISK and TAYLOR[42] have considered magnetic dipole radiation; HEBB and NELSON[43] have extended the calculations to higher multipole orders. Very recently calculations have been made for an extended range of atomic number and quantum energy by GRIFFITH and STANLEY[44] for electric dipole, and DRELL[45] for magnetic transitions of high multipole order. LOWEN and TRALLI[46] give the ratio of the K and L conversion coefficients for a range of atomic numbers and quantum energy. None of the results can be expressed in a closed form, and very laborious numerical calculations have to be made to obtain results pertaining to even a single value of the quantum energy and atomic number. However it may be said that the conversion coefficient increases rapidly with the atomic number, approximately as Z^3 over part of the range. Also it decreases rapidly as the quantum energy increases. For low quantum energies (less than about 300 kev) the conversion coefficient is sensitively dependent on the multipole order of the transition, increasing very rapidly with the latter. The ratio of the K and L conversion coefficients also depends on the multipole order and, to a marked extent, on whether the transition is electric or magnetic, especially for high multipole orders. This is important because the K/L ratio is easy to determine experimentally, as most spectrometers are able to resolve the two lines in the relevant range of energies.

The conversion coefficient itself is a difficult quantity to determine experimentally with any accuracy. The calculations of HULME[40], and of

TAYLOR and MOTT[41], have been checked in the classical work of LATYSHEV[35]. He determined the ratio of the number of photoelectrons, corresponding to a given transition, to the number of primary β-particles in the continuous spectrum. A measurement of the relative intensities of the γ-rays by examination of the Compton recoil spectrum then gave the conversion coefficients. A further interesting method, which is however applicable only to a simple spectrum, consists in determining the conversion electron coincidence rate per recorded β-particle, with conversion electrons focused in a spectrometer in coincidence with β-particles recorded by a Geiger counter placed near the source. A knowledge of the transmission of the spectrometer then determines the conversion coefficient. This has been used by DOWNING, DEUTSCH and ROBERTS[47].

Internal pair production—In the case of high energy γ-rays, and where large sources of very high specific activity are available, information on the multipole order of the transition may be obtained either by examining the internal pair spectrum in a pair spectrometer, or the positron part of it in, say, a magnetic lens spectrometer. The theory of this effect has been developed by JAEGER and HULME[48] and the results confirmed by LATYSHEV[35] with experiments on Th(C+C′). The essential features are that there is little dependence on atomic number, and that in contradistinction to internal conversion the conversion coefficient is greater for dipole than for quadrupole transitions. The conversion coefficients increase almost linearly with quantum energy (above $2mc^2$), but they are small ($\sim 5{\cdot}10^{-4}$) at 2 Mev, and this together with the fact that the electrons and positrons are spread out in a continuous spectrum demands the use of very strong sources for the investigation of either component singly. For high atomic numbers the positron spectrum shows a sharp break at the upper limit of energy, which is useful in separating the components of a complex spectrum.

The above methods of determining the multipole order of γ-ray transitions are of very limited applicability, because for nuclei of low atomic number the internal conversion coefficient is small, $\sim 10^{-4}$, while for nuclei of high atomic number, at high energies, $\sim$ 1 Mev, the conversion coefficients are not only small but also are not markedly dependent on multipole order. The limitations in the method depending on internal pair production are indicated above. A method of more general applicability has been developed recently, principally by BRADY and DEUTSCH[49].

Angular correlation between successively emitted γ-rays—Consider a nucleus in an excited state having a spin different from zero. Then this spin will have a particular orientation in space, and the γ-ray will be emitted with a probability polar diagram characteristic of the multipole order of the transition, in the same way as for instance a classical dipole oscillator has a characteristic polar diagram. Unfortunately different nuclei are orientated at random, and

hence the polar diagram effect is obliterated. It is possible that at extremely low temperatures the nuclei could be lined up in a magnetic field, and the polar diagram of the emitted γ-rays could be measured directly. However, such low temperatures have not yet been produced. Yet it is possible under some circumstances to obtain information on the polar diagram, in a different way. Suppose that the γ-ray is followed by one or more further γ-rays in cascade, and that after the first γ-transition the nucleus again has a spin different from zero. Then the orientation of this spin will depend on the spin, if any, of the first excited state, and the direction of emission of the first γ-ray. Again the emission of the second γ-ray will be characterized by a polar diagram, depending for its orientation on the spin of the second excited state. Hence there will be a correlation between the directions of emission of the two γ-rays, depending on the multipole orders of the two transitions. The only case in which this fails is when the intermediate state is of spin zero or $\frac{1}{2}$; for neither can a direction in space be defined.

The theory was originally worked out by HAMILTON[50], for the case in which the effect of external fields on the nucleus, in the time between the emission of the two γ-rays, was neglected. Experimental work by KIKUCHI, WATASE, and ITOH[51], BERINGER[52], and GOOD[53], failed to show any angular correlation, although nuclei were chosen such as Co^{60}, which decays by the emission of a β-particle followed by two γ-rays in cascade to Ni^{60}, being an even nucleus, with zero spin in the ground state. This ensures that the state intermediate between the emission of the two γ-rays has a spin other than zero. It was thought that the correlation might have been disturbed by the precession of the nucleus in the field of the extra-nuclear electrons, and a more elaborate theory was put forward by GOERTZEL[54] which attempted to evaluate the effects of disturbing forces. In particular, he suggested that the nucleus be placed in a uniform magnetic field, and calculations were made of the field strengths required to decouple the nucleus from the extranuclear electrons under various circumstances.

However, the inaccuracies of the earlier experiments had been underestimated, and the experiments by BRADY and DEUTSCH[49] in 1947 were successful, although no magnetic field was used. The experiments consisted essentially in determining the change in coincidence counting rate when two γ-counters were placed either 90° or 180° apart, with respect to the source. A change of 21 per cent was found for Co^{60} and Sc^{46} and no effect for Y^{88} and Cs^{134}, though this last result was later found to be in error. In 1948 further results[49] were published from experiments using high efficiency scintillation counters, which enabled a complete exploration of the angular correlation pattern to be made. Although the spin changes derived from the latter are not uniquely determined they do provide a valuable limitation of possibilities. In an accompanying paper DEUTSCH and METZGER[55] describe experiments on the correlation between the direction and polarization of successive

γ-ray quanta, the results of which throw further light on the nature of the transition. The study of angular correlation is likely to open a wide field because many nuclei emit γ-rays in cascade.

MEASUREMENT OF MAXIMUM ENERGY OF β-RAYS

Absorption measurements—The measurement of the maximum range of β-particles in material of low density such as aluminium is still a good method when only small sources and limited equipment are available. The attenuation is roughly exponential over a factor of 10 to 100, provided the absorbers are placed in contact with the counter. If they are placed near the source they must be very small, so as to intercept just that part of the beam which would strike the counter. Various empirical formulae for the range energy relationship have been derived, notably by FEATHER[56] and FLAMMERSFELD[57]. Feather's formula is

$$R=0{\cdot}571E_e-0{\cdot}161$$

where R is the range in gm/sq cm aluminium and E_e the energy in Mev. It is fairly accurate for energies in excess of 1 Mev, but decreasingly accurate for smaller energies. Flammersfeld's formula represents an improvement, since it is applicable over the range of energies 50 kev—3 Mev, and is

$$E_e=1{\cdot}92(R^2+0{\cdot}22R)^{\frac{1}{2}}$$

These formulae are, however, rather difficult to apply in practice because the absorption curve near the endpoint gradually merges into the cosmic ray background of the counter, or, more usually, the γ-ray background. In these circumstances the endpoint is difficult to determine accurately. Feather has attempted to eliminate this difficulty by comparing the form of the absorption curves with that of a standard taken with the same geometry. BLEULER and ZÜNTI[31] calculated the form of the attenuation, with a standard geometry, on the basis that the energy spectrum of the β-rays is that given by Fermi's theory for an allowed transition for aluminium absorbers, and for energies less than 3 Mev, for which radiation losses are unimportant. In making use of their results, the thickness of absorber required to reduce the counting rate by factors of 2, 4, 8.....2^n respectively is determined. Each of these values of the thickness may be used to make a determination of the maximum energy of the β-rays. For a simple allowed spectrum all these values of the energy ought to coincide. Even in the case of RaE and P^{32}, which are second forbidden transitions, it was found experimentally that the various values of the energy derived in this way agreed very closely. The maximum energies of β-spectra have been determined to better than 5 per cent by the application of this method, which may moreover be used to determine whether a spectrum is complex.

Other methods—The cloud chamber has been used extensively in the measurement of β-ray energies, but the results obtained have until recently been very inaccurate. The most accurate method is to use a spectrometer with thin sources on thin backings, paying particular attention to the obtaining of good counting statistics near the upper limit of energy. This is then determined by the extrapolation of the straight line Kurie plot $\{N/(H\rho)^3\}^{\frac{1}{2}}$, where N is the counting rate, and $H\rho$ the electron momentum, or any quantity proportional to it. All spectra appear to have straight line Kurie plots in the upper energy region. As will be discussed later, complex spectra show breaks in the Kurie plot which may be used to determine the maximum energies of the lower energy partial spectra, provided that the breaks are in fact due to this cause.

Very recently the energies of low energy β-particles and also of γ-rays have been determined by means of calibrated proportional counters[58]. This is a method which will be increasingly important for work at low energies, because it eliminates many of the difficulties associated with spectrometer work in this region, caused principally by scattering and absorption.

NUCLEAR LEVEL SCHEMES

The β- and γ-ray energies pertaining to a given radioactive nucleus having been determined by one means or another, it remains to consider them in relation to the energy level scheme of the product nucleus. In the early investigations of the natural radioactive bodies using the semicircular focusing spectrometer it was often possible to group the γ-rays, by means of their energies as measured from internal conversion lines, into self-consistent schemes, but such schemes were almost invariably ambiguous. With the artificial radioactive nuclei of low atomic number, the number of γ-rays of different energies emitted is usually small, and in general the energies are not known to the same accuracy as those of the natural radioactive nuclei. This means that it is difficult, or frequently impossible, to use energy grouping as a means of identifying the level scheme.

Fortunately there is another method which is especially applicable when the number of possible γ-rays is small. This method relies on the fact that the nuclear lifetime against radiative transitions is usually very short $\sim 10^{-13}$ seconds, and that γ-rays when emitted in cascade with β-rays or other γ-rays, in the great majority of cases, appear with them coincident in time. This may be made the basis of identifying a given γ-ray in relation to a given β-ray or other γ-rays. The method has been developed by DUNWORTH[59] and others. Consider the simplest case of a nucleus which emits a β-particle followed invariably by a γ-ray of a certain energy. Suppose the source is placed between two counters, one of which responds only to the β-particles and the other only to γ-rays. Let the two counters be connected into a

coincidence circuit of resolving time τ, such that only pulses from the two counters separated by a time less than 2τ are recorded as coincidences. Then if N nuclei disintegrate per second, and the efficiencies of the counters for β-and γ-rays are respectively ϵ_β and ϵ_γ, the counting rates in the two counters will be

$$C_A = N\epsilon_\beta/\text{sec} \qquad C_B = N\epsilon_\gamma/\text{sec}$$

The coincidence counting rate will be

$$C_C = N\epsilon_\beta\epsilon_\gamma/\text{sec}$$

In addition there will be an accidental coincidence counting rate. This is caused by independent pulses from the two counters arriving by chance within a time 2τ of each other. This rate depends on the coincidence resolving time, and its value may be found by considering that each of the pulses arriving from the one counter opens a ' time gate ' of length 2τ, into which a pulse from the other counter may fall. This gives the accidental coincidence rate as $N\epsilon_\beta 2\tau N\epsilon_\gamma$/sec. There is a further contribution from background coincidences produced by cosmic rays, which in general is small.

Obviously it is unprofitable to work with an accidental coincidence rate larger than the genuine coincidence rate, because both accidental and genuine coincidences arrive in a random fashion. We see immediately that this sets an upper limit to the intensity of source which may be used. Equating the genuine to the accidental coincidence rate we obtain $N=1/2\tau$ as the upper limit of the source strength such that the genuine rate shall be as large, or larger than, the accidental rate. The resolving time is usually set by random delays in the counters, and is of the order of a few tenths of a microsecond for Geiger counters. The maximum source size useful for coincidence work using the latter is thus of the order of a hundred microcuries ($=3{\cdot}7\times10^6$/sec). By taking the ratio C_AC_B/C_C we obtain N, the source strength. The ratios C_C/C_B and C_C/C_A give respectively ϵ_β and ϵ_γ, the efficiencies of the two counters. This is true even if several γ-rays are emitted in cascade with the β-particle; the γ-ray efficiency obtained will then represent an average value.

Coincidence absorption measurements—The coincidence technique in conjunction with absorption measurements may be used to decide whether a given β- spectrum is simple or complex. If the β-spectrum is simple every β-particle is accompanied by the same γ-ray or γ-rays. Thus if absorbers are placed over the β-counter, the β-γ coincidence rate per recorded β-particle will be a constant, independent of the absorber thickness, for a simple spectrum, provided that none of the γ-rays is appreciably internally converted. Examples of β-spectra found to be simple by this method are Na^{24} and Co^{60}. In the case of complex spectra it may be possible to find the upper energy limit of the lower energy β-group by observing where the β-γ coincidence rate per recorded β-ray flattens out when absorbers are placed before the

β-counter. It is also possible to find out if the greatest energy β-transition leads to the ground state of the product nucleus, or not, by observing if the β-γ coincidence rate per recorded β-ray becomes zero, or remains at a finite value, for large thicknesses of absorber. Information on the decay scheme may also be obtained by measuring γ-γ coincidences as a function of absorbers placed before the γ-counters. Examples of the way in which the coincidence rate may be expected to vary for different types of decay schemes are given by MITCHELL[60] and others.

In the case of complex decay schemes with greater than two or three β-rays and γ-rays the coincidence absorption method is not very useful. Nevertheless it has been used very extensively for the investigation of decay schemes, because of the simplicity of the apparatus involved. Moreover, in the case of γ-γ coincidences the large solid angles obtainable in this type of measurement are of paramount importance. It is only very recently, with the introduction of scintillation counters, that γ-γ coincidence measurements with a spectrometer could be contemplated.

Coincidence measurements with the spectrometer—It will be useful to determine the order of magnitude of the coincidence rate to be expected in a typical case for coincidences between a Geiger counter placed near the source and the spectrometer counter. Consider the case in which coincidences are being measured between β-particles focused in the spectrometer, and γ-rays recorded by the Geiger counter near the source. If the spectrometer is of the magnetic lens type, working with a transmission of say 0·5 per cent, and a resolution of 5 per cent, then the efficiency for β-ray counting is of the order of $2{\cdot}5\times10^{-4}$. The overall efficiency, including the solid angle factor, for γ-ray counting with a Geiger counter is unlikely to exceed 10^{-3}. For a source strength of say 2×10^{6} disintegrations per second, and for a simple transition in which a single γ-ray invariably follows the β-particle, the β-γ coincidence rate will be of the order of 0·5/sec. It could easily be considerably smaller for a lower energy γ-ray, or if a branch reaction of low ratio is being studied. It is therefore highly desirable to use an instrument with as high a transmission as possible, together with a high efficiency γ-counter, such as a scintillation counter, for this application. In another application, coincidences between conversion electrons of one γ-ray focused in the spectrometer and a second γ-ray recorded by a Geiger counter, it is necessary to use the spectrometer with a high resolution in order to improve the line to background ratio, and so reduce background β-γ coincidences. Here a balance has to be struck between a good transmission and high resolution.

The application of conversion electron β-ray coincidence counting to the measurement of conversion coefficients has been mentioned earlier. It is also sometimes possible to decide if a particular γ-ray is associated with either a low or a high energy partial β-spectrum by placing absorbers

before the β-counter in a similar sort of measurement and noting the change in coincidence rate per recorded β-particle. If the γ-ray is associated with a low energy partial spectrum the coincidence rate will fall to zero faster than the single β-rate. A further application is in the determination of the partial β-spectra associated with γ-transitions in some simple cases. Much of this type of work has been done by DEUTSCH and his collaborators[61].

Although it is possible to obtain more detailed results for simple disintegration schemes by coincidence work with the spectrometer than by coincidence absorption work, it is nevertheless almost equally difficult to analyse more complicated schemes. To do this it is necessary to use two spectrometers in coincidence. This has been done by FEATHER[62], who has used a semicircular focusing spectrometer, and taken coincidences between two counters on which different parts of the same spectrum are focused. So far the method has been limited to coincidences between a highly converted γ-ray and the continuous spectrum. The difficulties of such measurements are obvious: the transmission, of what is in effect a second spectrometer, enters into the overall efficiency, and the coincidence counting rate is extremely low. The method has the merit that the two spectrometers are essentially independent of each other, but the semicircular focusing instrument does suffer from the disadvantage of its low transmission, which now enters as the square into the coincidence counting rate. One possible way of increasing the latter is to use detectors having a better ultimate resolving time than the Geiger counter. Scintillation counters may be used for this purpose, with resolving times[63] as low as 10^{-8} seconds. A further means of improving the counting rate is to use spectrometers with a larger transmission. Deutsch has suggested the possibility of using two short magnetic lens spectrometers back to back for coincidence work. Since the fields are fairly localized it should be possible, by means of neutralizing coils, to eliminate the effect of the field of one spectrometer over the other.

Although the level schemes of a number of nuclei, such as Co^{60} and Na^{24}, have been derived by the above methods, only in the simplest cases is there any degree of reliability. A great deal of work has been done in recent years in β- and γ-spectra, but coincidence work is so time consuming, as a rule, that little has been done in constructing rigorous decay schemes.

REFERENCES

1 BAEYER, L. V. and HAHN, O. *Physik* 11 (1910) 488
2 DANYSZ, J. *C. R. Acad. Sci., Paris* 153 (1911) 339
3 ELLIS, C. D. and WOOSTER, W. A. *Proc. roy. Soc.* 117 (1927) 109
4 MEITNER, L. and ORTHMANN, W. *Z. Phys.* 60 (1930) 143
5 CRANE, H. R. *Rev. mod. Phys.* 20 (1948) 278
6 FERMI, E. *Z. Phys.* 88 (1934) 161
7 KONOPINSKI, E. J. and UHLENBECK, G. E. *Phys. Rev.* 48 (1935) 7
8 SARGENT, B. W. *Proc. roy. Soc.* 139 (1933) 659
9 KONOPINSKI, E. J. and UHLENBECK, G. E. *Phys. Rev.* 60 (1941) 308

[10] WIGNER, E. P. *Phys. Rev.* 51 (1937) 106; 56 (1939) 519
[11] GAMOW, G. and TELLER, E. *ibid* 49 (1936) 895
[12] LI, K. T. *Proc. Camb. phil. Soc.* 33 (1937) 164
[13] TRICKER, R. A. R. *ibid* 22 (1924) 454
[14] WITCHER, C. M. *Phys. Rev.* 60 (1941) 32
[15] FRANKEL, S. *ibid* 73 (1948) 804
[16] PERSICO, E. *ibid* 73 (1948) 1475
[17] DEUTSCH, M., ELLIOTT, L. G. and EVANS, R. D. *Rev. sci. Instrum.* 15 (1944) 178
[18] SVARTHOLM, N. and SIEGBAHN, K. *Arkiv. Mat. Astra o Fysik* 33*A* No. 21 (1946) 22
[19] KERST, D. W. and SERBER, R. *Phys. Rev.* 60 (1941) 53
[20] SHULL, F. B. and DENNISON, D. M. *ibid* 71 (1947) 681; 72 (1947) 256
[21] ROSENBLUM, E. S. *ibid* 72 (1947) 731
[22] KURIE, F. N. D., OSOBA, J. S. and SLACK, L. *Rev. sci. Instrum.* 19 (1948) 771
[23] SHULL, F. B. *Phys. Rev.* 74 (1948) 917
[24] LANGER, L. M. and COOK, C. S. *Rev. sci. Instrum.* 19 (1948) 257
[25] KORSUNSKY, M. *J. Phys. U.S.S.R.* 9 (1945) 14
[26] SIDAY, R. E. *Proc. phys. Soc.* 59 (1947) 905
[27] WALKER, R. L. and MCDANIEL, B. D. *Phys. Rev.* 74 (1948) 315
[28] PURCELL, E. M. *ibid* 54 (1938) 818
[29] EVANS, R. D. and EVANS, R. O. *Rev. mod. Phys.* 20 (1948) 305
[30] FEATHER, N. *Rep. Progr. Phys.* 7 (1940) 66
[31] BLEULER, E. and ZÜNTI, W. *Helv. Phys. Acta* 19 (1946) 375
[32] FOWLER, W. A., LAURITSEN, C. C. and LAURITSEN, T. *Rev. mod. Phys.* 20 (1948) 236
[33] KLEIN, O. and NISHINA, Y. *Z. Phys.* 52 (1929) 853
[34] HEITLER, W. *The Quantum Theory of Radiation* Oxford, 1944 p 119
[35] LATYSHEV, G. D. *Rev. mod. Phys.* 19 (1947) 132
[36] HULME, H. R., MCDOUGALL, J., BUCKINGHAM, R. A. and FOWLER, R. H. *Proc. roy. Soc.* 149 (1935) 131
[37] BETHE, H. and HEITLER, W. *ibid* 146 (1934) 83
[38] BRADT, H., GUGELOT, P. C., HUBER, O., MEDICUS, H., PREISWERK, P. and SCHERRER, P. *Helv. Phys. Acta* 19 (1946) 77
[39] WIEDENBECK, M. L. *Phys. Rev.* 69 (1946) 567
[40] HULME, H. R. *Proc. roy. Soc.* 138 (1932) 643
[41] TAYLOR, H. M. and MOTT, N. F. *ibid* 138 (1932) 665; 142 (1933) 215
[42] FISK, J. B. and TAYLOR, H. M. *ibid* 146 (1934) 178
[43] HEBB, M. H. and NELSON, E. *Phys. Rev.* 58 (1940) 486
[44] GRIFFITH, B. A. and STANLEY, J. P. *ibid* 75 (1949) 534
[45] DRELL, S. D. *ibid* 75 (1949) 132
[46] LOWEN, I. S. and TRALLI, N. *ibid* 75 (1949) 529
[47] DOWNING, J. R., DEUTSCH, M. and ROBERTS, A. *ibid* 61 (1942) 686
[48] JAEGER, J. C. and HULME, R. H. *Proc. roy. Soc.* 148 (1935) 708
[49] BRADY, E. L. and DEUTSCH, M. *Phys. Rev.* 72 (1947) 870; 74 (1948) 1541
[50] HAMILTON, D. R. *ibid* 58 (1940) 122
[51] KIKUCHI, S., WATASE, Y. and ITOH, J. *Z. Phys.* 119 (1942) 185
[52] BERINGER, R. *Phys. Rev.* 62 (1943) 23
[53] GOOD, W. M. *ibid* 70 (1946) 978
[54] GOERTZEL, G. *ibid* 70 (1946) 897
[55] DEUTSCH, M. and METZGER, F. *ibid* 74 (1948) 1542
[56] FEATHER, N. *Proc. Camb. phil. Soc.* 34 (1938) 599
[57] FLAMMERSFELD, A. *Naturwiss* 33 (1946) 280
[58] CURRAN, S. C., ANGUS, J. and COCKCROFT, A. L. *Nature, Lond.* 162 (1948) 302
[59] DUNWORTH, J. V. *Rev. sci. Instrum.* 11 (1940) 167; *Nature, Lond.* 144 (1939) 152
[60] MITCHELL A. C. G. *Rev. mod. Phys.* 20 (1948) 296
[61] DEUTSCH, M. *et al Phys. Rev.* 60 (1941) 544; 61 (1942) 686; 62 (1942) 3
[62] FEATHER, N., KYLES, J. and PRINGLE, R. W. *Proc. phys. Soc. Lond.* 61 (1948) 466
[63] BELL, R. E. and PETCH, H. E. *Phys. Rev.* 76 (1949) 1409

7

THE SZILARD-CHALMERS PROCESS

H. A. C. McKay

ATOMS newly produced as a result of nuclear changes—'hot' atoms—possess exceptional properties. They may carry a large amount of kinetic energy, or they may be short of some of their orbital electrons, or both. They show, therefore, an abnormal chemical reactivity. The phenomena observed are similar whether the activation is kinetic or electronic, so it is convenient to consider both cases in one report. We shall, however, confine our attention to hot atoms which are isotopic, or isomeric, with their parent atoms. The non-isotopic atoms differ in important practical respects, and are less ripe for review.

Of the various nuclear processes which take place without change of atomic number, the nγ-process provides the chief source of kinetically activated hot atoms, while γ-radioactivity yields electronically activated atoms. There is also an example in the literature of the use of the γn-process[24]. Processes which can only be carried out in the direct beam of a particle accelerator, such as the dp-process, are less suitable owing to the heat developed in the target material.

In the nγ-process the γ-ray causes a recoil which is generally powerful enough to sever the bonds holding the recoiling atom in its molecule, and to provide a surplus of energy for further chemical reaction. In γ-radioactivity, however, the γ-ray is usually insufficient to break up the molecule. Chemical phenomena seem to occur only when the γ-ray is internally converted, *i.e.* when the hot atom is produced as a positive ion.

EXAMPLES OF THE PROCESS

SZILARD and CHALMERS' original experiment[2] in 1934 was to irradiate ethyl iodide with neutrons from a radium-beryllium source. After irradiation a large part of the active iodine could be extracted by shaking with an aqueous reducing solution containing a trace of free iodine as carrier. The ejection of the radio-iodine atoms at the moment of formation had evidently taken

place as predicted, and I^{128} of relatively high specific activity could be obtained by a simple chemical operation, despite the fact that large amounts of isotopic material were present.

Many similar examples have since been discovered, and a list is given in *Table I.* One or two of the earlier results seem a little suspicious and the work merits repetition. An obvious condition for success is that there shall be no exchange between the active and the inactive material. For non-metals this is usually an easy condition to fulfil, but for metals it may be difficult. Ordinary inorganic salts, containing simple metallic ions, cannot be used and recourse must be had either to compounds in which the metal appears at the centre of a complex ion (see, for example, Fe^{59} in *Table I*), or to organic complexes in which the metal does not ionize (see, for example, Cu^{64}).

Nevertheless, many complexes undergo exchange reactions much more rapidly than one might have supposed, or hoped. DREHMANN[48] found, for example, that manganous ions exchange quite quickly with manganese acetylacetonate and benzoylacetonate, DUFFIELD and CALVIN[53] tested a number of complex copper compounds before they found one which does not exchange, and LEVENTHAL and GARNER[69] failed to find a zinc complex which does not exchange completely in 30 seconds. STEIGMAN[40] has introduced a useful aid in such searches. He pointed out that when a complex can be resolved into non-racemizing optical isomers, then it can be assumed that it is stable enough not to exchange. He applied this principle to cobalt, rhodium, iridium and platinum (see *Table I*), but was unsuccessful with ruthenium.

Even when there is no exchange under normal conditions, the Szilard-Chalmers process may still fail for reasons to be discussed later. The neutron bombardment of phosphites, for example, yields no separable P^{32}.

The extension of the process to γ-radioactivity was made in 1939, when the separation of the 18 minute isomer of Br^{80} from the 4·4 hour isomer was announced simultaneously by SEGRÈ, HALFORD and SEABORG[22], and by DEVAULT and LIBBY[15]. Since then the study of such isomeric transitions has paralleled that of the $n\gamma$-reactions, though it was soon realized that the details of the process must be quite different. *Table II* gives a list of successful separations of nuclear isomers by the Szilard-Chalmers method.

Table I. Applications of the Szilard-Chalmers Process to nγ-reactions

Isotope	*Half-life*	*Material irradiated*	*Method of separation*
Cl^{36}	2×10^6 *yr*	*Sodium chlorate or perchlorate*	*Precipitation as silver chloride*[38]
Cl^{38}	38 *min*	*Halates, perhalates*	*Precipitation as silver halide*[3, 4, 10, 11, 29, 43]
Br^{80}	4·4 *hr*	*Organic halogen compounds*	*Extraction into aqueous solution*[2, 3, 7, 10, 19]
Br^{82}	34 *hr*		*Shaking with charcoal, alumina, metal powders*[5, 8, 19]
I^{128}	25 *min*		*By applying an electric field*[3, 9]
P^{32}	14·3 *day*	*Triphenyl phosphate in benzene solution*	*Shaking with water or charcoal*[12]
S^{35}	87 *day*	*Carbon disulphide*	*Remains behind after evaporation*[6]
V^{52}	3·8 *min*	*Vanadium 8-hydroxyquinolate*	*Precipitation as silver vanadate*[51]
		Vanadium cupferronate in benzene solution	*Extraction into aqueous solution*[51]
		Sodium vanadate	*Adsorption on silver vanadate precipitate*[51]
Mn^{56}	2·6 *hr*	*Potassium permanganate or manganate*	*As manganese dioxide*[1, 29, 37, 50]
Fe^{59}	46 *day*	*Potassium ferrocyanide*	*Carried on aluminium hydroxide precipitate*[55, 63]
		Hydroferrocyanic acid	*Ether extraction of ferric chloride*[61, 74]
Co^{60}	5·3 *yr*	*Sodium cobalticyanide*	*Precipitation of α-nitroso-β-naphthol complex*[14]
		Tris-ethylenediamine cobaltic nitrate	*Displacement from solution by zinc dust*[40]
Cu^{64}	12·8 *hr*	*Copper salicylaldehyde-ortho-phenylenediamine in pyridine solution*	*Precipitation as copper sulphide*[53]
As^{76}	26·8 *hr*	*Arsine*	*By applying an electric field*[9]
		Cacodylic acid	*Precipitation as arsenious sulphide*[1, 49]
		Sodium cacodylate	*Shaking with magnesia*[32]
Se^{81}	59 *min*	*Selenites, selenates*	*Precipitation of elementary selenium*[35, 43]
Rh^{104}	4·7 *min*	*Tris-ethylenediamine rhodium nitrate*	*As with cobalt*[40]
Sb^{124}	60 *day*	*Triphenylstibine*	*Shaking with water*[63]
		Antimony pentafluoride	*Remains behind after evaporation*[63]
		Ammonium metafluoantimonate	*Precipitation as antimony sulphide*[63]
*Te		*Tellurates*	*Precipitation of elementary tellurium*[43]
*Ir		*Tris-ethylenediamine iridium nitrate*	*As with cobalt*[40]
*Pt		*Bis-ethylenediamine platinous nitrite*	*As with cobalt*[40]
Au^{193}	2·3 *day*	*Alkaline auric chloride*	*On colloidal gold precipitate*[13, 20]
		Sodium gold thiosulphate	*Shaking with mercury*[13, 20]
U^{239}	23·5 *min*	*Ammonium uranyl acetate*	*Precipitation of sodium uranyl acetate*[17]
		Uranyl benzoylacetonate	*Dissolved in acetone and shaken with barium carbonate*[45]

* It is not clear from the literature which isotope has been separated.

Table II. Applications of the Szilard-Chalmers Process to Isomeric Transitions

Isomeric Pair	*Half-lives*	*Material containing the activity*	*Method of separation*
Se^{81}	59 *min* ↓ 17 *min*	*Selenic acid*	*Reduction with sulphur dioxide to elementary selenium*[28]
Br^{80}	4·4 *hr* ↓ 18 *min*	*Sodium bromate*	*Precipitation as silver bromide*[15,36]
		Organic bromides	*Shaking with water etc*[18, 22, 25, 36, 44, 62, 64]
			By applying an electric field[52, 58]
			Reaction with inorganic bromides[26]
		Aqueous bromide	*Differential adsorption on aged silver chloride*[27]
		Bromine dissolved in ether, carbon tetrachloride etc	*Lower isomer enters into organic combination*[34, 41, 62]
Te^{127}	90 *day* ↓ 9·3 *hr*	*Telluric acid*	*Reduction with sulphur dioxide or hydrogen sulphide to elementary tellurium*[21, 30, 31, 60]
Te^{129}	32 *day* ↓ 72 *min*	*Alkaline or slightly acid tellurite*	*Remains behind as tellurate when tellurite is precipitated*[60]
Te^{131}	30 *hr* ↓ 25 *min*	*Tellurium diethyl*	*Accumulates on walls of vessel*[30]
		Tellurium hexafluoride	*Remains behind after evaporation of starting material*[60]

MECHANISM OF THE PROCESS

The initial activation in nγ*-reactions*—The energy emitted as γ-rays in an nγ-reaction amounts to several Mev. If the whole of this energy is concentrated into a single γ-ray of energy E_γ, in Mev, then it will cause an atom of mass M to recoil with energy E, in ev, given by

$$E=536E_\gamma^2/M$$

Typical values of 8 Mev for E_γ and 100 mass units for M lead to 343 ev for E. The energies required to disrupt chemical bonds, on the other hand, seldom exceed 5 ev (=115 kcals), so the γ-ray recoil should normally be amply sufficient to throw the hot atom out of its parent compound.

SUESS[23] appears to have been the first to question whether the molecule may not occasionally remain intact. One possible reason is the emission of two or more γ-rays in cascade; the most recent work[68] indicates that although there is always a significant proportion of single γ-rays most of the energy is in fact emitted in two or three γ-ray steps. For two γ-rays of energies $E_{\gamma 1}$ and $E_{\gamma 2}$, the directions of emission of which are unrelated, there is a uniform probability of the recoil having any energy from $536(E_{\gamma 1}-E_{\gamma 2})^2/M$ to $536\ (E_{\gamma 1}+E_{\gamma 2})^2/M$. If $E_{\gamma 1}$ and $E_{\gamma 2}$ are roughly equal there is therefore a definite small probability of the recoil being inadequate to decompose the molecule. If there are several γ-rays in cascade this probability may be rather larger. Only in very exceptional circumstances, however, would more

than one or two per cent of the molecules fail to break up. The directions of emission of the γ-rays would not only have to be very highly correlated, but correlated in a specialized manner, to wit, so as nearly to cancel one another's effects. It has recently been reported by BALL, SOLOMON and COOPER[65] that in the activation of cystine in the pile, about 0·07 per cent of the S^{35} is found combined as cystine. This may, just possibly, be an effect of the kind discussed here.

A second reason for incomplete disruption occurs when the recoiling atom is bonded to one of low mass. If m is the mass of the light atom, then only a fraction $m/(m+M)$ of the recoil energy is available for bond rupture, the remainder appearing as kinetic energy of the molecule as a whole. When the light atom is hydrogen or deuterium, the effect may be large enough to preserve the molecule intact. SUESS[23, 33] made an ingenious attempt to show that the HBr molecule does indeed survive the γ-ray recoil. He carried out the activation in the gas phase in the presence of acetylene, which is known to react with Br atoms but not with HBr or Br_2 molecules. It was hoped that there would be very little reaction with the acetylene, when it could have been assumed that very few Br atoms were formed. Unfortunately there was considerable reaction, and no definite conclusion could be drawn: the effect might be ascribed equally reasonably either to Br atoms or to HBr molecules with high translational energy. More recently HAMILL and WILLIAMS[60, 75] have followed up SUESS's work using stronger neutron sources, and conclude from a careful comparison of the results for HBr and C_2H_5Br that 10 per cent of the HBr molecules remain intact in the nγ-process.

It seems clear nevertheless that the two suggestions made by SUESS do not affect the conclusion that normally the disruption of the parent molecule is the first step. Where there are no chemical complications it is indeed possible in the nγ-processes to separate the whole of the active material from its parent compound. 100 per cent yields of separable activity have, for example, been reported for various oxy-acid salts under favourable conditions (see *Table VII*). Even organic halogen compounds, which usually only yield about 50 per cent of free radiohalogen, give nearly 100 per cent yields when activated in the gas phase[23,33,36,67].

The fact that practically every molecule is disrupted initially does not, however, imply that the process always proceeds as far as free atoms of the radioactive isotope. The recoil energy may not be sufficient for this. When a permanganate, for example, is irradiated with neutrons it is probable that one or two oxygen ions are ejected from each molecule, but not more:

$$MnO_4^- \begin{cases} \nearrow MnO_3^+ + O^{2-} \\ \searrow MnO_2^{3+} + 2\,O^{2-} \end{cases}$$

The initial activation in isomeric transitions—The state of affairs after an isomeric transition is very different from that after an nγ-process. The γ-rays are much softer, and only cause a recoil amounting to a small fraction of an electron volt, so no chemical effects would be expected. There is a somewhat larger recoil, due to the conversion electron, when the γ-ray is internally converted; a hot Br^{80} atom, for example, recoils with about 0·16 ev after *K*-shell conversion. This is still much less than the energies necessary to account for the observed chemical reactions; the decomposition of ethyl bromide, for instance, requires about 2·6 ev. The value 0·16 ev, however, is comparable with thermal energies, yet WILLARD[34] has shown that the chemical phenomena are independent of temperature. Clearly there must be some disruptive mechanism which taps a much larger fraction of the γ-ray energy.

It is now generally accepted that ionization of the hot atom during internal conversion is responsible[23, 25, 33, 34, 36, 42, 46]. The hot atom loses an electron in the conversion process, often from the *K*-shell. An electron from a higher shell will drop down to fill the *K*-shell, with emission of an x-ray, which may be internally converted in its turn, and so on. Altogether the atom may lose several electrons. For Br^{80} COOPER[42] has calculated that the average loss should be 4·7 electrons[42]. The multiply charged bromine ions formed hold a considerable store of energy: even the first ionization potential of bromine amounts to 11·8 ev. Moreover, some of the electrons lost are bonding electrons. Chemical effects such as the liberation of the hot atom from its parent molecule are therefore to be expected.

Molecular disruption should, then, occur only with internal conversion. Unfortunately the experimental evidence on this point is still far from conclusive. There is a striking difference between zinc and tellurium diethyls in the gaseous state at 110°C: $Zn^{69}Et_2$ is not disrupted by the isomeric transition of the zinc nucleus, the γ-rays of which are not internally converted, whereas both $Te^{127}Et_2$ and $Te^{129}Et_2$ are decomposed, and the daughter species accumulate on the walls of the containing vessel[30]. However, a quantitative correlation has never been established between the internal conversion coefficient and the maximum yield of separable daughter. With Br^{80} it was at first believed that the maximum yield was 85 to 90 per cent[36, 44], and that this corresponded to 85 to 90 per cent probability of internal conversion, but HAMILL and YOUNG[67] have recently obtained practically 100 per cent yield in a carefully selected instance *viz* the decomposition of gaseous methyl bromide mixed with inactive hydrogen bromide. Similarly the early claims of 100 per cent separation of the Te^{129} daughter from telluric acid[30], agreeing with 100 per cent internal conversion, have been disproved by WILLIAMS[64], who obtained only 55 per cent separation. Even when steps were taken to minimize subsequent chemical reaction of the hot Te^{129} atoms, by using gaseous tellurium hexafluoride in presence of other (inactive) gases, this same figure

of 55 per cent was obtained. There is obviously a need to re-examine the physical data on the conversion process in this instance.

'Cooling' of the hot atoms—Although the hot atoms produced in $n\gamma$-reactions carry energies which are large compared with those of chemical bonds, they are still not as energetic as, for example, fission fragments, and they cannot cause much ionization. They lose energy chiefly by elastic collisions with other atoms, so the 'cooling' process is analogous to the slowing down of neutrons in matter.

As LIBBY[39, 56] has emphasized, the mass ratio μ between the struck atom and the hot atom is of great importance. If the initial energy of the hot atom is E, its energy after collision may assume any value from $\left(\frac{\mu-1}{\mu+1}\right)^2 E$ to E with equal probability. The cooling process will therefore be most effective for equal masses ($\mu=1$), which means that inactive atoms of the element irradiated will generally be the best cooling agents. The worst will be hydrogen atoms.

The average number of collisions, n, necessary for a given degree of cooling may be calculated from the expression well known in neutron diffusion theory:

$$\xi n = \log E/E'$$

where E and E' are the initial and final energies, and

$$\xi = 1 + \frac{(\mu-1)^2}{4\mu} \log \left(\frac{\mu-1}{\mu+1}\right)^2$$

For the two limiting cases of $\mu=1$ and μ large we have, respectively, $\xi=1$ and $\xi \sim 2/\mu$.

Consider, for example, an atom of mass 100 cooled until its energy has been reduced by a factor of 50 *i.e.* into the range of chemical bond energies. If the atoms of the cooling agent also have mass 100, $\mu=1$, $\xi=1$ and $n=3{\cdot}9$. If on the other hand the cooling agent is hydrogen, $\mu=100$, $\xi \sim 0{\cdot}02$ and $n \sim 200$. In the former case there are a few large energy jumps; in the latter a large number of small steps.

Towards the end of the cooling process the simple billiard ball picture just given is no longer valid. Excitation of molecular vibrations becomes significant, and inelastic collisions occur.

In the whole process it is convenient to distinguish three energy ranges with distinct properties:

1 *The high energy range*—The hot atom has ample energy for chemical reaction, greatly in excess of chemical activation energies. The phenomena observed should therefore be independent of temperature.

2 *The epithermal range*—The hot atom has only just enough energy for reaction. When the atoms of the cooling agent are of low mass every hot

atom will pass through the epithermal range, but when heavy atoms are present there is a chance of the last energy jump carrying a hot atom direct to the thermal range. Some temperature dependence might be expected for epithermal reactions.

3 *The thermal range*—The hot atoms have cooled completely. They may still undergo ordinary temperature-dependent thermal reactions, and as atoms rather than molecules they may still be quite reactive.

CHEMISTRY OF HOT HALOGEN ATOMS

The theory just outlined has been applied, principally by LIBBY[39,56,66] to explain the phenomena observed in the neutron irradiation of organic halogen compounds. The initial step is the production of hot halogen atoms, which, as GLUECKAUF and FAY[10] were the first to show, are capable of a variety of chemical reactions. When methyl iodide, for example, is activated, only 44 per cent of the I^{128} is separable as free radio-iodine. The remainder is retained in organic form, 45 per cent as methyl radio-iodide and 11 per cent as methylene radio-iodide. Other organic halogen compounds behave similarly (*Table III*).

Table III. Neutron Irradiation of Organic Halogen Compounds

Compound irradiated	*Activity retained in organic form per cent*	*References*
CCl_4	45	19
C_6H_5Cl	50 = 35% C_6H_5Cl + 15% $C_6H_4Cl_2$	10
CH_2Br_2	57 = 43% CH_2Br_2 + 14% $CHBr_3$	10
$CHBr_3$	66 = 47% $CHBr_3$ + 19% CBr_4	10
CBr_4 *solid*	60	29
C_2H_5Br *liquid*	75	29, 36
C_2H_5Br *gas*	4·5	36
	<3	23, 33
$(CH_2Br)_2$ *liquid*	49	19
	31	36
$(CH_2Br)_2$ *gas*	6·9	36
n-C_3H_7Br	50·0 = 42·6% C_3H_7Br + 8·3% $C_3H_6Br_2$	66
iso-C_3H_7Br	42·1 = 33·7% C_3H_7Br + 8·4% $C_3H_6Br_2$	66
n-C_4H_9Br	60	19
C_6H_5Br	70 (<0·4% $C_6H_4Br_2$)	19, 39
$CH_2Br{\cdot}CO_2H$	22 as CH_2Br_2	10
CH_3I	56 = 45% CH_3I + 11% CH_2I_2	10
CHI_3 *solid*	60	29
C_2H_5I	37	29
n-C_4H_9I	53	19
C_6H_5I	65	19

We might argue from this that 45 per cent of the methyl iodide molecules survive the γ-ray recoil, though this would provide no explanation of the formation of active methylene iodide. Nor could we account for the results with mixtures (*Table IV*). The formation of $C_6H_5Cl^{38}$, for instance, by irradiation of a mixture of benzene with carbon tetrachloride, can hardly imply anything other than a reaction between hot Cl^{38} atoms and benzene molecules.

Table IV. Formation of New Products by Neutron Irradiation of Mixtures

Material irradiated	*New products*	*Fraction of total activity per cent*	*References*
$CCl_4+C_6H_6$ (1:1)	C_6H_5Cl	10	10
NH_4Br *aq. sat. with* C_6H_5OH	$C_6H_4Br(OH)$?	—	59
$CH_3Br+C_6H_5OH$ (1:1)	C_6H_5Br $C_6H_4Br(OH)$	2 2	10
$CBr_4+C_6H_6$ (1:1)	C_6H_5Br	15	10
$C_6H_5NH_3Br$	C_6H_5Br $C_6H_4Br(NH_2)$	1 2	10
Br_2+CCl_4(0·7 *mol* % Br_2)	CCl_3Br CCl_2Br_2 *Higher-boiling compounds*	13 5 6	62
$Br_2+C_2Cl_4$(0·7 *mol* % Br_2)	*Not resolved*	37	62
$I_2+C_2H_5OH$ *sat.*	CH_3I C_2H_5I	6 4	10
$I_2+CH_3CO_2H$ *sat.*	CH_3I	10	10
$I_2+C_5H_{12}$(0·45 *mol* % I_2)	$C_5H_{11}I$	23—38	54
$CH_3I+C_6H_6$ (1:10)	C_6H_5I	15	10

Returning to methyl iodide we are led to assume the reactions:

$$I^{128} + CH_3I \begin{cases} \longrightarrow CH_3I^{128} + I \\ \longrightarrow CH_2II^{128} + H \end{cases}$$

Alternatively, of course, the CH_3I^{128} may be produced by recombination of the fragments formed in the initial disruption.

Parallel effects have been found to accompany the isomeric transition of Br^{80}. *Table V* gives some comparisons between reactions caused by nγ-processes, and reactions caused by the isomeric transition. Complete parallelism is not, of course, to be expected; in particular, the cooling process must be quite different.

The phenomena are in general remarkably independent of temperature, and in some cases even a change of state from solid to liquid has little effect[10, 34, 62, 66]. This is good evidence that we are dealing with true hot atom reactions involving energies much greater than thermal. FRIEDMAN and

LIBBY[66] have, however, found an interesting difference between $C_3H_7Br^{82}$ and $C_3H_6BrBr^{82}$, formed by irradiation of C_3H_7Br. The yield of the former was unaffected even by solidification at liquid nitrogen temperatures, whereas that of the latter was greatly enhanced. This suggests that the reaction

$$Br^{82} + C_3H_7Br \rightarrow C_3H_6BrBr^{82} + H$$

is an epithermal one. The suggestion is a reasonable one because high energy Br^{82} atoms would be unable to get rid of enough energy to the light hydrogen atom to yield a stable $C_3H_6BrBr^{82}$ molecule.

Vaporization always reduces the proportion of radiohalogen which is

Table V. Comparison of Results for Neutron Irradiation and Isomeric Transition

Material	*Activity retained in organic form*		*References*
	nγ-process per cent	*Isomeric transition per cent*	
C_2H_5Br *liquid*	75	42	36
C_2H_5Br *gas*	5	*c* 15	36
$(CH_2Br)_2$ *gas*	6·9	31	36
Br_2+CCl_4 *liquid*	24	34	41, 62
Br_2+CCl_4 *gas*	1·9	1·1	41, 62
$Br_2+C_2Cl_4$ *liquid*	37	85	41, 62
$Br_2+C_2Cl_4$ *gas*	0	19	41, 62

retained in organic combination[23, 33, 36, 67], whether nγ-activation or the isomeric transition of Br^{80} is involved. It is usually supposed that in the liquid or solid state other molecules form a ' cage ' around the disrupted molecule, holding the hot halogen atom in close juxtaposition to the remainder of the molecule until the excess energy is dissipated and the molecule re-forms[19, 36]. Only in a limited number of cases do the hot atoms escape from the cage. In the gas, on the other hand, the disrupted fragments are free to move apart, and seldom re-combine. Vaporization is therefore an important means of minimizing the subsequent chemical reactions of hot atoms in order to study the initial activation process[60, 67].

Dilution with an inert solvent is to some extent comparable with vaporization. The atoms of the solvent will generally be much lighter than the hot halogen atoms, and will be relatively inefficient cooling agents. The hot atoms will therefore have a greater chance of escaping from their cage, which explains why the retentions fall towards zero on dilution[29] (*Table VI*). LIBBY[56] has attempted to treat the phenomenon quantitatively, and has used it to estimate the initial energy of a hot Br^{82} atom; when a numerical error is corrected the not unreasonable figure of 270 ev is obtained, corresponding to a γ-ray energy of 6·4 Mev. Dilution data are at present very sketchy, so it is welcome to learn that more extensive experimental work is in hand[72], with

emphasis on the relative masses of the halogen and diluent atoms. Some of the early results are proving difficult to reconcile with Libby's 'billiard ball' theory.

Table VI. Dilution Effect in the Neutron Irradiation of Organic Halogen Compounds

Solution irradiated	*Concentration mol per cent*	*Activity retained in organic form per cent*
$CHBr_3$ *in* CS_2	41	62
	10·5	47
	3	*small*
CBr_4 *in* C_2H_5OH	1·15	28
	0·74	13
	0·45	2
	0·064	0
CHI_3 *in* C_5H_5N	6·3	25
	1·1	1

There are certain further chemical effects which may be given a brief mention. The radiohalogen seems always to have a preference for the form in which it was originally combined, rather than for new products. This may be because the original molecule can be re-formed by simple re-combination of the initial fragments in their cage. Also, a reaction such as $I^{128} + CH_3I \rightarrow CH_3I^{128} + I$ involves on an average a much greater energy transference than $I^{128} + CH_3I \rightarrow CH_2II^{128} + H$. The product is therefore much more likely to be 'cold' *i.e.* stable.

Isomerization reactions may be induced by the γ-ray recoil *e.g.* neutron irradiation of either propyl or *iso*-propyl bromide yields both propyl and *iso*-propyl radiobromides in roughly 2·4 to 1 ratio[66]. The great energy of recoil evidently sets up an equilibrium between the two chemical isomers.

Aromatic amines such as aniline, and to a less extent phenols, increase the yields of separable activity from organic halogen compounds[19]. The optimum amount of aniline is 4 per cent. The phenomenon accompanies the isomeric transition of Br^{80} as well as the nγ-reactions of chlorine, bromine and iodine. It is usually assumed that a Menschutkin reaction:

$$RX + C_6H_5NH_2 \rightarrow [C_6H_5NH_2R]^+X^-$$

occurs with hot or disrupted RX molecules, transforming some of the radiohalogen from non-extractable form (as RX) to extractable (as X^-). WINTERINGHAM[76] has, however, shown that aniline added to bromobenzene *after* irradiation causes a slow release of extractable Br^{82} over a period of several days, without producing corresponding amounts of inactive bromine. Some other mechanism must therefore operate.

It remains to indicate the ultimate state of such radiohalogen as escapes reaction, and can therefore be extracted into an aqueous phase. At least two

chemical species are normally present, since alkalis or thiosulphate remove an appreciably larger fraction of the total activity than acids. This applies both to nγ-activations[19] and to Br^{80} formed by isomeric transition[36]. Moreover, part at least of the free radiohalogen is ionized and moves towards the electrodes when an electric field is applied[9, 52, 58]; the activity appears chiefly but not exclusively on the anode. These facts are in harmony with the theory that the larger part of the extractable activity exists in the form of negative halide ions, along with a smaller proportion of halogen atoms or molecules, and sometimes positive halogen ions as well (see WEXLER and DAVIES[78]).

Finally, a practical warning is necessary. The activation and the chemical operations must all be completed in a relatively short time, say an hour, even if the activity measurements are postponed to allow decay of the shorter-lived isotopes. Otherwise the extractable radiohalogen slowly disappears, perhaps by reaction with trace impurities in the organic materials[66] or by exchange[76].

DISRUPTION OF OXY-ACIDS AND THEIR SALTS

Extensive studies have been made of one other class of substances besides the organic halogen compounds, namely those containing oxy-acid anions. The experimental results for nγ-processes are summarized in *Table VII*, and are arranged so as to bring out the grouping according to position in the periodic table, first pointed out by DAUDEL[43].

Table VII. Disruption of Oxy-acids and their Salts

Group of periodic table	*Material irradiated*	*Retention in original anion per cent*	*Chemical form of separable activity*
VB	*Phosphate*	50	*Probably phosphite*[29]
	Phosphite	*Complete*	—[29]
	Arsenate	*Complete*	—[29]
		50	*Arsenite*[43]
	Arsenite	*Complete*	—[29]
	Antimonate	*Complete*	—[43]
VA	*Vanadate*	*Not complete*	*Not identified*[51]
VIB	*Selenate*	*None*	*Probably as free element*[43]
	Selenite	<50	*Probably as free element, definitely not selenide*[35]
	Tellurate	*None*	*Probably as free element*[43]
VIA	*Chromate*	*Between 55 and 76*	*Not identified*[77]
	Dichromate	*Nearly complete*	*Not identified*[57, 77]
VIIB	*Perchlorate*	*None*	*Free halogen or halide (not distinguishable owing to exchange)*[4, 10, 11, 29]
	Chlorate		
	Bromate		
	Periodate		
	Iodate		
VIIA	*Permanganate*	*Between 0 and 94 according to conditions*	*Manganese dioxide*[29, 50]
	Manganate	*Less than for permanganate*	*Manganese dioxide*[29]

As with the organic halogen compounds, there may be considerable retention of activity in the parent compound, though the reason for such retention must be different. There is generally either complete retention or 100 per cent yield of separable activity.

LIBBY[29] has suggested that although the γ-ray recoil always breaks up the ion concerned, the valency of the activated atom need not necessarily be changed thereby. The arsenate ion, for example, may eject one or more O^{2-} ions, yielding AsO_3^-, AsO_2^+ *etc* in which the arsenic remains penta-valent. Such ions may then revert to their normal state by simple hydrolysis *e.g.*

$$AsO_2^+ + 2H_2O \rightarrow AsO_4^{3-} + 4H^+$$

Any alternative process, such as the ejection of the oxygen as a neutral atom, is likely to result in the production of separable activity.

Phosphate and permanganate—These are particularly instructive because the retention of activity is partial, indicating competition between different processes. Phosphates always give about 50 per cent retention whether a solid or a solution is irradiated, and whatever the conditions of acidity or alkalinity. It may be surmised that the initial disruption may occur by either of two almost equally probable routes, one leading back to phosphate and the other giving lower valency states *e.g.*

$$PO_4^{3-} \begin{cases} \rightarrow PO_3^- + O^{2-} \\ \rightarrow PO_3^{3-} + O \end{cases}$$

In permanganate, on the other hand, the percentage retention varies over practically the whole possible range from zero to 100 per cent as the conditions are changed. It is probable therefore that the divergence of behaviour occurs *after* the initial disruption, according to some such scheme as

$$4MnO_3^+ + 2H_2O \rightarrow 4MnO_2 + 4H^+ + 3O_2$$

$$MnO_3^+ + OH^- \rightarrow H^+ + MnO_4^-$$

$$Mn^{56}O_3^+ + MnO_4^- \rightarrow MnO_3^+ + Mn^{56}O_4^-$$

In neutral or dilute acid solution the first reaction predominates, and the retention is low. In alkaline solution the second reaction becomes important, and the retention rises steeply to nearly 100 per cent. In strongly acid solution or with increasing permanganate concentration, the third reaction, an exchange, comes into play, and the retention again rises somewhat. BRODA and RIEDER [71] have recently made the interesting observation that fast neutrons give the same results with permanganate as slow neutrons.

Isomeric transitions—Instances of similar phenomena induced by isomeric transitions have already been given in *Table II.* Here, however, the valency of the central atom must increase in the initial activation, owing to the loss of electrons, which means that the intermediates must be very highly oxidized molecules. The most curious case is that of Te^{129}, studied by WILLIAMS[64],

who found that the isomeric transition not only reduces tellurate to a lower valency state, probably tellurite, but also oxidizes tellurite to tellurate. Moreover, although these two processes are observed in different experiments, they are intimately related : the yields vary according to acidity, yet the sum of the yields is always 55 per cent except in strongly alkaline solution. The probable explanation is the formation of the same intermediate in both cases, reacting to give tellurite and tellurate in proportions determined by the conditions.

APPLICATIONS

Preparation of material of high specific activity—The Szilard-Chalmers process was of great value in the days when artificial radioelements were often best prepared by the agency of radium-beryllium sources. ERBACHER and PHILIPP[7,8,12], for example, applied it to the preparation of carrier-free P^{32} and radiohalogens. Without its aid a number of early researches would have been impossible.

With the advent of the cyclotron the Szilard-Chalmers process became of less importance as a preparative method. However, it contributed materially to the discovery and study of Cl^{36}, which was first made by leaving a specimen of sodium chlorate or perchlorate for several months near the target holder in a cyclotron[38].

Fresh interest has arisen now that the nγ-process in chain-reacting piles forms the major source of radioactivity. KENNY and MATON[61, 74], for example, have made Fe^{55}, Fe^{59} of high specific activity by the pile irradiation of hydroferrocyanic acid. At least 90 per cent of the Fe^{59} produced was separable from its parent compound.

There may, however, be complicating side reactions induced by the neutron- and γ-radiation field of the pile. Lead shields can be used to reduce the γ-radiation. Two main types of effect have been recognized by WILLIAMS[63]:

1 Decomposition of the parent substance—When potassium ferrocyanide is irradiated, roughly the same proportion of the radio-iron is separable on an aluminium hydroxide precipitate, however long the irradiation, but the specific activity of the separated material falls off with time (*Figure 1*). Evidently the irradiation produces inactive iron which separates along with the active; and as only the active iron decays with time the specific activity decreases progressively.

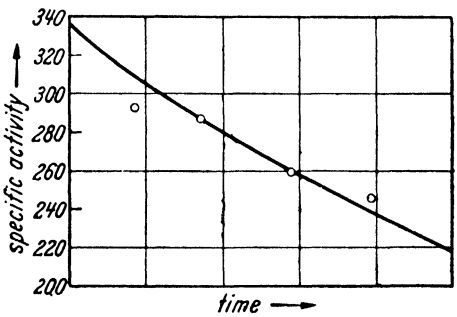


Figure 1. Decrease with time of specific activity of radio-iron separated from potassium ferrocyanide

2 Back reaction of the separable material—With antimony pentafluoride, the proportion of separable activity is not constant, as with potassium ferrocyanide, but decreases with time (*Figure 2*). The pile radiations must therefore convert the separable trifluoride back to the pentafluoride. By using a boron carbide shield, WILLIAMS was able to show that slow neutrons are not the agent responsible.

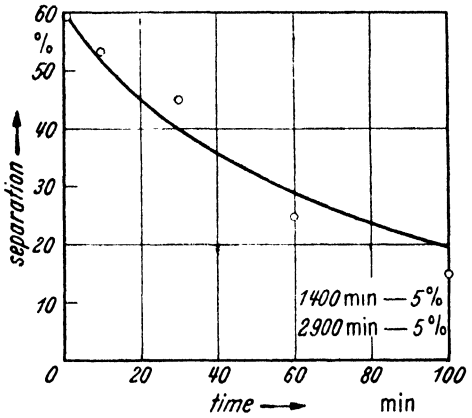


Figure 2. Decrease with time of percentage separation of radio-antimony from antimony pentafluoride

Preparation of organic radiohalogen compounds—A particular application of the Szilard-Chalmers process is to the preparation of organic radiohalogen compounds. Thus GLUECKAUF and FAY[10] have described a method of obtaining a continuous supply of methyl radioiodide by neutron irradiation of 80 per cent acetic acid saturated with potassium iodide. Other examples may be found in *Table IV*. The process is very much quicker than most ordinary synthetic chemical methods, so it is particularly valuable with such short-lived isotopes as Cl^{38} and I^{128}. Moreover, the new products may be prepared in carrier-free condition[73].

Measurement of low neutron fluxes—Neutron fluxes are commonly measured by means of the radioactivity they produce *e.g.* in silver or rhodium foils. The sensitivity can be increased by several powers of ten by using the Szilard-Chalmers process. VON HALBAN, KOWARSKI and MAGAT[16] have employed this principle in determining the intensity of neutrons in cosmic radiation, and have shown that the intensity is much greater at 9,500 m than at the level of Paris. They took as their measure the activity of the 4·4 hr Br^{80} liberated from ethyl bromide. BRODA[50] has used the Mn^{56} from potassium permanganate in a similar way, and SHAW and COLLIE[70] the I^{128} from ethyl iodide. There would probably be fewer chemical complications if iodobenzene were chosen.

Parent-daughter relationships between isomeric pairs—The most conclusive way of proving that one radioelement, A, is the parent of a second, B, is by means of a chemical separation. If B reappears after a time in a sample of A from which it has once been removed, then B must be a daughter of A. Without the Szilard-Chalmers process this type of proof would scarcely be possible for isomeric pairs. With its aid, however, genetical relationships have been established for Se^{81}, Br^{80}, Te^{127}, Te^{129} and Te^{131}. For tellurium

the separations were instrumental in pairing off the tellurium activities into isomeric pairs.

Estimation of internal conversion coefficients—The relation between Szilard-Chalmers separation data for isomeric transitions and internal conversion coefficients has already been discussed. It seems that chemical information may provide a useful check on results obtained by physical means.

REFERENCES

[1] AMALDI, E., D'AGOSTINO, O., FERMI, E., PONTECORVO, B., RASETTI, F. and SEGRÈ, E. *Ric. Sci.* 5 (1934) 467
[2] SZILARD, L. and CHALMERS, T. A. *Nature, Lond.* 134 (1934) 462, 494
[3] AMALDI, E., D'AGOSTINO, O., FERMI, E., PONTECORVO, B., RASETTI, F. and SEGRÈ, E. *Proc. roy. Soc. A* 149 (1935) 522
[4] D'AGOSTINO, O. *Gazz. chim. ital.* 65 (1935) 1071
[5] ROGINSKY, S. and GOPSTEIN, N. *Phys. Z. Sowjet.* 7 (1935) 672
[6] ANDERSEN, E. B. *Z. phys. Chem. B* 32 (1936) 237
[7] ERBACHER, O. and PHILIPP, K. *ibid A* 176 (1936) 169
[8] — — *Ber. dtsch. chem. Ges.* 69*B* (1936) 893
[9] FAY, J. W. J. and PANETH, F. A. *J. chem. Soc.* (1936) 384
[10] GLUECKAUF, E. and FAY, J. W. J. *ibid* (1936) 390
[11] BAKKER, C. J. *Physica* 4 (1937) 863
[12] ERBACHER, O. and PHILIPP, K. *Z. phys. Chem. A* 179 (1937) 263
[13] MAJER, V. *Naturwiss.* 25 (1937) 252
[14] CHATTERJEE, S. and RAY, P. *Trans. Bose Res. Inst., Calcutta* 13 (1937-8) 43
[15] DEVAULT, D. C. and LIBBY, W. F. *Phys. Rev.* 55 (1939) 322
[16] VON HALBAN, H., KOWARSKI, L. and MAGAT, M. *C. R. Acad. Sci. Paris* 208 (1939) 572
[17] IRVINE, J. W. *Phys. Rev.* 55 (1939) 1105
[18] LEROUX, L. J., LU, C. S. and SUGDEN, S. *Nature, Lond.* 143 (1939) 517
[19] LU, C. S. and SUGDEN, S. *J. chem. Soc.* (1939) 1273
[20] MAJER, V. *Chem. Listy* 33 (1939) 130
[21] SEABORG, G. T. and KENNEDY, J. W. *Phys. Rev.* 55 (1939) 410
[22] SEGRÈ, E., HALFORD, R. S. and SEABORG, G. T. *ibid* 55 (1939) 321
[23] SUESS, H. *Z. Elektrochem.* 45 (1939) 647
[24] BARKAS, W. H., CARLSON, P. R., HENDERSON, J. E. and MOORE, W. H. *Phys. Rev.* 58 (1940) 477
[25] DEVAULT, D. C. and LIBBY, W. F. *ibid* 58 (1940) 688
[26] FAIRBROTHER, F. *Nature, Lond.* 145 (1940) 307
[27] IMRE, L. *Naturwiss.* 28 (1940) 158
[28] LANGSDORF, A. and SEGRÈ, E. *Phys. Rev.* 57 (1940) 105
[29] LIBBY, W. F. *J. Amer. chem. Soc.* 62 (1940) 1930
[30] SEABORG, G. T., FRIEDLANDER, G. and KENNEDY, J. W. *ibid* 62 (1940) 1309
[31] — LIVINGOOD, J. J. and KENNEDY, J. W. *Phys. Rev.* 57 (1940) 363
[32] STARKE, K. *Naturwiss.* 28 (1940) 631
[33] SUESS, H. *Z. phys. Chem. B* 45 (1940) 297, 312
[34] WILLARD, J. E. *J. Amer. chem. Soc.* 62 (1940) 3161
[35] DAUDEL, R. *C. R. Acad. Sci. Paris* 213 (1941) 479
[36] DEVAULT, D. C. and LIBBY, W. F. *J. Amer. chem. Soc.* 63 (1941) 3216
[37] DREHMANN, U. *Naturwiss.* 29 (1941) 708
[38] GRAHAME, D. C. and WALKE, H. J. *Phys. Rev.* 60 (1941) 909
[39] LIBBY, W. F. *Science* 93 (1941) 283
[40] STEIGMAN, J. *Phys. Rev.* 59 (1941) 498
[41] BOHLMANN, E. G. and WILLARD, J. E. *J. Amer. chem. Soc.* 64 (1942) 1342
[42] COOPER, E. P. *Phys. Rev.* 61 (1942) 1
[43] DAUDEL, R. *C. R. Acad. Sci. Paris* 214 (1942) 547
[44] KREBS, A. *Naturwiss.* 30 (1942) 121
[45] STARKE, K. *ibid* 30 (1942) 577
[46] DAUDEL, R. *C. R. Acad. Sci. Paris* 216 (1943) 46
[47] — *ibid* 216 (1943) 341

[48] DREHMANN, U. *Z. phys. Chem. B* 53 (1943) 227
[49] SUE, P. *J. Chim. phys.* 40 (1943) 17
[50] BRODA, E. *BDDA* 46 (1944)
[51] SUE, P. and YUASA, T. *J. Chim. phys.* 41 (1944) 160
[52] CAPRON, P. C., STOKKINK, G. and VAN MEERSSCHE, M. *Nature, Lond.* 157 (1946) 806
[53] DUFFIELD, R. B. and CALVIN, M. *J. Amer. chem. Soc.* 68 (1946) 557, 1129
[54] REID, A. F. *Phys. Rev.* 69 (1946) 530
[55] DEWHURST, H. and MILLER, N. *Rep. Nat. Res. Counc. Canada CRC* 351 (1947)
[56] LIBBY, W. F. *J. Amer. chem. Soc.* 69 (1947) 2523
[57] MUXART, R., DAUDEL, P., DAUDEL, R. and HAISSINSKY, M. *Nature, Lond.* 159 (1947) 538
[58] RUSINOV, L. I. and KARAMIAN, A. S. *Compt. rend. Acad. Sci. U.R.S.S.* 55 (1947) 599
[59] SUE, P. and MELANDER, L. *C. R. Acad. Sci. Paris* 225 (1947) 413
[60] HAMILL, W. H. and WILLIAMS, R. R. *J. chem. Phys.* 16 (1948) 1171
[61] KENNY, A. W. and MATON, W. R. E. *Nature, Lond.* 162 (1948) 567
[62] WILLARD, J. E. *J. Phys. coll. Chem.* 52 (1948) 585
[63] WILLIAMS, R. R. *ibid* 52 (1948) 603
[64] — *J. chem. Phys.* 16 (1948) 513
[65] BALL, E. G., SOLOMON, A. K. and COOPER, O. *J. biol. Chem.* 177 (1949) 81
[66] FRIEDMAN, L. and LIBBY, W. F. *J. chem. Phys.* 17 (1949) 647
[67] HAMILL, W. H. and YOUNG, J. A. *ibid* 17 (1949) 215
[68] KUBITSCHEK, H. E. and DANCOFF, S. M. *Phys. Rev.* 76 (1949) 531
[69] LEVENTHAL, L. and GARNER, C. S. *J. Amer. Chem. Soc.* 71 (1949) 371
[70] SHAW, P. F. D. and COLLIE, C. H. *J. chem. Soc.* (1949) 1217
[71] BRODA, E. and RIEDER, W. *ibid* (1944) S. 356
[72] MILLER, J. M. and DODSON, R. W. *Brookhaven National Laboratory Report No. C-7* (1948) 19
[73] GLUECKAUF, E., JACOBI, R. B. and KITT, G. P. *J. chem. Soc.* (1949) S330
[74] KENNY, A. W. and MATON, W. R. E. Private communication
[75] WILLIAMS, R. R. and HAMILL, W. H. *Brookhaven National Laboratory Report No. C-7* (1948) 28
[76] WINTERINGHAM, F. D. W. Private communication
[77] GREEN, J. H. and MADDOCK, A. G. *Nature, Lond.* 164 (1949) 788
[78] WEXLER, S. and DAVIES, T. H. *J. chem. Phys.* 18 (1950) 376

8

THE SCATTERING OF NEUTRONS BY CRYSTALS

J. M. Cassels

A GREAT DEAL of interesting information has been obtained by studying the transmission of slow neutrons through various materials. For neutrons with energies between 1/10 and 1,000 ev, the data can be fitted very accurately by the well known dispersion formula, a result which was expected from the very general nature of the theoretical arguments involved.

In the energy region from 1/10 to 1 ev the dispersion formula usually reduces to the $1/v$ law: the scattering cross section is constant while the absorption cross section is inversely proportional to the velocity of the neutrons. (Cross sections will be given as multiples of 1 barn $= 10^{-24}$ sq cm.) When this is so it can be predicted with confidence that the effect of a single nucleus continues to obey the $1/v$ law below 1/10 ev.

Nevertheless large deviations from the law are found under actual experimental conditions where a scatterer containing a very large number of nuclei is used. These deviations below 1/10 ev are due to the fact that the atoms in the scattering material are not acting independently. This interpretation is at once indicated by the fact that the scattering can be affected by altering the temperature or physical state of the sample.

Such interference effects can be expected because the wavelengths of the de Broglie waves associated with very low energy neutrons are comparable with the interatomic spacings. The interference is particularly strong when the scattering sample is crystalline, although effects can be observed with molecular gases, liquids and amorphous solids. Here we shall be concerned only with materials that are crystalline.

In the course of the inquiry, account will be taken of the fact that the masses of the various scattering atoms are not infinitely large. This circumstance makes possible inelastic collisions, in which there is transfer of energy to or from vibrations of the crystal lattice. A further complication arises as will be seen, if a scattering element contains nuclei with spin or with several isotopes.

The first two of the following sections are devoted to a theoretical study of the subject. In the first the scattering produced by a single nucleus is discussed. The scattered neutron wave is spherically symmetrical and takes

the form $-a\exp(ikr)/r$ for spinless nuclei; $a \equiv \alpha + i\beta$ is termed the scattering length. For many nuclei the scattering length is of the same order as the nuclear radius, with α almost constant and β very small. The interaction between the neutron and the nucleus can then be represented by a fictitious potential energy which, if it alone were present, would produce the scattered wave which is actually observed. This is the Fermi pseudo-potential which is used below to calculate the inelastic scattering. Finally, the effect of the nucleus having a spin I is explained. When the nucleus combines with the neutron, the spin of which is $\frac{1}{2}$, two compound systems may be formed. The spins of these compound systems are $I + \frac{1}{2}$ and $I - \frac{1}{2}$, and two different scattering lengths, a_+ and a_- respectively, are associated with them. HALPERN and JOHNSON have shown that two scattering cross sections are constructed from a_+ and a_-. Only one of them represents scattering which is coherent with that of other nuclei; the other is incoherent.

In the second section the scattering of a polycrystalline sample containing one element only is discussed. At first the element is assumed to have only one infinitely heavy isotope which has no nuclear spin. The infinite mass of the nuclei precludes inelastic scattering, so that there is just one cross section to calculate.

Next, the element is allowed to have several isotopes and/or nuclear spin, while remaining infinitely heavy. This has the effect of splitting the scattering into two terms which are labelled ordered and disordered. The former shows interference effects and the latter does not.

Thirdly, the element is allowed to have finite mass, but is supposed to have only one isotope with no nuclear spin. This is the problem considered by WEINSTOCK in a fundamental paper. The scattering is naturally divided into elastic and inelastic components.

Finally, the general case of a finitely heavy element with several isotopes and/or nuclear spin is discussed. There are altogether four terms to distinguish, the ordered elastic, the ordered inelastic, the disordered elastic and the disordered inelastic. Formulae are derived for all these.

The results for the elastic scattering are easy to understand and compute. The inelastic terms, on the other hand, are finally presented in the form of complicated definite integrals which have to be evaluated afresh for every new element, neutron wavelength and sample temperature. This difficulty is alleviated to some extent by the computational results presented at the end of this section. The inelastic scattering turns out approximately proportional to $1/m\Theta$, where m and Θ are respectively the mass and the Debye temperature of the element concerned. A simple scaling by the appropriate combination of masses and Debye temperatures will yield results for other crystals which are probably correct to 10 or 20 per cent.

At the end of this section some attention is given to the scattering of mixed crystals containing more than one element. Expressions are given for the ordered and disordered elastic scattering cross sections which are valid when the masses of the various elements are not too different.

Lastly there is a brief discussion of the extinction effects which may modify the ordered elastic scattering. These can be avoided by grinding the scattering material into a fine powder.

Throughout the theoretical treatment the scattering is assumed to be caused by the nuclei alone. This is not always true because there can be quite strong interaction between the magnetic moment of the neutron and that of the atomic electrons. Fortunately, the magnetic moment of many atoms is due to the valence electrons in the outer shell. In crystals these electrons are detached from the parent atoms to form the Fermi gas, in which the various levels are occupied by pairs of electrons with opposed spins. There will obviously be no magnetic scattering under these conditions. On the other hand transition elements, such as manganese, iron and nickel, owe their magnetic moments to uncompleted inner shells. These magnetic moments are retained in the crystal and give rise to some additional scattering. No attempt will be made here to outline the theory of this effect, though in the final section we shall have occasion to refer to it in connection with a discrepancy between the simple theory and some experimental results obtained with an iron scatterer.

Apart from the magnetic effects, we can ignore any direct scattering of neutrons by electrons. The interaction is so small that very specialized experiments give only slight indications of a positive effect.

In the last section some experimental investigations of the scattering of neutrons by crystals will be considered. The information available is growing rapidly as a result of various technical developments which make possible the use of monochromatic neutron beams. For convenience the results are divided into three groups.

In the first group those experiments which have as their object the determination of the scattering constants of the elements are considered. It is essential to know not only the total amount of scattering by every element, but also the ratio in which it is divided into ordered and disordered components. This programme is already far advanced.

Secondly, some experiments on the variation with temperature of the inelastic scattering will be discussed briefly. As mentioned above, the results with iron are not at all in agreement with the theory of this section. However, a similar trial with aluminium shows good accord with theory.

The third group of experiments is concerned with neutron crystallography, a subject which includes not only the determination of crystal

structures but also the investigation of such problems as order-disorder transitions in alloys. Work along these and other lines is only just beginning, and undoubtedly it will be rapidly extended as instruments with better resolving power are brought into use.

SCATTERING OF NEUTRONS BY A SINGLE NUCLEUS

The incident neutron beam—Let us consider a uniform beam of neutrons moving along the z axis of a set of Cartesian coordinates. The wave function representing the neutrons must satisfy the Schrodinger equation for free space,

$$\nabla^2\psi + k^2\psi = 0 \qquad k = 2\pi/\lambda = m_0 v/\hbar \qquad \ldots . (1)$$

where k is the wave-number, λ the wavelength, m_0 the mass and v the velocity of the neutrons; $\hbar$ is Planck's constant divided by 2π. The appropriate solution of equation 1 is clearly the plane wave

$$\psi_0 = \exp(ikz) \qquad \ldots . (2)$$

Consider now the changes in this wave function which occur when a nucleus is clamped to the origin. For this, it will be very convenient to use spherical coordinates defined by

$$\begin{cases} x = r\sin\theta\cos\phi \\ y = r\sin\theta\sin\phi \\ z = r\cos\theta \end{cases} \qquad \ldots . (3)$$

Now rewrite ψ_0 in terms of r, θ, ϕ by means of the expansion[1]

$$\psi_0 = \exp(ikz) = \sum_{l=0}^{\infty} (2l+1)\, i^l (\pi/2kr)^{\frac{1}{2}} J_{l+\frac{1}{2}}(kr)\, P_l(\cos\theta) \equiv \sum_{l=0}^{\infty} \psi_0^l \ldots . (4)$$

where $J_{l+\frac{1}{2}}$ is the Bessel function of the first kind of order $l + \frac{1}{2}$ and P_l is the Legendre function of order l.

Each term ψ_0^l in the expansion of equation 4 is individually a solution[2] of the wave equation 1. It is not difficult to show that ψ_0^l represents neutrons of total angular momentum $[l(l+1)]^{\frac{1}{2}}\hbar$ with respect to the origin. (The operator $\{-(1/\sin\theta)(\partial/\partial\theta)\sin\theta(\partial/\partial\theta) - (1/\sin^2\theta)(\partial^2/\partial\phi^2)\}$ applied to ψ_0^l gives the result $l(l+1)\psi_0^l$.) The $l = 0, 1, 2 \ldots$ terms are usually known as $s, p, d \ldots$ waves.

At large radii

$$\lim_{r\to\infty} \psi_0^l = \left\{(l+\tfrac{1}{2})\, i^{-l} P_l(\cos\theta)\right\} \frac{1}{kr} \{\exp[-i(kr - l\pi/2)] - \exp[i(kr - l\pi/2)]\} \qquad \ldots . (5)$$

As we can see from the dependence on r, this expression represents the superposition of two waves, one moving inwards and one outwards.

Wave function with a nucleus present—When a nucleus is clamped to the origin the situation is altered in the following way. Outside the range of the nuclear forces the wave equation is still given by equation 1, but now there is a different boundary condition for the wave function to satisfy at small radii. Formerly ψ/r had to remain bounded at the origin; now we require that ψ fits smoothly at the nuclear radius, $r = b$, where the nuclear forces take over.

The general solution[2] of the wave equation 1 has the form

$$\psi = \sum_{l=0}^{\infty} \left\{ A_l J_{l+\frac{1}{2}}(kr) + B_l J_{-(l+\frac{1}{2})}(kr) \right\} (\pi/2kr)^{\frac{1}{2}} P_l(\cos\theta) \equiv \sum_{l=0}^{\infty} \psi^l \ldots . \quad (6)$$

The complex coefficients A_l and B_l are determined by two conditions :

a at the nuclear radius the ψ^l must satisfy the l^{th} order boundary condition

b at large radii, equation 6 becomes the sum of an ingoing and outgoing wave. Obviously the part that represents an ingoing wave must be identical with the ingoing part of equation 5. This actually means

$$A - i^{2l+1}B = (2l + 1)\, i$$

At small radii there is a very important difference between the behaviour of the two Bessel functions. When kr is small $(1/kr)^{\frac{1}{2}} J_{l+\frac{1}{2}}(kr)$ behaves like $(kr)^l$, whereas $(1/kr)^{\frac{1}{2}} J_{-(l+\frac{1}{2})}(kr)$ becomes infinite as $(kr)^{-l-1}$. It is for this reason that the expansion 4 contained no terms of the type $J_{-(l+\frac{1}{2})}(kr)$.

Now, for the values of k appropriate to slow neutrons, kb will always be very small ($\sim 10^{-4}$). Accordingly, rather small amounts of the $J_{-(l+\frac{1}{2})}(kr)$ solutions are sufficient to distort the wave function very violently at the nuclear radius, especially as l increases. Because of this the boundary conditions can be satisfied by very small values of B_l, except possibly for the s, or $l = 0$, wave. For large kr and $l > 0$ we can neglect altogether the disturbances to the ψ_0^l.

The wave function with the nucleus present can thus be written

$$\psi = (\pi/2kr)^{\frac{1}{2}} \left\{ A_0 J_{\frac{1}{2}}(kr) + B_0 J_{-\frac{1}{2}}(kr) \right\} + \sum_{l=1}^{\infty} \psi_0^l, \qquad r \gg b \quad \ldots . \quad (7)$$

since $P_0(\cos\theta) = 1$. Because

$$(\pi/2kr)^{\frac{1}{2}} J_{\frac{1}{2}}(kr) = \sin(kr)/kr$$

and

$$(\pi/2kr)^{\frac{1}{2}} J_{-\frac{1}{2}}(kr) = \cos(kr)/kr$$

this can be rewritten in a form which makes sure that the ingoing s wave is the same as in equation 5,

$$\psi = \sum_{l=0}^{\infty} \psi_0^l - \frac{a}{r}\exp(ikr) = \exp(ikz) - \frac{a}{r}\exp(ikr), \qquad r \gg b \qquad \ldots.(8)$$

This equation defines a complex length $a \equiv \alpha + i\beta$, which is called the scattering length[3] of the nucleus.

Scattering and absorption cross sections—The wave function ψ given by equation 8 is easily interpreted. It represents the uniform incident wave together with a spherically symmetrical outgoing scattered wave.

The incident flux of neutrons is given by

$$v|\exp(ikz)|^2 = v \text{ neutrons-cm}^{-2}\text{-sec}^{-1}$$

The outgoing current of scattered neutrons is

$$v.\ 4\pi r^2 |a \exp(ikr)/r|^2 = 4\pi v|a|^2 \text{ neutrons-sec}^{-1}$$

The scattering cross section σ is therefore given by

$$\sigma = 4\pi \mid a \mid^2 = 4\pi(\alpha^2 + \beta^2) \qquad \ldots.(9)$$

The absorption cross section of the nucleus is calculated by considering the complete s wave function, which by equation 8 is

$$\psi^0 = \psi_0^0 - \frac{a}{r}\exp(ikr) = (i/2kr)\left\{\exp(-ikr) - (1-2ika)\exp(ikr)\right\} \qquad \ldots.(10)$$

This represents ingoing and outgoing streams of s neutrons; the ingoing current is

$$v.\ 4\pi r^2 \mid i\exp(-ikr)/2kr \mid^2 = \pi v/k^2 \text{ neutrons-sec}^{-1}$$

while the corresponding outgoing current is

$$v.4\pi r^2 \mid -i(1-2ika)\exp(ikr)/2kr \mid^2 = (\pi v/k^2)\mid 1 - 2ika \mid^2 \text{ neutrons-sec}^{-1}.$$

The number of neutrons per second absorbed by the nucleus is the difference between these two currents, so that the absorption cross section σ_a is

$$\sigma_a = (\pi/k^2)\left\{1 - \mid 1 - 2ika \mid^2\right\} = -4\pi\beta/k - \sigma \qquad \ldots.(11)$$

The total cross section is the sum of the scattering and absorption cross sections

$$\sigma_t = \sigma + \sigma_a = -4\pi\beta/k \qquad \ldots.(12)$$

From equations 9 and 12

$$\alpha^2/\beta^2 = -1 + 4\pi\sigma/k^2\sigma_t^2 \qquad \ldots.(13)$$

Later, when considering interference effects in the scattering, it will often be assumed that the scattering length is completely real. This approximation is legitimate so long as

$$4\pi\sigma/k^2\sigma_t^2 \gg 1 \qquad \ldots\ldots(14)$$

which is nearly always true.

Dispersion formula (Breit-Wigner formula)—As has been seen, the actual value of the scattering length is determined by the boundary conditions at the nuclear surface. At present these conditions cannot be discussed in detail except for the very lightest nuclei. Instead we have to be guided by rather general reasoning[4, 5, 6] which leaves undetermined certain constants the values of which have to be found by experiment. These constants are the neutron and absorption 'widths', $\Gamma_n^{(r)}$ and $\Gamma_a^{(r)}$, and the resonance energies $E_r + B$ of the compound system formed by the nucleus and an added neutron, B being the binding energy of the neutron. In the neighbourhood of the rth resonance the scattering and absorption cross sections are found to be

$$\sigma = \frac{4\pi}{k^2}\left|\frac{\frac{1}{2}\Gamma_n^{(r)}}{(E-E_r)+\frac{1}{2}i(\Gamma_n^{(r)}+\Gamma_a^{(r)})}+kb\right|^2 \qquad \ldots\ldots(15)$$

$$\sigma_a = \frac{\pi}{k^2}\frac{\Gamma_a^{(r)}\Gamma_n^{(r)}}{(E-E_r)^2+\frac{1}{4}(\Gamma_n^{(r)}+\Gamma_a^{(r)})^2} \qquad \ldots\ldots(16)$$

Now it can be shown that $\Gamma_a^{(r)}$ is independent of E while $\Gamma_n^{(r)}$ is proportional to $E^{\frac{1}{2}}$, or k; also the approximation $|E+\frac{1}{2}i\Gamma_n^{(r)}| \ll |-E_r+\frac{1}{2}i\Gamma_a^{(r)}|$ is valid for most nuclei and very slow neutrons. In good approximation, then, σ_a is proportional to $E^{-\frac{1}{2}}$, $1/k$, or $1/v$, while σ and a are constant.

The constancy and spherical symmetry of the amplitude of the scattered neutron wave is in marked contrast to the situation in X-ray scattering. There, the amplitude of the scattered wave becomes rapidly smaller at small wavelengths and large scattering angles, because of the electronic form factor.

The X-ray scattering amplitude increases smoothly and predictably with the atomic number of the scattering element. The neutron scattering amplitude, on the other hand, may vary sharply from one nucleus to the next. In the approximate expression

$$a \sim -\frac{\Gamma_n^{(r)}}{2kE_r}+b \qquad \ldots\ldots(17)$$

the first, or resonance, term may be large or small, and either positive or negative ($\Gamma_n^{(r)}$ is essentially positive, but E_r may be positive or negative). The potential term, b, is expected to vary more smoothly, since the nuclear radius should be proportional to $A^{\frac{1}{3}}$, A being the atomic weight. The presence of the potential term is responsible for the fact that the large majority of scattering lengths are positive.

Nuclear pseudo-potential—For many scattering calculations it is convenient to have an analytical form for the interaction between the nucleus and the neutron. Since it is the scattering only which is of interest here, we can represent the interaction by means of a fictitious potential which replaces the nucleus at the origin. This potential $V(r)$ is required to give the scattering length a.

Schrödinger's equation in the presence of $V(r)$ reads

$$\left\{\nabla^2 + k^2 - 2m_0V(r)/\hbar^2\right\}\psi = 0 \qquad \ldots . (18)$$

This equation is readily solved with the help of Born's approximation. The solution is (MOTT and MASSEY[1], chapter VII)

$$\psi = \exp(ikz) - \frac{m_0}{2\pi\hbar^2}\int_{\text{all space}}\frac{\exp(ik|\boldsymbol{r}-\boldsymbol{r}'|)}{|\boldsymbol{r}-\boldsymbol{r}'|}V(r')\exp(ikz')\,dv' \ldots . (19)$$

At large radii ψ behaves like $\exp(ikz) + f(\theta)\exp(ikr)/r$, where

$$(\theta) = -\frac{2m_0}{\hbar^2}\int_0^\infty \frac{\sin(2kr'\sin\frac{1}{2}\theta)}{2kr'\sin\frac{1}{2}\theta}V(r')r'^2dr' \qquad \ldots . (20)$$

If we identify $f(\theta)$ with $-a$, it is now easy to verify that the potential

$$V(r) = \frac{\hbar^2 a}{2m_0}\delta(r) = \frac{2\pi\hbar^2 a}{m_0}\delta(\boldsymbol{r}) \qquad \ldots . (21)$$

gives correct results. The δ- function of vectorial argument is defined by the equations

$$\int_{\text{all space}}\delta(\boldsymbol{r}'-\boldsymbol{R})dv' = 1 \qquad \ldots . (22)$$

$$\int_{\text{all space}}F(\boldsymbol{r}')\delta(\boldsymbol{r}'-\boldsymbol{R})dv' = F(\boldsymbol{R}) \qquad \ldots . (23)$$

The potential defined in equation 21 was originally introduced by FERMI[7]; it is valid so long as $|ka| \ll 1$.

Free scattering cross section—So far we have kept the nucleus rigidly clamped to the origin when making our calculations. If the nucleus is allowed to recoil, the free scattering cross section σ' is smaller than σ by a factor $(A/A+1)^2$. This makes a large difference in the case of hydrogen; the bound scattering cross section is 80 barns, whereas the free scattering cross section is only 20 barns.

Scattering by a nucleus with a spin—The theory has not yet allowed for the possibility that the nucleus has a spin I. HALPERN and JOHNSON[8] have discussed the necessary modifications and have shown that the scattering is divided into two essentially different parts.

The expression for the incoming wave must now include spin wave functions. Let us suppose that the neutron is in the spin state χ_n while the nucleus is in the spin state Λ_m. Then

$$\psi_0 = \exp(ikz)\,\chi_n \Lambda_m \qquad \ldots . (24)$$

There are two independent χ_n's and $2I + 1$ independent Λ_m's; we shall average over all these states later.

The interaction between the neutron and the nucleus depends on how the nuclear spin I and the neutron spin $\frac{1}{2}$ are combined. When the total spin is $I + \frac{1}{2}$ the scattering length is a_+. If, on the other hand, the total spin is $I - \frac{1}{2}$ then the scattering length a_- is to be used.

The outgoing wave from the nucleus is thus

$$-\frac{\exp(ikr)}{r}\left(a_+\eta_+ + a_-\eta_-\right)\chi_n \Lambda_m \qquad \ldots . (25)$$

When the total spin is $I + \frac{1}{2}$ the operators η_+ and η_- are equal to 1 and 0 respectively. These values are reversed when the total spin is $I - \frac{1}{2}$.

If $\boldsymbol{\sigma}$ and $\boldsymbol{i}$ are the neutron and nuclear spin operators respectively, then

$$(\boldsymbol{i} + \boldsymbol{\sigma})^2 = \boldsymbol{i}^2 + 2\boldsymbol{i}.\boldsymbol{\sigma} + \boldsymbol{\sigma}^2 = I(I+1) + 2\boldsymbol{i}.\boldsymbol{\sigma} + \tfrac{3}{4} \qquad \ldots . (26)$$

Now $(\boldsymbol{i} + \boldsymbol{\sigma})^2$ is equal to $(I + \frac{1}{2})(I + \frac{3}{2})$ when the total spin is $I + \frac{1}{2}$, and $(I - \frac{1}{2})(I + \frac{1}{2})$ when the total spin is $I - \frac{1}{2}$. With the help of equation 26 it is easy to find

$$\begin{aligned} \eta_+ &= (I + 1 + 2\,\boldsymbol{i}.\boldsymbol{\sigma})/(2I+1) \\ \eta_- &= (I - 2\boldsymbol{i}.\boldsymbol{\sigma})/(2I+1) \end{aligned} \qquad \ldots . (27)$$

The scattered wave (equation 25) can now be rewritten

$$-\frac{1}{2I+1}\cdot\frac{\exp(ikr)}{r}\left\{(I+1)a_+ + Ia_- + 2\boldsymbol{i}.\boldsymbol{\sigma}(a_+ - a_-)\right\}\chi_n \Lambda_m \qquad \ldots . (28)$$

Just as before, the total outgoing current is found by multiplying equation 28 by its conjugate complex quantity and putting in the factor $4\pi r^2 v$. The operator in the brackets, being a real observable, is self-conjugate. Accordingly, the total scattering cross section is

$$\sigma = \frac{4\pi}{(2I+1)^2}\left[\Lambda_m^* \chi_n^* \left\{(I+1)a_+ + Ia_- + 2\boldsymbol{i}.\boldsymbol{\sigma}(a_+ - a_-)\right\}^2 \chi_n \Lambda_m\right]_{Av} \qquad \ldots . (29)$$

where the average is taken over all the spin states χ_n, Λ_m. The expression 29 shows that σ is equal to the product of $4\pi/(2I+1)^2$ and the average value of $\{(I+1)a_+ + Ia_- + 2\boldsymbol{i}.\boldsymbol{\sigma}(a_+ - a_-)\}^2$. In working out the latter we can ignore terms linear in $\boldsymbol{i}.\boldsymbol{\sigma}$ which vanish on the average since the neutron and nuclear spins are uncorrelated. Similarly we can neglect the terms in $(\boldsymbol{i}.\boldsymbol{\sigma})^2$ which are of the type $i_x\sigma_x i_y\sigma_y$. Finally we remember that, on the average,

$i_x^2\sigma_x^2 = i_y^2\sigma_y^2 = i_z^2\sigma_z^2 = \frac{1}{3}\boldsymbol{i}^2.\frac{1}{3}\boldsymbol{\sigma}^2 = I(I+1)/12$. The contributions made by the two squared terms in equation 29 are therefore

$$4\pi(p_+a_+ + p_-a_-)^2 \equiv S \qquad \ldots\ldots(30)$$

and

$$4\pi p_+p_-(a_+ - a_-)^2 = 4\pi\{(p_+a_+^2 + p_-a_-^2) - (p_+a_+ + p_-a_-)^2\} \equiv s \qquad \ldots\ldots(31)$$

where the ' weights ' p_+ and p_- are equal to $(I+1)/(2I+1)$ and $I/(2I+1)$ respectively. The total scattering cross section σ is the sum of S and s.

It is important to realize that only the scattering represented by S is coherent with scattering by other nuclei. If, for example, two identical nuclei are placed very close together, then the combined scattering cross section is $4S + 2s$.

The reason for this is very simple. When we work out the new problem we find that the combined cross section is equal to $4\pi/(2I+1)^2$ multiplied by the average value of $\{2(I+1)a_+ + 2Ia_- + (2\boldsymbol{i}^{(1)}.\boldsymbol{\sigma} + 2\boldsymbol{i}^{(2)}.\boldsymbol{\sigma})(a_+ - a_-)\}^2$, where $\boldsymbol{i}^{(1)}$ and $\boldsymbol{i}^{(2)}$ are the spin operators for the first and second nuclei respectively. On averaging, the term proportional to $(\boldsymbol{i}^{(1)}.\boldsymbol{\sigma})(\boldsymbol{i}^{(2)}.\boldsymbol{\sigma})$ drops out because the spins of the two nuclei are not correlated.

Since a_+ and a_- can have opposite signs, it is quite possible for a nucleus to give no coherent scattering at all. This is very nearly so with hydrogen, where the triplet and singlet states (spins 1 and 0) of the deuteron have positive and negative scattering lengths respectively. The coherent cross section of hydrogen is only 2 barns, although the total scattering cross section is as much as 80 barns.

SCATTERING OF NEUTRONS BY POLYCRYSTALLINE SOLIDS

The interaction of slow neutrons with a single nucleus has been considered; in practice experiments are done with samples containing a very large number of nuclei, the mutual interaction of which cannot be ignored.

In the sections that follow, the scattering of a polycrystalline sample containing a single element only will be discussed. In the most general case, as will be seen, there are no less than four separate contributions to the total scattering. The complicating features will be introduced in turn until the most general theory is reached, p 203.

Scattering by an element with one infinitely heavy spinless isotope—If the mass of the scattering nuclei is infinite, transfers of energy to or from the crystal lattice are obviously not possible; all the collisions are elastic and the final velocity of the neutron is the same as the incident velocity.

Let us assume that a typical microcrystal has the same shape as the unit cell, and that it consists of rows of g_1+1, g_2+1, g_3+1 atoms in the

directions of three basic lattice vectors $\boldsymbol{a}_1$, $\boldsymbol{a}_2$, $\boldsymbol{a}_3$. We assume that the vector $\boldsymbol{\rho}$ describing any lattice point can be written in the form

$$\boldsymbol{\rho} = \rho_1\boldsymbol{a}_1 + \rho_2\boldsymbol{a}_2 + \rho_3\boldsymbol{a}_3 \qquad \ldots.(32)$$

where ρ_1, ρ_2, ρ_3 are integers which run from 0 to g_1, g_2, g_3 respectively; $g_1\, g_2\, g_3 \equiv N$. Suitable basic vectors can be found for the Bravais lattices, which include the body and face centred cubic structures.

If the wave vector of the neutron is $\boldsymbol{k}$ before and $\boldsymbol{k}'$ after scattering, then the wave function at large radii has the form

$$\psi = \exp(ikz) - \frac{a}{r}\exp(ikr)\sum_{\boldsymbol{\rho}} \exp\left\{(i\boldsymbol{\rho}.(\boldsymbol{k} - \boldsymbol{k}')\right\} \qquad \ldots.(33)$$

The phase factors $\exp\left\{i\boldsymbol{\rho}.(\boldsymbol{k} - \boldsymbol{k}')\right\}$ are introduced in the usual way by the path difference between scattering by the various nuclei.

The differential (*i.e.* per unit solid angle) cross section per nucleus for scattering in the direction of $\boldsymbol{k}'$ is therefore

$$G(\boldsymbol{k}') = \frac{a^2}{N}\left|\sum_{\boldsymbol{\rho}} \exp\left\{i\boldsymbol{\rho}.(\boldsymbol{k} - \boldsymbol{k}')\right\}\right|^2 \qquad \ldots.(34)$$

To get the scattering cross section per nucleus we must integrate over all scattering angles and average over all possible orientations of the micro-crystal. As usual, we introduce the basic vectors $\boldsymbol{b}_1$, $\boldsymbol{b}_2$, $\boldsymbol{b}_3$ of the reciprocal lattice. They are defined by the equations

$$\boldsymbol{b}_1 = \frac{\boldsymbol{a}_2 \times \boldsymbol{a}_3}{\boldsymbol{a}_1\cdot\boldsymbol{a}_2 \times \boldsymbol{a}_3} \qquad \boldsymbol{b}_2 = \frac{\boldsymbol{a}_3 \times \boldsymbol{a}_1}{\boldsymbol{a}_1\cdot\boldsymbol{a}_2 \times \boldsymbol{a}_3} \qquad \boldsymbol{b}_3 = \frac{\boldsymbol{a}_1 \times \boldsymbol{a}_2}{\boldsymbol{a}_1\cdot\boldsymbol{a}_2 \times \boldsymbol{a}_3} \qquad \ldots.(35)$$

We can check by straightforward calculation that

$$\boldsymbol{a}_i \cdot \boldsymbol{b}_j = \delta_{ij} \qquad \ldots.(36)$$

$$(\boldsymbol{a}_1 \cdot \boldsymbol{a}_2 \times \boldsymbol{a}_3)(\boldsymbol{b}_1 \cdot \boldsymbol{b}_2 \times \boldsymbol{b}_3) = 1 \qquad \ldots.(37)$$

and note that $\boldsymbol{a}_1.\boldsymbol{a}_2 \times \boldsymbol{a}_3 \equiv B$ is the volume per nucleus in the ordinary space. We now write

$$\boldsymbol{\rho} = \sum_{i=1}^{3} \rho_i\boldsymbol{a}_i \qquad \boldsymbol{k} - \boldsymbol{k}' = \sum_{i=1}^{3} (k_i - k_i')\boldsymbol{b}_i \qquad \ldots.(38)$$

so that from equation 36

$$\boldsymbol{\rho}\,(\boldsymbol{k} - \boldsymbol{k}') = \sum_{i=1}^{3} \rho_i(k_i - k_i') \qquad \ldots.(39)$$

With the help of this equation

$$\left|\sum_{\boldsymbol{\rho}} \exp\left\{i\,\boldsymbol{\rho}\cdot(\boldsymbol{k} - \boldsymbol{k}')\right\}\right|^2 = \prod_{i=1}^{3}\left|\sum_{\rho_i=0}^{g_i} \exp\left\{i\rho_i(k_i - k_i')\right\}\right|^2$$

$$= \prod_{i=1}^{3} \frac{\sin^2\tfrac{1}{2}\left\{g_i(k_i - k_i')\right\}}{\sin^2\tfrac{1}{2}(k_i - k_i')} \qquad \ldots.(40)$$

Clearly this expression is small unless $k_i - k_i' = 2\pi\tau_i$ for all i, where the τ_i are positive or negative integers. To each triple set of integers $\tau_1\tau_2\tau_3$ there corresponds a reciprocal lattice vector $\boldsymbol{\tau}$ defined by

$$\boldsymbol{\tau} = \sum_{i=1}^{3} \tau_i \boldsymbol{b}_i \qquad \ldots . (41)$$

The sharply varying form of function 40 suggests a representation in terms of δ-functions, and it turns out that we can replace it by

$$(2\pi)^3 N \prod_{i=1}^{3} \delta(k_i - k_i' - 2\pi\tau_i) \qquad \ldots . (42)$$

To obtain this result, write $k_i - k_i' - 2\pi\tau_i = \phi$ (say) and examine the integral properties of $\sin^2 \frac{1}{2} g_i\phi / \sin^2 \frac{1}{2}\phi$ in the neighbourhood of $\phi = 0$. By elementary calculations

$$\int_{-\Phi}^{\Phi} \frac{\sin^2 \frac{1}{2} g_i\phi}{\sin^2 \frac{1}{2}\phi} d\phi = 2\pi g_i = 2\pi g_i \int_{-\Phi}^{\Phi} \delta(\phi) d\phi , \quad \frac{\pi}{2g_i} \ll \Phi \ll \frac{\pi}{2} \qquad \ldots . (43)$$

At this point, it is convenient to go over from the reciprocal lattice space, defined by the vectors $\boldsymbol{b}_i$, to an ordinary Cartesian frame of reference. The triple product of the δ-functions equation 42 is transformed by

$$\prod_{i=1}^{3} \delta(k_i - k_i' - 2\pi\tau_i) = B^{-1} \delta(\boldsymbol{k} - \boldsymbol{k}' - 2\pi\boldsymbol{\tau}) \qquad \ldots . (44)$$

The factor B^{-1} is introduced because δ-functions are defined by integral equations, and the transformation of integrals from one space to another involves the Jacobian, or ratio of unit volumes in the two spaces.

The differential cross section (equation 34) has now been put in the form

$$G(\boldsymbol{k}') = \frac{a^2(2\pi)^3}{B} \delta(\boldsymbol{k} - \boldsymbol{k}' - 2\pi\boldsymbol{\tau}) \qquad \ldots . (45)$$

The utility of the reciprocal lattice now becomes apparent. Every term in the scattering is associated with a reciprocal lattice vector $\boldsymbol{\tau}$; as the micro-crystal is rotated the reciprocal lattice also rotates and the end of each $2\pi\boldsymbol{\tau}$ vector traces out a sphere of radius $2\pi\tau$. The vector $\boldsymbol{k}$ remains fixed and there is scattering in the directions of $\boldsymbol{k}'$ for which $\boldsymbol{k} - \boldsymbol{k}'$ can start from the centre and end on the surface of the sphere. The vector $\boldsymbol{k}'$ thus traces out a cone (the Debye-Scherrer cone) of semi-vertical angle θ_τ, with

$$k \sin \frac{\theta_\tau}{2} = \pi\tau \qquad \ldots . (46)$$

This can alternatively be written in the form of the Bragg condition

$$2d \sin \frac{\theta_\tau}{2} = \lambda \qquad \ldots . (47)$$

where $d = 1/\tau$ is the distance between Bragg planes in the crystal.

It is clear from equation 45 that any particular reciprocal lattice vector $\boldsymbol{\tau}$ can only contribute to the scattering if it satisfies the inequality $\tau \leqslant k/\pi$. For all such reciprocal lattice vectors we must integrate equation 45 over all directions of $\boldsymbol{k}'$ and average over all directions of $\boldsymbol{\tau}$ (for details see WEINSTOCK[9], equations 27—31). It is found that the scattering cross section given by each $\boldsymbol{\tau}$ is

$$E^\tau = \frac{\pi\sigma}{2k^2B\tau} \qquad \ldots . (48)$$

and the total scattering cross section is the sum of this over all the suitable $\boldsymbol{\tau}$:

$$E = \frac{\pi\sigma}{2k^2B} \sum_{\tau \leqslant k/\pi} 1/\tau \qquad \ldots . (49)$$

In carrying out the summation it must be remembered that it is common for many reciprocal lattice vectors to have the same length.

The behaviour of E is readily understood. As λ increases and k decreases, the factor $\pi\sigma/2k^2B$ rises steadily while the Σ term falls abruptly at each of the points $k = \pi\tau$ where reciprocal lattice vectors 'cut out'. At very long wavelengths there will be no $\boldsymbol{\tau}$ short enough to satisfy $\tau \leqslant k/\pi$, and therefore no scattering at all. (The function labelled 100° K in *Figure 1*a behaves somewhat similarly to E.) At short wavelengths it is not very difficult to prove that E becomes equal to σ and that the scattering is isotropic.

Scattering by an element with several infinitely heavy spinless isotopes—We are going to consider now the scattering of an element with several infinitely heavy isotopes which have no nuclear spin, the rth isotope having an abundance p_r and a scattering length a_r. If there are no interference effects, then each nucleus scatters independently with the average cross section

$$\sigma = 4\pi \sum_r p_r a_r^2 = 4\pi \overline{a_r^2} \qquad \ldots . (50)$$

This quantity will be termed the amorphous scattering cross section of the element. It is the scattering cross section which would be observed if the atoms were randomly arranged in space; it is also the cross section measured at short wavelengths.

At wavelengths comparable with interatomic distances, interference cannot be neglected and the differential cross section (*cf* equation 34) becomes

$$G(\boldsymbol{k}') = \frac{1}{N} \left| \sum_{\boldsymbol{\rho}} a_{\boldsymbol{\rho}} \exp\{i\boldsymbol{\rho} \cdot (\boldsymbol{k} - \boldsymbol{k}')\} \right|^2 \qquad \ldots . (51)$$

where a_ρ is the scattering length of the isotope which happens to occupy the lattice point ρ. Clearly, we must consider all possible distributions of the isotopes among the lattice points and find the average value of $G(\boldsymbol{k}')$.

This lengthy but essentially simple operation yields the obvious result

$$\overline{G(\boldsymbol{k}')} = \Sigma_r p_r a_r^2 - \left(\Sigma_r p_r a_r\right)^2 + \frac{1}{N}\left(\Sigma_r p_r a_r\right)^2 \left| \sum_\rho \exp\{i\rho\cdot(\boldsymbol{k}-\boldsymbol{k}')\}\right|^2 \quad \ldots\ldots(52)$$

$$= \left(\overline{a_r^2} - \overline{a_r}^2\right) + \frac{1}{N}\overline{a_r}^2 \left| \sum_\rho \exp\{i\rho\cdot(\boldsymbol{k}-\boldsymbol{k}')\}\right|^2 \quad \ldots\ldots(53)$$

$$= \frac{1}{4\pi}\left\{s + \frac{S}{N}\left| \sum_\rho \exp\{i\rho\cdot(\boldsymbol{k}-\boldsymbol{k}')\}\right|^2\right\} \quad \ldots\ldots(54)$$

where the constants $S = 4\pi\overline{a_r}^2$ and $s = 4\pi\left(\overline{a_r^2} - \overline{a_r}^2\right)$ will be called respectively the ordered and disordered scattering cross sections of the element. By definition we have

$$\sigma = S + s \quad \ldots\ldots(55)$$

The total scattering cross section is found, as usual, by integrating the expression 54 over all directions of $\boldsymbol{k}'$ and averaging over all orientations of the microcrystal.

The second term in equation 54 is identical with the differential cross section 34 except for the replacement of $a^2 = \sigma/4\pi$ by $S/4\pi$. The ordered scattering is therefore

$$E(S) = \frac{\pi S}{2k^2 B} \sum_{\tau \leqslant k/\pi} 1/\tau \quad \ldots\ldots(56)$$

The first term in equation 54 is easily handled. Since s is a constant the integration over all directions of $\boldsymbol{k}'$ is accomplished simply through multiplication by 4π. The disordered scattering is thus

$$E(s) = s \quad \ldots\ldots(57)$$

The total scattering of the element is the sum $E(S) + E(s)$, which varies from the value σ at short wavelengths to the value s at long wavelengths, where $E(S) = 0$.

Extension to nuclei with spin—If an element has one or more isotopes with a spin, only a small extension of the work is needed. We saw on p 192 that the scattering cross section of a spinning nucleus is divided into two parts coherent and non-coherent. Only the first part is able to contribute to the ordered scattering, while the second part increases the disordered scattering.

We can retain the previous definitions of σ, S and s by generalizing the definition of the abundance factors p_r. There have to be two p_r terms for each isotope with a spin, equal to the isotopic abundance multiplied by $(I+1)/(2I+1)$ and $I/(2I+1)$ respectively. With the first p_r is associated the scattering length belonging to the compound state with total spin $I+\frac{1}{2}$; correspondingly the second p_r is linked with the scattering length for the state with spin $I-\frac{1}{2}$. We find σ, S and s as before from the summations $(\sum_r p_r a_r)^2$ and $\sum_r p_r a_r^2$.

For example, hydrogen has the cross sections

$$\begin{aligned} \sigma &= 4\pi(\tfrac{3}{4}a_+^2 + \tfrac{1}{4}a_-^2) \\ S &= 4\pi(\tfrac{3}{4}a_+ + \tfrac{1}{4}a_-)^2 \\ s &= \sigma - S \end{aligned} \qquad \ldots\ldots(58)$$

where a_+, a_- are the scattering lengths for the triplet and singlet states of the deuteron.

Table I sets out the scheme of abundances for lead, which has one isotope with a spin and three without. There are five p_r and a_r terms.

Table I. Abundance and Spin of Lead Isotopes

Atomic weight of isotope	204	206	207		208
Isotopic abundance	0·015	0·236	0·226		0·523
Spin	0	0	$\frac{1}{2}$		0
p_r	0·015	0·236	0·170 +	0·056 −	0·523

Scattering by an element with one finitely heavy spinless isotope—This is the problem which has been considered by WEINSTOCK[9], whose treatment will be followed here.

The finite mass of the scattering nuclei makes it possible for a neutron to transfer energy to the lattice vibrations, its final velocity being correspondingly reduced. Such a process is referred to as phonon emission by the neutron. Alternatively, the neutron energy may be increased by phonon absorption, at the expense of vibrational energy already present in the lattice as a result of thermal agitation. Elastic collisions with no energy interchange are, of course, still possible.

The problem is to obtain E_{el} and E_{in}, the cross sections for elastic and inelastic collision, in terms of $\sigma = 4\pi a^2$. Use is made of a simple extension of

the Born approximation to allow for the internal motion of the scatterer; the usual formula (*cf* MOTT and MASSEY[1], chapter VIII) is

$$G(\boldsymbol{k}') = \frac{{m_0}^2}{4\pi^2\hbar^4 N} \cdot \frac{k'}{k} \left| \int\int\int \exp\{i\boldsymbol{r}.(\boldsymbol{k}-\boldsymbol{k}')\}\ V\Phi^{*'}(\gamma,\mu)\Phi(\gamma,\mu)dv\,d\gamma\,d\mu \right|^2 \quad \ldots\ (59)$$

for the differential cross section per scattering nucleus. In this expression $\boldsymbol{r}$ is the position vector of the neutron and $\boldsymbol{k}$, $\boldsymbol{k}'$ are its incident and final propagation vectors. Since inelastic collisions may now occur, k' is not always equal to k; the factor k'/k is present because the ingoing current is proportional to v and the outgoing to v'.

The function V represents the interaction between the neutron and the crystal; it can be written

$$V = \sum_{\rho} \frac{2\pi\hbar^2 a}{m_o} \delta(\boldsymbol{r} - \boldsymbol{R}_\rho) \quad \ldots\ (60)$$

with the help of the Fermi pseudo-potential (equation 31). Here $\boldsymbol{R}_\rho$ is the position vector of a nucleus the equilibrium position of which is ρ. Because of the lattice vibrations the nucleus is slightly displaced by the vector $\boldsymbol{u}_\rho$, so that

$$\boldsymbol{R}_\rho = \rho + \boldsymbol{u}_\rho \quad \ldots\ (61)$$

The crystal wave function Φ (a function of the $3N$ components of the $\boldsymbol{u}_\rho$ vectors) represents the displacements of the N nuclei. The final crystal wave function Φ' differs from Φ if an inelastic collision has occurred.

In order to find the analytical form of Φ, it is customary to change its argument from the $\boldsymbol{u}_\rho$ vectors to new coordinates defined by

$$\boldsymbol{u}_\rho = (2/mN)^{\frac{1}{2}} \sum_s \alpha_s(\gamma_s \cos \rho\cdot\boldsymbol{q}_s - \mu_s \sin \rho\cdot\boldsymbol{q}_s) \quad \ldots\ (62)$$

Here m is the mass of each nucleus; γ_s and μ_s are the two independent amplitudes of a plane polarized standing elastic wave with propagation vector $\boldsymbol{q}_s$ and unit polarization vector α_s. The suffix s takes on $3N/2$ values to give $3N$ independent amplitudes in all. The set of propagation vectors $\boldsymbol{q}_s$ (inversely proportional to the wavelengths) is such as to make the corresponding elastic waves periodic in the microcrystal. The lengths of the $\boldsymbol{q}_s$ vectors accordingly vary from near zero to a maximum value rather smaller than the length of the basic reciprocal lattice vectors.

The utility of the expansion 62 lies in the fact that the potential energy U of the crystal can be written

$$U = \sum_s \tfrac{1}{2}\omega_s^2(\gamma_s^2 + \mu_s^2) \quad \ldots\ (63)$$

in which the coefficients ω_s depend on the forces which bind each atom to its neighbours. The expression 63 is analytically identical with the potential

energy of $3N$ simple harmonic oscillators with angular frequencies ω_s. The appropriate wave function for each 'γ-oscillator' accordingly has the form

$$\phi_n\left(\gamma(\omega/\hbar)^{\frac{1}{2}}\right) = (1/2^n n!)^{\frac{1}{2}}\,(\omega/\pi\hbar)^{\frac{1}{4}} \exp\left(-\omega\gamma^2/2\hbar\right) H_n\left(\gamma(\omega/\hbar)^{\frac{1}{2}}\right) \quad \ldots . (64)$$

when the oscillator is in its nth eigenstate with an energy $(n + \frac{1}{2})\hbar\omega$; H_n is the Hermite polynomial of nth order. A μ-oscillator is represented by the same expression with μ substituted for γ and the total wave function is the product

$$\Phi = \prod_{s_1 s_2} \phi_{n\,s_1}\,\phi_{n\,s_2} \quad \ldots . (65)$$

with the s_1 and s_2 suffixes referring to the γ and μ-oscillators respectively. Physically $\Phi^*\Phi \prod_{s_1 s_2} d\gamma_{s_1} d\mu_{s_2}$ is the probability of finding the $3N$ standing waves with a set of energies $(n_{s_1} + \frac{1}{2})\hbar\omega_{s_1}$, $(n_{s_2} + \frac{1}{2})\hbar\omega_{s_2}$ and a set of amplitudes lying between γ_{s_1}, μ_{s_2} and $\gamma_{s_1} + d\gamma_{s_1}, \mu_{s_2} + d\mu_{s_2}$.

To complete the formulation of the problem, the frequencies ω_s of the elastic waves are determined from the corresponding propagation vectors q_s by taking the sound velocity c to be independent of mode and frequency, so that $\omega_s = cq_s$. This is the Debye approximation, familiar in specific heat theory; it gives rise to a frequency spectrum which increases as the square of ω up to a maximum $\omega_0 = k_0\Theta/\hbar$ where Θ is the Debye temperature of the crystal and k_0 is Boltzmann's constant.

Weinstock finds, for the elastic component, the differential cross section

$$G_0(\boldsymbol{k}') = \frac{\sigma \exp(-2W)}{4\pi N}\left|\sum_{\rho} \exp\left\{i\rho\cdot(\boldsymbol{k} - \boldsymbol{k}')\right\}\right|^2 \quad \ldots . (66)$$

$$W = \frac{3\hbar^2}{2mk_0\Theta}(\boldsymbol{k} - \boldsymbol{k}')^2\left[\tfrac{1}{4} + (T/\Theta)^2\int_0^{\Theta T/} \frac{\beta}{(e^\beta - 1)}d\beta\right] \quad \ldots . (67)$$

As usual, the total elastic cross section is evaluated from equation 66 with the help of the reciprocal lattice. The final result is

$$E_{el} = \frac{\pi\sigma}{2k^2B}\sum_{\tau \leqslant k/\pi} \frac{\exp\left(-2W_0^\tau\right)}{\tau} \quad \ldots . (68)$$

$$W_0^\tau = \frac{6\pi^2\hbar^2\tau^2}{mk_0\Theta}\left[\tfrac{1}{4} + (T/\Theta)^2\int_0^{\Theta/T} \frac{\beta}{(e^\beta - 1)}d\beta\right] \quad \ldots . (69)$$

Comparison with equation 49 shows that the only novelty is the presence of the factors $\exp(-2W_0^\tau)$, which are responsible for a rapid decrease of E_{el} at short wavelengths.

The expression for the inelastic cross section is much more complicated. Weinstock shows that, at medium and long wavelengths, the important transitions are those in which a single oscillator changes its energy by one quantum only (single phonon emission and absorption). At short wavelengths

multiple phonon emission becomes probable and an alternative theory developed by FINKELSTEIN[10] should be used. Finkelstein assumes that the thermal oscillators have just one frequency, which is the Einstein approximation. The simplicity thus introduced makes it possible to calculate the probability of multiple transitions; but the results must be less accurate than Weinstock's at medium and long wavelengths.

The differential cross section for single phonon emission to the oscillators of frequency ω (γ and μ modes and all 3 polarizations included) is found to be

$$G_{+1}(\boldsymbol{k}') = \frac{\sigma\hbar\exp(-2W)}{8\pi m\omega(1-x)N^2}\cdot\frac{k'}{k}(\boldsymbol{k}-\boldsymbol{k}')^2\cdot\left|\sum_{\boldsymbol{\rho}}\exp\{i\boldsymbol{\rho}\cdot(\boldsymbol{k}-\boldsymbol{k}'+\boldsymbol{q})\}\right|^2 \quad \ldots.(70)$$

with $x = \exp(-\hbar\omega/k_0T)$. To find the total cross section for scattering with phonon emission, the expression 70 must be integrated over all directions of $\boldsymbol{k}'$, averaged over all orientations of the microcrystal and integrated over all $\boldsymbol{q}$ space. The result, with two unimportant terms omitted as suggested by Weinstock, is

$$E_{+1} = \sum_{\tau} E_{+1}^{\tau} \quad \ldots.(71)$$

$$E_{+1}^{\tau} = \sigma\cdot\frac{k_0^2T^2\exp(-2W_0^{\tau})}{16\pi\tau\hbar k^2mc^3}\left\{4\pi^2\tau^2\int_0^{\beta_0}\frac{(\lambda_2-\lambda_1)\beta}{(1-e^{-\beta})}d\beta\right\} \quad \ldots.(72)$$

where $\beta = \hbar\omega/k_0T$; $(\lambda_2 - \lambda_1)$ is a function of τ and β which can be found by means of a diagram described in section VI of Weinstock's paper.

Similar work finds the total cross section for phonon absorption

$$E_{-1} = \sum_{\tau} E_{-1} \quad \ldots.(73)$$

$$E_{-1}^{\tau} = \sigma\cdot\frac{k_0^2T^2\exp(-2W_0^{\tau})}{16\pi\tau\hbar k^2mc^3}\left\{4\pi^2\tau^2\int_0^{\beta_0}\frac{(\lambda_2-\lambda_1)\beta}{(e^{\beta}-1)}d\beta\right\} \quad \ldots.(74)$$

with $(\lambda_2 - \lambda_1)$ a different function of τ and β.

The total inelastic cross section E_{in} is the sum of E_{+1} and E_{-1}.

It is possible to show that E_{+1} is zero when the wavelength is long enough to make the smallest τ greater than k/π. On the other hand E_{-1} increases proportionately to λ at very long wavelengths.

Scattering by an element with several finitely heavy spinless isotopes— Weinstock's work needs extension to allow for the presence of several isotopes; this addition to the theory has been made by CASSELS[11].

As in the section dealing with infinitely heavy isotopes, the scattering divides into two parts depending on S and s respectively ; now there is a

further division into elastic and inelastic collisions, making four categories in all. The four terms will be called the ordered elastic cross section $E_{el}(S)$, the disordered elastic cross section $E_{el}(s)$, the ordered inelastic cross section $E_{in}(S)$ and the disordered inelastic cross section $E_{in}(s)$.

Consider first the elastic components. The differential cross section will be given by a simple generalization of equation 66

$$G_0(\boldsymbol{k}') = \frac{\exp(-2W)}{N} \left| \sum_{\rho} a_\rho \exp\{i\rho \cdot (\boldsymbol{k} - \boldsymbol{k}')\} \right|^2 \qquad \ldots . (75)$$

where, just as in equation 51, a_ρ is the scattering length of the element occupying the lattice point ρ. The average of $G_0(\boldsymbol{k}')$ over all possible distributions of the isotopes gives

$$\overline{G_0(\boldsymbol{k}')} = \frac{\exp(-2W)}{4\pi} \left\{ s + \frac{S}{N} \left| \sum_{\rho} \exp\{i\rho \cdot (\boldsymbol{k} - \boldsymbol{k}')\} \right|^2 \right\} \qquad \ldots . (76)$$

The second term of this is identical with the cross section 66 save for the replacement of σ by S. The ordered elastic cross section is therefore

$$E_{el}(S) = \frac{\pi S}{2k^2 B} \sum_{\tau \leqslant k/\pi} \frac{\exp(-2W_0{}^\tau)}{\tau} \qquad \ldots . (77)$$

The first term of equation 76, after integration over all directions of $\boldsymbol{k}'$, gives the disordered elastic cross section. Introducing θ, the angle of scattering, we have $(\boldsymbol{k} - \boldsymbol{k}')^2 = 4k^2 \sin^2(\theta/2)$. Thus

$$\mathrm{E}_{el}(s) = \frac{s}{4\pi} \int_0^{\pi} \exp\{ -4k^2 Y \sin^2(\theta/2) \}\, 2\pi \sin\theta \, d\theta \qquad \ldots . (78)$$

$$Y = \frac{3\hbar^2}{m k_0 \Theta} \left[\tfrac{1}{4} + (T/\Theta)^2 \int_0^{\Theta^T} \frac{\beta}{(\mathrm{e}^\beta - 1)} d\beta \right] \qquad \ldots . (79)$$

Carrying out the integration of equation 78 we finally get

$$E_{el}(s) = \frac{s}{4k^2 Y} \left\{ 1 - \exp(-4k^2 Y) \right\} \qquad \ldots . (80)$$

The cross sections for phonon emission are similarly obtained by generalizing equation 70 to read

$$G_{+1}(\boldsymbol{k}') = \frac{\hbar \exp(-2W)}{2m\omega(1-x)N^2} \cdot \frac{k'}{k} (\boldsymbol{k} - \boldsymbol{k}')^2 \cdot \left| \sum_{\rho} a_\rho \exp\{i\rho \cdot (\boldsymbol{k} - \boldsymbol{k}' + \boldsymbol{q})\} \right|^2$$

$$\ldots . (81)$$

After averaging over the distributions of the isotopes, the usual splitting into two terms is found

$$\overline{G_{+1}(\boldsymbol{k}')} = \frac{\hbar \exp(-2W)}{8\pi m\omega(1-x)N} \cdot \frac{k'}{k} (\boldsymbol{k}-\boldsymbol{k}')^2 \times$$
$$\times \left\{ s + \frac{S}{N} \left| \sum_{\rho} \exp\{ i\rho \cdot (\boldsymbol{k} - \boldsymbol{k}' + \boldsymbol{q}) \} \right|^2 \right\} \quad \ldots . (82)$$

The second term here gives the ordered cross section for phonon emission. It is identical with equation 70 except for the replacement of σ by S. Thus

$$E_{+1}(S) = \sum_{\tau} E^{\tau}_{+1}(S)$$
$$E^{\tau}_{+1}(S) = S \cdot \frac{k_0^2 T^2 \exp(-2W_0^{\tau})}{16\pi\tau\hbar k^2 mc^3} \left\{ 4\pi^2\tau^2 \int_0^{\beta_0} \frac{(\lambda_2 - \lambda_1)\beta}{(1-e^{-\beta})} d\beta \right\} \quad \ldots . (83)$$

in accord with equation 72.

The first term in equation 82 must be averaged over all directions of $\boldsymbol{k}'$ and integrated over the whole of $\boldsymbol{q}$ space to give the disordered cross section for phonon emission. Introducing again the scattering angle θ we have $(\boldsymbol{k} - \boldsymbol{k}')^2 = k^2 + k'^2 - 2kk'\cos\theta$, now that k' is no longer equal to k. The integration over all scattering angles yields the quantity

$$s \cdot \frac{\hbar}{8\pi m\omega(1-x)N} \cdot \frac{k'}{k} \int_0^{\pi} (k^2 + k'^2 - 2kk'\cos\theta) \times$$
$$\exp\{ - Y(k^2 + k'^2 - 2kk'\cos\theta) \} 2\pi \sin\theta d\theta \quad \ldots . (84)$$
$$= s \cdot \frac{\hbar \exp\{ - Y(k^2 + k'^2) \}}{2mNY\omega(1-x)} \left\{ \left(\frac{k'^2 + k'^2 + (1/Y)}{2k^2} \right) \sinh(2Ykk') - \right.$$
$$\left. - \frac{k'}{k} \cosh(2Ykk') \right\} \quad \ldots . (85)$$

In this expression we now substitute for k' by means of the condition for conservation of energy, $k'^2 = k^2 - 2m_0\omega/\hbar$. Finally, $E_{+1}(s)$ is obtained by integrating over the usual Debye frequency spectrum, wherein the number of frequencies between ω and $\omega + d\omega$ is $\{ BN/(2\pi)^3 \} 4\pi q^2 dq$ up to a cut-off frequency $\omega_0 = k_0\Theta/\hbar$. Introducing again $\beta = \hbar\omega/k_0 T$, we at length have

$$E_{+1}(s) = s \cdot \frac{k_0^2 T^2 B}{4\pi^2 mc^3 \hbar Y} \int_0^{\beta'} \frac{\beta \exp\left\{ - 2Yk^2 \left(1 - \frac{m_0 k_0 T\beta}{\hbar^2 k^2} \right) \right\}}{1 - e^{-\beta}} \times$$
$$\times \left[\left(1 - \frac{m_0 k_0 T\beta}{\hbar^2 k^2} + \frac{1}{2Yk^2} \right) \sinh \left\{ 2Yk^2 \left(1 - \frac{2m_0 k_0 T\beta}{\hbar^2 k^2} \right)^{\frac{1}{2}} \right\} - \right.$$
$$\left. - \left(1 - \frac{2m_0 k_0 T\beta}{\hbar^2 k^2} \right)^{\frac{1}{2}} \cosh \left\{ 2Yk^2 \left(1 - \frac{2m_0 k_0 T\beta}{\hbar^2 k^2} \right)^{\frac{1}{2}} \right\} \right] d\beta \quad \ldots . (86)$$

The upper limit β' of the integration is either $\beta_0 = \Theta/T$ or $\beta_1 = \hbar^2k^2/2m_0k_0T$, whichever happens to be smaller. The reason for this is that at long wavelengths the neutron has not enough energy to excite the oscillators of higher frequency.

Similar treatment of the phonon absorption processes yields the ordered and disordered cross sections:

$$E_{-1}(S) = \sum_\tau E^\tau_{-1}(S)$$

$$E^\tau_{-1}(S) = S \cdot \frac{k_0^2T^2 \exp(-2W_0^\tau)}{16\pi\tau\hbar k^2mc^3} \left\{ 4\pi^2\tau^2 \int_0^{\beta_0} \frac{(\lambda_2-\lambda_1)\beta}{(e^\beta-1)} d\beta \right\} \quad \ldots . (87)$$

and

$$E_{-1}(s) = s \cdot \frac{k_0^2T^2B}{4\pi^2mc^3\hbar Y} \int_0^{\beta_0} \frac{\beta \exp\left\{ -2Yk^2\left(1 + \frac{m_0k_0T\beta}{\hbar^2k^2}\right)\right\}}{e^\beta - 1} \times$$

$$\times \left[\left(1 + \frac{m_0k_0T\beta}{\hbar^2k^2} + \frac{1}{2Yk^2}\right) \sinh\left\{2Yk^2\left(1 + \frac{2m_0k_0T\beta}{\hbar^2k^2}\right)^{\frac{1}{2}}\right\} - \right.$$

$$\left. - \left(1 + \frac{2m_0k_0T\beta}{\hbar^2k^2}\right)^{\frac{1}{2}} \cosh\left\{2Yk^2\left(1 + \frac{2m_0k_0T\beta}{\hbar^2k^2}\right)^{\frac{1}{2}}\right\} \right] d\beta \quad \ldots . (88)$$

The total inelastic cross sections are, of course, given by $E_{in}(S) = E_{+1}(S) + E_{-1}(S)$ and $E_{in}(s) = E_{+1}(s) + E_{-1}(s)$. At long wavelengths the probability of phonon emission is very small, but both the cross sections for phonon absorption increase as λ.

Extension to nuclei with spin—The extension to nuclei with spin is done, as on p 198, by enlarging the definitions of S and s.

Figure 1 (a-d) shows the results of a practical application to a body centred cubic crystal with lattice constant $a = 2{\cdot}90$ Å, $m = 9{\cdot}22 \times 10^{-23}$ gm and $\Theta = 453°$ K. (These are the constants of iron crystals, but the theory cannot be applied directly to that element because of magnetic scattering by the atomic electrons.) $E_{in}(S)$ was calculated by CASSELS and LATHAM[12], and the remaining cross sections by Cassels. It is interesting to note the close similarity between the behaviours of $E_{in}(S)$ and $E_{in}(s)$. This result is expected because there are always several values of τ contributing to $E_{in}(S)$, so that interference effects are not very important. By the same token $E_{el}(S) + E_{el}(s)$ is probably well represented at short wavelengths by the approximation

$$E_{el}(S) + E_{el}(s) \sim \frac{\sigma}{4k^2Y} \left\{ 1 - \exp(-4k^2Y) \right\} \quad \ldots . (89)$$

The inelastic cross sections are roughly proportional to $1/m\Theta$, so that approximate results for other crystals can be obtained from the data in *Figures 1* c and d.

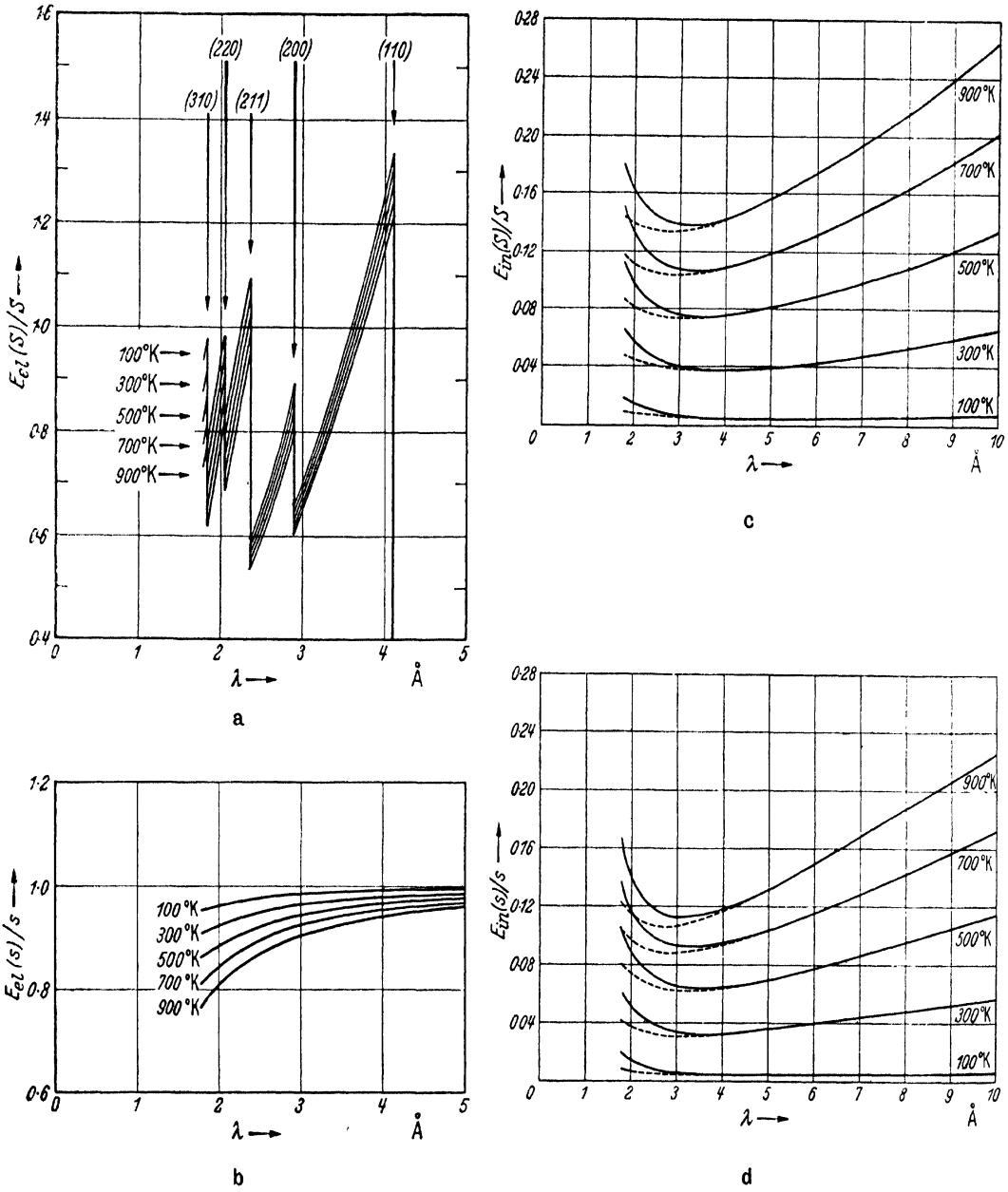


Figure 1. The four scattering cross sections of a body centred cubic crystal ($a = 2{\cdot}90$ Å, $m = 9{\cdot}22 \times 10^{-23}$ gm, $\Theta = 453°$ K):

- **a** *ordered elastic scattering cross section, $E_{el}(S)$,*
- **b** *disordered elastic scattering cross section, $E_{el}(s)$,*
- **c** *ordered inelastic scattering cross section, $E_{in}(S)$,*
- **d** *disordered inelastic scattering cross section, $E_{in}(s)$*

Scattering by mixed crystals—The previous work on p 197 is easily extended to crystals containing several elements of infinite mass.

The disordered cross sections are not subject to interference effects, so that a simple addition of the separate contributions is possible. For example, the disordered scattering per molecule in a body centred cubic crystal containing two elements A and B is

$$E(s) = s^{A} + s^{B} \qquad \ldots . (90)$$

The ordered scattering is slightly more complicated because the effective amplitude of scattering depends on the relative phases of the scattered waves from the various elements. This means that we must make the value of S a function of τ, so that the ordered scattering cross section per molecule is

$$E(S) = \sum_{\tau \leqslant k/\pi} E^{\tau}(S^{\tau})$$

$$E^{\tau}(S^{\tau}) = \frac{\pi S^{\tau}}{2k^2 B} \cdot \frac{1}{\tau} \qquad \ldots (91)$$

Using again the example of a body centred cubic crystal containing two elements A and B, S^{τ} is $4\pi(\overline{a_r^{A}} + \overline{a_s^{B}})^2$ if $h + k + l$ is even and $4\pi(\overline{a_r^{A}} - \overline{a_r^{B}})^2$ if $h + k + l$ is odd. Here the Miller indices h,k,l are defined by $\tau = h\boldsymbol{b}_1 + k\boldsymbol{b}_2 + l\boldsymbol{b}_3$. In the mixed body centred cubic crystal the basic lattice vectors $\boldsymbol{a}_i$ define the unit cube and $\boldsymbol{a}_1 . \boldsymbol{a}_2 \times \boldsymbol{a}_3 = B$ is the volume per molecule in the ordinary space.

When the masses of the atoms are not infinite the lattice vibrations again modify the scattering. The situation is rather complicated in a mixed crystal, because the frequency spectrum divides into several 'branches'. In some of these branches the angular frequency ω does not tend to zero when the wave vector $\boldsymbol{q}$ is small, so that the Debye approximation, $\omega = cq$, is obviously not a good one.

If the masses of the various elements are not too different, the ordered elastic cross section is approximately given by equation 91 with every mean scattering length multiplied by its corresponding $\exp(-W_0^{\tau})$. For instance, in the mixed body centred cubic crystal we substitute $(\overline{a_r^{A}} \exp(-W_0^{\tau,A}) + \overline{a_s^{B}} \exp(-W_0^{\tau,B}))$ for $(\overline{a_r^{A}} + \overline{a_s^{B}})$ and $(\overline{a_r^{A}} \exp(-W_0^{\tau,A}) - \overline{a_s^{B}} \exp(-W_0^{\tau,B}))$ for $(\overline{a_r^{A}} - \overline{a_s^{B}})$. Here $\exp(-W_0^{\tau,A})$, $\exp(-W_0^{\tau,B})$ contain the common Debye temperature Θ and the masses m_A and m_B respectively.

SHULL, WOLLAN, MORTON and DAVIDSON[13] have described an empirical method of correcting the ordered elastic scattering for the effects of lattice vibrations. This method was used to analyse the scattering of NaH, where the masses of the two elements are very different.

Extinction effects—In the theoretical work it is often assumed that the microcrystals are large enough to make g_1, g_2 and g_3, the numbers of atoms

along the three edges of the microcrystal, very large compared with unity. This assumption is usually, but not always[14], well justified.

It is possible, however, for the microcrystals to be too large. The ordered elastic scattering is produced by comparatively few microcrystals which scatter rather strongly. This is because the vast majority of the microcrystals are not oriented properly for satisfying the relation $\boldsymbol{k} - \boldsymbol{k}' = 2\pi\tau$, while the very few microcrystals that are correctly oriented scatter intensely because of constructive interference. The neutron beam may therefore be attenuated appreciably in passing through a single microcrystal, which results in a smaller ordered elastic scattering than predicted by our formulae. The magnitude of this effect has been investigated theoretically by BACON and LOWDE[15].

In practice, investigations of the ordered elastic scattering are made with samples which are finely ground in order to eliminate extinction. The grains should have linear dimensions not greater than about 5×10^{-5}cm.

The ordered inelastic and the two disordered cross sections are not affected by extinction, since all the microcrystals are able to take part.

EXPERIMENTAL RESULTS

In 1939 WHITAKER and BEYER[16] demonstrated that polycrystalline substances were more transparent to neutrons when the microcrystals were large. They drew the correct conclusion that crystalline scattering was being modified by extinction effects.

In this and other early work there was the great difficulty that the neutron beam contained particles of all energies in the thermal range. The measured quantities were averages over a broad energy spectrum, the shape of which was not precisely known. Consequently precise results could not be obtained.

In recent years the experimental work has been stimulated by great improvements in neutron technique. With the help of velocity and crystal spectrometers, and the filtering technique, we can now use neutrons of selected energy instead of being forced to accept the whole thermal spectrum of energies. As a result, the field is rapidly expanding.

Obviously, the first task is to determine the scattering constants (σ,S,s and the sign of $\bar{a}_r$) for the elements. Investigations which have this object are now reviewed and the results are summarized in *Table II.*

Once the scattering constants are known the inelastic scattering can be measured and compared with the theory already described. There is of course a connection here with solid state physics, where the frequency spectrum of the lattice vibrations is a subject of perennial interest.

Finally, we shall mention experiments concerned with neutron crystallography. The determination of crystal structures containing light elements

and the study of order-disorder transitions in alloys are among the useful applications of neutron technique.

Determination of σ, S, *and* s—Two experiments are usually necessary to find the scattering constants of an element, since very few elements have a single spinless isotope (if so, $\sigma = S$ and $s = 0$).

The value of σ is easily found by measuring the total cross sections of the element for neutron wavelengths less than about 1 Å. In this region interference effects are small and the total cross section is the sum of two parts. As predicted by the $1/v$ law, one part is proportional to λ while the other is constant ; the former is due to absorption while the latter is equal to σ. For very light elements the change over from bound to free scattering may complicate the issue.

Having found σ, a measurement of either S or s is required. The former is obtained from studies of the ordered elastic scattering and the latter by examining the disordered elastic scattering.

FERMI and MARSHALL[3] used a single crystal of calcium fluoride to produce a monochromatic neutron beam of wavelength 1·5 Å. In this beam they placed single crystals containing two or more elements, and measured the neutron intensity in three or more orders of reflection from various Bragg planes. The results showed up the variation of S^{τ} with τ which occurs in a mixed crystal. This made possible a comparison of the values of $\bar{a}_r$ and hence of S for the elements concerned.

This technique was improved by WOLLAN and SHULL[17]. The single crystals were replaced by powdered samples, eliminating extinction effects which may have affected Fermi and Marshall's results. The measurements were also made absolute by calibration with diamond and graphite scatterers. (Carbon has only one spinless isotope, so that $s = 0$.)

Figure 2 illustrates their apparatus. A collimated thermal neutron beam emerges from a pile and falls on a single crystal of sodium chloride. Another collimator is set at such an angle as to receive neutrons of wavelength 1·057 Å,

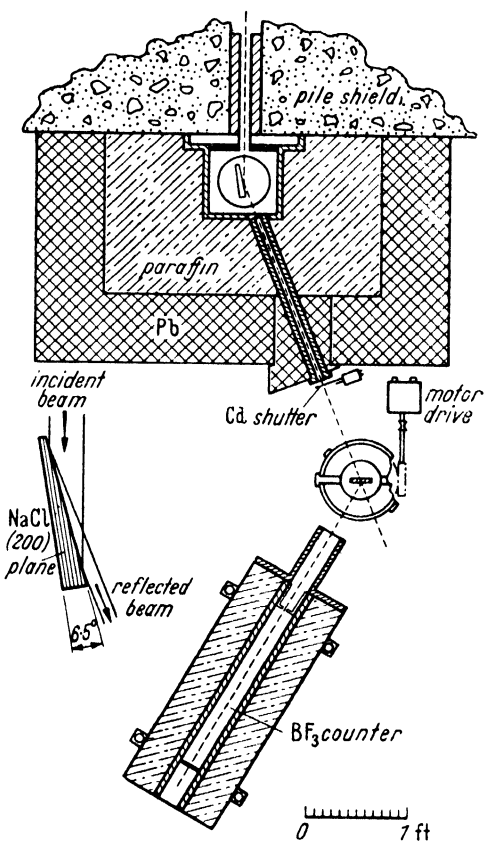


Figure 2. The apparatus used by WOLLAN *and* SHULL[17] *for determining scattering constants*

reflected by the 200 planes in the crystal. This monochromatic beam is then directed on to a powdered sample.

The boron trifluoride neutron detector is moved round the sample in order to investigate the angular distribution of the scattered neutrons. *Figure 3* shows some of the results obtained for four crystals containing sodium. There are a number of sharp peaks as the counter moves through the Debye-Scherrer cones into which the ordered elastic scattering is concentrated. From the size of the peaks S^T can be found for a number of values of τ. The observations show that the 111 peak is smaller than the 200 in every case. This means that sodium, bromine, fluorine, and chlorine all scatter in the same phase *i.e.* have the same sign for $\bar{a}_r$. The results also show that a large part of the scattering by sodium is disordered. The

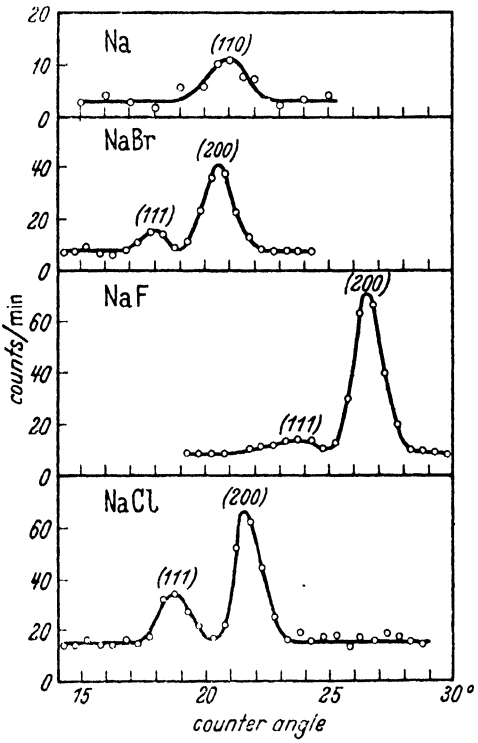


Figure 3. Some experimental results[17] *for four crystals containing sodium. The fact that the* 111 *peaks are smaller than the* 200 *shows that sodium, bromine, fluorine and chlorine all scatter in the same phase*

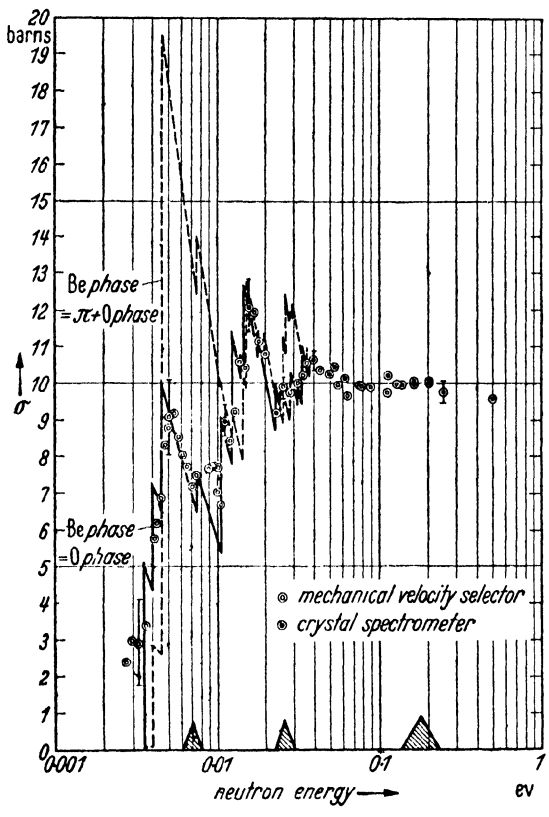


Figure 4. Scattering cross section of beryllium oxide[18]*, showing that beryllium and oxygen scatter in phase*

amorphous scattering cross section σ is 3·5 barns while the ordered cross section S is only 1·5 barns.

The ordered elastic scattering can also be studied in transmission. The total cross section shows sharp breaks at the wavelengths where reciprocal lattice vectors ' cut-out'. The magnitude of these discontinuities is proportional to S, or S^T in the case of mixed crystals. By this method FERMI, STURM and SACHS[18] showed convincingly that beryllium and oxygen have the same sign

for $\bar{a}_r$. Their results are illustrated in *Figure 4;* they were obtained with pile neutrons using both a mechanical velocity selector and a crystal spectrometer. The same method has been used by WINSBERG, MENEGHETTI and SIDHU[19].

The disordered elastic cross section can be observed in the long wavelength region ($\lambda > 2d_{max}$), where the ordered elastic cross section has disappeared.

A measurement of s is usually the most satisfactory way of determining the constants, since σ and S are normally very nearly equal. A disadvantage is that no information about the sign of $\bar{a}_r$ is obtained.

Transmission measurements in the long wavelength region were made by FERMI and MARSHALL[20] in order to study the spin dependence of scattering in beryllium, aluminium and bismuth. The total cross section as measured includes the absorption cross section, though this can be subtracted with fair accuracy.

Also included are the cross sections for inelastic scattering which are usually small enough to allow a fairly low limit to be placed on s. The effect of inelastic scattering can be reduced by cooling the sample in liquid air.

LATHAM and CASSELS[21, 22] observed directly the scattered neutrons in the long wavelength region, and found s/σ by comparison with the similar measurement in the short wavelength region. One advantage of this approach is that the absorption cross section is not directly involved in the measurements. The effect of inelastic scattering was also reduced at long wavelengths because the boron trifluoride neutron detector was energy sensitive, and so discriminated against the neutrons which had absorbed a phonon. There was correspondingly some difficulty at the short wavelength end where the neutrons which have emitted a phonon are too easily detected.

Probably the most satisfactory technique for determining the scattering constants would be to observe the scattered neutrons at long wavelengths only, in an arrangement made absolute by calibration with some suitable scatterer. This would ensure minimum disturbance from the absorption and inelastic cross sections and would fix the value of s, which is usually the small quantity in the equation $\sigma = S + s$.

The signs of the $\bar{a}_r$ can be compared by the experiments with mixed crystals, so that if one $\bar{a}_r$ is known the others follow. For theoretical reasons $\bar{a}_r$ for hydrogen is believed to be negative, which provides one starting point. Another is given by the work of FERMI and MARSHALL[3], who showed that the scattering length was positive in a number of metals by demonstrating total reflection at small angles of incidence. This is a result of a refractive index[23] smaller than unity inside a sample with positive scattering length.

As expected the majority of scattering lengths have turned out to be positive. *Table II* shows the results obtained so far (April 1949).

Table II. Scattering Constants of the Elements (April 1949)

Element (separated isotopes have mass number indicated)	*σ barns*	*S barns*	*s barns*	*Sign of ā, (+ unless otherwise indicated)*
H	81	2·0 [13]		—
H^2	7·4	4·1 [13], 5·0 [24]		
Li	2·2	0·4 [24]		—
Li^6		~6 [24]		
Li^7		0·8 [24]		—
Be	7·5	7·7 [24]	<0·47 [20]	
C	5·2	5·2 [17]		
N	11	4·6 [24]		
O	4·15	4·2 [24]		
F	3·7	5·2 [17], ~4 [24]		
Na	3·5	1·51 [17]		
Mg	3·7	2·4 [24]		
Al	1·5	1·5 [24]	<0·21 [20], <0·10 [22]	
S	1·0	1·2 [24]		
Cl	15	12·8 [17], 12·2 [24]		
K	~ 2	1·5 [24]		
Ca	2·3	2·7 [19], 2·9 [24]		
Ti	~ 6	0·78 [19], 1·8 [24]		—
V	5	<0·1 [24]		
Mn	2·2	1·3 [24]		—
Fe	11·0	10·3 [24]	<0·70 [12]	
Co	6·7	1·76 [24]		
Ni	17·0	13·5 [24]		
Ni^{58}		26 [24]		
Ni^{60}		2 [24]		
Cu	7·8	7·3 [24]		
Zn	4·2	4·2 [19], 4·3 [24]		
Ge	8·5	8·8 [24]		
As	7–8	5·0 [24]		*probably+*
Br	7·5	5·3 [17]		
Rb	5·5	3·8 [24]		
Sr	9·5	4·1 [24]		
Zr	6·8	4·9 [24]		
Nb	6·4	6·0 [24]		?
Mo	7·4	5·2 [24]		?
Pd	6·6	4·8 [24]		?
Ag	6·7	4·6 [24]		
Ag^{107}		8·7 [24]		
Ag^{109}		2·3 [24]		
Sn	4·9	4·6 [24]		
Sb	4·2	3·7 [24]		
I	3·8	3·4 [24]		
Cs	~ 7	3·0 [24]		
Ta	7·2	6·1 [24]		
W	5·7	3·3 [24]		
Au	~ 9	7·5 [24]		
Tl	9·7	7·1 [19]		
Pb	11·0	11·5 [24]	<0·85 [20], <0·70 [21]	
Bi	9·2	10·1 [24]	<0·85 [20], <0·65 [22]	?

The quantities shown are those actually measured; application of the equation $\sigma = S + s$ yields all the constants when only S or s has been determined. Experimental errors are responsible for S being given as larger than σ in a few cases. Most of the determinations of σ are taken from the work of RAINWATER, HAVENS, WU and DUNNING at Columbia University, New York (for references see GOLDSMITH, IBSER and FELD[25]).

Inelastic scattering—Measurements of the inelastic scattering are most easily made at long wavelengths where the ordered elastic scattering has disappeared.

The scattering constants are first found by a transmission experiment at 90° K, or by other means. Once these are known, the total cross section at higher temperatures can be calculated by means of the theory described earlier. The results can then be compared with the total cross sections which are measured at these higher temperatures.

CASSELS and LATHAM[12] have carried out such an experiment with iron, using a cyclotron and an electronic velocity selector. The total cross section was found to increase with temperature much faster than expected. It is believed that this discrepancy is due to magnetic scattering, which can only appear at these wavelengths if the atomic spins are not completely aligned within the magnetic domains. The degree of misalignment must depend on the temperature if the magnetic scattering is to vary from near zero at 90° K to ~ 2·3 barns at 800° K and 6 Å. The results could not have been affected by a small angle magnetic scattering effect recently discovered by HUGHES, BURGY, HELLER and WALLACE[26].

A similar investigation with aluminium has recently been made by CASSELS[11], who has obtained good agreement between theory and experiment.

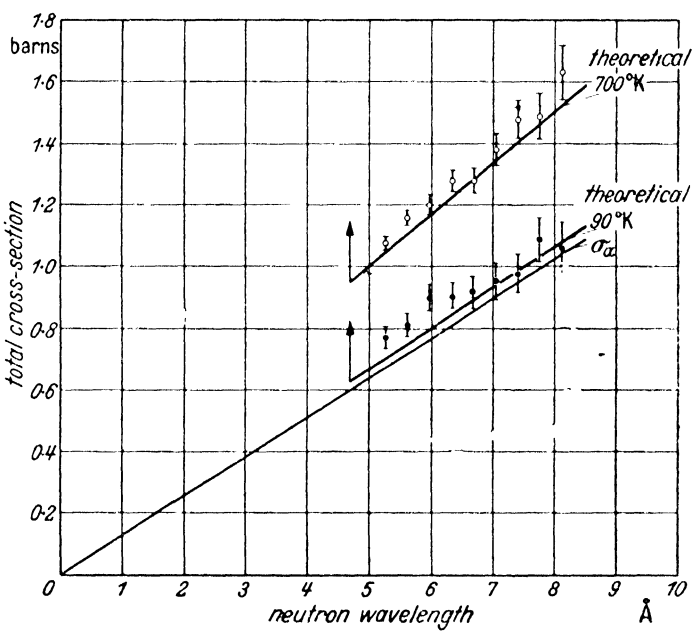


Figure 5. Transmission measurements on the total cross section of aluminium at long wavelengths. The theoretical curves are based on the constants $\sigma = S = 1{\cdot}50$ barns, $s = 0$ barns, $\sigma_\alpha/\lambda = 0{\cdot}128$ barns/Å, $\Theta = 398°K$. The experimental points were taken at 90°K (•) and 700°K (○). There is a discontinuity in the total cross section at $\lambda = 2d_{max} = 4{\cdot}67$ Å

Some of these results are reproduced in *Figure 5* ; they show that the increase with temperature of the total cross section of aluminium is predicted to within 15 per cent.

An ideal experiment on the inelastic scattering would require selection of both the incident and final wavelengths of the neutron together with the use of a single crystal as scatterer. This would enable the observer to define all four vectors in the equation, $\boldsymbol{k} - \boldsymbol{k}' = 2\pi\boldsymbol{\tau} - \boldsymbol{q}$, which is involved in the ordered inelastic scattering. A lot of useful information about the lattice vibrations could be obtained. Such an experiment may be possible in laboratories which have a pile available.

Neutron crystallography—For some time it has been anticipated that the use of neutrons would make possible the investigation of crystal structures containing light elements. The scattering lengths of the light elements are not particularly small, in contrast to the situation in x-ray or electron scattering. At the moment neutron technique is not refined enough to allow work with complicated structures but the limitation will undoubtedly disappear soon.

The first structures to have been determined solely by neutrons are those of NaH and NaD, which were found[13] to be face centred cubic like the alkali halides. For more complicated structures it will probably be necessary to use deuterated samples since the very large disordered scattering by hydrogen will cause difficulties.

Other phenomena which have been studied with neutrons include order-disorder transitions[27, 28] in alloys and the preferred orientation of the microcrystals[29] which may be induced by cold working.

I am very grateful to Drs Wollan and Shull for sending data for inclusion in Table II in advance of publication. I wish also to thank Mr Lowde for reading the proofs and making many valuable suggestions.

REFERENCES

1 MOTT, N. F. and MASSEY, H. W. S. *The Theory of Atomic Collisions* Oxford, 1933
2 MARGENAU, H. and MURPHY, G. M. *The Mathematics of Physics and Chemistry* New York, 1943
3 FERMI, E. and MARSHALL, L. *Phys. Rev.* 71 (1947) 666
4 BREIT, G. and WIGNER, E. *ibid* 49 (1936) 519
5 KAPUR, P. L. and PEIERLS, R. *Proc. roy. Soc. A* 166 (1938) 277
6 FESHBACH, H., PEASLEE, D. C. and WEISSKOPF, V. L. *Phys. Rev.* 71 (1947) 145
7 FERMI, E. *Ric. Sci.* 1 (1936) 13
8 HALPERN, O. and JOHNSON, M. H. *Phys. Rev.* 55 (1939) 898
9 WEINSTOCK, R. *ibid* 65 (1944) 1
10 FINKELSTEIN, R. J. *ibid* 72 (1947) 907
11 CASSELS, J. M. In press
12 — and LATHAM, R. *Phys. Rev.* 74 (1948) 103
13 SHULL, C. G., WOLLAN, E. O., MORTON, G. A. and DAVIDSON, W. L. *ibid* 73 (1948) 842
14 KUEGER, H. H. A., MENEGHETTI, D., RINGO, G. R. and WINSBERG, L. *ibid* 75 (1949) 1098

[15] BACON, G. E. and LOWDE, R. D. *Acta Crystallogr.* 1 (1948) 303
[16] WHITAKER, M. D. and BEYER, H. G. *Phys. Rev* 55 (1939) 1101
[17] WOLLAN, E. O. and SHULL, C. G. *ibid* 73 (1948) 830
[18] FERMI, E., STURM, W. J. and SACHS, R. G. *ibid* 71 (1947) 589
[19] WINSBERG, L., MENEGHETTI, D. and SIDHU, S. S. *ibid* 75 (1949) 975
[20] FERMI, E. and MARSHALL, L. *ibid* 72 (1947) 408
[21] LATHAM, R. and CASSELS, J. M. *Nature, Lond.* 161 (1948) 282
[22] — — Unpublished
[23] GOLDBERGER, M. L. and SEITZ, F. *Phys. Rev.* 71 (1947) 294
[24] WOLLAN, E. O. and SHULL, C. G. Unpublished
[25] GOLDSMITH, H. H., IBSER, H. W. and FELD, E. T. *Rev. mod. Phys.* 19 (1947) 259
[26] HUGHES, D. J., BURGY, M. T., HELLER, R. B. and WALLACE, J. W. *Phys. Rev.* 75 (1949) 565
[27] NIX, F. C., BEYER, H. G. and DUNNING, J. R. *ibid* 58 (1940) 1031
[28] SHULL, C. G. and SIEGEL, S. *ibid* 75 (1949) 1008
[29] ARNOLD, G. P., MEYERS, V. W. and WEBER, H. H. *ibid* 75 (1949) 217
See also WOLLAN, E. O. and SHULL, C. G. Neutron Diffraction and Associated Studies *Nucleonics* 3/1 (1948) 8; 3/2 (1948) 17

NAME INDEX

ALBERT, R. D. 121, 138
ALBOUY, G. 46, 70
ALLEN, J. S. 132, 139
ALLISON, S. K. 36
AMALDI, E. 183
ANDERSEN, E. B. 183
ANGUS, J. 138, 167
ARNOLD, G. P. 215

BACHER, R. F. 138
BACKUS, J. 121, 138
BACON, G. E. 208, 215
BAEYER, L. V. 166
BAGGE, E. 67, 72
BAKKER, C. J. 183
BALL, E. G. 172, 184
BARBOUR, I. 52, 60, 61, 70, 71
BARKAS, W. H. 54, 70, 183
BARNES, J. R. 68, 72
BARNES, S. W. 20
BARSCHALL, H. H. 47, 70
BARTON, H. A. 25, 26, 36
BATES, W. J. 52, 70
BECQUEREL, H. 37
BELL, R. E. 167
BENNETT, W. E. 36
BENNETT, W. H. 36
BERG, W. F. 40, 46, 69, 70
BERINGER, R. 161, 167
BERRIMAN, R. W. 39, 42, 69
BETHE, H. A. 57, 71, 138, 139, 158, 167
BEYER, H. G. 208, 215
BISHOP, A. S. 54, 70
BLAU, M. 38, 45, 48, 57, 59, 69, 70, 71
BLEULER, E. 120, 138, 156, 162, 167
BLOCH, F. 134, 139
BLUM, J. 43, 54, 69
BOHLMANN, E. G. 183
BOHM, D. 5, 9, 20, 138
BORST, L. B. 45, 70
BOSE, D. M. 59, 60, 71
BOUCHEZ, R. 139
BOUSSER, F. 72
BOUWERS, A. 36
BOWER, J. C. 71
BRADEN, C. H. 139
BRADNER, H. 54, 70
BRADT, H. L. 61, 62, 63, 67, 71, 72, 134, 139, 158, 167
BRADY, E. L. 160, 161, 167
BREIT, G. 214
BREMNER, J. W. 67, 72
BROBECK, W. M. 20
BRODA, E. 45, 70, 180, 182, 184
BROSTRÖM, K. J. 36
BROWN, F. W. 46, 70
BROWN, H. 133, 138
BROWN, R. H. 42, 43, 57, 66, 67, 69, 72
BUECHNER, W. W. 36
BURCH, C. R. 52, 70
BURCHAM, W. E. 24, 36
BURG, A. B. 139
BURGER, E. E. 36
BURROWS, H. B. 64, 65, 71

CALVIN, M. 169, 184
CAMERINI, U. 66, 69, 72
CAPRON, P. 184
CARLSON, P. R. 183
CASIMIR, H. B. G. 120
CASSELS, J. M. 202, 205, 211, 213, 214, 215
CHADWICK, J. 64, 70
CHALMERS, T. A. 168
CHAMPION, F. C. 51, 63, 70
CHASTEL, R. 70, 71
CHATTERJEE, S. 183
CHAUMAT, H. 36
CHEKA, J. S. 46, 68, 70
CHILTON, L. V. 69
CHOUDHURI, B. 59, 60, 71
CHRISTY, R. F. 132, 138
COCKROFT, A. L. 138, 167
COHEN, E. R. 132, 138
COLE, J. F. I. 36
COLLIE, C. H. 182, 184
CONNER, C. H. 72
CONVERSI, M. 139
COOK, C. S. 121, 138, 152, 167
COOPER, D. 66, 72
COOPER, E. P. 138, 173, 183
COOPER, F. S. 36
COOPER, O. 172, 184
COPPENS, R. 46, 68, 70, 72
CORK, J. M. 138
COSYNS, M. 62, 71
COTTON, E. 54, 70, 71
CRANBERG, L. 138
CRANE, H. R. 115, 116, 138, 166
CUER, P. 40, 45, 54, 56, 65, 68, 69, 70, 71, 72
CURIE, I. 67, 72
CURRAN, S. C. 138, 167

CURRY, W. J. J. 65, 71
CURTIS, N. W. 53, 70

D'AGOSTINO, O. 183
DANCOFF, S. M. 184
DANFORTH, W. E. 36
DANYSZ, J. 140, 166
DAUDEL, P. 139, 184
DAUDEL, R. 128, 130, 139, 179, 183, 184
DAVIDSON, W. L. 207, 214
DE FELICE, J. A. 47, 48, 70
DEMERS, P. 37, 39, 40, 43, 45, 46, 47, 53, 56, 57, 65, 66, 69, 70, 72
DENNISON, D. M. 151, 167
DEUTSCH, M. 129, 139, 147, 158, 160, 161, 166, 167
DE VAULT, D. C. 169, 183
DEWHURST, H. 184
DILWORTH, C. C. 47, 48, 70, 71
DIRAC, P. A. M. 116, 119, 120, 133
DODSON, R. W. 184
DOWNING, J. R. 160, 167
DREHMANN, U. 169, 183, 184
DRELL, S. D. 159, 167
DUFFIELD, R. B. 169, 184
DUNBAR, D. N. F. 71
DUNNING, J. R. 213, 215
DUNWORTH, J. V. 163, 167
DYSON, F. J. 139
DYSON, J. 52, 70

EDELFSEN, N. E. 20
EGGLER, C. 121, 138
ELLIOTT, L. G. 147, 158, 167
ELLIS, C. D. 140, 166
ELMORE, W. C. 83
ENDICOTT, K. M. 69, 72
ERBACHER, O. 181, 183
EVANS, J. 47, 70
EVANS, R. D. 147, 158, 167
EVANS, R. O. 167

FAIRBROTHER, F. 183
FALKOFF, D. L. 139
FARAGGI, H. 46, 70
FARLY, G. M. 15, 20
FAY, J. W. J. 175, 182, 183
FEATHER, N. 126, 127, 139, 155, 162, 166, 167
FEENBERG, E. 139
FELD, B. T. 67, 72, 213, 215
FERMI, E. 115, 117, 120, 121, 124, 126, 127, 138, 141, 162, 166, 183, 192, 209, 210, 211, 214, 215
FERTEL, G. E. F. 69
FESHBACH, H. 214
FINKELSTEIN, R. J. 202, 214
FINKELSTEIN, A. T. 36
FIREMAN, E. L. 131, 139
FISK, J. B. 159, 167
FLAMMERSFELD, A. 162, 167
FLOYD, J. J. 70
FOLDY, L. L. 5, 9, 20
FONG, H. T. 72
FOSTER, J. S. 20
FOWLER, P. H. 54, 65, 69, 70, 71, 72
FOWLER, R. H. 167
FOWLER, W. A. 132, 138, 156, 167
FRANK, F. C. 121, 138
FRANKEL, S. 145, 167
FRANZINETTI, C. 61, 71
FREDETTE, V. 69, 72
FREIER, P. 61, 62, 71
FRIEDLANDER, G. 183
FRIEDMAN, L. 176, 184
FURRY, W. H. 131, 139

GAMOW, G. 117, 124, 126, 127, 132, 138, 141, 167
GARDNER, E. 66, 71, 139
GARNER, C. S. 169, 184
GEORGE, E. P. 47, 67, 70, 72
GIBSON, W. M. 45, 54, 63, 65, 70, 71
GLUECKAUF, E. 175, 182, 183, 184
GOEPPERT-MAYER, M. 131, 139
GOERTZEL, G. 161, 167
GOLDBERGER, M. L. 215
GOLDHABER, G. 45, 70
GOLDHABER, M. 115, 138
GOLDSCHMIDT-CLERMONT, Y. 59, 71
GOLDSMITH, H. H. 213, 215
GOOD, W. M. 161, 167
GOPSTEIN, N. 183
GORDY, W. 139
GOSSLING, B. S. 36
GOUDSMIT, S. A. 60, 71
GOWARD, F. K. 66, 71
GRAHAME, D. C. 183
GRAY, L. H. 24, 36
GREEN, L. L. 45, 46, 47, 54, 63, 65, 70, 71
GREULING, E. 126, 139
GRIFFITH, B. A. 159, 167
GROSSKREUTZ, J. C. 65, 71
GUGELOT, P. C. 139, 167
GUGGENHEIMER, K. M. 64, 71
GURNEY, R. W. 40, 69

HAHN, O. 166
HAISSINSKY, M. 184
HALFORD, R. S. 169
HALPERN, J. 116, 138
HALPERN, O. 186, 192, 214
HAMILL, W. H. 172, 173, 184
HAMILTON, D. R. 132, 139, 161, 167
HANSON, A. O. 36
HARDING, J. B. 45, 67, 70, 72

HAVENS, W. W. 213
HAXBY, R. O. 36
HEBB, M. H. 159, 167
HEIDMANN, J. 72
HEITLER, H. 64, 71, 72
HEITLER, W. 62, 69, 139, 157, 158, 167
HELLER, R. B. 213, 215
HELMHOLTZ, A. C. 20
HENDERSON, J. E. 183
HENRICH, L. R. 20
HERB, R. G. 26, 27, 34, 36
HERZ, R. H. 54, 71
HILDEBRAND, R. 16, 20
HIRST, F. 71
HO ZAH-WEI. 71
HODGSON, P. E. 45, 62, 70
HORNBOSTEL, J. 67, 72
HOROWITZ, J. J. 139
HOUGH, P. V. C. 53, 70
HOYLE, F. 118, 138
HUBER, O. 36, 167
HUBER, P. 139
HUGHES, D. J. 121, 138, 213, 215
HULL, A. W. 36
HULME, H. R. 158, 159, 160, 167
HUUS, T. 36

IBSER, H. W. 213, 215
IMHOF, A. 36
IMRE, L. 183
IRVINE, J. W. 183
ITOH, J. 161, 167

JACOB, L. 36
JACOBI, R. B. 184
JACOBSEN, J. C. 132, 139
JAEGER, J. C. 160, 167
JASON, A. C. 67, 72
JAUNEAU, L. 72
JDANOFF, A. 38, 39, 40, 65, 69, 71
JEAN, M. 139
JENKINS, F. A. 139
JENSEN, E. N. 139
JOHNSON, M. H. 186, 192, 214

KAPLAN, M. F. 61, 71
KAPLAN, N. 44, 46, 47, 70, 72
KAPUR, P. L. 214
KARAMIAN, A. S. 184
KEEPIN, G. R. 65, 71
KEMMER, N. 139
KENNEDY, J. W. 183
KENNY, A. W. 181, 184
KERST, D. W. 150, 167
KIKUCHI, S. 161, 167
KING, D. T. 71, 72
KING, T. 71
KINOSHITA, S. 37, 69
KITT, G. P. 184
KLEIN, O. 157, 167
KNOWLES, W. 43, 69
KOFOED-HANSEN, O. 121, 132, 138, 139
KONOPINSKI, E. J. 115, 118, 121, 124, 125, 138, 139, 141, 166
KORSUNSKY, M. 152, 167
KOWARSKI, L. 182, 183
KREBS, A. 183
KUBITSCHEK, H. E. 184
KUEGER, H. H. A. 214
KURIE, F. N. D. 68, 72, 121, 151, 163, 167
KYLES, J. 167

LAMAR, E. S. 36
LAMB, W. A. 46, 70
LANGER, L. M. 121, 138, 139, 152, 167
LANGSDORF, A. 183
LA PALME, J. 46, 70
LARK-HOROWITZ, K. 45, 70
LASLETT, L. J. 139
LATHAM, R. 205, 211, 213, 214, 215
LATTES, C. M. G. 49, 54, 55, 56, 58, 59, 63, 65, 66, 70, 71, 139
LATTIMORE, S. 59, 71, 72
LATYSHEV, G. D. 158, 160, 167
LAUDA, J. 45, 70
LAURITSEN, C. C. 156, 167
LAURITSEN, T. 132, 138, 156, 167
LAWRENCE, E. O. 1
LAWSON, J. L. 138
LECOIN, M. 139
LEITH, C. E. 20
LEPRINCE-RINGUET, L. 67, 72
LEROUX, L. J. 183
LEVENTHAL, L. 169, 184
LEWIS, H. 138
LI, K. T. 143, 167
LI, T. T. 72
LIBBY, W. F. 169, 174, 175, 177, 178, 180, 183, 184
LIEBERMANN, L. N. 47, 70
LINDHARD, J. 139
LIVESEY, D. L. 46, 47, 63, 65, 69, 70, 71
LIVINGOOD, J. J. 183
LIVINGSTON, M. S. 1, 4, 13, 20, 57, 71
LOCQUEREUX, R. 71
LOFGREN, E. J. 71
LONGMIRE, C. 133, 135, 138, 139
LOWDE, R. D. 208, 215
LOWEN, I. S. 159, 167
LU, C. S. 183
LUHR, O. 36

MACKENZIE, K. R. 12, 20
MAGAT, M. 182, 183
MAJER, V. 183
MAJORANA, E. 131

MARGENAU, H. 214
MARSHAK, R. E. 120, 125, 126, 130, 138, 139
MARSHALL, L. 209, 211, 214, 215
MARTIN, L. H. 64, 71
MASSEY, H. S. W. 192, 200, 214
MATHER, K. B. 46, 68, 70, 72
MATHIEU, R. 53, 70
MATON, W. R. E. 181, 184
MAUER, P. B. 44, 69
MAY, A. N. 64, 70, 71
MCDANIEL, B. D. 153, 154, 157, 167
MCDOUGALL, J. 167
MCKIBBEN, J. 27, 31, 36
MCMILLAN, E. M. 20, 66, 71
MEDICUS, H. 139, 167
MEITNER, L. 140, 166
MELANDER, L. 184
MENEGHETTI, D. 211, 214, 215
MENSCHUTKIN, B. N. 178
METZGER, F. 161, 167
MEYERS, V. W. 215
MILLER, L. C. 139
MILLER, N. 184
MITCHELL, A. C. G. 139, 165, 167
MITCHELL, R. G. 36
MOAK, C. D. 71
MØLLER, C. 129, 134, 139
MOORE, W. H. 183
MORAND, M. 70, 71
MOREL, R. 36
MORELLET, D. 72
MORRISH, A. H. 132, 139
MORRISON, A. 52, 70
MORRISON, P. 134, 139
MORTON, F. 52, 70
MORTON, G. A. 207, 214
MOTT, N. F. 40, 62, 69, 71, 159, 160, 167, 192, 200, 214
MOYER, B. J. 16, 20
MUIRHEAD, H. 69, 70, 71, 72
MÜLLER, H. 36
MURPHY, G. M. 214
MUXART, R. 139, 184
MYSSOWSKY, L. 38, 65, 69, 71

NAHMIAS, M. E. 4, 20
NELSON, E. 139, 159, 167
NEY, E. P. 71
NISHINA, Y. 157, 167
NIX, F. C. 215
NORDHEIM, L. W. 139
NOVICK, A. 138

OCCHIALINI, G. P. S. 37, 46, 48, 51, 52, 63, 65, 66, 67, 69, 70, 71, 72
OLIPHANT, M. L. E. 4, 20, 36
OPPENHEIMER, F. 71
ORTHMANN, W. 140, 166
OSBORNE, L. S. 53, 67, 70, 72
OSOBA, J. S. 139, 151, 167

PANCINI, E. 139
PANETH, F. A. 183
PANETH, H. R. 132, 139
PARKINSON, D. B. 36
PAULI, W. 115, 141
PAUTHENIER, M. 36
PAYNE, R. M. 51, 70
PEACOCK, C. L. 139
PEACOCK, W. C. 138
PEASLEE, D. C. 214
PECK, R. A. 54, 65, 71
PEIERLS, R. E. 60, 214
PENNING, F. M. 33
PERFILOV, N. A. 45, 46, 70
PERKINS, D. H. 45, 59, 62, 67, 70, 71, 72
PERSICO, E. 145, 146, 167
PETCH, H. E. 167
PETERS, B. 61, 62, 63, 67, 71, 72
PETERSON, J. M. 66, 71
PHILIPP, K. 181, 183
PICCIONI, O. 139
PICCIOTTO, E. 45, 47, 67, 70, 72
PICKAVANCE, T. G. 20, 70
PICKUP, E. 67, 72
PLOOS VAN AMSTEL, J. J. A. 36
POLLOCK, H. C. 36
PONTECORVO, B. 183
POOLE, J. H. J. 67, 72
POWELL, C. F. 37, 38, 39, 45, 46, 48, 49, 51, 54, 56, 60, 61, 63, 64, 65, 66, 67, 69, 70, 71, 72
POWELL, W. M. 15, 20
PREISWERK, P. 139, 167
PRICE, H. C. 138, 139
PRIMAKOFF, H. 139
PRINGLE, R. W. 167
PURCELL, E. M. 154, 167
PURSLOW, E. T. 49, 70

RAINWATER, L. J. 213
RASETTI, F. 183
RAY, P. 183
REGENER, V. 107, 108
REID, A. F. 184
REINGANUM, M. 38, 69
REYNOLDS, H. L. 69
REYVAL, J. 24, 36
RICHARDS, H. T. 63, 65, 71
RICHARDS, J. 139
RICHARDSON, J. O. W. 126, 139
RICHARDSON, J. R. 13, 17, 18, 20
RIEDER, W. 180, 184
RING, H. 139
RINGO, G. R. 214

RITSON, D. M. 69, 71, 72
ROBERTS, A. 160, 167
ROBERTS, J. H. 65, 71
ROGINSKY, S. 183
ROSE, M. E. 3, 9. 10, 20
ROSEN, L. 71, 139
ROSENBLUM, E. S. 151, 167
ROSENBLUM, S. 60, 61, 71
ROSENFELD, L. 67, 72
ROSS, M. A. S. 54, 71
ROTBLAT, J. 49, 54, 56, 57, 68, 69, 70, 71, 72
ROZENTAL, S. 139
RUBIN, S. 64, 71
RUSINOV, L. I. 184
RUTHERFORD, LORD 36, 38, 140
RUTHERGLEN, J. G. 36

SACHS, R. G. 210, 215
SAKATA, S. 139
SALANT, E. O. 67, 72
SAMPSON, M. B. 138
SARGENT, B. W. 115, 126, 138, 141, 166
SAWYER, R. B. 71
SAXON, D. 139
SCHARFF-GOLDHABER, G. 138
SCHERRER, P. 139, 167
SCHIFF, L. I. 134, 139
SCHMIDT, F. H. 11, 20
SCHMITT, O. H. 85
SCHÖNBERG, M. 71
SCHWINGER, J. 138
SCOTT, W. T. 60, 71
SEABORG, G. T. 169, 183
SEGRÈ, E. 130, 139, 169, 173, 183
SEITZ, F. 215
SERBER, R. 18, 150, 167
SEWELL, D. C. 16, 20
SHAPIRO, M. M. 37, 38, 68, 69, 72
SHAW, P. F. D. 182, 184
SHERWIN, C. W. 132, 139
SHULL, C. G. 207, 209, 214, 215
SHULL, F. B. 139, 151, 167
SIDAY, R. E. 152, 167
SIDHU, S. S. 211, 215
SIEGBAHN, K. 139, 150, 151, 167
SIEGEL, S. 215
SLACK, L. 139, 151, 167
SNELL, A. H. 139
SOLOMON, A. K. 172, 184
SÖRENSEN, S. O. C. 62, 71
STANLEY, B. A. 159
STANLEY, J. P. 167
STARKE, K. 183
STEFFEN, R. 139
STEIGMAN, J. 169, 183
STEVENS, G. W. W. 47, 70
STOKKINK, G. 184
STRACHAN, C. 139
STURM, W. J. 210, 215
SUE, P. 184
SUESS, H. 169, 172, 183
SUGDEN, S. 183
SVARTHOLM, N. 150, 151, 167
SZILARD, L. 168

TAI, C. T. 49, 70
TALLMADGE, F. K. 71
TAYLOR, H. J. 38, 69
TAYLOR, H. M. 159, 160, 167
TELLER, E. 117, 124, 126, 127, 132, 138, 141, 167
TEMPLE, G. D. 154
THOMSON, G. P. 67, 72
THONEMAN, P. C. 36
TITTERTON, E. W. 66, 68, 71, 72
TOWNSEND, A. A. 138
TRALLI, N. 159, 167
TRICKER, R. A. R. 145, 167
TRUMP, J. G. 27, 36
TSCHISHOW, P. 38, 69
TSIEN, S. T. 54, 65, 70, 71
TUVE, M. A. 25, 26, 36

UHLENBECK, G. E. 118, 125, 138, 139, 141, 166

VALE, J. 20
VAN DE GRAAFF, R. J. 24, 25, 26, 27, 32, 36
VAN DEN GRINTEN, W. 47, 59, 70, 71
VAN DER TUUK, J. H. 36
VANESLOW, S. 48, 49, 70
VAN GEEL, W. C. 36
VAN MEERSCHE, M. 184
VEKSLER, V. 4, 20
VIGNERON, L. 70, 71
VOELRATH, R. E. 36
VON ARDENNE, M. 36
VON HALBAN, H. 182, 183
VOYVODIC, L. 67, 72

WÄFFLER, H. 45, 70
WAGNER, N. 66, 72
WAITHMAN, V. B. 20
WALKE, H. J. 183
WALKER, R. L. 153, 154, 157, 167
WALLACE, J. W. 213, 215
WAMBACHER, H. 38, 69
WANG, C. S. 139
WATASE, Y. 161, 167
WEBB, J. H. 37, 40, 54, 69
WEBER, H. H. 215
WEINSTOCK, R. 186, 199, 201, 202, 214
WEISSKOPF, V. F. 214
WENTZEL, G. 138

WESTÖÖ, R. 45, 70
WHITAKER, M. D. 208, 215
WHITE, E. L. C. 80
WIEDENBECK, M. L. 159, 167
WIEGAND, C. E. 130, 139
WIENER, M. 47, 70
WIGNER, E. P. 127, 139, 141, 167, 214
WILKINS, J. R. 38, 69
WILKINSON, D. H. 65, 71
WILLARD, J. E. 173, 183, 184
WILLIAMS, E. J. 59, 71
WILLIAMS, J. H. 36, 64, 71
WILLIAMS, R. R. 172, 173, 180, 181, 182, 184
WILSON, M. J. 48, 49, 70
WILSON, R. R. 3, 20
WINSBURG, L. 211, 214, 215
WINTERINGHAM, F. D. W. 178, 184
WITCHER, C. M. 145, 167
WOLLAN, E. O. 65, 71, 207, 209, 214, 215
WOOSTER, W. A. 166
WU, C. S. 121, 138, 213

YAGODA, H. 37, 44, 46, 47, 66, 68, 69, 70, 72
YANG, C. N. 139
YOST, F. L. 139
YOUNG, J. A. 173, 184
YOUNIS, S. 45, 70
YUASA, T. 184
YUKAWA, H. 117, 135, 138, 139

ZAJAC, B. 54, 57, 71
ZHDANOW, A. (See Jdanoff, A.)
ZINN, W. H. 36
ZÜNTI, W. 120, 138, 156, 162, 167

SUBJECT INDEX

ACCELERATING tubes 29
Allowed transitions (in beta decay) 117
Alpha particle, from fission 65
— — range in emulsion 55
— — tracks in emulsions 37, 38, 42, 62
Amplifier, D.C. 92, 113
— negative feedback 76
— pulse 93, 100
— noise 94
Angular correlation in beta decay 131
Anode follower 78
Anti-coincidence circuit 103

BETA decay 115 *et seq*
— — allowed 117
— — angular correlation in 131
— — double 130
— — forbidden 122
— — in light nuclei 127
Beta-ray, energy measurement 162
— — spectrum 120, 124, 140
Born approximation 200
Breakdown, in dielectrics 25, 27
— *in vacuo* 30, 31
Breit-Wigner formula 190

CATHODE coupled pair 88
— follower 77, 80
Coincidence absorption method 164
— circuit 101
— measurements 163, 165
Compton electrons 156
Counting rate meter 111
Critical absorption 155
Crystal lattice 194, 205
Current feedback 74, 79, 81
Cyclotron 1
— frequency modulated (*See* Synchrotron)
— relativity effects 3

DEBYE temperature 201
Delay lines 89
Densitometer 52
Deuteron, tracks in emulsions 42
Diodes 86
Discriminators 97
Dispersion formula 190

ELECTRON, tracks in emulsions 42
Electrostatic generator 21, 24
— — characteristics 28
— — voltage control 33
Emulsions, photographic 37, 39, 40
— — applications of 63, 66, 67, 68
— — characteristics 42, 43, 44
— — loaded 44
— — shrinkage of 49
— — treatment of 47

Extinction effects (neutron scattering) 207

FEEDBACK 74, 77
— amplifier 76
— negative 76
— positive 83
Fermi plot 121
— pseudo-potential 186, 192
— selection rules 124, 141
Fission 65

GAMMA rays, energy measurement 155
— — in beta decay 134
Gamow-Teller selection rules 124, 126, 127, 141
Generating voltmeter 34
Grain density, in emulsions 57

HIGH voltage rectifier sets 22
'Hot' atoms 168
— — chemistry of 175, 179
— — cooling of 174

INELASTIC neutron scattering 205
Internal conversion 159
— pair production 160
Ion sources 14, 32
Isomeric transitions 159, 169, 171, 173

K-CAPTURE 128
— — forbidden 129
Klein-Nishina formula 157
Kurie plot 121

LATENT image, fading of 45, 46
Lattice vibrations 199, 207
Leptons 117

MASS determination (in emulsions) 60
Meson 60, 66, 117
— fields 136
— pairs 137
— theory 135
Microcrystals, neutron scattering by 194, 208
Microscope, projection 51
— reflecting 52
— universal 49

NEUTRINO 115, 116
Neutron 65
— absorption 190
— beam 209
— irradiation 175, 176
— — dilution effects 178
— scattering 185 *et seq*
— — and lattice vibrations 199

Neutron scattering by polycrystals 194
— — by single nucleus 188
— — case of several isotopes 197, 202
— — extinction effects 207
— — inelastic 205
— — influence of nuclear spin 192, 198
Noise in amplifiers 94
Nuclear forces 67
— level schemes 163
— pseudo-potential 192

PAIR production 152, 158
— — internal 160
— spectrometer 152
Penning gauge 33
Phonons 199, 201, 202, 203, 204, 205, 211
Photographic emulsions (*See* Emulsions)
Photomicrograph 52
Polycrystal, neutron scattering by 194
Positron emission 129
Proton, track in emulsions 39
— range, in aluminium 19
— — in emulsion 55
Pulse shapers 86, 90, 97, 101

QUENCHING circuit 100

RANGE-ENERGY relation 19, 54
Ring decade circuit 106

SCALING circuits 105, 106, 109
Scattering, small angle 59
— constants 198, 209, 212
— cross section 190, 197, 209
— — — differential 195
— — — elastic 199, 206, 210, 211
— — — inelastic 199, 205, 206, 211, 213
Scattering cross section, total 193, 198, 202
— length 186, 190
Schmitt circuit 85
Selection rules, in beta decay 123, 141
Shielding from neutrons 15
Spectrometer, beta-ray 142, 143, 145, 146
— — — double focusing 149, 151, 152
Stabilizer, current 113
— voltage 112, 113
Straggling 56
Synchrotron 4
— beam 16
— magnet 7, 8
— R. F. system 10
— vacuum system 13
Szilard-Chalmers reaction 168 *et seq*
— — — applications 181
— — — recoil effects 171
— — separations 170

TRACK, alpha particle 42, 62
— deuteron 42
— electron 42
— heavy nuclei 62, 63
— proton 42
— measurement 53
Transformers 80
Transition effect (soft gamma-rays) 155
Trigger circuits 83

VACUUM systems 13
Van de Graaff machine 24
Voltage control 34
— feedback 74

WILSON seal 13

X-RAYS 29